Molecular mechanisms underlying presynaptic plasticity: characterization of the RIM1α and SV2A interactome

Dissertation

zur

Erlangung des Doktorgrades (Dr. rer. nat.)

der

Mathematisch-Naturwissenschaftlichen Fakultät

der

Rheinischen Friedrich-Wilhelms-Universität Bonn

vorgelegt von

Ana-Maria Oprişoreanu

aus

Târgovişte, Rumänien

Bonn 2014

Angefertigt mit Genehmigung der Mathematisch-Naturwissenschaftlichen Fakultät der Rheinischen Friedrich-Wilhelms-Universität Bonn

1. Gutachter Prof. Dr. Susanne Schoch
2. Gutachter Prof. Dr. Albert Haas

Tag der Promotion: 13.01.2015

Erscheinungsjahr: 2015

Erklärung

Diese Dissertation wurde im Sinne von § 4 der Promotionsordnung vom 17.06.2011 am Institut für Neuropathologie und Klinik für Epileptologie der Universität Bonn unter der Leitung von Frau Prof. Dr. Susanne Schoch angefertigt.
Hiermit versichere ich, dass ich die vorliegende Arbeit selbständig angefertigt habe und keine weiteren als die angegebenen Hilfsmittel und Quelle verwendet habe, die gemäß § 6 der Promotionsordnung kenntlich gemacht sind.

Bonn, den _____ _____

Ana-Maria Oprişoreanu

1.Introduction 1
1.1 The synapse 1
1.2 Cytometrix at the active zone (CAZ) 1
1.2.1 Active Zone Ultrastructure 1
1.2.2 Active Zone composition 3
1.3 The synaptic vesicle cycle 4
1.4 Synaptic plasticity 5
1.4.1 Presynaptic dormancy 6
1.4.2 Molecular mechanisms involved in presynaptic LTP 7
1.5 Two major players in synaptic plasticity 7
1.5.1 RIMs 8
1.5.1.1 RIM gene structure 8
1.5.1.2 RIM protein structure and binding partners 9
1.5.1.3 RIM function 11
1.5.1.3.1 RIM in invertebrates (*C.elegans* and *D.melanogaster*) 11
1.5.1.3.2 RIM in vertebrates (*M.musculus*) 12
1.5.1.3.2.1 RIM1α knock-out mice 12
1.5.1.3.2.2 RIM1αβ double knock-out mice 13
1.5.1.3.2.3 RIM2α knock-out mice 13
1.5.1.3.2.4 RIM1α/RIM2α double knock-out mice 13
1.5.1.3.2.5 RIM conditional knockout mice 14
1.5.2 Synaptic vesicle protein 2A (SV2A) 15
1.5.2.1 SV2A function 15
1.5.2.2 SV2A knock-out mice 16
1.6 Aim of the study 17
2. Materials 18
2.1 Equipment 18
2.2 Chemicals 19
2.3 Cell culture media 20
2.4 Kits 20
2.5 Enzymes 20
2.6 Inhibitors 20
2.7 Diverse materials 20
2.8 Cloning primers 21
2.9 Sequencing primers 22
2.10 Site-directed mutagenesis 22
2.11 Oligonucleotides used for HA-tag cloning 22
2.12 Oligonucleotides used for shRNA cloning 22
2.13 Generated constructs 23
2.14 Plasmids obtained from other sources and used in this thesis 23
2.15 Primary and secondary antibodies 24
3. Methods 25
3.1 Molecular Biology 25

3.1.1 RNA extraction and cDNA synthesis 25
3.1.2 Polymerase chain reaction (PCR) 25
3.1.3 Site directed mutagenesis 25
3.1.4 Sequencing 26
3.1.5 Cloning technique 26
3.1.5.1 Oligonucleotides cloning 26
3.2 Cell Culture 26
3.2.1 HEK (AAV) 293T cell culture 26
3.2.2 HEK (AAV) 293T transfection methods 27
3.2.2.1 Ca^{2+}-phosphate method 27
3.2.2.2 Lipofectamine method 27
3.2.3 Neuronal primary cell culture 27
3.2.3.1 Generation of primary cell culture 27
3.2.3.2 Transfection of neurons 28
3.2.3.3 Infection of neurons 28
3.3 Virus Production 28
3.3.1 rAAV serotype 1/2 and 8 production (Ca^{2+}-phosphate method) 28
3.3.2 rAAV serotype 8 purification 29
3.3.3 P0-P3 animal injection 29
3.4 Biochemistry 30
3.4.1 Preparation of crude synaptosomes 30
3.4.2 Protein-protein interaction assays 30
3.4.2.1 Protein induction and purification from BL21 bacteria 30
3.4.2.2 GST-pull down assay 31
3.4.2.3 Co-immunoprecipitation (co-IP) 31
3.4.2.4 Immunoprecipitation (IP) 31
3.4.3 Protein concentration determination 32
3.4.4 Western Blotting (WB) 32
3.5 Identification of novel binding partners by tandem-affinity purification (TAP) 32
3.5.1 Protein cross-linking 32
3.5.2 Strep/FLAG tandem affinity purification 33
3.5.3 Protein purification from HEK293T cells 34
3.5.4 Binding assays between the different regions of RIM1α and crude synaptosomes 34
3.5.5 Sample preparation for mass spectrometer analysis 34
3.6 Immunochemical methods 36
3.6.1 Pre-treatment of primary neurons with various inhibitors 36
3.6.2 Immunofluorescence (IF) 36
3.6.3 Immunohistochemistry (IHC) 36
3.7 Imaging 37
3.8 Quantifications and statistical analysis 37
3.8.1 Image quantification 37
3.8.2 WB quantification 37
3.9 Programmes and URLs 37

4. Results 38
4.1 Impact of phosphorylation status on the properties of RIM1α 38
4.1.1 Distribution of RIM1α in synaptic boutons is altered by hyperphosphorylation events 38
4.1.2 Identification of novel phosphorylation-dependent RIM1α binding proteins 40
4.1.2.1 Identification of protein complexes associated with the C-terminal region of RIM1α 41
4.1.2.2 Analysis of protein complexes associated with the N-terminal region of RIM1α 44
4.1.2.3 Analysis of the protein complexes co-purified with the overexpressed C-terminal region of RIM1α in primary cultured neurons 45
4.1.3 Validation of the newly identified RIM1α binding proteins 48
4.1.3.1 Unc-51-like kinase (ULK) 48
4.1.3.1.1 ULK proteins bind RIM1α 48
4.1.3.1.2 The ULK-kinase domain mediates binding to RIM1α 49
4.1.3.1.3 ULK1/2 partially co-localize with endogenous RIM1/2 at synapses 50
4.1.3.1.4 Generation of a short-hairpin RNA against ULK2 54
4.1.3.2 Serine-arginine protein kinase 2 (SRPK2) 55
4.1.3.2.1 SRPK2 targets RIM1α 56
4.1.3.2.2 Non-kinase core regions do not mediate direct binding to RIM1α 60
4.1.3.2.3 The effect of SRPIN340 inhibitor on the SRPK2 co-localization with endogenous RIM1α 62
4.1.3.3 Vesicle-associated membrane protein (VAMP) associated-protein A/B (VAPA/VAPB) 63
4.1.3.3.1 VAPA/VAPB binds RIM1α 63
4.1.3.3.2 Kinase inhibition strengthens the VAPA-RIM1α interaction 65
4.1.3.3.3 The T812/814A point mutations in the RIM1α C2A-domain impair binding to VAPA 66
4.1.3.3.4 VAP proteins bind RIM1α in co-IP assays 66
4.1.3.3.5 Co-localisation of VAP proteins with endogenous RIM1/2 in neuronal cell culture 67
4.1.3.4 Copine VI 71
4.1.3.4.1 Copine VI binds RIM1α 71
4.1.3.4.2 The Copine VI-RIM1α interaction is calcium dependent 72
4.1.3.4.3 Copine VI and RIM1/2 co-localized at a subset of synapses 72
4.2 SV2A 73
4.2.1 Generation and characterisation of the TAP-tagged SV2A constructs 73
4.2.2 Optimization of SV2A protein purification from primary rat cortical neurons 75
4.2.2.1 One-step purification yields good recovery of TAP-tagged SV2A 75
4.2.2.2 Two-step purification of fusion proteins leads to a decrease in elusion efficiency 76
4.2.3 SV2A overexpression and affinity purification from mouse brain 78

4.2.3.1 Analysis of mouse brain transduced with rAAV-SV2A-GFP indicates high levels of expression of recombinant protein 79
4.2.3.2 N- and C-tagged SV2A affinity purification from transduced mouse brain 80
4.2.3.2.1 Analysis of single-step purification method 80
4.2.3.2.2 Two-step purification procedure 82
4.2.4 Analysis of protein complexes co-immunprecipitated with overexpressed SV2A in primary neuronal cell culture 83
4.2.4.1 Enrichment of bound protein complexes to SV2A by using cross-linkers and primary neurons from hetero- and homozygous SV2A mice 83
4.2.4.2 Identification of novel potential binding partners for SV2A by mass-spectrometry 85
5. Discussion 86
5.1 Hyperphosphorylation alters the distribution of the presynaptic protein RIM1α at synapses 86
5.2 Identification of novel phosphorylation-dependent RIM1α binding proteins 89
5.2.1 Two novel potential kinases associate with RIM1α protein 90
5.2.1.1 Unc-51-like kinase (ULK) binds the C2-domains of RIM1α 91
5.2.1.2 Serine Arginine protein kinase 2 (SRPK2) targets specifically the C2A-domain of RIM1α 93
5.2.2 VAPA/B proteins bind specifically the C2A-domain of RIM1α 96
5.2.3 Copine VI binds RIM1α in a calcium-dependent manner 98
5.3 Identification of novel SV2A binding partners: new experimental approaches 99
6. Outlook 102
7. Summary 103
8. Appendix 105
9. Abbreviations 113
10. References 115
11. Acknowledgments 128

1. Introduction

1.1 The synapse

Already in 1897 Foster and Sherrington introduced the term synapse (from Greek *synapsis* "conjunction", from *synaptein* "to clasp", from *syn-* "together" and *haptein* "to fasten)[1] (WESTFALL et al., 1996). By 1962 the first nervous system, though a simple one, in Phylum *Cnidaria* (corals, anemones, and jellyfish) was defined by Horridge and Mackay. After Santiago Ramón y Cajal, the founder of modern neuroscience (LLINÁS, 2003), many scientists dedicated themselves in understanding the structure and function of synapses. In 1954 Palade and Palay described for the first time the structure of a vertebrate synapse using electron microscopy (EM). Since that time our understanding of synapse architecture has deepened, facilitated also by enhanced imaging techniques.

The synapse is an asymmetrical structure composed of a presynaptic terminal, a synaptic cleft and a postsynaptic terminal. The presynaptic terminal is important in regulating synaptic vesicle docking, priming, fusion and neurotransmitter release into the cleft, where the neurotransmitter molecules bind to the postsynaptic terminal's receptors. In the postsynaptic terminal the chemical signal is converted into an electrical one and further propagated within the neuron. Several steps of synaptic vesicle (SV) fusion take place at a specialized structure in the presynaptic terminal, which contains an electron-dense cytoskeletal matrix, known as **c**ytometrix at the **a**ctive **z**one (CAZ) (review: SCHOCH and GUNDELFINGER, 2006; review: SÜDHOF, 2012).

1.2 Cytometrix at the active zone (CAZ)

1.2.1 Active Zone Ultrastructure

In a simplistic model the active zone consists of a proximal zone close to the plasma membrane, where the docking of synaptic vesicles (SV) takes place and a more distal zone where vesicles are tethered. Over the decades electron microscopy and tomography (EM) techniques have revealed the existence of an electron-dense structure expanding into the cytoplasma. These observed dense projections differ considerably between species (review: ZHAI and BELLEN, 2004). At the neuromuscular junction (NMJ) of *C.elegans* the dense projection has been described as a plaque surrounded within 100nm by a subpopulation of vesicles (*Fig. 1.1A*; WEIMER et al., 2006); while in *D.melanogaster,* the dense structure takes the shape of a pedestal and a platform (T-bars) enclosed by synaptic vesicles and closely associated with calcium channels (*Fig. 1.1B*; PROKOP and MEINERTZHAGEN, 2006). In vertebrates (frog), the NMJ has

[1] ONLINE ETYMOLOGY DICTIONARY: *www.etymonline.com*

a more complex structure formed by a tight and ordered connection of structural elements (different classes of active zone material-AZM-macromolecules) that connect the correctly orientated SVs (the luminal assembly of macromolecules orientated towards the AZM macromolecules) in order to facilitate the docking process with the presynaptic membrane (*Fig. 1.1E and 1.1F*; HARLOW et al., 2001, 2013; SZULE et al., 2012). In mammalian neurons, EM using fixed and stained samples highlighted the active zone as a hexagonal grid of dense projections with synaptic vesicles in between (review: SÜDHOF, 2012). Sensory synapses exhibit a striking dense structure, in the shape of a ribbon, where synaptic vesicles are primed. The shape of the ribbon is dictated by the sensory cell type; dense structure in rod and cone photoreceptors, plate-like in bipolar cells, whereas in hair cells a spherical form is displayed (dense bodies) (MERCER and THORESON, 2011).

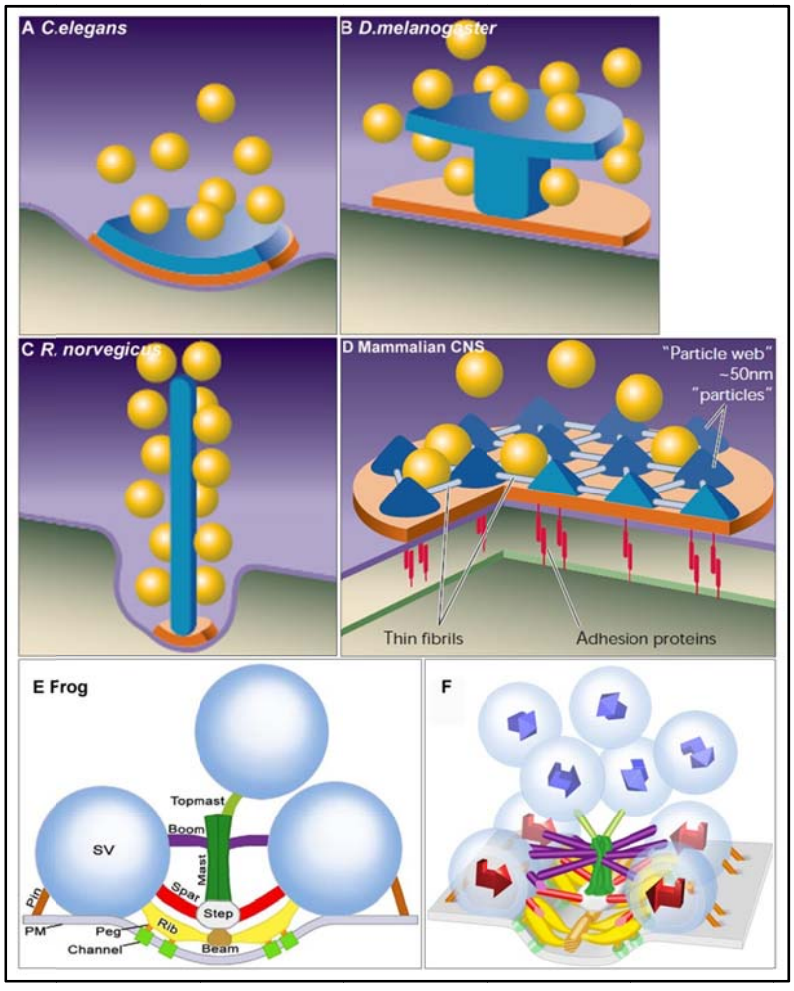

***Figure 1.1*: Electron micrographs of the active zone structure.** (**A**) plaque-like dense projection in *C.elegans* NMJ; (**B**) T-bar dense projection in *D.melanogaster* NMJ; (**C**) ribbon synapse in *R.norvegicus*; (**D**) active zone structure in mammalian CNS. (**E**) Dense projection structure in frog NMJ; (**F**) 3D arrangement of the docked and undocked SVs relative to the AZM and the presynaptic membrane. Pictures were taken from: ZHAI et al., 2004; SZULE et al., 2012 and HARLOW et al., 2013.

The difference in the size of the dense projection is dictated not only by the cell type but also by the activity of the cell. The large dense projections allow an increase in the size of the RRP (readily releasable pool) without an increase in the active zone area (T-bars and ribbon synapses), conferring a sustained release of neurotransmitters upon continuous stimulation. At vertebrate neuromuscular junctions (NMJs) and central nervous system (CNS) synapses, where stimulations are not continuous and the size of the nerve terminal is not restricted, the active zone may expand (review: ZHAI and BELLEN,2004).

To uncover the architecture of the active zone, different electron tomography (EM) techniques have been applied. EM of fixed and stained samples showed the dense material of the AZ as a regular array of thick projections surrounded by SVs. Due to the different treatments samples must undergo before imaging, it has been argued that the native structure is lost due to protein aggregation as a consequence of protein cross-liking, thus leading to a false interpretation of the data. New EM techniques based only on fast freezing of the tissue sample to immobilize the entire structure in the native state, did not reveal the presence of any dense projections. Instead a less organized architecture with fine filaments connecting SVs between each other (*connectors*) and to the plasma membrane (*tethers*) was observed (*Fig. 1.2*; FERNANDEZ-BUSNADIEGO et al., 2010; review: SIKSOU et al., 2011).

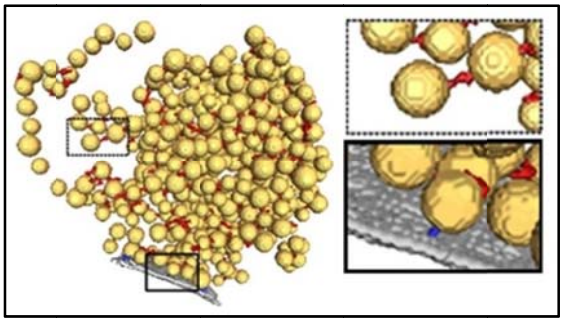

Figure 1.2: 3D segmentation of synaptic vesicles (yellow), AZ (gray), synaptic vesicle connectors (red), and synaptic vesicle tethers (blue). All pictures were taken from FERNANDEZ-BUSNADIEGO et al., 2010.

1.2.2 Active Zone composition

Despite the differences between cryo-EM and classical EM, both approaches revealed the diversity of the active zone ultrastructure. The nature of the intricate web of proteins underlying the plasma membrane is very complex. In addition to proteins involved in adhesion, cytoskeletal formation, scaffolding and the fusion machinery, the active zone is composed of a set of proteins highly enriched in this area (RIM, RIM-BP, Liprin, Munc13, Piccolo and Bassoon, and ELKS (CAST/ERC)) and proteins associated with these (CASK/Veli/Mint1) (*Fig. 1.3*; review: SCHOCH and GUNDELFINGER, 2006; SÜDHOF, 2012).

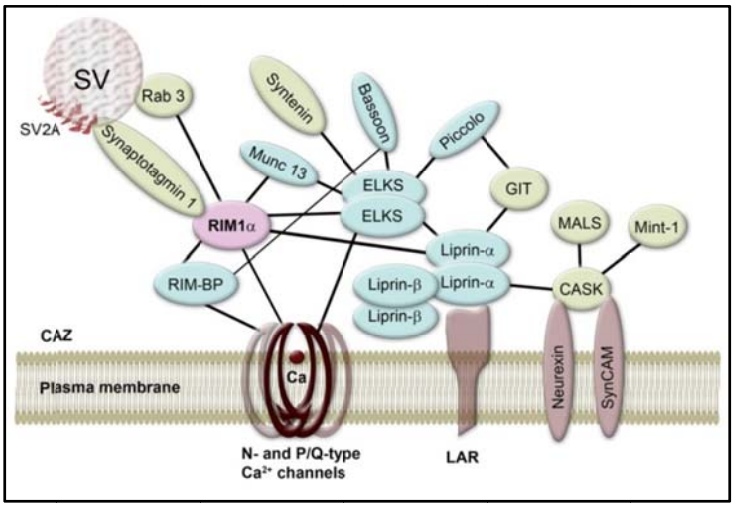

Figure 1.3: **Active Zone protein composition.** Proteins highly enriched at the active zone are depicted in light blue. CAZ, cytometrix at the active zone; RIM-BP, RIM binding protein; LAR, leukocyte common antigen related; GIT, G-protein-coupled receptor kinase-interacting protein; RIM, Rab3 interacting protein; SV2A, synaptic vesicle protein 2A; CASK, calcium/calmodulin-dependent serine protein kinase. Adapted from review: SCHOCH, MÜLLER und OPRISOREANU,2014.

The active zone, due to its complex organization, has four principle functions in neurotransmitters release: (*1*) SV docking and priming; (*2*) calcium channels recruitment, in order to facilitate fast synchronous excitation/release coupling; (*3*) precise localization of pre- and postsynaptic compartments; (*4*) mediation of both short- and long-term presynaptic plasticity. As a result, all these functions guarantee that presynaptic vesicle exocytosis is performed with the requisite speed and plasticity needed for the information transfer (SÜDHOF, 2012).

1.3 The synaptic vesicle cycle

The active zone is the specialized structure in the presynaptic terminal, where neurotransmitter release takes place. When an action potential reaches the presynaptic terminal, the voltage gated calcium channels open followed by an increase in Ca^{2+}- ion influx. The transient Ca^{2+} elevation stimulates SV exocytosis. In the synaptic bouton SVs undergo repeated cycles of exocytosis-endocytosis. During exocytosis vesicles are filled actively with neurotransmitters followed by docking, priming, fusion and neurotransmitters release (Fig. 1.4; reviews: SÜDHOF, 2004, 2013).

After the synaptic vesicles are filled with neurotransmitters and docked, they undergo several changes until they become fusion-competent (priming step). This priming step is mediated on one side by the formation of the SNARE complex (soluble N-ethylmaleimide-sensitive factor attachment protein receptor) consisting of synaptobrevin-SNAP25-Syntaxin1 and on the other side by Munc18, Munc13, RIM and Synaptotagmin1 (reviews: SÜDHOF, 2004, 2013). Originally Munc18-1 was reported to bind syntaxin1 in a 'closed' conformation, competing with core-complex formation (DULUBOVA et al., 1999).

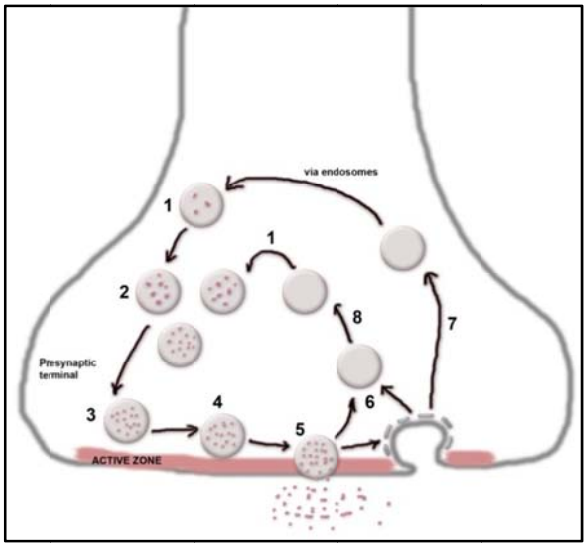

Figure 1.4: **Synaptic vesicle cycle.** ***1***- SVs are actively filler with neurotransmitters; ***2***- reserve pool of SVs; ***3***- docking; ***4***- priming; ***5***- fusion and neurotransmitter release; ***6***- recycling via kiss-and-run; ***7***- clathrin mediated endocytosis and recycling via the endosome compartment; ***8***- clathrin mediated endocytosis and recycling without endosomal intermediate. Adapted from review: SÜDHOF, 2004.

Other candidate proteins to facilitate SV priming are Munc13 and RIM. Munc13, activated by binding to the RIM Zn^{2+}-finger domain (DENG et al., 2011), was suggested to assist the transition to an 'open' conformation of syntaxin1, enabling SNARE complex

assembly and thereby the priming step (BETZ et al., 1997; review: RIZO and SÜDHOF, 2002; STEVENS et al., 2005; review: SÜDHOF, 2013).

After the action potential reaches the presynaptic terminal, voltage gated calcium channels open and the calcium concentration builds up in a microdomain near the priming complex. The calcium sensor synaptotagmin1 (present on the synaptic vesicle) together with the SNARE complex further enables membrane fusion (DAI et al., 2008; CHOI et al., 2010; VRLJIC et al., 2010) with the formation of the pore to release the neurotransmitters into the synaptic cleft. Following neurotransmitter release SVs are recycled via different routes, like *kiss-and-run* (vesicles undock and recycle locally), clathrin mediated endocytosis (vesicles are reacidified and refilled directly or by passing via the endosome compartment) (review: SÜDHOF, 2004) or via bulk endocytosis. Activity-dependent bulk endocytosis (ADBE) is the dominant retrieval pathway after an elevated stimulation activity (CHEUNG and COUSIN, 2013).

In accordance with the network's needs, the amount of SVs ready to release neurotransmitter may very as well. SV recycling is tightly regulated by the action of different proteins, resident at the AZ. Therefore, fluctuations in the activity of synapses could be mediated by the actions of various AZ proteins, as well as by the SVs cycle. These changes represent the fundament of presynaptic plasticity.

1.4 Synaptic plasticity

The concept of synaptic plasticity, which was for the first time formulated by Hebb in 1949, refers to the capacity of synapses to react accordingly to the network's needs either be weakening (depression) or strengthening (potentiation) its activity. These types of changes may well extend over short periods (short-term plasticity) or long periods of time (long-term plasticity). The Hebbian theory is used to describe these synaptic changes as being associative and rapidly induced, shortly explained as a positive feedback process (HEBB., 1949). For example, upon LTP induction, synapses become more excitable and the entire network activity would increase leading to a runaway potentiation. To prevent such extremes, the homeostatic process, which hinders the network to reach high levels of activity and preserve the stored information, has an important role (review: POZO and GODA, 2010).

In the active state or basal conditions synaptic transmission is mediated by the release of neurotransmitters from presynaptic terminals into the synaptic cleft, followed by the activation of different receptors on the postsynaptic terminal. Under increased network activity presynaptic neurons decrease their release probability (LTD-long-term depression), while the postsynaptic cells decrease the number of their receptors. To offset reduced network

activity, presynaptic neurons enhance the recycling, the number of docked vesicle and the release probability (LTP-long-term potentiation) (review: POZO and GODA, 2010; CASTILLO, 2012). There are multiple parallel mechanisms responsible for controlling pre- and postsynaptic homeostasis, and consequently affecting synapse activity. The molecular mechanisms that govern the negative feedback (homeostatic plasticity) rely on the efficiency of different intracellular signalling cascades to detect and to respond accordingly to changes in the network. These fine-tuned mechanisms include: gene expression induction, protein synthesis and degradation. Besides the two major mechanisms: transcription and translation, post-translational modifications have emerged as an important factor in controlling plasticity (review: POZO and GODA., 2010). Several post-translational modifications have been suggested to modulate the function of various pre- and postsynaptic proteins, like: palmitoylation (review: EL-HUSSEINI and BREDT 2002), myristilation and prenylation (KUTZLEB et al., 1998; O'CALLAGHAN et al., 2003), SUMOylation (**S**mall **U**biquitin-like **Mo**difier) (GIRACH et al., 2013) and phosphorylation (review: BARRIA, 2001).

1.4.1 Presynaptic dormancy

Presynaptic dormancy is induced as a response to a prolonged strong depolarization or increased action potential firing. Dormant synapses display a decrease in neurotransmitter release. The molecular mechanism is based on the inhibitory action of G proteins on adenylyl cyclase (AC), which causes a decrease in the level of cAMP and thereby directly affects the activity of protein kinase A (PKA) (*Fig. 1.5*). Therefore, presynaptic proteins are less phosphorylated and become susceptible to degradation through the proteasome (review: CRAWFORD and MENNERICK, 2012). The protein levels of RIM1α and Munc13-1 were shown to be decreased upon induction of presynaptic dormancy through the action of the ubiquitin-proteasome system, while an overexpression of RIM1α in cultured neurons prevented the induction of silencing (JIANG et al., 2010). Recently two other presynaptic proteins, Piccolo and Bassoon were identified as negative regulators of the E3 ligase Siah1. In the DKO neurons the rate of presynaptic protein degradation was increased, leading to the observation that these two proteins are important regulators of the protein ubiquitination in the presynaptic terminal, therefore maintaining synapse integrity (WAITES et al., 2013).

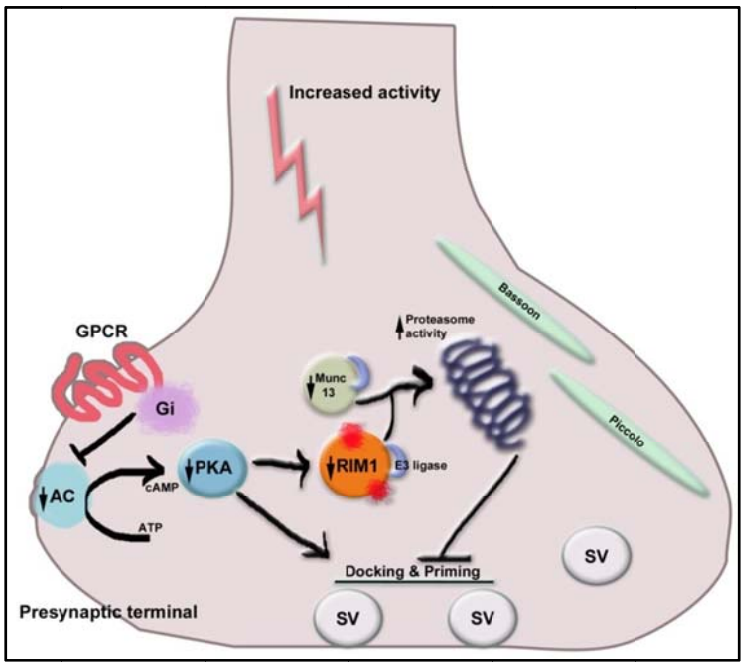

Figure 1.5: **Presynaptic dormancy.** Increased action potential firing activates the inhibitory G protein (Gi, pink), Adenylyl cyclase (AC, light blue) action is impaired and protein kinase A (PKA, dark blue) activity is decreased. As a consequence RIM1α, is less phosphorylated (red markings) and susceptible to degradation, via the proteasome. Together with RIM1, Munc13 protein (green) is also degraded. Model adapted after CRAWFORD and MENNERICK, 2012.

1.4.2 Molecular mechanisms involved in presynaptic LTP

At the mossy fibres (MF) presynaptic long-term potentiation (LTP) is induced by an increase in Ca^{2+} influx via voltage gated calcium channels (VGCG). The increase in calcium in the presynaptic terminal will activate the Ca^{2+} /calmodulin dependent-adenylyl cyclase, leading to an increase in cAMP and activation of PKA (review: CASTILLO, 2012). One of the PKA targets is RIM1α, a highly enriched protein in the active zone. Although RIM1α has been reported to be important in several cAMP/PKA-dependent forms of presynaptic plasticity (CASTILLO et al., 2002; review: CASTILLO, 2012) its direct phosphorylation by PKA could not be linked to any significant function in presynaptic LTP (KAESER et al., 2008a; YANG and CALAKOS, 2010). Additionally, PKA may regulate LTP independently of RIM1α phosphorylation. Another kinase, PKC was reported to be responsible for LTP in MF-dentate gyrus basket cells (review: CASTILLO, 2012). Overall, the precise molecular mechanism governing presynaptic LTP and LTD are still not fully elucidated.

1.5 Two major players in synaptic plasticity

Even though the exact mechanisms governing the presynaptic plasticity are not fully elucidated, several cellular processes, like SV priming or posttranslational modifications, were suggested to modulate this event. Since SV priming is one of the most important events leading to neurotransmitters release, it's imperious to be under a tight control. Two proteins, one resident of the AZ (RIM1α), the other a component of synaptic vesicle (SV2A), were described to be actively involved in taking part in the regulation of priming. Moreover, their function could be altered, via posttranslational modifications, triggering changes in synaptic transmission.

1.5.1 RIMs

1.5.1.1 RIM gene structure

The RIM protein family consist of 7 members encoded by 4 separate genes (RIM1, RIM2, RIM3 and RIM4). RIM1 and RIM2 genes can direct the synthesis of different isoforms using distinct promoters: 2 isoforms for RIM1 (α, β) (KAESER et al., 2008b), and 3 isoforms for RIM2 (α, β, γ) (WANG and SÜDHOF, 2003). RIM3 and RIM4 genes encode each for one transcript only, RIM3γ and RIM4γ, respectively (*Fig. 1.6A*; WANG and SÜDHOF, 2003).

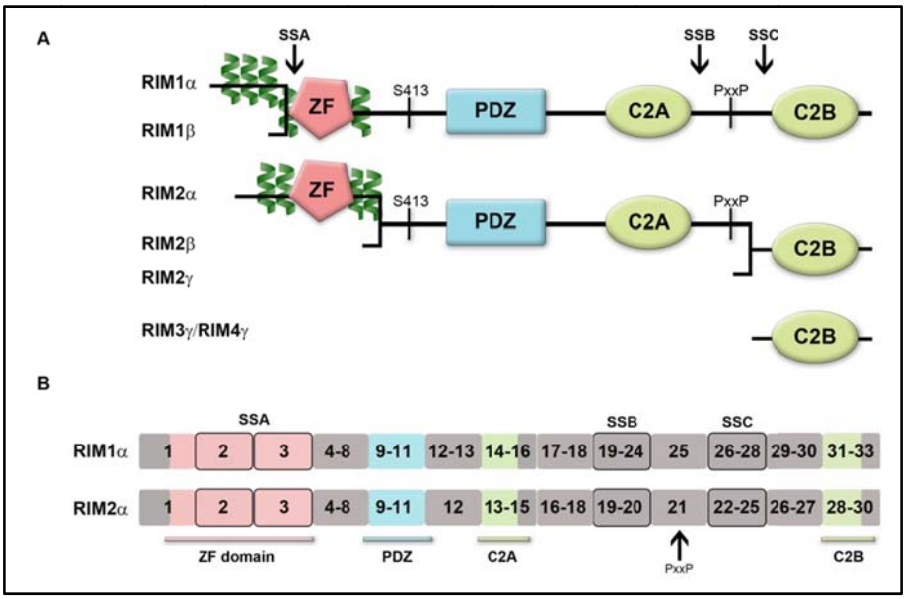

***Figure 1.6*: Schematic representation of the RIM protein family.** (**A**) Domain structure of different RIM family members. α-isoforms (RIM1 and RIM2) contain the full set of domains: ZF (zinc finger domain), PDZ (post synaptic density protein -PSD95, Drosophila disc large tumor suppressor- Dlg1, and zonula occludens-1 protein- zo-1), C2A and C2B domains. RIM1β lacks the Rab3 binding site, while RIM2β lacks the entire N-terminal domain containing the α-helixes and the ZF. All γ-isoforms are composed of only the C2B domain. (**B**) Scheme depicting the alternative splicing of the α-isoforms.

With the exception of the γ-transcripts all other transcripts are subject to intense alternative splicing (*Fig. 1.6B*). The α- isoforms have three conserved splicing sites: splice site A in the N-terminal Zn^{2+}-finger domain and splice site B and C between the C2A and C2B domains. Splice site A contains 2 exons, conserved in both RIM1 and RIM2 (exons 2 and 3) (WANG and SÜDHOF, 2003). In brain exons 2 and 3 can be spliced either as a block or separately (FUKUDA, 2003). Splice site B contains 6 exons (19-24) in RIM1, spliced not as a block, but independently, giving rise to 64 possible variants, and only 2 exons (19 and 20) in RIM2. Splice site C, spliced as a block to prevent the disruption of the reading frame in the protein sequence, has 3 exons in RIM1 (26-28) and 4 exons in RIM2 (22-25). The last exon (28 in RIM1 respectively 25 in RIM2) includes an alternative splice acceptor site responsible for either the deletion or the insertion of a small 9 residue sequence. The two splicing sites, B and C, are separated by only one exon, 25 in RIM1 and 21 in RIM2, which contains a proline rich-domain (WANG and SÜDHOF, 2003). In comparison to rat and mouse, splice site A and exon 3

are missing from the human transcript, while exon 22 is retina specific and exon 24 and 26 are brain specific. Another interesting feature is the alternative splice site involving exon 17 that may be responsible for the generation of two other splice variants in the retina (JOHNSON et al., 2003). In invertebrates (*C.elegans, D.melanogaster*) only one gene was identified to be responsible for the synthesis of the RIM protein (unc-10) (KOUSHIKA et al., 2001; GRAF et al., 2012; MÜLLER et al., 2012).

1.5.1.2 RIM protein structure and binding partners

RIM1α and RIM2α proteins contain the complete set of domains: an N-terminal Zn^{2+}-finger domain, a central PDZ domain, and two C- terminal C2 domains: C2A and C2B (WANG et al., 1997, 2000). RIM1β lacks the α1-helix in the N-terminal position, responsible for Rab3 binding (KAESER et al., 2008b), RIM2β lacks the entire N terminal Zn^{2+}- finger domain, while the γ-isoforms contain only the last C-terminal C2B domain and a short isoform specific sequence (*Fig.1. 6A*; WANG et al., 2000; WANG and SÜDHOF, 2003).

The *N-terminal domain,* containing two α-helices (α1 and α2) flanking the Zn^{2+}-finger domain, is important for the formation of the tripartite complex: Rab3/RIM/Munc13. The N-terminal α1 helix of RIM1α is sufficient to mediate binding to GTP- bound Rab3A/B/C/D and for other Rab molecules (Rab10, Rab26 and Rab37 bind RIM1α; Rab3A/B/C/D and Rab8A bind RIM2α) (*Fig.1.7*; SUN et al., 2001; WANG et al., 2001; FUKUDA, 2003), while the module composed of the zinc domain, α2 helix and SGAWFY motif displays a high affinity for Munc13-1 and ubMunc13-2 (BETZ et al., 2001; DULUBOVA et al., 2005; ANDREWS-ZWILLING et al., 2006). Munc13 exists in an inactive homodimerization state unable to perform its function in priming. The interaction of RIM1α with Munc13 activates vesicle priming by impairing Munc13 homodimerization (DENG et al., 2011).

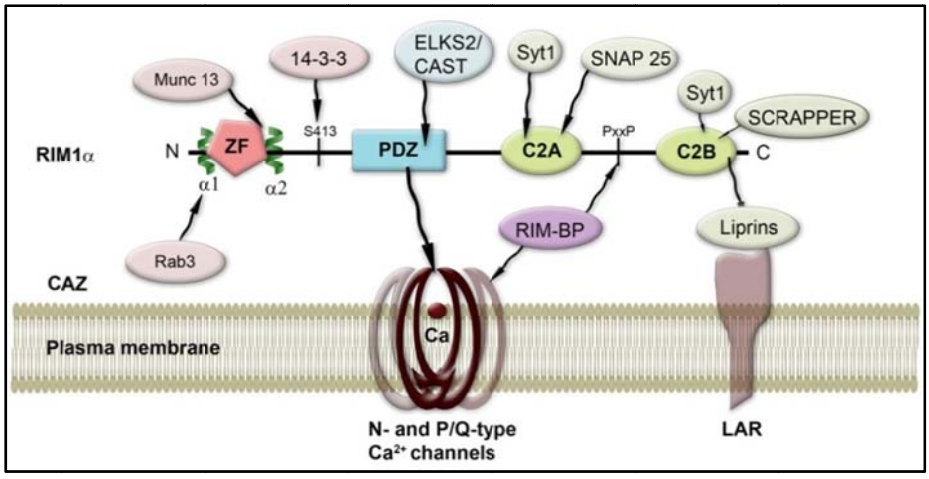

Figure 1.7: **Schematic representation of RIM1α binding partners.** Adapted after MITTELSTAEDt, 2010.

The *sequence between the zinc and PDZ domains* contains several amino acid residues that have been suggested to be important in modulating RIM's function (*Fig. 1.7*). Serine 413 was identified as a phospho-switch that triggers presynaptic LTP in cultured cerebellar granular and Purkinje cell neurons, upon phosphorylation by PKA (LONART et al., 2003). These findings however were not confirmed by studies in knockin mice, bearing the S413A mutation. The phosphorylation of serine 413, although important in binding 14-3-3 proteins, displayed no significant role in presynaptic plasticity or in learning and memory (KAESER et al., 2008a; YANG and CALAKOS, 2010). Other phosphoserines (Ser241 and Ser287 in RIM1α, and Ser335 in RIM2α) were also associated with binding to 14-3-3 proteins, when phosphorylated by the Ca^{2+}/calmodulin dependent kinase II (CaMKII). The ability of RIM to bind 14-3-3 proteins does apparently not impair the binding between RIM-Munc13 and RIM-Rab3A (SUN et al., 2003). The same linker region between zinc finger and PDZ domain may also act as a substrate for ERK2 kinase, which phosphorylates Ser447, a residue linked to the enhancement of glutamatergic transmission in hippocampal CA1 after stimulation with BDNF (SIMSEK-DURAN and LONART, 2008).

The *central PDZ domain* that interacts with the ELKS2/CAST protein (OHTSUKA et al., 2002; WANG et al., 2002), plays an important role in RIM1's distribution in cultured neurons; the truncated form lacking this domain being diffusely localized (*Fig. 1.7*; OHTSUKA et al., 2002). CAST binds directly not only RIM1, but also Bassoon and Piccolo, and the entire ternary complex RIM1-CAST-Bassoon is involved in controlling neurotransmitter release (TAKAO-RIKITSU et al., 2004). Two reports from 2011 attribute to RIM1/2 a key role in controlling not only the number of docked vesicles but also the distribution and/or density of calcium channels at the active zone (HAN et al., 2011; KAESER et al., 2011). By generating RIM1/2 floxed mouse lines, in which all RIM isoforms containing a PDZ domain can be deleted by cre-recombinase *in vitro*, it was shown that the PDZ domain alone was required for the proper localization of N- and P/Q type calcium channels (KAESER et al., 2011).

The α- and β-RIMs contain two *C-terminal domains: C2A and C2B* that are separated by a proline-rich domain and two splice sites (B and C) (*Fig. 1.7*; WANG and SÜDHOF, 2003). Both domains do not contain the consensus calcium binding sites present in synaptotagmin's C2-domains (WANG et al., 2000; DAI et al., 2005). The *C2A domain* was shown to have affinity in a calcium dependent manner for SNAP25 and Synaptotagmin1 (COPPOLA et al., 2001), even though NMR studies suggested that there was little binding between these proteins (DAI et al., 2005). Very intriguing is a point mutation in human RIM1 (R844H) that was identified in a patient with autosomal dominant cone-rod dystrophy-CORD7, characterized by impaired vision due

to the reduction in the cone and rod sensitivity (JOHNSON et al., 2003; MICHAELIDES et al., 2005). The *C2B domain* has been shown to interact with several proteins that may have an impact on RIM1α function at the active zone, among them Synaptotagmin1, identified to bind with high affinity to the C2B domain in biochemical assays (COPPOLA et al., 2001; SCHOCH et al., 2002), results not reproduced by NMR studies (GUAN et al., 2007). Other proteins that bind the C2B domain are: liprins-α (SCHOCH et al., 2002); the E3 ubiquitin ligase SCRAPPER (YAO et al., 2007) that controls RIM1 turn-over, facilitating ubiquitination and degradation; SAD kinase (INOUE et al., 2006); and the β4 subunit of voltage gated calcium channels (COPPOLA et al., 2001; KIYONAKA et al., 2007). In addition the interaction between RIM1 and the α1 subunit of the N-type calcium channel is regulated by cyclin-dependent kinase 5 (Cdk5), which enhances channel opening and facilitates neurotransmitters release (SU et al., 2012).

SUMOylation was recently reported by the group of Hanley to act as a molecular switch for RIM1α. SUMOylated RIM1α confers affinity for Cav2.1, therefore promoting calcium channel clustering and synchronous synaptic vesicle release, while non-SUMOylated form is responsible only for vesicle priming and docking (GIRACH et al., 2013).

Other proteins that couple RIM1/2 to calcium channels are RIM-BPs. On one hand RIM-BP binds the *proline-rich domain* of RIM1/2 (WANG et al., 2000) and on the other hand calcium channels, bringing these proteins in close proximity at the active zone (HIBINO et al., 2002).

1.5.1.3 RIM function

1.5.1.3.1 RIM in invertebrates (*C.elegans* and *D.melanogaster*)

Analysis of RIM protein function in *C.elegans* demonstrated that UNC-10 has a major role in coordinating vesicle docking and priming by regulating UNC-13 activity. It has been hypothesised that UNC-10/RIM may signal syntaxin, via UNC-13, to change its conformation from a closed to an open state. UNC-10 mutants exhibit a decrease in vesicle fusion at release sites, an effect suppressed by the expression of the open form of syntaxin (KOUSHIKA et al., 2001). Furthermore, disruption of the unc-10 gene triggers a depletion of docked synaptic vesicles since the normal connections between SVs and dense projection filaments are impaired (STIGLOHER et al., 2011).

D.melanogaster RIM mutants show decreased evoked synaptic transmission as a consequence of the reduction in the size of the RRP of SVs and altered Ca^{2+}-channels clustering together with a decreased calcium influx. Mutants present a normal cellular morphology with no major changes in active zone architecture (GRAF et al., 2012; MÜLLER et al., 2012).

1.5.1.3.2 RIM in vertebrates (*M.musculus*)

In the recent years several reports have been published, providing new data about the possible role of RIMs at the active zone. Different mouse models have been generated, knocking out either one or more isoforms, in order to gain new insights into how different variants of RIMs influence neurotransmitter release and presynaptic plasticity as well as to understand ability of the various isoforms to compensate for each other.

1.5.1.3.2.1 RIM1α knock-out mice

The first model generated targeted the most abundant isoform in the brain, RIM1α (SCHOCH et al., 2002). Homozygous mice were viable and fertile, with no evident structural abnormalities or changes in brain architecture. Overall, active zone architecture was comparable to WT littermates. Among the AZ proteins, Munc13-1 showed a major decrease of 60% in KOs, while several postsynaptic density proteins (SynGAP, PSD95, SHANK) exhibited a moderate increase, suggesting a role for RIM1α in synaptic remodelling (SCHOCH et al., 2002). Electrophysiological recordings revealed that RIM1α knockout caused a decrease in the size of the RRP, with no effect on synaptic vesicle recycling. These data together with findings from *D.melanogaster* and *C.elegans* suggest a role for RIM1α in vesicle maturation, from priming to calcium triggered fusion (KOUSHIKA et al., 2001; SCHOCH et al., 2002; CALAKOS et al., 2004; MÜLLER et al., 2012). Additionally, the RIM1α protein seems to be involved both in short-term plasticity as well as in presynaptic long-term potentiation (LTP) (review: MITTELSTAEDT et al., 2010).

Cryo-electron tomography revealed a series of changes in the AZ with regard to vesicle tethering and vesicle concentration in synaptosomes from RIM1α KO mice (40% reduction in proximal vesicles compared to control) that may account for the decrease in the size of the RRP. Blocking proteasome activity with MG132, the KO phenotype was rescued and the treated KO synaptosomes became indistinguishable from WT synaptosomes, displaying an increase in the number of vesicles at the AZ. This recent study highlights the importance of the ubiquitin-proteasome system (UPS) in the turn-over of RIM proteins, emerging as a key factor in controlling presynaptic plasticity (FERNANDEZ-BUSNADIEGO et al., 2013).

Besides deficits in synaptic transmission, KO mice display impaired learning and memory (POWELL et al., 2004), schizophrenia-like behaviour (BLUNDELL et al., 2010), and a higher susceptibility to develop spontaneous seizures after status epilepticus (PITSCH et al., 2012).

1.5.1.3.2.2 RIM1αβ double knock-out mice

Mutant mice lacking both RIM1 isoforms, α and β, display a more severe impairment in synaptic transmission and significant changes in the solubility of different active zone proteins. Both isoforms are expressed in a similar pattern in the brain, with a slight increase of RIM1β levels in the brainstem. During development RIM1β is highly expressed in the early postnatal phase in this region, which may account for the lethality of the DKO mice. Interestingly, in RIM1α KO mice the level of RIM1β is increased 2 fold, indicating a compensatory effect. Among the presynaptic proteins, ELKS1/2, RIM-BP2 and the remaining Munc13-1 (reduced to 30% in these mutant mice), showed a higher dissociation rate from the insoluble protein matrix, supporting the notion of RIMs acting as scaffolding proteins for various AZ proteins. Synaptic transmission is severely impaired in the DKO mice with the observation that presynaptic long-term plasticity is not aggravated by this double deletion compared to RIM1 KO. Therefore, it has been suggested that RIM1α mediates both long-term plasticity via Rab3 as well as short-term plasticity via Munc13, while RIM1β (since it lacks the binding motif for Rab3) is involved only in short-term plasticity (KAESER et al., 2008b).

1.5.1.3.2.3 RIM2α knock-out mice

Since RIM1α and RIM2α, which is much less abundant, display high homology, it was expected that the knockout of RIM2α might partially resemble the phenotype of the RIM1α KO. However, deletion of the RIM2α gene did not trigger any change in release probability compared to the impairment in synaptic transmission and facilitation observed in the RIM1α KO mice (CASTILLO et al., 2002; SCHOCH et al., 2002, 2006). RIM2α KO mice were viable and fertile, and displayed normal brain morphology (SCHOCH et al., 2006).

1.5.1.3.2.4 RIM1α/RIM2α double knock-out mice

Deletion of both α isoforms (RIM1 and RIM2) turned out to be lethal, RIM1α/2α DKO mice die immediately at birth, not due to changes in brain development but due to breathing problems. No obvious alterations in brain morphology were detected by conventional EM. Protein composition analysis revealed no additional decrease in the level of Munc13-1 compared to RIM1α KO mice. Nonetheless, immunostaining analysis of the whole-mount diaphragm muscle at E18.5 revealed an increased innervation or expansion of innervation with no major changes in the ultrastructure of the NMJ in the DKO mice. These changes were accompanied by impairment in synaptic transmission. Spontaneous or Ca^{2+}-dependent exocytosis was not abolished, only evoked synaptic transmission (Ca^{2+}- triggering exocytosis) was strongly impaired in these mutants (SCHOCH et al., 2006).

1.5.1.3.2.5 RIM conditional knockout mice

As both RIM1α/RIM1β (KAESER et al., 2008b) and RIM1α/RIM2α (SCHOCH et al., 2006) DKO mice were lethal, conditional knockouts (floxed mouse lines) were generated to further study the consequences of a deficiency of all RIMs isoforms. Deletion of both RIM genes *in vitro* supported the role of RIMs in controlling vesicle priming and neurotransmitter release (KAESER et al., 2012). Furthermore, RIMs were shown to be responsible for proper tethering of the Ca^{2+} channels via the PDZ domain (HAN et al., 2011; KAESER et al., 2011).

Single deletions (RIM1αβ or RIM2αβγ) altered SV priming, while double deletion (RIM1αβ/RIM2αβγ) impaired not only the priming but also the calcium responsiveness and synchronization of release. In HEK293T cells and in RIM1/2 double deficient neurons, RIM2γ wasn't able to rescue the phenotype, suggesting that the C2 domain alone neither contributes to calcium channel activity modulation nor plays an important role in the synaptic function of RIM proteins (KAESER et al., 2012).

Taken together, RIM1α plays an important role in synaptic vesicle priming, and in both presynaptic short-term and long-term plasticity. Moreover, the level of RIM1α seems to be correlated with the synaptic activity.

1.5.2 Synaptic vesicle protein 2A (SV2A)

1.5.2.1 SV2A function

Synaptic vesicle proteins (SV2s) are a class of transmembrane glycosylated proteins, integrated in the synaptic vesicles membrane (*Fig.1.8*), with three characterised isoforms (SV2A, SV2B and SV2C), expressed only in neurons and endocrine cells. SV2A is known to have a more ubiquitous expression throughout the brain, while SV2B has a more limited distribution. However, both isoforms, SV2A and B, can be found at varying ratios though in the same neurons and even on the same synaptic vesicles (BAJJALEH et al., 1992; 1993; 1994). SV2A, but not SV2B, was reported to interact directly through its N-terminal region with the C2B domain of synaptotagmin1 (SCHIVELL et al., 1996). This binding was reported to be facilitated by phosphorylation events of different serine/threonine residues, potentiating presumably the affinity of the N-terminal domain toward the calcium sensor synaptotagmin1 (PYLE et al., 2000), and inhibited by high concentration of calcium, which induce conformational changes in synaptotagmin1, determining its dissociation from SV2A (SCHIVELL et al., 1996).

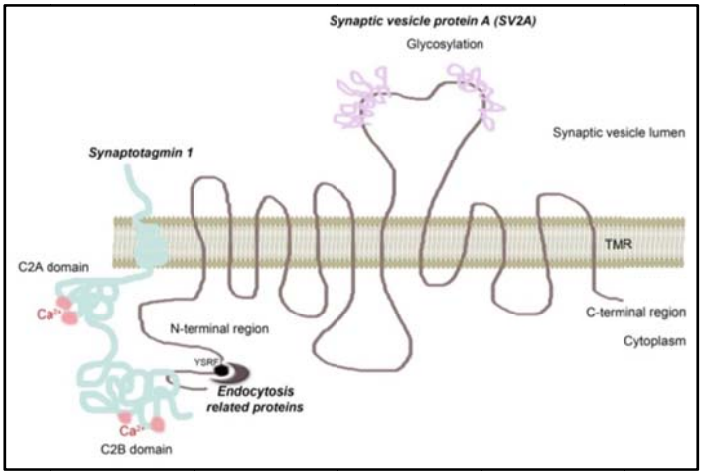

Figure 1.8: **Schematic representation of SV2A structure and its binding partners.** SV2A is a 12-pass transmembrane (TMR) glycoprotein (glycosylation depicted in pink). The N-terminal region was reported to bind to the C2B domain of Synaptotagmin 1(light blue) and different clathrin adaptor proteins (grey).

The endocytosis motif in the N-terminal region of SV2A (YSRF) was identified to be required for binding to different clathrin adaptor proteins, controlling thus the trafficking of Synaptotagmin1 and affecting in this manner its amount on the synaptic vesicles (YAO et al., 2010). Chang and Südhof (2009), whose results showed that the N-terminal region appears not to play, if any, a major role in SV2A function, contradicted this hypothesis however. Additionally, mutations of different amino acid residues in transmembrane region 1 (TMR1) and in the glycosylation site were reported to either impair SV2A subcellular localization or abolish completely SV2A function, by altering its normal processing and folding (CHANG and SÜDHOF, 2009; NOWACK et al., 2010).

Interestingly, SV2 proteins bind with high specificity adenine nucleotides (ATP and NAD), pointing to the fact that these proteins' activity may be modulated by different energy levels (YAO and BAJJALIEH, 2008).

1.5.2.2 SV2A knock-out mice

In spite of all the data collected until now the exact function of SV2A still remains enigmatic. To gain further insights into SV2A function, SV2A deficient mice were generated (CROWDER et al., 1999; JANZ et al., 1999). Albeit SV2A KO littermates appeared normal at birth, mice experienced severe seizures and died about three weeks after birth. No obvious alterations of synaptic density or morphology in the brain of SV2A KO mice were observed (CROWDER et al., 1999; JANZ et al., 1999). Therefore, SV2A seems not to be required in embryonic development but rather its presence is essential for survival afterwards. Electrophysiological studies further revealed that inhibitory (CROWDER et al., 1999; CHANG and SÜDHOF, 2009) as well as excitatory (CUSTER et al., 2006) neurotransmission in these mice were impaired. A similar impairment was also detected in adrenal chromaffin cells from SV2A KO mice, where the exocytotic burst defining the size of the readily releasable pool (RRP) was observed to be decreased with no evident alterations in the calcium level (XU and BAJJALIEH, 2001). A role in priming after vesicle tethering was suggested by Custer et al. (2006), who observed a similar decrease in RRP in the SV2A deficient mice's brain, with no oscillation in calcium level.

However, earlier studies using SV2A/SV2B double knockout mice with a phenotype resembling SV2A KO, proposed a role in regulating the calcium level during repetitive stimulation trains rather than priming (JANZ et al., 1999). The described decrease in the RRP size (CUSTER et al., 2006) was not reproduced by Chang (CHANG and SÜDHOF, 2009). A further observation that the protein components of SNARE complexe were reduced in SV2A KO mice supported the hypotheses that SV2A may have a role in the fusion mechanism (XU and BAJJALIEH, 2001).

Taken together, the collected data suggest a role of SV2A in SV priming. Moreover, SV2A act as a receptor for the anti-epileptic drug Keppra. It has been suggested that Keppra may inhibit inappropriate interactions to occur when SV2A is overexpressed in neuronal cell cultures. Neurons with elevated amount of overexpressed SV2A display similar impairments in synaptic transmission as neurons from SV2A KO mice (NOWACK et al., 2011). It seems that the protein amount plays an important role in maintaining the neuronal function as well. The molecular mechanism of action of Keppra on SV2A is not fully elucidated.

Aim of the study

One of the most important properties of the synapse is the capacity to remodel itself in response to ongoing activity in its environment. The synapse's ability to weaken or strengthen over time in response to different stimuli is called synaptic plasticity. One way of inducing changes in presynaptic plasticity is to modulate SV priming and the protein machinery involved in this process, like RIM1α and SV2A proteins. Over the years it has been proposed that regulated phosphorylation/dephosphorylation events may play a role in plasticity-induced remodelling of established and the assembly of novel active zones. To date the molecular mechanism governing these changes are not understood in detail.

In this thesis two goals will be pursued:

1. *Examine how phosphorylation events affect RIM1α binding affinities*

RIM1α, a scaffold multi-domain protein residing in the active zone (AZ), has been shown to be involved in synaptic vesicle priming and in different forms of presynaptic plasticity. Both synaptic abundance and function have been suggested to be regulated by posttranslational modifications. However, the precise mechanisms involved in controlling RIM1α protein levels and function in the presynaptic terminal are not yet resolved.

To understand the impact that RIM1α phosphorylation has on active zone reorganisation and presynaptic function, we aim at identifying novel phospho-dependent binding partners. Combining various stimulation protocols, in order to block or enhance kinases activity, different protein complexes binding to RIM1α will be identified by mass-spectrometry. Next, these newly identified binding partners will be verified by protein-protein interaction assays, and the functional role of these new proteins addressed in neuronal cell culture.

2. *Identify novel binding partners for SV2A*

The last part of this study will be focused on the synaptic vesicle protein 2A (SV2A) protein, whose involvement in vesicle priming or in controlling calcium levels is not yet elucidated. Although SV2A is targeted by the antiepileptic drugs Keppra that only acts in case of strong pathophysiological activity, its mode of action is still unresolved.

Therefore, to gain insight into the SV2A function identification of novel binding partners will be addressed. Different affinity methods in combination with rAAV injections in mice will be applied in order to find the best approach possible to purify the entire complex of proteins under native conditions, followed by mass-spectrometry.

The results of this study will provide new insight into the molecular mechanisms by which the functional properties of the presynaptic release machinery might be modulated.

2. Materials

2.1 Equipment

	Application	Model	Company
A	Acrylamid electrophoresis system	Mini-PROTEAN Tetra Cell/ Power Pac Basic Power Supply	BioRad
	Agarose electrophoresis system	SUB-CELL GT	BioRad
	Analytical balance	JP	Mettler Toledo
	Autoclave	Laboklav	Steriltechnik AK
B	Balance	SBC53	Scaltec
C	Capillary Sequencer	3130/xl/Genetic Analyzer	Applied Biosystems
	Cell-culture hood	MSC-Advantage	Thermo Scientific
	Cell-culture hood	HERA Safe KS	Thermo Scientific
	Centrifuge	Rotina 420R	Hettich
	Centrifuge	Mikro 200R	Hettich
	Centrifuge	-	Abimed
	Chamber for MS	X Cell SureLock Mini-Cell	Life Technologies
	Confocal laser scanning microscope	A1/Ti	Nikkon
	Confocal microscope	FV1000	Olympus
	Controller	Micro4 Controller, 4- Channel	World Precision Instruments
G	Gel documentation system	AlphaImager	Alpha Innotech
I	Incubator	HERA Cell 150i	Thermo Scientific
	Incubator	-	Binder
	Incubator	Incubator 1000	Heidolph
	Incubator	Incubator Mini Shaking	VWR
	Infrared imaging system	Odyssey	Li-cor
	Inverse microscope	Axio Observer 1A	Zeiss
	Inverse microscope	Axiovert 40 CFL	Zeiss
M	Magnetic Separator	-	Sigma
	Mass-spectrometer (IBMB, Bonn)	LTQ OrbitrapVelos/ Thermo DionexUlti Mate 3000 RSLCnano HPLC	Thermo Scientific
	MilliQ -Ultra pure water	Advantage A10	Millipore
	Microsyringe pump controller	Micro4	World Precision Instruments
P	PCR Machine	MY Cycler	BioRad
	Peristaltic pump	P-1	GE Healthcare
	pH-Meter	InLab@ExpertDIN	Mettler Toledo
	Potter	Potter S	B. Braun
	Power Supply	PHERO-stab.500	Biotec-Fischer
	Power Supply	Power Pack 25	Biometra
R	Rocking Platform	Polymax 1040	Heidolph
	Rotator	SB 3	Stuart
S	Shaker	TH 15	Edmund Bühler
	Shaker	TH 30	Edmund Bühler
	Sonicator	Labsonic 2000	B. Braun
	Spectrophotometer	BIO	Eppendorf
	Spectrophotometer	ND 1000	NanoDrop
	Syringe	Nanofil	World Precision Instruments
T	Thermo shaker	Compact	Eppendorf
	Thermo shaker	MB-102	Bioer
	Transfer System	Mighty Small Transphor/ Hoefer TE22	Amersham
U	Ultracentrifuge	WX ULTRA Series	Thermo Scientific
	Ultracentrifuge	Optima L series, S class	Beckman Coulter
	Ultrasonicator	UP50H	Hilscher
V	Vacuum concentrator	Concentrator plus	Eppendorf
	Vortex	Vortex-Genie 2	Scientific Industries

2.2 Chemicals

Chemicals	Company
A	
Acetic acid	Roth
Acetonitril LC-MS Grade	Roth
Agarose	Sigma
Ammonium hydrogencarbonate	Roth
Ammonium peroxodisulphate	Roth
Ampicillin	Roth
Ampuwa	Fresenius
Antioxidant Agent	Life Technologies
Arginine-HCl	Sigma
B	
ß-Marcaptoethanol	Roth
Bensonase	Sigma
BES (N,N, Bis-(2-hydroxyethyl)-2-amino-ethansulfonic acid)	Roth
Bovine serum albumin (BSA)	Roth
C	
Calcium chloride ($CaCl_2$)	Sigma
Chlorhidric acid (HCl)	Roth
Chloroform	Roth
Citric acid	Sigma
ComplexiolLyte114 (CL114)	LogoPharm
CL114 Dilution Buffer	LogoPharm
Cold Water Fish Gelatine	Sigma
D	
Dimethyl 3,3'-dithiobispropionimidate-2HCl (DTBP)	Pierce
Dimethylsulfoxide (DMSO)	Roth
Disodiumhydrogenphosphat	Merk
Dithiobis (succinimidylpropionate) (DSP)	Pierce
Ditiothreitol (DTT)	Roth
DNA 6 x loading buffer	Thermo Scientific
E	
Ethanol	Roth
Ethidium bromide	Merck
EDTA	Sigma
G	
Glucose	Roth
Glycerol	Sigma
Glycine	Roth
H	
HEPES	Roth
I	
Iodixanol (OptiPrep)	Axis-Shield
Iodoacetamide (IAA)	Sigma
Isofluran	Abbott
Isopropanol	Roth
IPTG	Roth

Chemicals	Company
L	
LB-Agar	Roth
LB-Medium	Roth
Laemmli Buffer	Life Technologies
Lysozym	Roth
M	
Magnesium chloride ($MgCl_2$)	Roth
Magnesium sulphate ($MgSO_4$)	Roth
Methanol	Roth
Mowiol 4-88	Roth
N	
n-dodecyl-β-maltoside (DDM)	Roth
Normal goat serum (NGS)	Gibco BRL
NuPAGE MOPS SDS Running Buffer	Life Technologies
P	
Paraformaldehyd (PFA)	Merk
Phenol red	Sigma
Phosphate Buffer Saline (PBS)	Biochrom AG
Potasium chloride (KCl)	Roth
Potasium dihydrogenphosphate	Roth
R	
Reduction Agent	Life Technologies
Roti-Blue	Roth
Roti-Phenol/C/I	Roth
Rotiphorese Gel 30	Roth
S	
Saccharose	Roth
Sodium acetate	Roth
Sodium carbonate	Roth
Sodium chloride (NaCl)	Roth
Sodium dodecylsulfat (SDS)	Roth
Sodium dihydrogenphosphat	Roth
Sodium hydroxide (NaOH)	Roth
T	
TEMED	Roth
Tris-Base	Roth
Tris-chlorhidric acid	Roth
Triton-X-100	Sigma
Trypan-Blue	Life Technologies
V	
Vectashield mounting medium	Vectorlabs
X	
Xylene	Roth

2.3 Cell culture media

» B27 supplement (*17504*)	Gibco BRL	Eagle (MEM) (*M2279*)	
» Basal Medium Eagle (BME) (*41010*)	Gibco BRL	» Neurobasal medium (*21103*)	Gibco BRL
		» Opti-MEM (*31985*)	Gibco BRL
» DNaseI (*11284932001*)	Roche	» Penicillin-Streptomycin (*15140*)	Gibco BRL
» Dulbecco's Modified Eagle Medium (DMEM)(*41966*)	Gibco BRL		
		» Phosphate Buffer Saline (PBS) (*14190*)	Gibco BRL
» Fetal calf serum (FCS)(*16170*)	Life Technologies		
» Hanks' Balanced Salt Solution (HBSS) (*14170*)	Gibco BRL	» Poly-D-Lysine (*P1149*)	Sigma
		» Poly-L-Lysine (*P1399*)	Sigma
» Iscove's Modified Dulbecco's Medium (IMDM) (*21980*)	Gibco BRL	» Trypsin	Sigma
		» Trypsin EDTA (*25300*)	Gibco BRL
» L-Glutamine (*25030*)	Gibco BRL		
» Minimal Essential Medium	Sigma		

2.4 Kits

» BigDye Terminator v3.1cycle Sequencing kit	Applied Biosystems	» Trypsin Profile IGD Kit (*PP0100*)	Sigma
» DNA Clean and Concentration kit	Zymo Research	» QuickChangeII XL Site Directed Mutagenesis kit	Stratagene
» Dynabeads mRNA direct	Life Technologies	» Pure link Midi kit	Life
» EndoFree Plasmid Maxi kit	Qiagen	(DNA purification)	Technologies
» First-strand cDNA Synthesis kit (*K1632*)	Thermo Scientific	» Zymoclean Gel DNA recovery kit	Zymo Research
» GeneJET Plasmid Miniprep kit	Thermo Scientific		
» Lipofectamine 2000	Life Technologies		

2.5 Enzymes

» *pfu*DNA polymerase » Restriction enzymes: *AvrII, BamHI*, *BglII*, *ClaI*, *EcoRI*, *HindIII*, *NotI*, *SalI*, *XbaI*, *XhoI*	Thermo Scientific	» Shrimp alkaline phosphatase » T4 DNA Ligase » T4 Polynucleotide Kinase	Thermo Scientific

2.6 Inhibitors

» Calyculin A (*208851*)	Calbiochem	» phosSTOP	Roche
» Complete Mini EDTA free proteinase inhibitors	Roche	» SRPIN340	Axon Medchem
		» Staurosporine (*S5921*)	Sigma
» Okadaic acid (*495604*)	Calbiochem		

2.7 Diverse materials

» Amicon Ultra Centrifigal filters (3000 MWCO/100000 MWCO)	Millipore	» Strep-tactin MacroPrep	IBA
		» Thinwall Polyallomer Centrifuge Tubes (*03141*)/ Sealing Cap Assemblies (*52572*)	Sorvall
» FLAG-magnetic beads	Sigma		
» GFP- magnetic beads	Biozol		
» Glutathion-agarose beads	Sigma	» Whatman Protran Nitrocellulose Membrane 0.45uM	Whatman, GE Healthcare
» HA- magnetic beads	Pierce		
» LoBind Eppendorf tubes	Eppendorf	» Vectashield mounting medium with DAPI	Vectorlabs
» NuPAGE 4-12% Bis-Tris Gel	Life Technologies		

2.8 Cloning primers

Vector	Primer Name		Sequence (5'-3')	Restriction Enzymes
AAV-MCS	N-TAP	Fw	gcg*gaattc*accatggattataaagatgatgatg	EcoRI
		Rev	gcg*ggatcc*tggtcctggtttctcgaactgcgggtg	BamHI
	C-TAP	Fw	gcg*ggatcc*ccggaccctggagccaccctcag	BamHI
		Rev	gcg*gtcgac*tcatttatcatcatcatctttataatc	SalI
	GFP (N)	Fw	gcg*gaattc*accatggtgagcaagggcg	EcoRI
		Rev	gcg*ggatcc*gggtccgggcttgtacagctcgtcc	BamHI
	Copine VI	Fw	gcg*gaattc*accatgtcggacccagagatg	EcoRI
		Rev	gcg*ggatcc*tgggctagggctgggag	BamHI
	SRPK2	Fw	gcg*atcgat*accatgtcagttaactctgagaagtc	ClaI
		Rev	gcg*tctaga*agaattcaaccaaggatgtcg	XbaI
		Fw	gcg*tctaga*cccgggccaatgtcagttaactctgagaagtcg	XbaI
		Rev	gcg*gtcgac*tcaagaattcaaccaaggatgccg	SalI
	SV2A	Fw	gcg*ggatcc*atggaagaaggctttcgag	BamHI
		Rev	gcg*aagctt*tcactgcagcacctgtcc	HindIII
		Fw	gcg*gaattc*accatggaagaaggctttcgag	EcoRI
		Rev	gcg*ggatcc*ctgcagcacctgtcc	BamHI
	ULK1	Fw	gcg*tctaga*atggagccgggccgc	XbaI
		Rev	gcg*aagctt*tcaggcatagacaccactc	HindIII
	ULK2	Fw	gcg*tctaga*atggaggtggtgggcg	XbaI
		Rev	gcg*gtcgac*tcacacagttgcagtgctac	SalI
	VAPA	Fw	gcg*tctaga*accatggcgtccgcctccg	XbaI
		Rev	gcg*aagctt*tcacaagatgaatttccctagaaag	HindIII
	VAPB	Fw	gcg*tctaga*atggcgaaggtggaacagg	XbaI
		Rev	gcg*agatct*tcacaaggcaatcttccctataatgac	BglII
CMV-MCS	C-TAP	Fw	gcg*gtcgac*cccggaccctggagccaccctcagttc	SalI
		Fw	gcg*cctagg*cccggaccctggagccaccctcagttc	AvrII
		Rev	gcg*aagctt*tcatttatcatcatcatctttataatc	HindIII
	C2A RIM1α	Fw	gcg*gaattc*accatgaggccttctatttctgttatttctc	EcoRI
		Rev	gcg*ggatcc*cgggcttcgggaggcatc	BamHI
	C2A-C2B RIM1α	Fw	gcg*gaattc*accatgaggccttctatttctgttatttc	EcoRI
		Rev	gcg*gtcgac*tgaccggatgcagggagg	SalI
	Zn-PDZ RIM1α	Fw	gcg*gaattc*tatgtcctcggccgtggg	EcoRI
		Rev	gcg*cctagg*gatcctggggatgtcacc	AvrII
	KD-ULK1	Fw	gcg*tctaga*atggagccgggccgc	XbaI
		Rev	gcg*aagctt*tcagaaagggtggtggaaaaattc	HindIII
	SPD-ULK1	Fw	gcg*tctaga**ttgga*tgccagcaccccc	XbaI
		Rev	gcg*aagctt*tcaagcctcgaaggtcacagc	HindIII
	CTD-ULK1	Fw	gcg*tctaga*cctgacctcccagaggag	XbaI
		Rev	gcg*aagctt*tcaggcatagacaccactc	HindIII
	KD-ULK2	Fw	gcg*tctaga*atggaggtggtgggcg	XbaI
		Rev	gcg*gtcgac*tcaaaggaaaggatggctgaaaaatg	SalI
	SPD-ULK2	Fw	gcg*tctaga*gagcaagttccagttaaaaaatc	XbaI
		Rev	gcg*gtcgac*tcaggcttcaaaggtgatgagac	SalI
	CTD-ULK2	Fw	gcg*tctaga*cctgaactaccagaggagac	XbaI
		Rev	gcg*gtcgac*tcacacagttgcagtgctac	SalI
pGEX	C2A RIM1α	Fw	gcg*gaattc*cgaggccttctatttctgttatttc	EcoRI
		Rev	gcg*ctcgag*tcatggctgaggcagaggtagt	XhoI
	SRPK2	Fw	gcg*cctagg*cccgggccaaccatgtcagttaactctgagaagtcg	AvrII
		Rev	gc*gtcgac*ctatctagaagaattcaaccaaggatgtcg	SalI
	MSP-VAPA	Fw	gcg*gaattc*cggcgaagcacgagcagatc	EcoRI
		Rev	gcg*aagctt*tcaaacagctttgctaggttccat	HindIII
	CC-VAPA	Fw	gcg*gaattc*cggatatggaacctagcaaagctg	EcoRI
		Rev	gcg*aagctt*tcaatctctgaaggacacggctg	HindIII
	MSP-CC VAPA	Fw	gcg*gaattc*cggcgaagcacgagcagatc	EcoRI
		Rev	gcg*aagctt*tcaatctctgaaggacacggctg	HindIII

2.9 Sequencing primers

Vector	Primer Name	Sequence (5'-3')
pGEX	Fw	gggctggcaagccacgtttggtg
	Rev	ccgggagctgcatgtgtcagagg
CMV	Fw	gagtccaaggtaggcccttt
pAMU6	Fw	tacgatacaaggctgttagagag

2.10 Site-directed mutagenesis

Target gene		Sequence (5'-3')	Amino acid Exchange
C2A (RIM1α)	Fw	gtctactcacacgtacatcatagagattttcgagagcgaatgttag	*R844H*
	Rev	ctaacattcgctctcgaaaatctctatgatgtacgtgtgagtagac	
ULK1	Fw	ggaggtggccgtcagatgcattaacaagaag	*K46R*
	Rev	cttcttgttaatgcatctgacggccacctcc	
ULK2	Fw	gggaggtggctattacaagtattaataaaaag	*K39T*
	Rev	ctttttattaatacttgtaatagccacctccc	

2.11 Oligonucleotides used for HA-tag cloning

Vector	Primer Name		Sequence (5'-3')	Restriction Enzymes
AAV-MCS	HA (N)	Fw	*aattc*accatgtacccatacgatgttccagattacgcta	EcoRI
		Rev	*gatct*agcgtaatctggaacatcgtatgggtacatggtg	BglII

2.12 Oligonucleotides used for shRNA cloning

Vector	Primer Name		Sequence (5'-3')	Position	Restriction Enzymes
pAMU6	ULK2 ≠1 (Xiang et al., 2007)	Fw	*gatct***cg***tgcctagtattcccagaga***ttcaagaga***tctctggg aatactaggca***tttttt***a*	699-717 (KD)	BglII
		Rev	*agctt***aaaaaa***tgcctagtattcccagaga***tctcttgaa***tctct gggaatactaggca***cg***a*		HindIII
	ULK2 ≠2	Fw	*gatct***cg***ggatagaatggactttgaagc***ttcaagaga***gcttc aaagtccattctatcc***tttttt***a*	772-792 (KD)	BglII
		Rev	*agctt***aaaaaa***ggatagaatggactttgaagc***tctcttgaa***g cttcaaagtccattctatcc***cg***a*		HindIII
	ULK2 ≠3	Fw	*gatct***cg***gctcaccatcttgtcgctttg***ttcaagaga***caaagc gacaagatggtgagc***tttttt***a*	894-914 (SPD)	BglII
		Rev	*agctt***aaaaaa***gctcaccatcttgtcgctttg***tctcttgaa***caa agcgacaagatggtgagc***cg***a*		HindIII
	ULK2 ≠4	Fw	*gatct***tc***cgcatagaacagaatcttata***ctcgag***tataagattc tgttctatgcg***ttttttggaa***a*	1235-1255 (SPD)	BglII
		Rev	*agctt***ttccaaaaa***cgcatagaacagaatcttata***ctcgag***ta taagattctgttctatgcg***ga***a*		HindIII

2.13 Generated constructs

Plasmids generated and used in this study.

Vector backbone	Insert	Plasmid name
AAV-FLAG/Strep (N-terminal/ C-terminal)	ULK1/KD-ULK1	AAV-CMV-FLAG/Strep-ULK1 AAV-CMV-FLAG/Strep-KD-ULK1
	ULK2/ KD-ULK2	AAV-CMV-FLAG/Strep-ULK2 AAV-CMV-FLAG/Strep-KD-ULK2
	SV2A	AAV-CMV/Synapsin-FLAG/Strep-SV2A
	SV2A	AAV-CMV/Synapsin-SV2A-FLAG/Strep
	- (Negative control)	AAV- CMV/Synapsin-FLAG/Strep
AAV-HA (N-terminal/ C-terminal)	Copine VI	AAV-CMV-Copine VI-HA
	SRPK2 (WT, DM, ΔSI, ΔNSI)	AAV-CMV-HA-SRPK2
	VAPA	AAV-CMV-HA-VAPA
	VAPB	AAV-CMV-HA-VAPB
AAV-GFP (N-terminal/ C-terminal)	GFP-ULK2	AAV-CMV-GFP-ULK2
	SRPK2-GFP	AAV-CMV-SRPK2-GFP
	SV2A- GFP	AAV-CMV/Synapsin-SV2A-GFP
CMV- FLAG/Strep (N-terminal/ C-terminal)	Kinase dead-domain (ULK1)	CMV-FLAG/Strep-KD-D-ULK1
	Kinase dead-domain (ULK2)	CMV-FLAG/Strep-KD-D-ULK2
	Kinase domain (ULK1)	CMV-FLAG/Strep-KD-ULK1
	Kinase domain (ULK2)	CMV-FLAG/Strep-KD-ULK2
	Serine proline rich domain (ULK1)	CMV-FLAG/Strep-SPRD-ULK1
	Serine proline rich domain (ULK2)	CMV- FLAG/Strep-SPRD-ULK2
	C-terminal domain (ULK1)	CMV-FLAG/Strep-CTD-ULK1
	C-terminal domain(ULK2)	CMV-FLAG/Strep-CTD-ULK2
	ZF-PDZ (RIM1α)	CMV-ZF-PDZ-FLAG/Strep
	C2A (RIM1α)	CMV-C2A- FLAG/Strep
	C2A-C2B (RIM1α)	CMV-C2A-C2B-FLAG/Strep
pGEX	C2A domain (RIM1α) (WT, R844H, T812/814A)	pGEX-C2A
	C2B domain (RIM1α)	pGEX-C2B
	SRPK2	pGEX-SRPK2
	Major sperm protein domain (VAPA)	pGEX-MSP-VAPA
	Coil coiled domain (VAPA)	pGEX-CC-VAPA
	Major sperm protein domain- Coil coiled domain (VAPA)	pGEX-MSP-CC-VAPA
pAMU6	shRNA (ULK2)	

2.14 Plasmids obtained from other sources and used in this thesis

Source	Plasmid name
Gyorgy Lonart (EVMS, Norfolk, USA)	CMV-RIM1α
Ngo Jacky (Hong Kong, China)	SRPK2 (human): WT, DM, ΔSI, ΔNSI
Open Biosystems – Thermo Scientific	ULK1 (Image clones-ID:6406755)
	ULK2 (Image clones-ID:5709559)
	VAPA (Image clones-ID:3490082)
	SRPK2 (Image clone-ID: 4507346)
	Copine VI (Image clones-ID:6591063)

2.15 Primary and secondary antibodies

Primary Antibodies

Antibody	*Assay*	*Dilution*	*Company*
α-Tubulin DM1A *(ab7291)*	IB	1:1000	Abcam
Bassoon *(clone SAP7F407)*	IF	1:200	Enzo Life Science
Copine VI	IF	1:100	Ege Kavalali
FLAG M2 *(F1804)*	IB/IF	1:1000/1:200	Sigma
GFP *(ab290)*	IB/IHC	1:5000/1:500	Abcam
HA.11 *(Clone 16B12)*	IB/IF	1:1000/1:100	Convance
PSD95 *(K28/43)*	IF	1:200	NeuroMab
RIM1/2	IB/IF	1:1000/1:200	BD Bioscience
RIM1/2 *(115.IT)*	IB/IF	1:1000/1:600	Frank Schmidt
SRPK2 *(bs-7923R)*	IF	1:100	Bioss
SRPK2 (*23*)	IB/IF	1:1000/1:100	Santa Cruz
SV2A *(119002)*	IB/IF	1:1000/1:200	Synaptic Sytems
Synapsin 1/2*(106004)*	IF	1:200	Synaptic Sytems
Synaptotagmin 1 *(105011)*	IB	1:1000	Synaptic Sytems
ULK1 *(ab65056)*	IF	1:100	Abcam
ULK1 *(OAAB05707)*	IF	1:100	Aviva
ULK1 *(bs-3602R)*	IF	1:100	Bioss
ULK1 *(D8H5)*	IF	1:100	Cell Signalling
ULK2 *(ab97695)*	IF	1:100	Abcam
ULK2*(PA5-22173)*	IF	1:100	Pierce
VAPA *(H-20)*	IB/IF	1:1000/1:100	Santa Cruz
VAPB *(H-20)*	IF	1:100	Santa Cruz

Secondary Antibodies

Antibody	*Assay*	*Dilution*	*Company*
Alexa Fluor 488 goat anti-mouse	IF	1:200	Life Technologies
Alexa Fluor 568 goat anti-rabbit	IF	1:200	Life Technologies
Alexa Fluor 488 goat anti-rabbit	IF	1:200	Life Technologies
Goat anti-guinea pig Cy5	IF	1:400	Jackson immunoreagents Europe Ltd
Goat anti-mouse Cy5	IF	1:400	Jackson immunoreagents Europe Ltd
Goat anti-mouse FITC	IF	1:400	Jackson immunoreagents Europe Ltd
Goat anti-rabbit Cy3	IF	1:400	Jackson immunoreagents Europe Ltd
Goat anti-rabbit FITC	IF	1:400	Jackson immunoreagents Europe Ltd
IRDye goat anti-mouse 800nm	IB	1:10000	Li-cor
IRDye goat anti-rabbit 680nm	IB	1:10000	Li-cor

3. Methods

3.1 Molecular Biology

3.1.1 RNA extraction and cDNA synthesis

mRNA was extracted from total or from different regions (cortex, hippocampus) of mouse or rat brain using Dynabeads mRNA direct kit (Life Technologies), according to the manufacturer's instructions. 1µg of mRNA was necessary for cDNA synthesis, using oligodT (First-strand cDNA Synthesis, Thermo Scientific). The resulting cDNA was used in further PCR reactions.

3.1.2 Polymerase chain reaction (PCR)

The following standard PCR protocol (*Table 3.1*) and program (*Table 3.2*) were applied to amplify different fragments, which were further used in cloning techniques. The only differences resided in the annealing and the strand elongation steps that were adjusted according to the product length and primers Tm. PCR primers are listed in section *2.8*.

Table 3.1A: **PCR protocol**

Final concentration
1x Buffer with $MgSO_4$
200µM dNTP
0.3µM Primer Fw
0.3µM Primer Rev
2.5 U *pfu* DNA polymerase (Thermo Scientific)
50-500ng DNA
dH_2O to a final volume of 50µl

Table 3.2: **PCR program**

Step	*Temperature*	*Time*	*Cycle*
1- Denaturation	95°C	5 min	1x
2- Denaturation	95°C	30 sec	35x
3- Annealing	55°C	40 sec	
4- Elongation	72°C	2min/1kb	
5- Final elongation	72°C	10 min	1x
	4°C	∞	1x

3.1.3 Site directed mutagenesis

Single point mutations were introduced using QuickChangeII XL Site Directed Mutagenesis kit (Stratagene). The applied PCR protocol and program were according to the manufacturer's instructions. Primers for site direct mutagenesis are listed in section *2.10*.

3.1.4 Sequencing

The sequencing of DNA plasmids was performed using BigDye Terminator v3.1cycle sequencing kit (Applied Biosystems) and specific sequencing primers (section *2.9*), followed by product purification (DNA Clean and Concentration kit, Zymo Research) and analysis (capillary sequencer, Applied Biosystems 3130/xl/Genetic Analyser). The sequencing results were analysed with BioEdit Sequence Alignment Editor v.7 and with BLAST from NCBI.

3.1.5 Cloning technique

The PCR products, purified from agarose gels (Zymoclean Gel DNA recovery kit, Zymo Research), and the vectors were digested with specific restriction enzymes (section *2.8*). Subsequent to digestion, both the insert and the dephosphorylated vector backbone were cleaned with DNA Clean and Concentration kit and ligated using the T4 DNA Ligase at 16°C/ON or 22°C for 2-3h. For a complete list of generated constructs see section *2.13*. The ligation reaction was used to transform chemically competent bacteria; 5-6 colonies from the agar plates were picked and incubated in 5ml LB-medium with appropriate antibiotic. 24h later DNA was extracted with the GeneJET Plasmid Miniprep kit and the presence of the insert was analysed with restriction enzymes followed by sequencing.

3.1.5.1 Oligonucleotides cloning

Oligonucleotides (sections *2.11* and *2.12*) were annealed and phosphorylated at the 5'-end using the T4 polynucleotide kinase. Next, the DNA oligonucleotides were extracted using phenol-chloroform (Molecular Cloning, Sambrook) and precipitated in the presence of sodium acetate (3M) and ethanol (99.9%) at -80°C/ON. After precipitation, DNA was pelleted at 14.000rpm/1h/4°C and the pellet washed one time in 70% ethanol and eluted in 10µl water. For ligation 1µl of annealed oligonucleotides was used in the presence of dephosphorylated vector backbone and T4 DNA Ligase. The ligation reaction was performed at 16°C/ON. The presence of the insert was verified in the same manner as previously described in cloning technique section *3.1.5*.

3.2 Cell Culture

3.2.1 HEK (AAV) 293T cell culture

Human embryonic kidney-293 cells (HEK293T or AAV293) were maintained in DMEM medium supplemented with penicillin/streptomycin (100units/ml penicillin and 100mg/ml streptomycin) and 10% FCS (fetal calf serum) in a humidified incubator at 37°C and supplied with 5% CO_2. Splitting was performed every 3 days.

3.2.2 HEK (AAV) 293T transfection methods

3.2.2.1 Ca^{2+}-phosphate method

For transfection, cells were seeded at a density of 1.5 x 10^6 cells/10cm dish and allowed to reach 50-60% confluence. 4h prior to transfection, DMEM medium was exchanged with IMDM medium, supplemented with 5% FCS. 2xHEBS (50mM HEPES, 280mM NaCl, 1.5mM Na_2HPO_4, pH 7.05) buffer was added to the transfection mixture containing water, $CaCl_2$ and DNA (*Table 3.3*), under vortexing in a drop-wise fashion, and further incubated for 2 minutes, to allow complex formation.

Table 3.3: **Transfection protocol**

Components	*Amounts*
dH_2O	1.1 ml
$CaCl_2$ (2.5 M)	145 µl
DNA plasmid	4-5 µg
2x HEBS (pH 7.05)	1.6 ml

The newly formed precipitate was quickly added drop-wise in a circular motion to the cells. After 24h the medium was replaced with fresh DMEM supplemented with 10% FCS and Pen/Strep and further incubated at 37°C and 5% CO_2. 48h post-transfection the cells were ready for harvesting.

3.2.2.2 Lipofectamine method

For shRNA transfection, the cells were seeded in a 12 well plate at a density of 1.5 x 10^4 cells/well. shRNA encoding plasmids and the DNA plasmids were co-transfected in a ratio of (µgr) 1:1, 1:3 and 1:6 using Lipofectamine2000 (Life Technologies) according to the manufacturer's instructions. 72h post-transfection, the cells were harvested and prepared for SDS-PAGE.

3.2.3 Neuronal primary cell culture

3.2.3.1 Generation of primary cell culture

The hippocampal and cortical neurons were prepared from rat and mouse embryos (E18/E19). Different brain regions (hippocampus or cortex) were trypsinized in HBSS, using trypsin to a final concentration of 0.25% for 20min/37°C. After trypsinization, the tissue was washed 3-5 times with HBSS and dissociated in 200µl DNaseI, passing the suspension 3-4 times through small size needles. Cells were counted (*Table 3.4*) and platted on poly-D-lysine pretreated glass coverslips (24-well plate) or on 6-wells plate in BME medium supplemented with: 1% FCS, 1% glucose (45%), 2% B27 and 0.5mM L-glutamine. After 24h the medium was

replaced with fresh DMEM medium and the neuronal cell culture incubated at 37°C/5% CO_2 for 2-3 weeks until ready to be used in experiments.

Table 3.4: **Counted cells per well**

Plate type	*Number of cells/ well*
6-well plate	120 000 cells
24-well plate	30 000-32 000 cells

3.2.3.2 Transfection of neurons

Primary cortical and hippocampal neurons were transfected at DIV4-6 according to the protocol of Köhrmann et al. (1999). Neurons transfection was performed in pre-warmed MEM medium, while the original medium was set aside in the incubator. 1.5µg of endofree DNA, 30µl $CaCl_2$ (250mM) and 30µl BES (280mM NaCl, 1.5mM Na_2HPO_4, 50mM BES, pH 7.11 to 7.14) were vortexted for 20sec. and quickly added to the neurons. The neurons were incubated for 30-40min at 2.5% CO_2. When the precipitates became visible under the microscope, neurons were washed twice with pre-warmed HBS (135mM NaCl, 4mM KCl, 1mM Na_2HPO_4, 2mM $CaCl_2$, 1mM $MgCl_2$, 10mM glucose, 20mM HEPES, pH7.35), one time with BME and after that the original medium was added. Transfected neurons were kept at 37°C and 5% CO_2 until DIV14, when they were prepared for immunocytochemistry.

3.2.3.3 Infection of neurons

Primary cortical neurons (24-well plate) were infected at DIV2-6 with 1-10µl crude viral particle extracts (rAAV serotype 1/2) per well. The infected neurons were further maintained at 37°C and 5% CO_2 until DIV14 or 21, when ready for immunocytochemistry.

3.3 Virus Production

3.3.1 rAAV serotype 1/2 and 8 production (Ca^{2+}-phosphate method)

The transfection protocol was based on the Ca^{2+}-phosphate method described above (section *3.2.2.1*), with some small additions, according to the following table *3.5*.

Table 3.5: **Transfection mixture amounts: per 10/15 cm dish**

Components	*Serotype 1/2 (10 cm dish)*	*Serotype 8 (15 cm dish)*
dH_2O	1.1 ml	2.4 ml
$CaCl_2$ (2.5 M)	145 µl	330 µl
AAV plasmid	5.5 µg	5 µg
pFdelta6- *helper virus*	11 µg	10 µg
pNLrep / *pRV1- serotype 1*	2.75 µg	-
pH21- *serotype 2*	2.75 µg	-
p5E18-VD2/8	-	5 µg
2x HEBS - added under vortexing	1.6 ml	2.6 ml

48h post-transfection cells were harvested in 1ml DMEM and frozen at -80°C. The cells were disrupted by three cycles of freezing-thawing, followed by a short spin to pellet the cellular debris. The supernatant containing the viral particles was kept at 4°C until further use.

3.3.2 rAAV serotype 8 purification

HEK293T cells were transfected using the Ca^{2+}-phosphate method (sections *3.2.2.1* and *3.3.1*) with p5E18-VD2/8 (AAV2 rep and AAV8 cap), pFdelta6 and the AAV plasmid. After 48h, cells were harvested in medium and centrifuged at 1.200rpm/20min. The pellet was resuspended in 10ml lysis buffer (150mM NaCl, 50mM Tris-HCl, pH 8.5) and three cycles of freezing-thawing were performed. In order to get rid of nucleic acids, 20µl benzonase (50U/ml suspension) was added to the lysate and incubated for 30min at 37°C. After the incubation, the suspension was centrifuged at 4.000rpm/30min/4°C and the clear suspension collected. The purification of the virus was performed using four layer discontinuous iodixanol gradients (ZOLOTUKHIN et al., 2002). The gradients were layered (*Table 3.6*) in ultracentrifuge tubes (Sorvall) using a peristaltic pump (P-1).

Table 3.6: **Iodixanol gradients**

Components	*15% Iodixanol*	*25% Iodixanol*	*40% Iodixanol*	*54% Iodixanol*
PBS 10x	5 ml	5 ml	5 ml	5 ml
Iodixanol	12.5 ml	20 ml	33.3 ml	45 ml
NaCl 5M	10 ml	-	-	-
KCl 2.5M	50 µl	50 µl	50 µl	50 µl
$MgCl_2$ 1M	50 µl	50 µl	50 µl	50 µl
0.5% Phenol red	75 µl	75 µl	-	75 µl
H_2O	22.3 ml	24.9 ml	11.6 ml	-
Volume used for one gradient				
	8-9 ml	5-6 ml	5 ml	2-4 ml

The cellular suspension (8-9ml) was layered on top of the iodixanol gradients; the tubes were sealed, and centrifuged at 60.000rpm/2h/4°C (fixed angle rotor T865, Thermo Scientific). rAAV particles were recovered from the 40% iodixanol layer and iodixanol was removed by several rounds of washing with PBS, using the Amicon centrifugal filters. The purity of the virus was determined by SDS-PAGE and Coomassie staining.

3.3.3 P0-P3 animal injection

New-born C57/BL6 mice were anesthetized for 30-40sec. on ice, followed by injection of 1µl purified rAAV, serotype8 in each hemisphere (2µl/brain). Injection was performed using a 10µl Hamilton syringe at a rate of 451nl/sec. After two to four weeks, mice were anesthetized with Isofluran and brains extracted and used for crude synaptosome preparation (section

3.4.1). All experiments were performed in agreement with the regulations of the University of Bonn Medical Centre Animal Care Committee.

3.4 Biochemistry

3.4.1 Preparation of crude synaptosomes

The preparation was performed at 4°C using detergent free equipment and buffers supplemented with proteinase inhibitors (Roche). C57/BL6 mice (6-8 weeks old) were euthanized with Isoflorane, decapitated and the brains extracted. The cerebellum together with the most of the white matter was removed. Both hemisphere were homogenized in ice-cold homogenization buffer (0.32M sucrose, 50mM EDTA, 2mM HEPES, pH 7.4), supplemented with proteinase inhibitor (Roche) in a Teflon-glass homogenizer (7strokes, 900rpm), followed by centrifugation at 3.000g/15min/4°C. The pellet (P1-nuclear fraction) was removed and the supernatant (S1-crude synaptosomal fraction) transferred into 2ml eppendorf tubes and centrifuged at 14.000rpm/25min/4°C. The synaptosomal cytosol fraction (S2) was discarded and the pellet (P2-crude synaptosomes) resuspended in either 500µl lysis buffer (CL114 detergent, Logopharm) or 100µl equilibration Krebs-Henseleit-HEPES buffer (118mM NaCl, 3.5mM KCl, 1.25mM $CaCl_2$, 1.2 mM $MgSO_4$, 1.2mM KH_2PO_4, 25mM $NaHCO_3$, 11.5mM glucose and 5mM HEPES-NaOH, pH 7.4).

In the case of SV2A protein purification, P0-P3 mice were injected with purified rAAV (serotype 8) and after several weeks crude synaptosomes were prepared as described above. The P2 fraction was resuspended in lysis buffer (50mM Tris-HCl, 150mM NaCl, pH 7.5) supplemented with proteinase, phosphatase inhibitors and 3.9mM n-dodecyl-β-maltoside (DDM**,** specific detergent for SV2A) as previously described by Lambeng et al. (2006). After 1h incubation at 4°C the solution was clarified by centrifugation and the supernatant used for immunoprecipitation (section *3.4.2.4*) or TAP purification (section *3.5.2*).

3.4.2 Protein-protein interaction assays

3.4.2.1 Protein induction and purification from BL21 bacteria

pGEX plasmids encoding for the protein of interest were retransformed in *Escherichia coli* BL21 (DE3). At an optic density (OD) of 0.6-0.8 of the bacterial culture, the expression of the GST-fusion proteins was induced by addition of IPTG (1mM) for 3-4h, under constant shaking at 37°C. After a centrifugation step at 4.500rpm/30min/4°C the bacterial pellet was resuspended in PBS supplemented with proteinase inhibitor (Roche) and lysozym (1mg/ml) and lysed on ice for 20min, followed by sonication and centrifugation at 4.500rpm/1h/4°C. To capture the protein of interest the clear supernatant was incubated for 1h with prewashed

Glutathion-agarose beads. Beads were extensively washed and resuspended in 1ml of PBS supplemented with proteinase inhibitors to reach 50% slurry, further used in GST-pull down assay (section *3.4.2.2*). In order to check the efficiency of protein induction a small aliquot was analyzed by Coomassie staining.

3.4.2.2 GST-pull down assay

To analyse the binding of different GST-fusion proteins to native or overexpressed proteins, GST-pull down assays were performed with crude synaptosomes (section *3.4.1*), primary cortical neurons and with transfected HEK293T cells by the Ca^{2+}-phosphate method (section *3.2.2.1*). HEK293T cells were lysed for 1h in ice-cold lysis buffer (50mM HEPES pH 7.4, 150mM NaCl, 1% Triton X-100, Complete Protease Inhibitor Cocktail Tablets), spun at 14.000rpm/10 min/4°C and the resulting clear supernatant was incubated for 1-2h with GST and GST-fusion proteins. Beads were washed five times with PBS-0.5% Triton X-100 washing buffer, boiled at 95°C/5min in Laemmli buffer with β-ME and resolved in SDS-PAGE gel. GST and GST-fusion proteins were incubated also with lysed crude synaptosomes or lysed cortical neurons for 2-4h. Bound protein complexes were washed with either CL-114 dilution buffer or PBS-0.5% Triton X-100, boiled in Laemmli buffer with β-ME at 95°C/5 min and resolved in SDS-PAGE gel.

3.4.2.3 Co-immunoprecipitation (co-IP)

HEK293T cells were co-transfected with DNA plasmids containing the sequence encoding for the proteins of interest using the Ca^{2+}-phosphate method as described in section *3.2.2.1*. 48h post-transfection the medium was discarded and the cells harvested in ice-cold lysis buffer (50mM HEPES pH 7.4, 150mM NaCl, 1% Triton X-100, Complete Protease Inhibitor Cocktail Tablets) and lysed on ice for 1h, followed by a short centrifugation step at 14.000rpm/10min/4°C. The supernatant was incubated at 4°C with pre-washed (in PBS) magnetic beads for 1h (FLAG M2 beads) or for 2-3h (HA- or GFP-magnetic beads) on a rotator. After the incubation time, the beads containing the protein complexes were washed with PBS-0.5% Triton X-100 buffer. The beads were boiled in Laemmli buffer with β-ME at 95°C/5 min and proteins resolved in SDS-PAGE gel (8% or 10%).

3.4.2.4 Immunoprecipitation (IP)

The P0-3 C57/BL6 mice were injected into the hemisphere with 2µl of purified virus (rAAV-SV2A-GFP, serotype 8) and two weeks after the injection crude synaptosomes were prepared (section *3.4.1*). After the P2 fraction was solubilised, the clear supernatant was mixed for 2-3h

with anti-GFP antibodies (abcam 290). The antibodies were collected overnight by incubation with protein A/G-agarose beads (Santa Cruz). The A/G-agarose beads were collected by centrifugation at low speed (2.000 rpm/5 min), washed five times in PBS and boiled in Laemmli buffer with β-ME at 95°C/5 min.

3.4.3 Protein concentration determination

The protein concentration was determined by measuring the optical density at 260nm using NanoDrop. For shRNA testing, the protein concentration of all samples was adjusted to the lowest one, before analysing by WB. In binding assays the protein concentration of the crude synaptosomes was adjusted to 3-5mg/ml/reaction.

3.4.4 Western Blotting (WB)

Prior to WB, samples were resolved in 8% or 10% SDS-polyacrylamide gel electrophoresis (SDS-PAGE) and separated by size. The separated proteins were transferred to nitrocellulose membrane, followed by protein detection. The membranes were blocked with 3% cold water fish gelatin in PBS for 1h, incubated with primary antibodies in blocking buffer for 2h, washed three times/15min with PBS-0.1% Tween 20 and further incubated with secondary antibodies (IRDye-1:10000, section *2.15*) for 40min. The detection was achieved with an infrared imaging system (Odyssey, Li-cor).

3.5 Identification of novel binding partners by tandem-affinity purification (TAP)

3.5.1 Protein cross-linking

Cultured cortical neurons (DIV2) obtained from wild-type (WT), SV2A +/- and SV2A -/- mice were infected with crude viral particles, serotype 1/2, expressing N- or C-TAP-tagged SV2A. At DIV14 neurons were washed one time with PBS and proteins were cross-linked using three different cross-linkers (*Table 3.7*): 1% formaldehyde (VASILESCU et al., 2004; KLOCKENBUSCH and KAST, 2010), 5mM DSP (dithiobis(succinimidylpropionate), Pierce), 5mM DTBP (dimethyl 3,3'-dithiobispropionimidate-2HCl, Pierce). The protein cross-linking was performed at room temperature or at 37°C/30-60 min, followed by quenching the reaction with 50mM Tris, pH 7.5 or 2.5mM glycine for 5-15min. Cells were lysed either in HEPES buffer (50mM HEPES, 150mM NaCl, pH 7.4) or in Tris-HCl buffer (50mM Tris-HCl, 150mM NaCl, pH 7.4) supplemented with proteinase, phosphatase inhibitors and 3.9mM n-dodecyl-β-maltoside (DDM) for 1h/4°C. The clear supernatant was subject to either one-step or tandem purification as described below (section *3.5.2*), with only one difference: the

elution was performed by boiling the beads in the presence of β-ME reducing agent at 95°C/5 min before SDS-PAGE.

Table 3.7: **Cross-linkers**

Cross-linker	*Functional group targeted*	*Cleavable*	*Solubility*	*Permeability*	*Arm length*
Formaldehyde	Amine to amine	Yes /95°C	Water soluble	Membrane permeable	2 Å
DSP		Yes/ β-ME/95°C thiol-cleavable	Organic solvents		12 Å
DTBP		Yes/DTT/37°C thiol-cleavable	Water soluble		11.9 Å

3.5.2 Strep/FLAG tandem affinity purification

Tandem affinity purification (*Fig.3.1*) is based on the protocol previously described by Glockner, C.J., et al. (Current Protocols in Protein Science, Unit 19.20, 2009). Briefly, crude synaptosomes (section *3.4.1*) or infected neurons (section *3.2.3.3*) were lysed under native conditions using cold lysis buffer (50mM Tris-HCl, 150mM NaCl, pH 7.5) supplemented with proteinase inhibitors and/or phosSTOP (Roche), and 3.9mM n-dodecyl-β-maltoside (DDM). Clear supernatant was applied directly to the Strep-Tactin MacroPrep columns (IBA). After the adsorption, the column was washed five times with buffer W (100mM Tris-HCl, pH 8.0, 150mM NaCl, 1mM EDTA) and elution performed with buffer E (100mM Tris-HCl, pH 8.0, 150mM NaCl, 1mM EDTA, and 2.5mM desthiobiotin). From each collected fraction a small aliquot was kept for further analysis by WB. All operations were performed either at 4°C or at room temperature.

In the case of two-step purification all elution fractions were pooled and mixed with anti-FLAG M2 affinity gel (A2220, Sigma) or anti-FLAG M2 magnetic beads (M8823, Sigma) for 1h/4°C. Beads were washed several times with TBS (Tris buffered saline) supplemented with DDM and elution was performed with: (a) 200µg/ml FLAG peptide (F3290, Sigma) in TBS for 10-30min; (b) 1M Arg-HCl pH 3.5 in TBS (FUTATSUMORI-SUGAI et al., 2009) or (c) SDS-PAGE sample buffer and boiled at 95°C/5 min.

In one-step FLAG purification, the clear supernatant resulted from neurons' lysis was directly incubated for 1h with anti-FLAG M2 beads, followed by the same washing and elution steps as described above.

For sample concentration, Amicon Ultra Centrifigal filters (Milipore, MWCO, 3000) were used (optional step). Proteins were separated in SDS-PAGE and the gel stained with Coomassie Colloidal Blue according to the manufacturer's instructions (Carl Roth).

3.5.3 Protein purification from HEK293T cells

HEK293T cells transfected with the FLAG/Strep-tagged truncated form of RIM1α (ZF-PDZ and C2A-C2B domains) were lysed for 1h in ice-cold lysis buffer (50mM HEPES, pH 7.4, 150mM NaCl, 1% Triton X-100, Complete Protease Inhibitor Cocktail Tablets), centrifuged at 14.000rpm/10min/4°C and the resulted supernatant was incubated for 1h with pre-washed FLAG-M2 magnetic beads. The beads were washed five times with lysis buffer and incubated with lysed crude synaptosomes.

3.5.4 Binding assays between the different regions of RIM1α and crude synaptosomes

Crude synaptosomes prepared as previously described (section *3.4.1*) were pre-equilibrated for 10min/37°C in Krebs-Henseleit-HEPES buffer (118mM NaCl, 3.5mM KCl, 1.25mM $CaCl_2$, 1.2mM $MgSO_4$, 1.2mM KH_2PO_4, 25mM $NaHCO_3$, 11.5mM glucose and 5mM HEPES-NaOH, pH 7.4) and studied under three treatment conditions for 15min/37°C: methanol control, Staurosporine (1μM) and 1xphosSTOP (Roche). After kinase or phosphatase inhibition, crude synaptosomes were lysed 1h/4°C in CL114 detergent (in the presence of the corresponding inhibitors), spun at 14.000rpm/20min/4°C and the supernatant incubated for 3-4h with purified ZF-PDZ and C2A-C2B domains of RIM1α, coupled to FLAG-magnetic beads. Subsequent to incubation, the magnetic beads were washed five times in CL114 dilution buffer and proteins denaturated at 95°C in 1x loading buffer (Life Technologies). Samples were separate by size in pre-cast NuPAGE4-12% Bis-Tris Gel, according to the manufacturer's instruction (Life Technologies) and stained with Coomassie Colloidal Blue (CCB).

3.5.5 Sample preparation for mass spectrometer analysis

Bands were excised with a cleaned scalpel, placed in 0.5ml LoBind Eppendorf tubes and destained using destaining solution, containing 200mM ammonium hydrogencarbonate and 40% acetonitrile (according to Sigma Protocol IGD profile kit). Gel pieces were dried using the vacuum concentrator for 30-40min/RT. For the maximum recovery of proteins, disulfuric bridges were reduced with 20mM DL-Dithiothreitol (DTT) in 100mM ammonium hydrogencarbonate for 30min/55°C and, the generated thiol groups were alkylated in the presence of 40mM iodoacetamide (IAA) in 100mM ammonium hydrogencarbonate for 30min/RT/in the dark (aminocarboxymethylation). The solution was removed and the gel pieces were incubated 5min with 100mM ammonium hydrogencarbonate, further dehydrated two times (5min each) with 50% acetonitrile and one time (5min) with 100% acetonitrile, and completely dried in the vacuum concentrator. In the tryptic digestion step, performed

according to the Sigma Protocol IGD profile kit, the dried gel pieces were digested with 0.4µg trypsin at 37°C/ON. After the incubation the resulted solution was transferred into a new tube and the peptides dried in the vacuum concentrator. The samples were analyzed by the mass spectrometry in the IBMB, Bonn.

***Figure 3.1*: Flow chart of tandem affinity purification.**

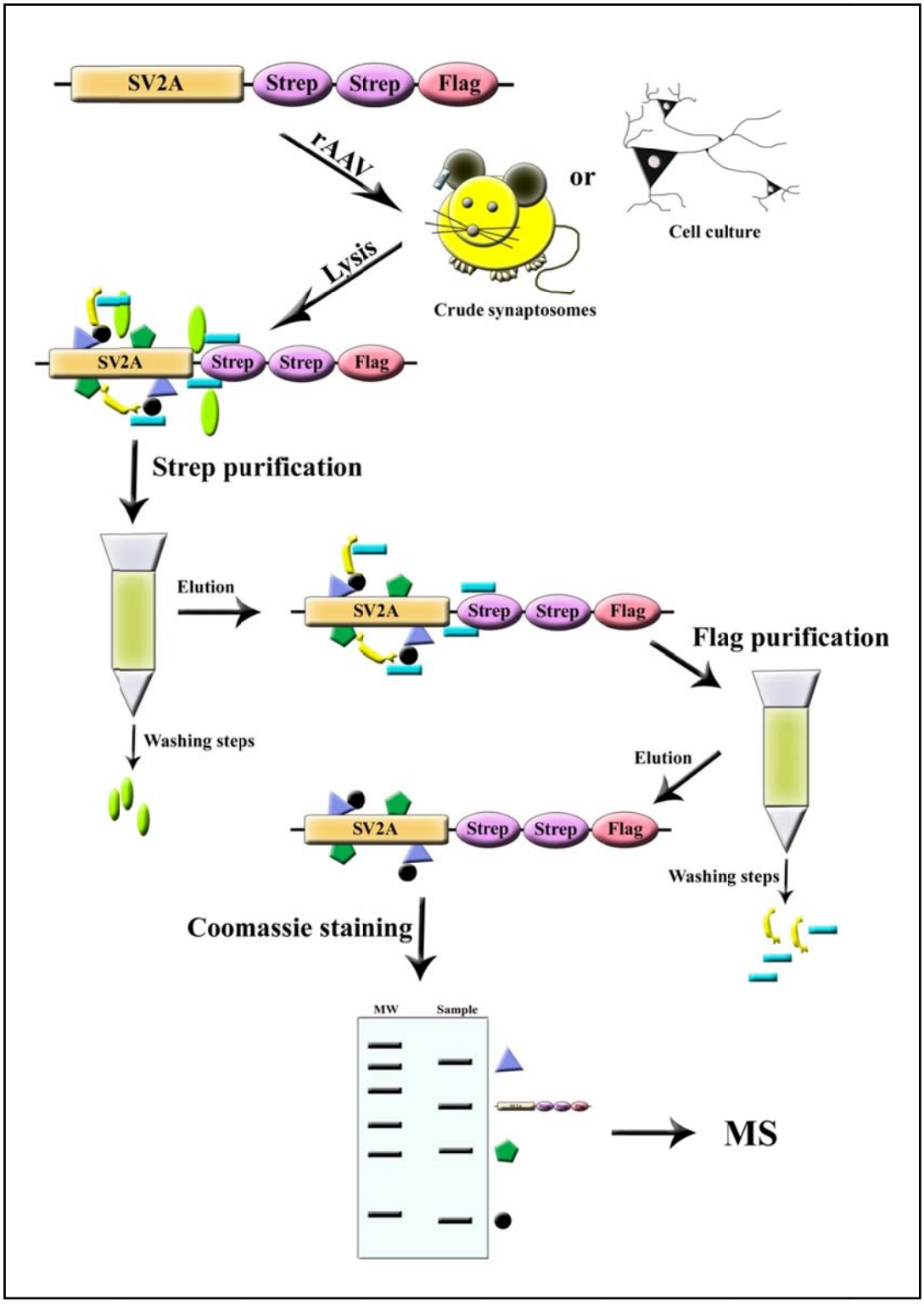

3.6 Immunochemical methods

3.6.1 Pre-treatment of primary neurons with various inhibitors

Rat primary cortical neurons were stimulated at DIV19-21 with different phosphatase inhibitors and at DIV12-14 with a specific inhibitor for SRPKs (table *3.8)*. As control the equivalent amount of methanol was used for Calyculin A and okadaic acid, DMSO for SRPIN340, while for phosSTOP, PBS was added to control cells (1 tablet of phosSTOP in 1ml PBS to obtain a concentration of 10x).

Table 3.8: **Phosphatase and kinase inhibitors**

	Inhibitor	*Target*	*Concentration*	*Inhibition time*
Phosphatase Inhibitors	Calyculin A	PP1, PP2A	2nM	30 min
	Okadaic acid	PP1, PP2A	10nM	60 min
	phosSTOP	all	0.1x	60 min
SRPK inhibitor	SRPIN340	SRPK1 SRPK2	10µM	12-16h

After the incubation time, neurons were washed 1x with PBS and fixed in 4% paraformaldehyde for 5min, followed by immunofluorescence (section *3.6.2*).

3.6.2 Immunofluorescence (IF)

Transfected or infected neuronal cultures were fixed for 5min in 4% paraformaldehyde and 4% glucose in PBS, permeabilised with 0.3% Triton X-100 and blocked for 1h/RT in blocking solution (10% BSA, 1% NGS, 0.1 Triton X-100 in PBS). Neurons were incubated with primary antibodies at 4°C/ON. Following the incubation, cells were washed three times with PBS and incubated with the secondary antibodies (section *2.15*) for 40min/RT/in dark. Subsequently to PBS washing, cover-slips were mounted in Mowiol (Sigma) and let to dry O.N.

3.6.3 Immunohistochemistry (IHC)

Brains were fixed in 4% paraformaldehyde and embedded in paraffin blocks. 4µm brain slices were deparaffinised in xylene and rehydrated in a series of ethanol baths (100%, 95% 70% and 50% in PBS) for 2min each. Heat mediated antigen retrieval was performed in citric buffer (10mM citric acid, pH 6.0), microwaved for 10min and cooled for 30min/RT. Slices were blocked in PBS with normal goat serum (1:100 to 1:200) and 10% fetal calf serum for 2h in a humidified chamber, followed by incubation with anti-GFP (ab290, 1:100), anti-FLAG (1:100, Sigma) and anti-SV2A (1:200, 119002 SySy) primary antibodies overnight. After several washings with PBS, secondary antibodies goat anti-mouse FITC and goat anti-rabbit Cy3 (Jackson ImmunoResearch) were applied at a concentration of 1:400 and

incubated for 2h in the dark. Several washing steps with PBS were followed by mounting the samples with Vectashield mounting medium containing DAPI (Vectorlabs).

3.7 Imaging

Images were acquired with a laser scanning Nikon A1/Ti confocal microscope using a CFI Plan APO IR 60x WI objective (NA 1.27), Nikon NIS-Elements 4.0 acquisition software or by using a confocal microscope Olympus FV1000, UPLS Apo60X WUIS2, 1.2 NA objective. IHC pictures were taken using a Zeiss Axio Observer A1 inverted microscope with a Plan-Apochromat 20x NA 0.8 air objective.

3.8 Quantifications and statistical analysis

3.8.1 Image quantification

Bouton size quantification was performed in ImageJ program. The maximal brightness was determined by subtracting the background (rolling ball radius of 1/3 of the pixel width of the image). A 30% threshold value was applied to all compared pictures, and the number of synapses counted. The pixel number, obtained for each synapse, was multiplied with the pixel size to obtain the area of each bouton. Obtained values were binned in 0.2- steps ranging from 0.2 to 2-2.5μm^2. Co-localization analysis was performed using the JACOp plug-in in ImageJ, and measuring Pearson's coefficient. Statistical analysis was performed either in Excel or in GraphPad Prism 6.

3.8.2 WB quantification

Images of the WB were quantified using the ImageJ program. Statistical analysis was performed in GraphPad Prism 6.

3.9 Programmes and URLs

ImageJ

GraphPad Prism 6

BioEdit v.7.1.3.0

Seqbuilder v.8.0.2

http://www.uniprot.org

http://www.ncbi.nlm.nih.gov

http://www.matrixscience.com

http://www.insilico.uni-duesseldorf.de (Ligation calculator)

http://www.bioinformatics.org/primerx (Designing primers for point mutations)

4. Results

4.1 Impact of phosphorylation status on the properties of RIM1α

It has been proposed that regulated phosphorylation/dephosphorylation events may play a role in plasticity- induced remodelling of established active zones, as well as in the assembly of new ones. The active zone protein RIM1α, a scaffolding multidomain protein, has been shown to be the substrate of two kinases, ERK2 (SIMSEK-DURAN and LONART, 2008) and PKA (LONART et al., 2003) and contains a large number of yet uncharacterized potential phosphorylation sites. Nevertheless, the impact of RIM1α phosphorylation on active zone reorganisation and function is not well understood. Moreover, such posttranslational events may impact the binding affinity of RIM1α to some of its binding partners, and subsequently trigger, directly or indirectly, a cascade of events culminating in the reorganization of active zone architecture and changes in synaptic activity.

4.1.1 Distribution of RIM1α in synaptic boutons is altered by hyperphosphorylation events

Both the UPS-system (JIANG et al., 2010) and the transcriptional/translational machinery (LAZAREVIC et al., 2011) have been suggested to control the level of RIM1α at the active zone. In addition, phosphorylation events may as well affect RIM1α's activity (*Fig. 4.1*).

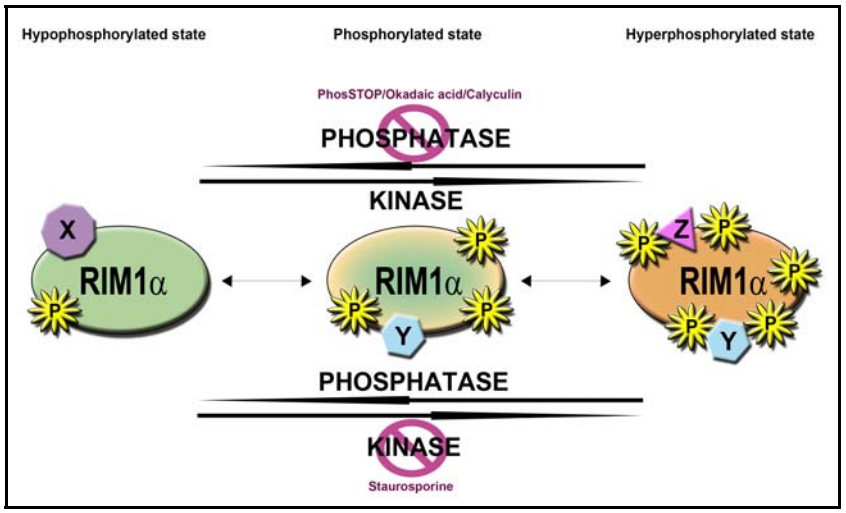

***Figure 4.1*: Regulation of RIM1α interactions by phosphorylation and dephosphorylation.** *In vivo*, under normal physiological conditions, the activity of the cell dictates the phosphorylation state of RIM1α. Phosphorylation of various amino acid residues may have a direct influence on the affinity of protein interactions of RIM1α. In a simplified model, RIM1α is phosphorylated and binds certain proteins (Y, blue). By applying a phosphatase inhibitor, the equilibrium is moved toward a hyperphosphorylated state and RIM1α may interact with additional proteins (Z, pink). By blocking kinase activity, RIM1α may lose some of its binding partners and bind new ones (X, violet). For the simplicity of the model, the influence of other posttranslational modifications has not been taken into the account.

Thus, to gain insight into the molecular mechanisms that dynamically regulate RIM1α levels and distribution, the effect of phosphatase inhibitors on RIM1α was assessed in neuronal cell culture. To this end different phosphatase blockers were applied and RIM1α's phosphorylation status was shifted artificially toward hyperphosphorylation. To analyze the distribution of endogenous RIM1α in boutons, rat primary cortical neurons were stimulated for different periods of time with various concentrations of phosphatse inhibitors at DIV21, followed by paraformaldehyde fixation and immunofluorescence against endogenous RIM1/2. Initially, two phosphatase inhibitors were tested: Calyculin A[2] 2nM for 30min and okadaic acid[3] 10nM for 60min. After the incubation, the bouton area labelled by endogenous RIM1/2 was quantified using the ImageJ software. In the case of okadaic acid application (*Fig. 4.2B*), a non-significant increase in the number of RIM1/2 labelled boutons with smaller area was observed compared to the methanol control. Accordingly, treatment with Calyculin A for 30min. (*Fig. 4.2A*), induced an increase in the number of small boutons labelled by RIM1/2 versus negative control (0.2-0.4μm^2, p=0.011). Interestingly, in both cases a small decrease in the area size was observed for bigger boutons, above 0.6μm^2 (Calyulin A, 0.6-0.8μm^2, p=0.016).

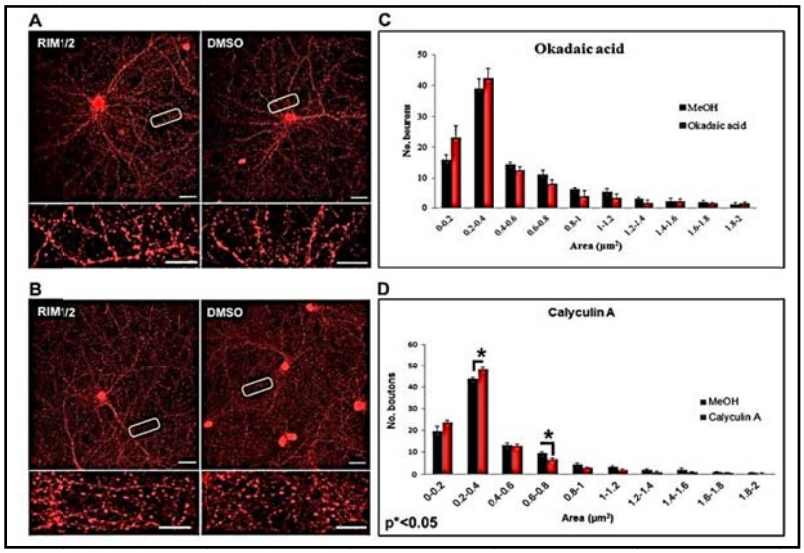

Figure 4.2: **The effect of PP1/PPA2 inhibitors on the bouton area labelled by endogenous RIM1/2.** Primary rat cortical neurons were treated with 10nM okadaic acid ***(A/C)*** for 60min and with 2nM Calyculin A. ***(B/D)*** for 30min, followed by IF against endogenous RIM1/2. ***(A/B)*** IF against endogenous RIM1/2 in the presence of different inhibitors. For each applied inhibitor, three independent experiments were performed (N=3). All pictures were taken using a laser-scanning confocal microscope (Nikon A1/Ti). The area of the boutons was binned in 0.2-step groups ranging from 0-0.2 μm^2 to 2 μm^2. Larger bouton sizes were excluded from the measurements in order to diminish staining artefacts. Within the same size group the measurements were compared to the methanol control and statistical analysis performed using Student's t-test student (p*<0.05). Scale bar: 20μm (overview) and 10μm (insets). N, number of independent experiments.

Since the spectrum of inhibition of okadaic acid and CalyculinA is limited to PP1 and PP2A, a more general phosphatase inhibitor, phosSTOP, was tested. Stimulation of rat cortical neurons at DIV21 with 0.1x phosSTOP for up to 60min reproduced the effects

[2] IC_{50} (PP1): 2nM; IC_{50} (PP2A): 0.5-1.0nM
[3] IC_{50} (PP1): 10-15nM; IC_{50} (PP2A): 0.1nM

observed after treatment with Calyculin A and okadaic acid (*Fig. 4.3*). Analysis of the intensity of RIM1/2 staining did not show any significant changes in samples treated with phosSTOP versus control *(Fig. 4.3C)*. In addition, between the same size groups no difference in RIM1/2 fluorescence intensity was detected (data not shown).

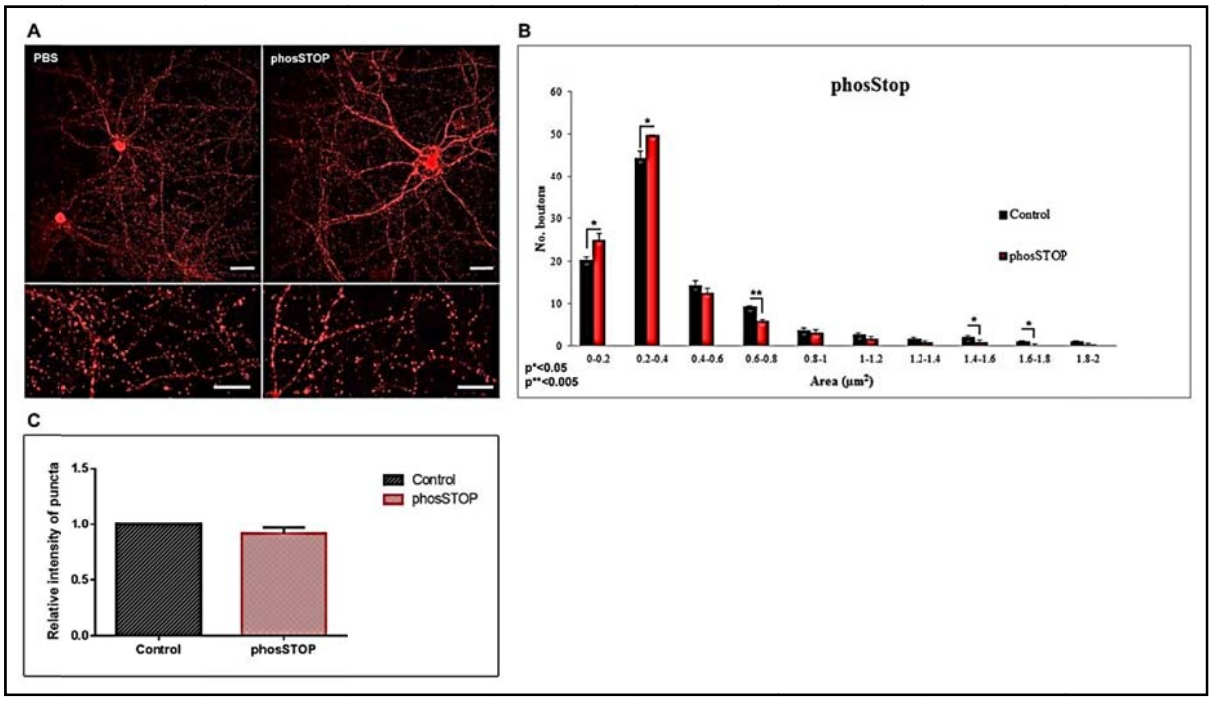

Figure 4.3: **The effect of phosSTOP inhibitor on the synaptic boutons.** ***(A)*** Rat primary cortical neurons were treated with 0.1x phosSTOP for 1h, followed by fixation and staining against the endogenous RIM1/2. All pictures were acquired using a laser-scanning confocal microscope (Nikon A1/Ti). ***(B)***The area of the boutons was binned in 0.2-step groups ranging from 0-0.2 μm^2 to $2\mu m^2$. Larger bouton sizes were excluded from the measurements in order to diminish staining artifacts. Within the same size group the measurements were compared to the methanol control and statistical analysis was performed using Student's t-test student (p*<0.05; p**<0.005). Three independent experiments were performed (N=3). ***(C)*** Quantification of the intensity of RIM1/2 staining. Bars represent mean values of three independent experiments; whiskers, SEM. Scale bar: 20µm (overview) and 10µm (insets).

These results indicate that by blocking phosphatase activity, the distribution of RIM1/2 seems to be altered at the AZ, while its total level remains unchanged. The molecular mechanisms behind these changes are not well understood.

4.1.2 Identification of novel phosphorylation-dependent RIM1α binding proteins

To gain better insight into how phosphorylation could affect RIM1α activity, we aimed at identifying possible phospho-dependent binding partners. Thus, an affinity purification approach coupled to mass spectrometry (MS) was applied. To this end, N- and C-terminal regions of RIM1α fused to a FLAG-tag, were overexpressed and purified from HEK293T cells by using FLAG magnetic beads. Purified fragments were further incubated with lysed mouse crude synaptosomes, in the presence of 1µM staurosporine or 1x phosSTOP (*Fig.4.4*),

followed by affinity purification and LC-MS/MS. Four independent experiments were performed, and each resulted in similar band pattern after Coomassie Colloidal Blue (CCB) staining (*Fig. 4.5*).

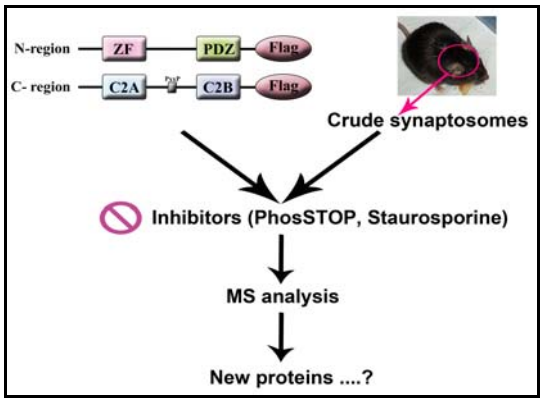

Figure 4.4: **Experimental approach to identify phospho-dependent binding partners for RIM1α**. The N- and C-terminal regions of RIM1α, fused to a FLAG/Strep-affinity tag and the respective control (tag alone) were overexpressed in HEK293T cells. After purification proteins were incubated with lysed mouse crude synaptosomes, in the presence of 1µM staurosporine, 1x phosSTOP, and the equivalent amount of methanol, as negative control. Samples were separated by SDS-PAGE. Bands were excised from the gel, digested with trypsine O.N. and peptides analysed by LC-MS/MS.

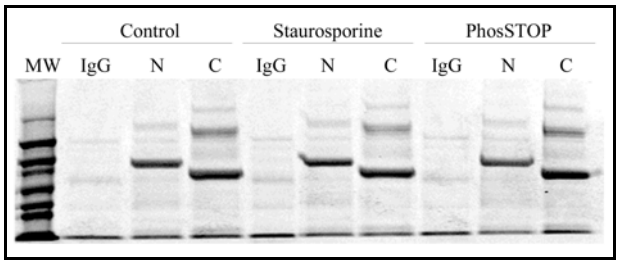

Figure 4.5: **Separation by SDS-PAGE of protein complexes from crude synaptosomes bound to either the N-terminal region (N) or C-terminal region (C) of RIM1α.** After elution, co-immunoprecipitated proteins were separated in NuPAGE 4-12% Bis-Tris and visualized by Coomassie Colloidal Blue (CCB) staining. Each lane was cut in 8 small pieces and prepared for mass spectrometry according to the protocol (n=4).

4.1.2.1 Identification of protein complexes associated with the C-terminal region of RIM1α

Four independent experiments were performed using lysed crude synaptosomes and the C2A-C2B region of RIM1α, overexpressed and purified from HEK293T cells. Immunopurified protein complexes were separated by SDS-PAGE and identified by mass-spectrometry. Three groups were analysed: control, staurosporine and phosSTOP. As negative control for unspecific binding, the FLAG-tag sequence alone was purified with FLAG magnetic beads.

The MS scores of treated samples were divided by the scores of negative samples (protein X – sample/protein X- control). Proteins with a ratio above 2- fold enrichment were considered to specifically bind RIM1α and not to the FLAG sequence or the magnetic beads. The remaining proteins were classified in five groups, according to their subcellular localization independent of the pharmacological treatment (*Fig. 4.6A*). A significant

proportion of these proteins were classified as components of various *signalling cascades* (24%), while other were present in the *CAZ* (19%) and in the membrane of *synaptic vesicles* (15%).

Moreover, the number of proteins binding the C- terminal region of RIM1α was increased by the application of either staurosporine or phosSTOP inhibitor. From a total of 174 identified proteins (*Table 4.1*), 41 were present in all three groups, 5 in the control and staurosporine, 14 in the phosSTOP and control, and 30 in the staurosporine and phosSTOP group. A considerable number of proteins bound to the C-terminal region of RIM1α in a treatment-dependent manner: 29 in response to staurosporine and 30 to phosSTOP (*Fig. 4.6B*).

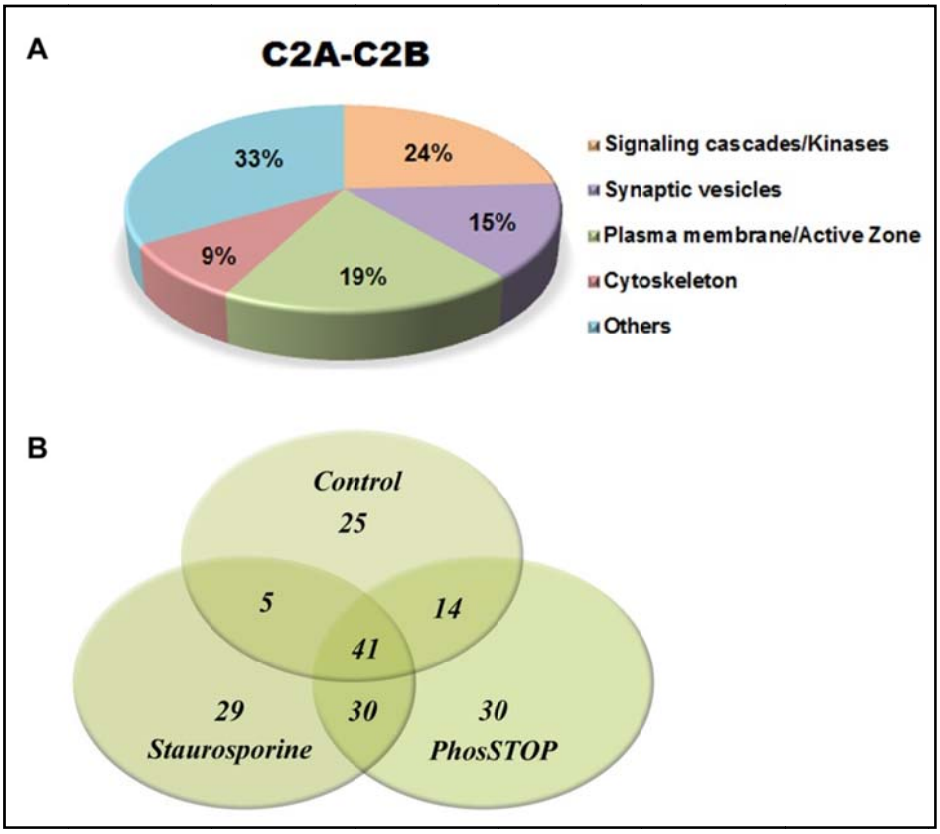

Figure 4.6*: Classification of the proteins identified to bind to the C2A-C2B domains of RIM1α.** ***(A) After elimination of the proteins binding unspecifically, the rest were classified according to their subcellular localization and function in five groups. ***(B)*** Comparative analysis between control, staurosporine (kinase inhibitor) and phosSTOP (phosphatase inhibitor) groups. Four independent experiments were performed.

Table 4.1: **Identification of proteins interacting with the RIM1α C2A-C2B region.** Proteins identified with a high score under different conditions are summarized in the table. Proteins were sorted according to their subcellular localization or function. *: best score from four independent measurements. Proteins of interest for this work are marked in bold italic. RIM1α, representing the input, is marked in italic. Proteins common for all *three groups* are marked in **green**, for *staurosporine and phosSTOP* in **orange**, *control and phosSTOP* in **lila**.

Protein name	*Control**	*Staurosporine**	*phosSTOP**	*Function/Localization*
14-3-3 protein beta/alpha	3788	3634	4952	**Signalling cascades**
14-3-3 protein epsilon	7724	7543	8543	
14-3-3 protein eta	4456	4405	5467	
14-3-3 protein gamma	5111	4811	6860	
14-3-3 protein theta	5775	4945	5607	
14-3-3 protein zeta/delta	6153	5327	6806	
Calcineurin subunit B type 1	1371	1686	2307	
Calcium/calmodulin-dependent protein kinase type II subunit alpha	419	2729	1028	
Calcium/calmodulin-dependent protein kinase type II subunit beta		1666	572	
Calcium/calmodulin-dependent protein kinase type II subunit delta		1445	560	
Calmodulin		154		
Casein kinase II subunit alpha	1343	1215	989	
Casein kinase II subunit alpha'	810	557	417	
Casein kinase II subunit beta	617	630	355	
Creatine kinase B-type	417	769	713	
Guanine nucleotide-binding protein G(I)/G(S)/G(T) subunit beta-1	99	149	145	
RasGTPase-activating protein SynGAP		58	57	
Serine/threonine-protein phosphatase 2A catalytic subunit beta isoform	166			
Serine/threonine-protein phosphatase 2B catalytic subunit alpha isoform	3437	4129	4420	
Serine/threonine-protein phosphatase 2B catalytic subunit beta isoform	2575	2576	3082	
Serine/threonine-protein phosphatase 2A 65 kDa regulatory subunit A alpha isoform	316	278	256	
SRSF protein kinase 2	***169***	***71***	***266***	
Rab GDP dissociation inhibitor alpha	101		58	
Septin-5	71		101	
AP-2 complex subunit alpha-2	191			**Synaptic vesicles**
AP-2 complex subunit beta	74	95	90	
Alpha-enolase	213		300	
Dynamin-1	144	109	403	
Gamma-enolase	201	405	337	
Ras-related protein Rab-3A		174	85	
Phosphoglycerate kinase 1	49		70	
Phosphoglyceratemutase 1		82	117	
Synapsin-1		124		
Synapsin-2			82	
Vesicle-associated membrane protein-associated protein A	***127***	***105***	***36***	
V-type proton ATPase subunit B, brain isoform		156	124	
V-type proton ATPase subunit D		124	73	
Copine-6	***747***	***574***	***423***	**Active Zone/ Plasma membrane**
Excitatory amino acid transporter 1	381			
Excitatory amino acid transporter 2	382			
ERC protein 2		360		
Neuronal membrane glycoprotein M6-a		300	128	
Protein bassoon	395	782	623	
Protein piccolo	33	290	117	
Regulating synaptic membrane exocytosis protein 1 (Input)	*11054*	*91764*	*114517*	
Regulating synaptic membrane exocytosis protein 2	13665	3302	10679	
RIMS-binding protein 2	819	453	697	
Synaptosomal-associated protein 25		146	116	
Syntaxin-1A			141	
Syntaxin-1B		302		

4.1.2.2 Analysis of protein complexes associated with the N-terminal region of RIM1α

An identical experimental approach with the N-terminal region of RIM**1**α was performed. The N-terminal region was included in the MS analysis in order to identify not only novel interacting partners but also to serve as internal control for the data obtained with the C-terminal region of RIM1α. Two independent experiments were performed. Three groups, control, staurosporine and phosSTOP, were analysed. Following the elimination of proteins binding unspecifically, the potential binding partners were sorted in five groups according to their subcellular localization or function.

Comparable to the C-terminal region, the *signalling cascades* group had the highest percentage (30%), followed by *active zone components* (23%) (*Fig. 4.7A*; *table 4.2*). Pre-treatment of crude synaptosomes with phosSTOP and staurosporine did not increase substancially the number of proteins binding specifically to the ZF-PDZ domain: only 3 were identified under phosSTOP and 17 under staurosporine treatment (*Fig. 4.7B*).

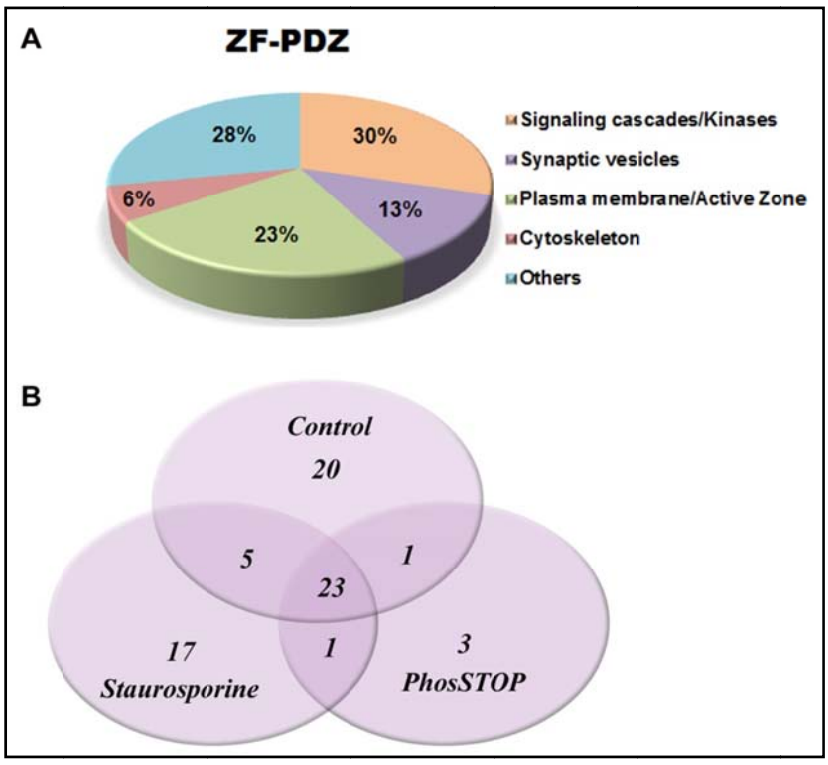

Figure 4.7*: Classification of the proteins identified by the mass spec approach for the ZF-PDZ region of RIM1α.** ***(A) Proteins binding specifically to the N-terminal region of RIM1α were sorted in five classes according to their subcellular localization and function. ***(B)*** Comparative analysis between control, staurosporine (kinase inhibitor) and phosSTOP (phosphatase inhibitor). Two independent experiments were performed.

***Table 4.2:* Proteins identified to interact with the RIM1α ZF-PDZ domain.** Proteins with the highest score binding the RIM1α ZF-PDZ under different conditions are summarized in the table. Proteins were sorted according to their subcellular localization or function. *: best score from four independent measurements. Proteins of interest for this work are marked in bold italic. Proteins common for all *three groups* are marked in **green**, for *staurosporine and phosSTOP* in **orange**, *control and phosSTOP* in **lila**, *control and staurosporine* in **aquamarine**

Protein name	Control*	Staurosporine*	phosSTOP*	Function/Localization
14-3-3 protein beta/alpha	3747	6375	4148	Signalling cascades
14-3-3 protein epsilon	8247	11102	8344	
14-3-3 protein eta	4243	6636	4681	
14-3-3 protein gamma	6227	9722	6737	
14-3-3 protein theta	3740	7859	5630	
14-3-3 protein zeta/delta	5091	8209	5650	
Calcium/calmodulin-dependent protein kinase type II subunit alpha	1447	2421	1080	
Calcium/calmodulin-dependent protein kinase type II subunit beta	684	1349	572	
Casein kinase II subunit alpha	2480	1974	1210	
Casein kinase II subunit alpha'	1242	1231	725	
Casein kinase II subunit beta	560	1161	527	
Guanine nucleotide-binding protein G(o) subunit alpha		435		
RasGTPase-activating protein SynGAP	125	495	92	
Serine/threonine-protein phosphatase 2A catalytic subunit alpha isoform	186	240	252	
Alpha-enolase		213		Synaptic vesicle
Ras-related protein Rab-15		80		
Synaptotagmin-1	73			
Vesicle-fusing ATPase	263	398		
V-type proton ATPase 116 kDa subunit a isoform 1		54		
V-type proton ATPase subunit E 1		224		
V-type proton ATPase catalytic subunit A	446		106	
ELKS/Rab6-interacting/CAST family member 1	1114	1349	1047	Plasma membrane/ Active Zone (AZ)
ERC protein 2	3179	5108	3790	
Protein piccolo	287	532	135	
Protein bassoon	1044	2078	783	
Protein unc-13 homolog A	175	558	174	
Regulating synaptic membrane exocytosis protein 2	1764	2861	2175	
Sodium/potassium-transporting ATPase subunit alpha-3	366			
Sodium/potassium-transporting ATPase subunit beta-1	147			
Voltage-dependent anion-selective channel protein 2	73	358		

4.1.2.3 Analysis of the protein complexes co-purified with the overexpressed C-terminal region of RIM1α in primary cultured neurons

In the previous MS data, obtained with crude synaptosomes, we identified several proteins as potential novel binding partners for RIM1α (*Table 4.1* and *4.2*, protein names are marked in ***bold italic***). Therefore, to confirm these results, rat primary cortical neurons were further used. Primary neuronal cultures were chosen because the detection of endogenous proteins binding the overexpressed C-terminal region of RIM1α was more reliable.

Rat primary cortical neurons were infected at DIV2 with rAAV (recombinant adeno associated virus) expressing only the C-terminal part of RIM1α and the FLAG-tag. Two weeks later C2A-C2B region was purified via FLAG-magnetic beads and bound protein complexes analysed by mass-spectrometry. The data was analysed as previously described in chapters *4.1.2.1* and *4.1.2.2*. The highest number of proteins was found in the *kinase/signalling group* (26%) and in the *CAZ* (22%), excluding the group of *others* (*Fig. 4.8A*; *Table 4.3*).

A comparative analysis between percentages acquired with crude synaptosomes and primary neurons, for the RIM1α C2-domains, revealed a similar distribution of the groups. Moreover, proteins belonging to the *kinase/signalling group* and the *active zone group* tended to have the highest probability of binding, directly or indirectly, the C-terminal region (*Fig. 4.8B*).

Additionally, RIM1α's known binding partners such as, liprins-α and RIM-BPs were also identified in the measurements (*Table 4.3*). However, the voltage-gated calcium channels (P/Q- and N- type) could not be detected using these methods and reagents.

Taken together, affinity purification coupled to mass-spectrometry analysis and pharmacological treatments resulted in the identification of both phospho-dependent as well as independent novel protein interactions for RIM1α.

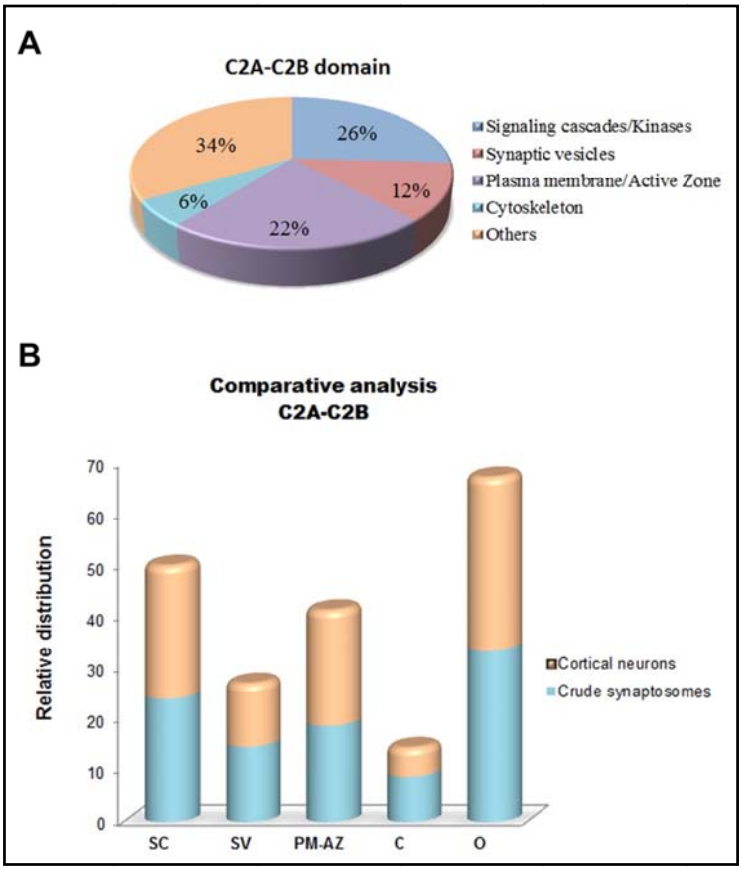

Figure 4.8: **Novel binding protein for the RIM1α C2A-C2B domain purified from rat cortical neurons.** (**A**) After unspecific bound proteins were excluded, the remaining ones were classified according to their subcellular localization. (**B**) Comparative analysis of the distribution of different groups obtained using the RIM1α C2A-C2B region. Data depicted in orange represents the co-IP experiment performed with rat cortical neurons (N=1), while in blue four independent measurements with crude synaptosomes are shown (N=4). The relative distribution of the groups is depicted in percentages. SC, signalling cascade group; SV, synaptic vesicle group; PM-AZ, plasma membrane and active zone group; C, cytoskeletal group; O, other group; N, number of independent experiments.

Table 4.3: **Identification of binding proteins binding to the RIM1α C2A-C2B domain overexpressed and purified from rat primary cortical neurons.** Proteins were grouped according to their subcellular localization or function. Proteins of interest for this work are marked in bold italic. In **bold lila** known binding partners for RIM1α are marked.

Protein name	*Score*	*Coverage*	*Localization/Function*
14-3-3 protein beta/alpha	1450	31,71	**Signalling cascades**
14-3-3 protein epsilon	4005	63,53	
14-3-3 protein eta	2665	50,41	
14-3-3 protein gamma	2504	46,96	
14-3-3 protein theta	1561	42,86	
14-3-3 protein zeta/delta	2750	47,76	
Calcium/calmodulin-dependent protein kinase type II subunit alpha	655	18,2	
Calcium/calmodulin-dependent protein kinase type II subunit beta	565	24,17	
Calmodulin	84	30,87	
Casein kinase II subunit alpha	739	43,48	
Casein kinase II subunit alpha'	224	23,14	
Casein kinase II subunit beta	318	29,77	
Creatine kinase B-type	101	13,65	
Serine/threonine-protein kinase 38	101	6,88	
Serine/threonine-protein phosphatase 2A 65 kDa regulatory subunit A alpha isoform	436	21,22	
Serine/threonine-protein phosphatase 2A catalytic subunit beta isoform	179	12,94	
Serine/threonine-protein phosphatase 2B catalytic subunit alpha isoform	2601	59,69	
Serine/threonine-protein phosphatase 2B catalytic subunit beta isoform	3306	67,43	
SRSF protein kinase 2	***92***	***6,75***	
Alpha-enolase	359	13,82	**Synaptic vesicle**
Clathrin heavy chain 1	62	2,69	
Phosphoglyceratemutase 1	118	10,63	
Pyruvate kinase isozymes M1/M2	74	5,08	
Ras-related protein Rab-6A	85	10,58	
Triosephosphateisomerase	225	9,36	
Vesicle-associated membrane protein-associated protein A	***636***	***41,37***	
V-type proton ATPase catalytic subunit A	209	9,56	
V-type proton ATPase subunit B, brain isoform	243	21,72	
V-type proton ATPase subunit E 1	194	11,95	
Adenylyl cyclase-associated protein 1	41	7,59	**Plasma membrane/ Active Zone (AZ)**
Contactin-1	112	5,1	
Copine-6	***682***	***26,39***	
Liprin-alpha-2	**583**	**10,1**	
Liprin-alpha-3	**296**	**8,53**	
Neuromodulin	48	9,25	
Regulating synaptic membrane exocytosis protein 2	5325	3,01	
RIMS-binding protein 2	**1018**	**31,06**	
Synaptosomal-associated protein 25	229	21,36	
Syntaxin-1B	100	12,85	
Voltage-dependent anion-selective channel protein 1	279	7,09	

4.1.3 Validation of the newly identified RIM1α binding proteins

All filtered proteins were analysed by screening the uniprot[4] and pubmed[5] databases, for their possible functions/involvement in CAZ architecture. Based on this analysis, four candidate proteins were chosen to be further tested: two kinases (ULKs, SRPKs) involved in controlling active zone assembly in invertebrates (JOHNSON et al., 2009; NIERATSCHKER et al., 2009; WAIRKAR et al., 2009); VAPA/VAPB, proteins associated with bouton formation (PENNETTA et al., 2002), and Copine VI, whose function in synaptic plasticity has not been yet elucidated.

4.1.3.1 Unc-51-like kinase (ULK)

ULK1 and ULK2 that were the first time described in mouse by Yan et al. (YAN et al., 1998, 1999), are protein kinases with a major role in autophagy (review: ALERS et al., 2012). Besides macroautophagy, ULKs play an important role in neurite outgrowth in cerebellar granular neurons (TOMODA et al., 1999).

In invertebrates (*C.elegans*) the function of Unc-51 in axon guidance is tightly regulated by protein phosphatase 2A, which dephosphorylates proteins phosphorylated by this kinase (OGURA et al., 2010). Moreover, Unc-51 acts in presynaptic motorneurons in *D. melanogaster*, where it regulates the localization of Bruchpilot opposite to glutamate receptors. In its absence a decrease in synaptic density, accompanied by abnormal active zone composition and impaired neurotransmitters release was detected (WAIRKAR et al., 2009).

So far, AZ protein substrates for ULK kinases have not been identified yet. In addition, the role of these kinases in the presynaptic terminal has not been fully elucidated.

4.1.3.1.1 ULK proteins bind RIM1α

Chromatography affinity coupled to MS analysis identified ULK2 to bind the biotin tagged C2 domain of RIM1α (*Table 4.4*). Although the score and the number of unique peptides were low, its association with CAZ and especially, with RIM1α protein was investigated, due to its involvement in controlling the assembly of the AZ in *D. melanogaster* (WAIRKAR et al., 2009).

***Table 4.4:* ULK2 protein was identified to bind with C2A-C2B domain of RIM1α.** The biotin tagged RIM1α C2-region was incubated with whole brain lysate and co-immunoprecipitated proteins were analysed by MS. Identification of ULK2 was performed using the human databank (international protein index). The generated score and the unique peptides are listed in table.

Accession Number (UniProtKB)	*Gene name*	*Score*	*Unique peptides*	*Type of experiments*	*Description*
O75385	ULK2-Human	45	2	Co-IP (Biotin)	**unc-51-like kinase 2**

[4] *http://www.uniprot.org/*
[5] *http://www.ncbi.nlm.nih.gov/pubmed*

To verify that ULK2 directly interacts with RIM1α, GST-pull down binding assays were performed between full-length ULK1, ULK2, and the C2-domains of RIM1α (C2A and C2B) (*Fig. 4.9A*). Purified GST-RIM1α C2A and GST- RIM1α C2B bound to FLAG-tagged ULKs overexpressed in HEK293T cells. Negative controls, represented by GST and the agarose matrix, did not reveal any unspecific binding to ULK proteins (*Fig.4.9B*).

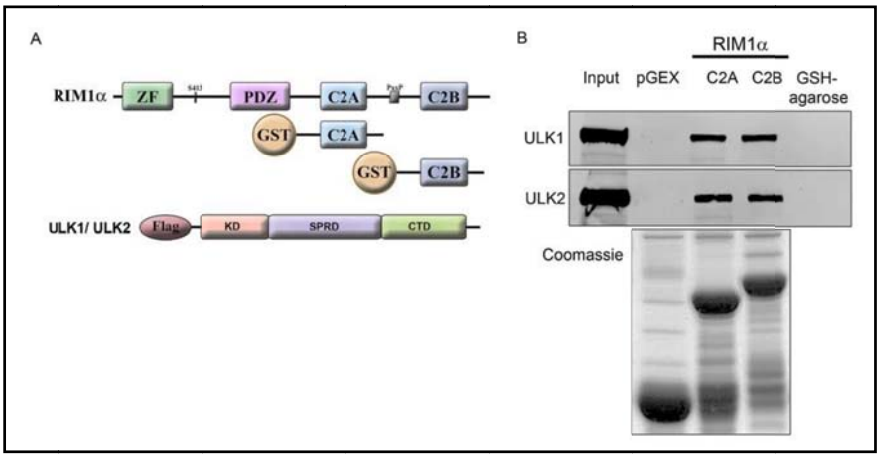

Figure 4.9: **ULK1 and ULK2 bind to RIM1α in GST-pull down assays.** ***(A)*** Schematic representation of the full-length ULK1 and ULK2 protein structure, and the RIM1α domains used in the pull-down assay. ***(B)*** ULK1 and ULK2 overexpressed in HEK293T cells, were incubated for 2h/4°C with GST-RIM1α C2A and GST-RIM1α C2B, respectively, followed by SDS-PAGE and immunoblotting with FLAG anti-mouse antibody. In the lower panel the amounts of GST fusion proteins used in the binding reaction were visualized by Coomassie staining. Number of independent experiments, N = 8. ZF, zinc finger domain; KD, kinase domain; SPRD, serine proline rich domain; CTD, C-terminal domain.

4.1.3.1.2 The ULK-kinase domain mediates binding to RIM1α

To identify which parts of ULK1/2 were responsible for the binding to the C2-domains of RIM1α, the individual ULK-domains (kinase domain, serine-proline rich domain, C-terminal domain; *Fig.4.10A*) were tested in GST-pull down assays. The individual FLAG-tagged ULK domains were overexpressed in HEK293T cells and respective proteins incubated with GST-RIM1α C2A and GST-RIM1α C2B. Of all domains tested, only the kinase domains displayed a strong and reproducible affinity for RIM1α (*Fig.4.10B*). A weak interaction was also observed in the case of the C-terminal domain of ULK1 to GST-RIM1α C2A and GST-RIM1α C2B, respectively. For the C-terminal domain of ULK2 no binding was detected.

Next, two reported point mutations in the kinase domain of ULK1 and ULK2 were analysed in binding assays. The lysine residue was exchanged with either arginine in the kinase domain of ULK1 (K46R-TOMODA et al., 1999) or with threonine in ULK2 (K39T- YAN et al., 1999). These mutations were reported to impair the ATP binding and as a consequence ULKs'autophosphorylation was abolished. GST-pull down assays showed that the association between the mutated ULK kinase domain and the GST-fusion proteins (C2A and C2B of RIMα) was abolished (*Fig. 4.10B)*. Full-length FLAG-tagged ULK1/2 kinase dead proteins

showed no binding to the C2-domains of RIM1α, as well (*Fig. 4.10 C*).

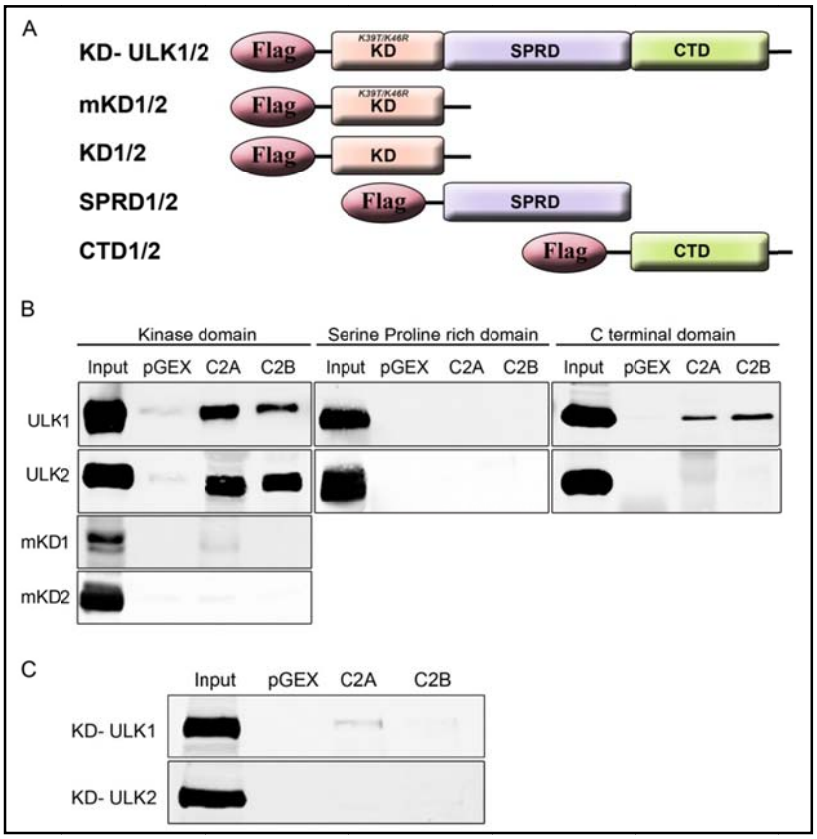

Figure 4.10:* RIM1α binds to the ULK kinase domain.** ***(A) Schematic representation of the FLAG-tagged kinase dead ULK1/2 and the FLAG-tagged ULK1/2 domains. ***(B)*** Different domains of ULK1/2 kinases, fused to a FLAG-tag, were overexpressed in HEK293T cells and tested for binding to GST-RIM1α C2A and GST-RIM1α C2B, respectively. Number of independent experiments, N=3-6. Mutations of the ATP binding site abolished the binding to the C2-domains of RIM1α (N=1). ***(C)*** Western blot of a GST- pull down assay revealed that full-length kinase dead mutants of ULK1 and ULK2 show no binding to GST-RIM1α C2A nor to GST- RIM1α C2B (N=1). N, Number of independent experiments.

4.1.3.1.3 ULK1/2 partially co-localize with endogenous RIM1/2 at synapses

To investigate if ULK kinases and RIM1α co-localize at the synapse, rat primary cortical neurons were fixed at DIV14 and labelled using antibodies against the endogenous proteins. Two of the antibodies tested against ULK1 showed a weak punctate staining, partially overlapping with RIM1/2 (*Fig.4.11A; Fig.4.12, upper panel*). Similar results were observed for ULK2 (*Fig. 4.11B, Fig.4.13, upper panel*). Moreover, ULK1 and ULK2 kinases seemed to co-localize to a certain degree also with the presynaptic marker, Bassoon (*Fig. 4.12 and 4.13, middle panel*), and the postsynaptic protein, PSD95 (*Fig. 4.12 and 4.13, lower panel*). In all immunofluorescence experiments a strong signal for the endogenous ULK1 and ULK2 was detected in the soma of the neurons.

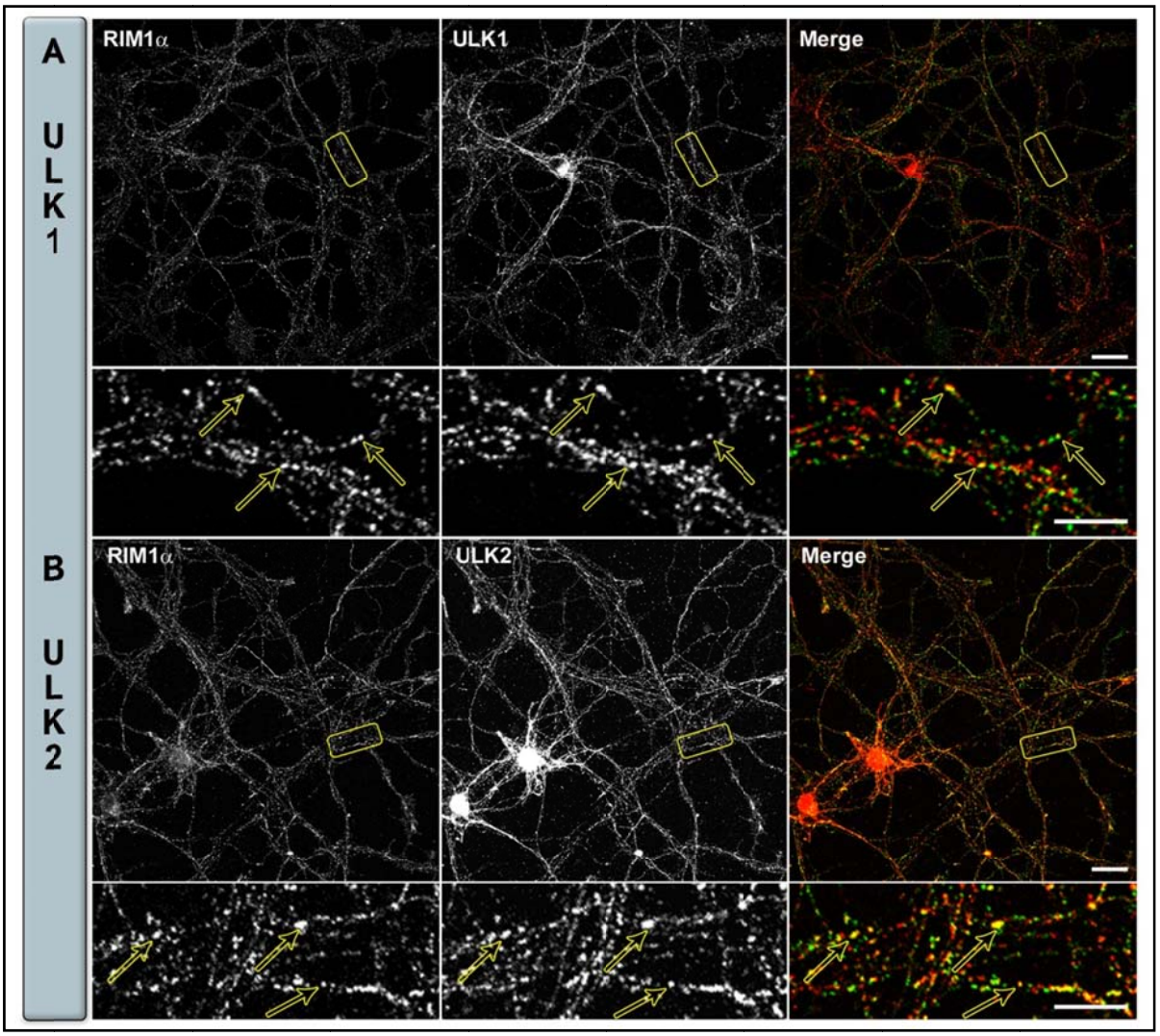

***Figure 4.11*: ULK1 and ULK2 partially co-localize with endogenous RIM1α.** At DIV 14, primary rat cortical neurons were fixed and stained against endogenous RIM1 (BD Bioscience) and ULK1 (Bioss) (panel **A**), and RIM1 (BD Bioscience) and ULK2 (Pierce) (panel **B**). Yellow arrows indicate a co-localization between these two proteins. Images were acquired using a laser-scanning confocal microscope (Nikon A1/Ti). Scale bar: 20µm (overview); 10 µm (insets).

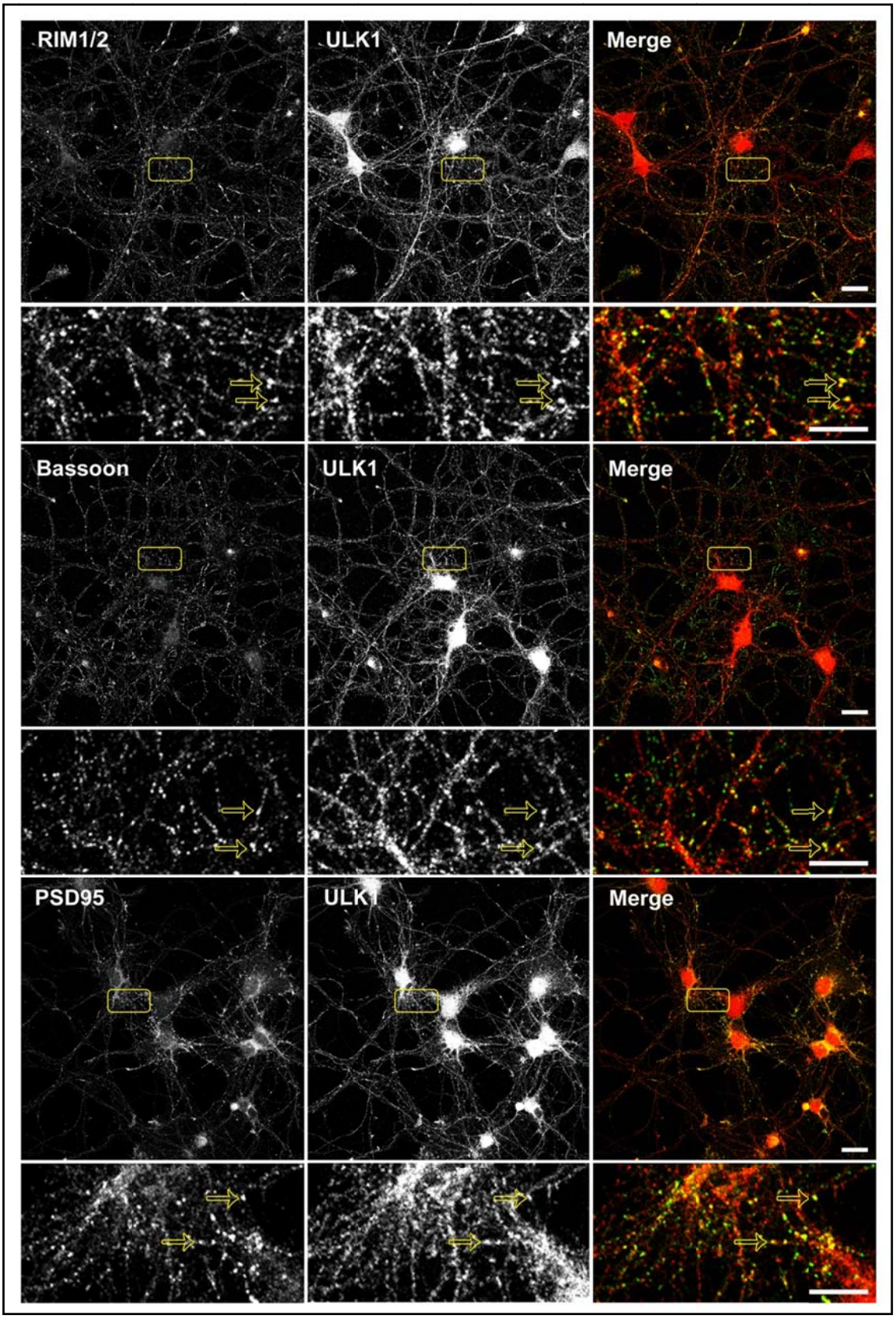

Figure 4.12: **Subcellular localization of endogenous ULK1 in rat cortical neurons.** At DIV 14, primary rat cortical neurons were fixed and stained against endogenous RIM1 (BD Bioscience) (*upper panel*), Bassoon (Covance) (*middle panel*), PSD95 (NeuroMab) (*lower panel*) and ULK1 (Aviva). Yellow arrows indicate a co-localization of these proteins. Images were acquired using a laser-scanning confocal microscope (Nikon A1/Ti). Scale bar: 20µm (overview); 10 µm (insets).

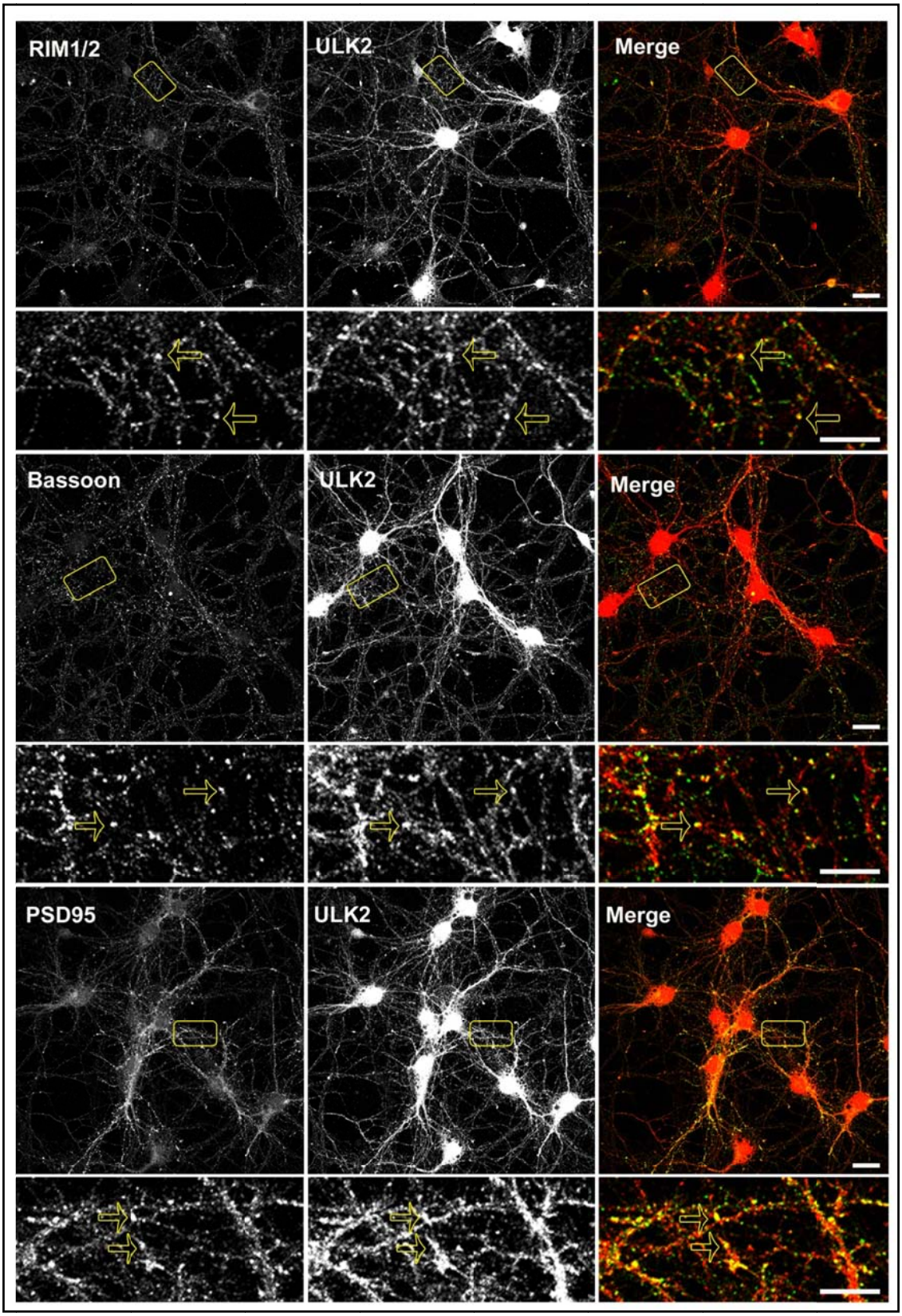

Figure 4.13: **Analysis of the subcellular distribution of endogenous ULK2 in rat cortical neurons.** At DIV 14, primary rat cortical neurons were fixed and stained against endogenous RIM1 (BD Bioscience) (*upper panel*), Bassoon (Covance) (*middle panel*), PSD95 (NeuroMab) (*lower panel*) and ULK2 (Pierce). Yellow arrows indicate a co-localization of the tested proteins. Images were acquired using a laser-scanning confocal microscope (Nikon A1/Ti). Scale bar: 20µm (overview); 10 µm (insets).

To measure the degree of co-localization between the ULK kinases and the pre- and postsynaptic markers, pictures were analysed using the JACOp plug-in in the ImageJ software (BOLTE and CORDELIERS, 2006). The calculated Pearson's coefficient indicated a high degree of co-localization between ULK1/2 kinases and the presynaptic proteins, Bassoon and RIM1/2. In addition, ULK1/2 seems to be present, even in higher amounts, in the postsynaptic site. This is suggested by a higher degree of co-localization between ULK1/2 and the postsynaptic marker, PSD95 (*Fig. 4.14*).

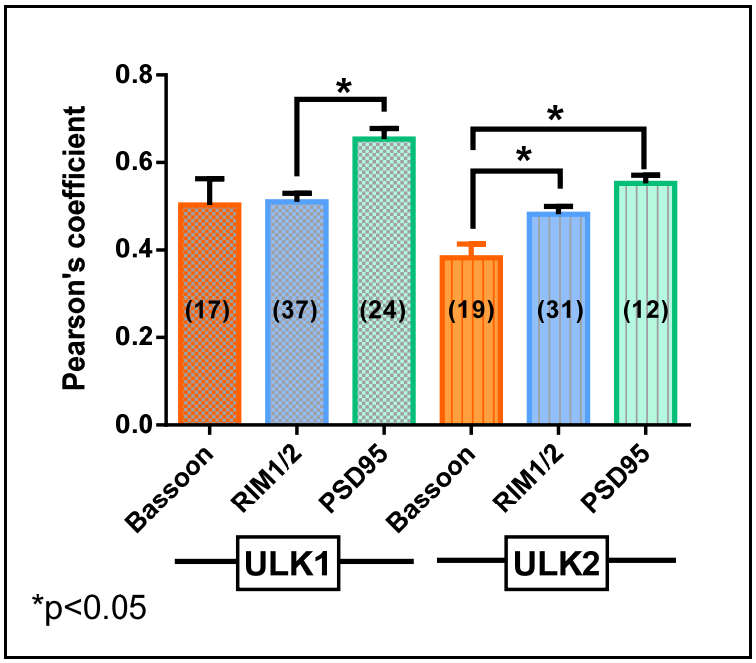

***Figure 4.14:* Quantitative analysis of the co-localization of ULK1/2 with different synaptic markers.** Pictures were analysed in ImageJ, measuring the Pearson's coefficient (JACOp plug-in). Values in bars indicate the number of cells analysed. Statistical analysis was performed in GraphPad Prism6, performing one-way ANOVA (Kruskal-Wallis test), followed by Dunn's multiple comparisons test. Bars show mean ± SEM. *p<0.05.

4.1.3.1.4 Generation of a short-hairpin RNA against ULK2

Biochemistry, as well immunofluorecence data suggest an interaction between RIM1α and ULK kinases. Therefore, to study the functional relevance of this interaction, shRNAs against ULK1 and ULK2, respectively, were designed and tested in HEK293T cells (*Fig.4.15A*). All four chosen shRNA efficiently knock-downed overexpressed FLAG-tagged ULK2. Three of these pairs had no effect on ULK1 protein levels, while pair no.4 reduced slightly the level of the ULK1 protein (*Fig. 4.15B*). Furthermore, these results were also confirmed by immunofluorescence using HEK293T cells (*Fig. 4.15C*). Overexpression of GFP-tagged ULK2 in HEK293T cells was accompanied by cells rounding up and detaching. These effects were abolished by shRNA-mediated knock-down of FLAG-tagged ULK2.

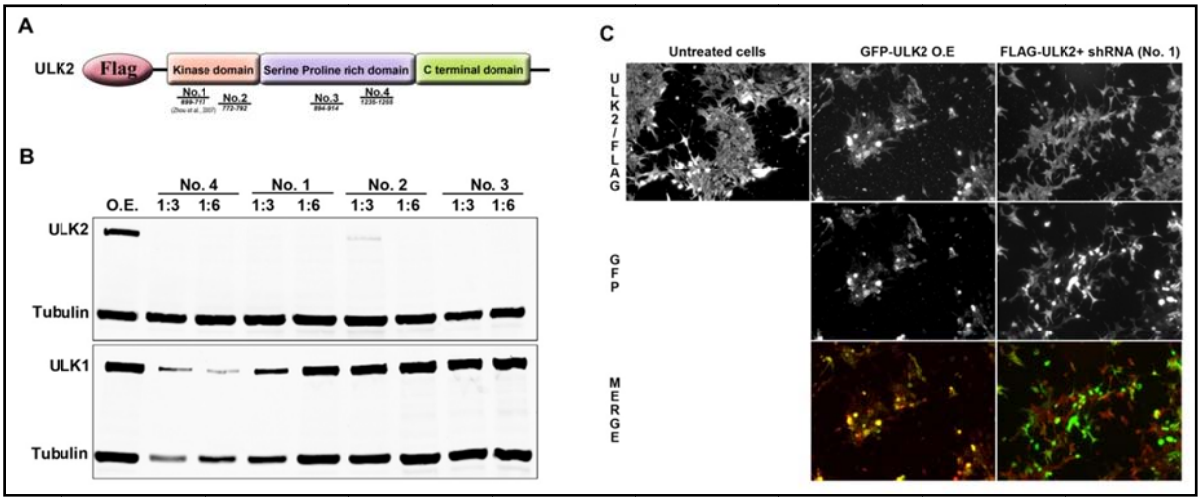

Figure 4.15:* shRNA mediated ULK2 knock down.** ***(A) Schematic representation of the full-length ULK2 and the position of the four different shRNA pairs. ***(B)*** 72h post transfection, overexpressed ULK2 was efficiently knocked down by all four shRNAs, while overexpressed ULK1 remained unaffected. The ratio represents the amount of transfected DNA in µgr (1µgr ULK2 or ULK1, and 3 and 6 µgr shRNAs) . ***(C)*** Immunofluorescence of HEK293T overexpressing either GFP-ULK2 alone or FLAG-ULK2 in the presence of shRNA (GFP). Cells were fixed and stained against the endogenous ULK2 (anti-rabbit Cy3) and FLAG (anti-mouse FITC). O.E, overexpression.

Five pairs of shRNAs targeting ULK1 were also tested in HEK293T cells, but none of them showed any efficiency in knocking-down overexpressed ULK1 (data not shown). As the available antibodies against either ULK1 or ULK2 did not give a specific signal in immunoblotting of lysates from either mouse brain or mouse primary cortical neurons, knock-down efficiency could not be analysed in these cells.

4.1.3.2 Serine-arginine protein kinase 2 (SRPK2)

At *D. melanogaster* SRPK79D kinase was shown to prevent the premature formation of T-bars in axons (JOHNSON et al., 2009; NIERATSCHKER et al., 2009). Furthermore, SRPK79D co-localizes with the T-bar associated protein, Bruchpilot (Brp) and its overexpression leads to a disruption of Brp localization at synapses and impairment in synaptic transmission (JOHNSON et al., 2009). The mammalian homolog SRPK2 was reported in Alzheimer's disease to hyperphosphorylate Tau protein, thus leading to impairment in microtubules polymerisation and axon elongation (HONG et al., 2012).

Due to the involvement of SRPK2 in active zone assembly, its possible association with the presynaptic protein RIM1α was investigated using different binding assays. Moreover, no presynaptic proteins to act as substrates for this kinase have been reported to date.

4.1.3.2.1 SRPK2 targets RIM1α

The analysis of our mass-spec data revealed that SRPK2 kinase associated exclusively with the C2A-C2B region of RIM1α, under all experimental conditions (*Table 4.5*).

In addition, co-immunoprecipitation of overexpressed FLAG-tagged RIM1α C2A-C2B from rat primary cortical neurons followed by MS, also revealed its association with SRPK2 protein (MS score: 92,24).

Experiments performed with crude synaptosomes showed the same affinity between the C2A-C2B domains of RIM1α and SRPK2 kinase, under all pharmacological treatments. However, in comparison to control and staurosporine conditions, application of phosSTOP increased the amount of the detected kinase. Therefore, the MS scores as well as the sequence coverage and the number of unique peptides were increased when phosphatase inhibitor was applied to mouse crude synaptosomes (*Table 4.6, phosSTOP; Fig. 4.16A*). RIM1α ZF-PDZ did not bind SRPK2 kinase. Therefore, this supports the specificity of the SRPK2 binding to the C2-domains of RIM1α.

***Table 4.5:* Detection of the SRPK2 kinase as RIM1α binding protein by mass-spec under different experimental conditions.** Mass scores are listed in correlation to various experimental conditions. Five independent experiments were performed.

Accession Number (UniProtKB)	*Gene name*	*Score*	*Sequence coverage*	*Unique peptides*	*Type of experiments*	*Description*
O54781	SRPK2-MOUSE	92,24	6,75	4	Co-IP from neurons	SRSF protein kinase 2
		32	4,41	2	Control	
		169,47	7,49	4		
		59,05	6,02	3	Staurosporine	
		175,72	9,54	5	phosSTOP	
		129	9,1	4		
		175,63	7,93	4		
		266,65	10,57	6		

Because the kinase SRPK2 was identified with high scores in MS to bind to the C2A-C2B domains of RIM1α, the direct interaction between these proteins was further investigated. Thus, GST-constructs containing either the C2A- or C2B-domain of RIM1α were used to examine the binding to endogenous SRPK2 from mouse brain or rat cortical neurons. GST-fusion proteins were incubated for several hours with either lysed crude synaptosomes or lysed rat primary cortical neurons, followed by SRPK2 detection by immunoblotting. In all cases, only the C2A-domain pulled down the native SRPK2, while the C2B domain did not bind the SRPK2 kinase (*Fig. 4.16B, control panels*).

Since in the MS data an increase in SRPK2 level was detected upon phosphatase blockade (*Fig. 4.16A*), the same pharmacological treatment was applied to either crude synaptosomes or primary cell culture, in order to test for changes in the binding affinity. Nevertheless, no detectable change in the binding affinity between SRPK2 and C2A-domain of RIM1α was observed compared to control (*Fig. 4.16B*, *staurosporine and phosSTOP panels*).

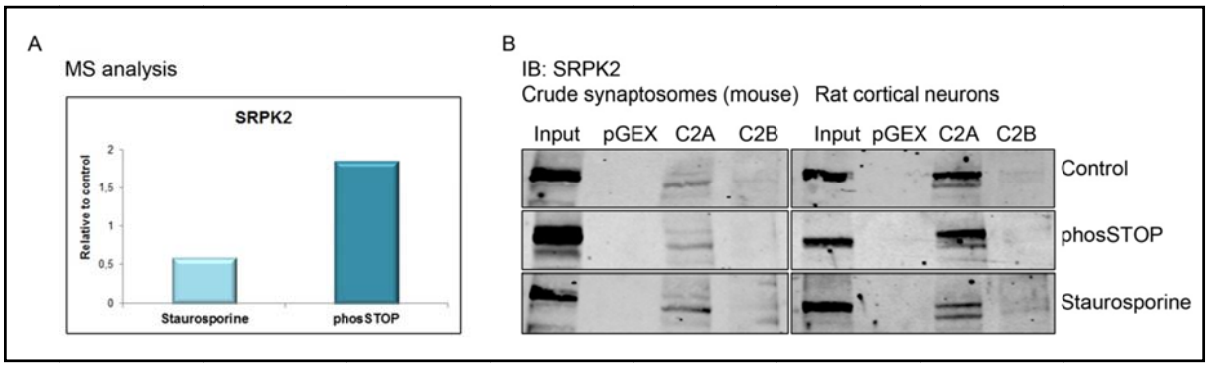

Figure 4.16:* SRPK2 binds specifically C2A-domain of RIM1α in GST-pull down assays**. ***(A) Mass spectrometry data revealed that SRPK2 was detected with higher scores in samples pre-treated with phosphatase inhibitors compared to staurosporine treatment. MS scores of staurosporine and phosSTOP were divided by the control's scores, and the remaining values plotted as relative to control (N=4). ***(B)*** GST-C2A RIM1α and GST-C2B RIM1α were incubated with crude synaptosomes obtained from mouse or with lysed rat cortical neurons for 2h/4°C, followed by SDS-PAGE and immunoblotting with mouse anti-SRPK2 antibodies (N=6). In parallel, samples (unlysed crude synaptosomes or cortical neurons) were treated with staurosporine (1μM) or with phosSTOP (1x) before the binding assay. The same concentration of inhibitors was maintained during the incubation with the GST-fusion proteins. N, number of independent experiments; IB, immunoblotting.

These positive results were further confirmed by using a GST-SRPK2 construct, which was able to capture either full-length untagged RIM1α or the FLAG-tagged C-terminal part of RIM1α, overexpressed in HEK293T cells (*Fig. 4.17*).

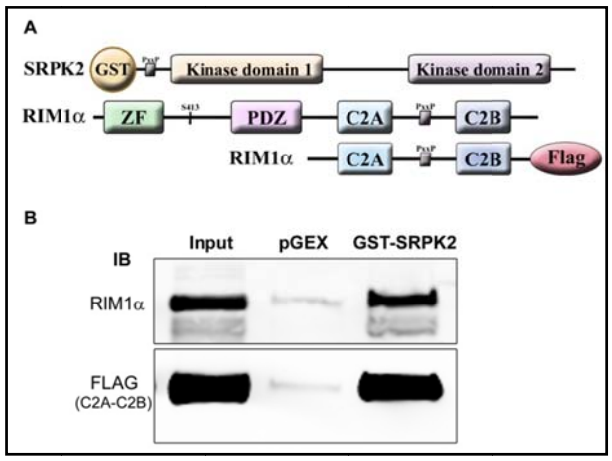

Figure 4.17*: GST-SRPK2 captures both full-length RIM1α as well as the C-terminal part of RIM1α, containing the C2-domains.** ***(A) Schematic representation of the constructs used in the GST-pull down assays. ***(B)*** HEK293T cell lysates containing either RIM1α or FLAG-tagged RIM1α C2A-C2B were incubated for 1h/4°C with GST-SRPK2. Beads were washed extensively and boiled in Laemmli buffer, followed by immunoblotting and detection using either an anti-RIM1/2 antibody or an anti-FLAG antibody (N=3). N, number of independent experiments; IB, immunoblotting.

To further confirm the positive interactions of the GST-pull down assays, co-imunoprecipitations using HEK293T cells were performed. HEK293T cell lysates containing overexpressed GFP- tagged SRPK2 and FLAG-tagged C2A-C2B of RIM1α were subject to

immunopurifications using either FLAG- or GFP-magnetic beads. The C-terminal region of RIM1α containing the entire set of C2-domains (C2A and C2B) was able to co-immunoprecipitate the GFP-tagged full-length SRPK2 (*Fig. 4.18B*). This positive binding was further validated by using also the GFP-magnetic beads (*Fig. 4.18C*).

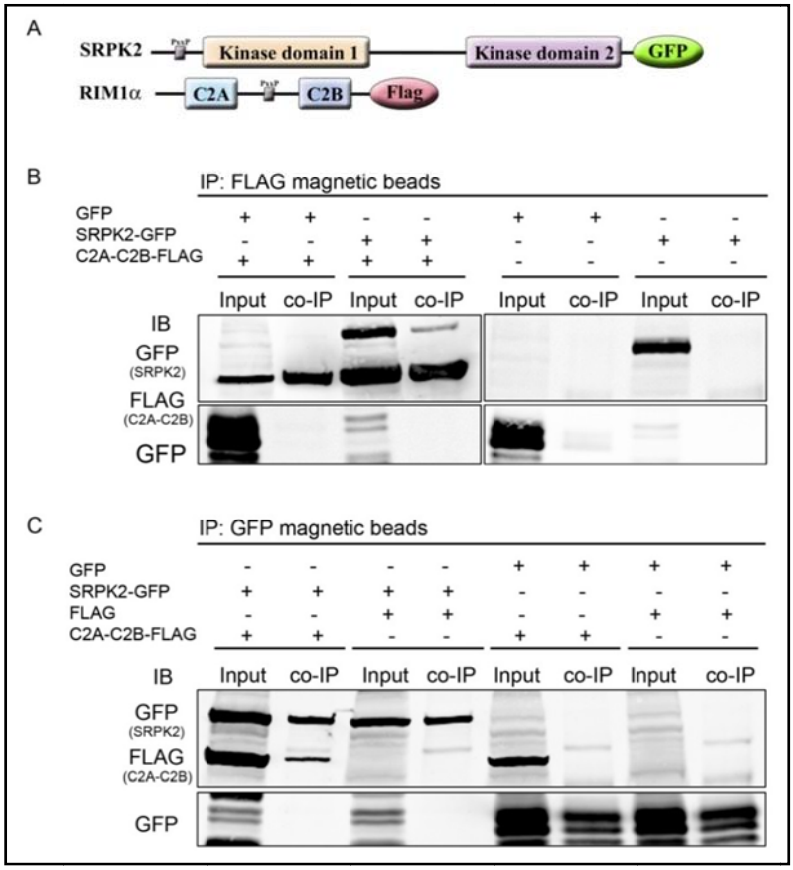

Figure 4.18: **GFP-tagged SRPK2 binds the RIM1α C2-domains in co-IP assay**. ***(A)*** Schematic representation of the GFP-tagged full-length SRPK2 and the FLAG-tagged C2A-C2B domain of RIM1α. ***(B/C)*** HEK293T cells were transfected with the above shown constructs and co-IP was performed with either FLAG- (N=1) or HA-magnetic beads (N=1). After the incubation the beads were washed and boiled in SDS-Laemmlli buffer followed by SDS-PAGE and immunoblotting using anti-GFP and anti-FLAG antibodies. Constructs containing only GFP or FLAG sequence were additionally used as negative controls. N, number of repetitions; IB, immunoblotting; IP, immunoprecipitations.

SRPK2 contains two kinase domains, one in the N-terminal region and the other one in the C-terminal region. The fusion to GFP protein may affect not only the proper folding of SRPK2 but also its kinase activity. Thus, HA-tagged SRPK2 was further analysed in binding assays with RIM1α. Full-length SRPK2 co-immunoprecipitated with full-length RIM1α from HEK293T cells (*Fig. 4.19B*). These results were further confirmed by co-IPs using only the truncated version of RIM1α containing the C2-domains and full-length SRPK2 (*Fig. 4.19D and E*).

Serine arginine kinases, like SRPK2, are able to phosphorylate serines from RS or SR dipeptides in a basic environment with arginine or histidine (WANG et al., 1998). Substrate phosphorylation mediated by SRPK2 kinase requires three elements: (1) SR or RS dipeptides; (2) a basic environment around the dipeptides; and (3) the absence of the Lysine (K) residue at position -2. Moreover, substrate specificity of SRPK2 determined by peptide selection indicates proline (P), polar (N and Q) and acidic amino acids (D and E) as possible residues surrounding the RS dipeptides (WANG et al., 1998).

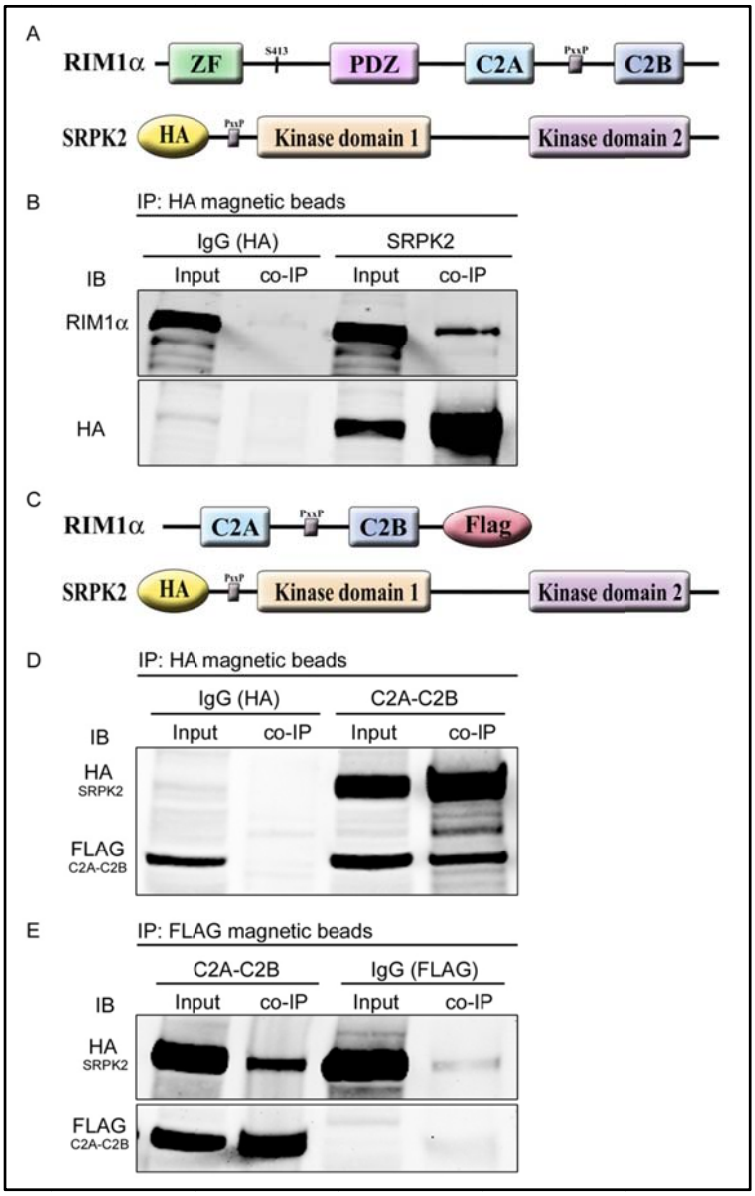

Figure 4.19: **HA-tagged SRPK2 binds the C2A-C2B domains of RIM1α.** ***(A/C)*** Schematic representation of the HA tagged full-length SRPK2, RIM1α and FLAG tagged C2A-C2B. ***(B)*** SRPK2 was able to capture full-length RIM1α. Lysates of transfected HEK293T were incubated with HA magnetic beads for 2h/4°C, followed by RIM1α detection by immunoblotting (N=4). ***(D)*** Immunoprecipitation with HA-magnetic beads showed SRPK2 to bind strongly the truncated form of RIM1α containg only the C2-domains (N=5). ***(E)*** Truncated form of RIM1α was also able to pull SRPK2 from the HEK293T lysates (N=3). N, number of repetitions; IB, immunoblotting; IP, immunoprecipitations.

The *R. norvegicus* RIM1α protein sequence was screened for similar recognition sites, excluding, however, the alternatively spliced exons from the analysis. In the end, similar motifs were identified in RIM1α: two close to the Zn^{2+}- finger domain and another two in the vicinity of the C2A-domain (*Fig. 4.20; Table 4.6*). Nevertheless, SRPK2 may recognize also other unconventional sites, like 'PSLP', described in tau proteins (HONG et al., 2012). Therefore, such unconventional sites may have been overlooked.

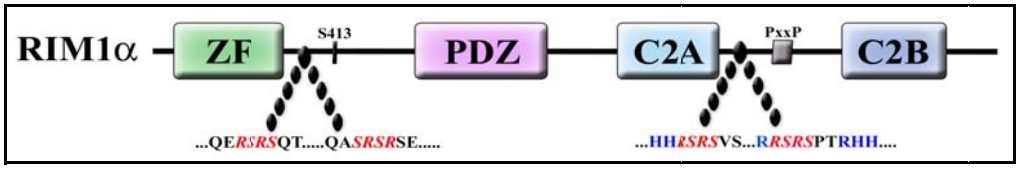

Figure 4.20: **Schematic representation of full-length RIM1α with its possible SRPK2 recognition motifs.** Two motifs are in the vicinity of the zing finger (ZF), and the other two near the C2A-domain. In red the RS/SR dipeptides are marked, while in blue the positively charged amino acid are depicted. Splice site B and C were excluded from the analysis.

***Table 4.6*: The distribution of amino acids surrounding the RS dipeptides.** Position 0 represents the serine phosphorylated by SRPK2. The other amino acid residues are represented as follows: in blue arginine (R) and in red histidine (H) residues necessary for conferring the basic environment; proline (P) preferred in position +1, depicted in green; glutamine (Q) and glutamic acid (E) in lila. The positions of the amino acid residues are in accordance with the study of Wang et al. (WANG et al., 1998).

Region/position	Amino acid residues									
	-4	-3	-2	-1	0	+1	+2	+3	+4	+5
ZF	E	R	S	R	**S**	Q	T	P	L	S
	Q	A	S	R	**S**	R	E	P	P	R
C2A	H	R	S	R	**S**	V	S	P	H	R
	R	R	S	R	**S**	P	T	R	H	H

To test the implication of these recognition motifs in the direct binding of SRPK2, co-IP assays were performed with HEK293T cells overexpressing GFP-tagged SRPK2 and a construct harbouring two of the identified possible RS motifs (RIM1α C2A). The RIM1α C2A-domain was able to bind full-length GFP-tagged SRPK2 (*Fig. 4.21B*). The other two recognition motifs in the vicinity of the ZF domain were not tested in the binding assays, since the construct containing both the zinc-finger and the PDZ domain did not show any association with SRPK2 in the mass-spec experiments.

Taken together, multiple biochemical assays revealed the specific interaction between the SRPK2 kinase and the C2A-domain of the RIM1α protein.

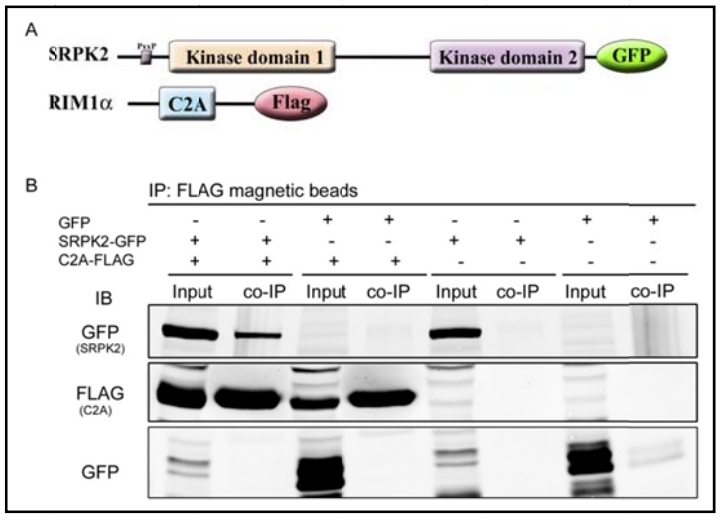

Figure 4.21:* The RIM1α C2A-domain binds to SRPK2.** ***(A) Schematic representation of the GFP-tagged full-length SRPK2 and the C2A-domain of RIM1α. ***(B)*** HEK293T cells were transfected with above depicted constructs and a co-IP was performed with FLAG magnetic beads (N=1). After the incubation the beads were washed and boiled in SDS-Laemmlli buffer followed by SDS-PAGE and immunoblotting using anti-GFP and anti-FLAG antibodies. Constructs containing only GFP or FLAG sequence were additionally used as negative controls. N, number of repetitions; IB, immunoblotting; IP, immunoprecipitations.

4.1.3.2.2 Non-kinase core regions do not mediate direct binding to RIM1α

To identify which region of the SRPK2 kinase might mediate the binding to RIM1α, three different constructs were tested in co-IP binding assays using HEK293T cells. SRPK2-DM (docking groove mutant), with a domain organization identical to SRPK2-WT, contained four mutated amino acids in the docking groove of the catalytic domain 2, in order to weaken the phosphorylation and binding to different substrates (*Fig. 4.22A*). SRPK2-ΔNSI had all the non-kinase core regions (linker region, N-terminal region) deleted; while in SRPK2-ΔSI only

the linker region was removed (LIANG et al., 2014). These constructs were overexpressed in HEK293T cells together with full-length untagged RIM1α, followed by co-IP using HA-magnetic beads, and detection of binding by immunoblotting using an anti-RIM1/2 antibody.

The binding experiments, using WT-SRPK2 and the mutated SRPK2 variants, revealed small changes in the affinity for full-length RIM1α (*Fig.4. 22B*). Even though all SRPK2 mutants displayed a weaker binding affinity for RIM1α versus WT, SRPK2-ΔNSI showed the strongest reduction in the binding affinity (p= 0.0049; *Fig. 4.22C*).

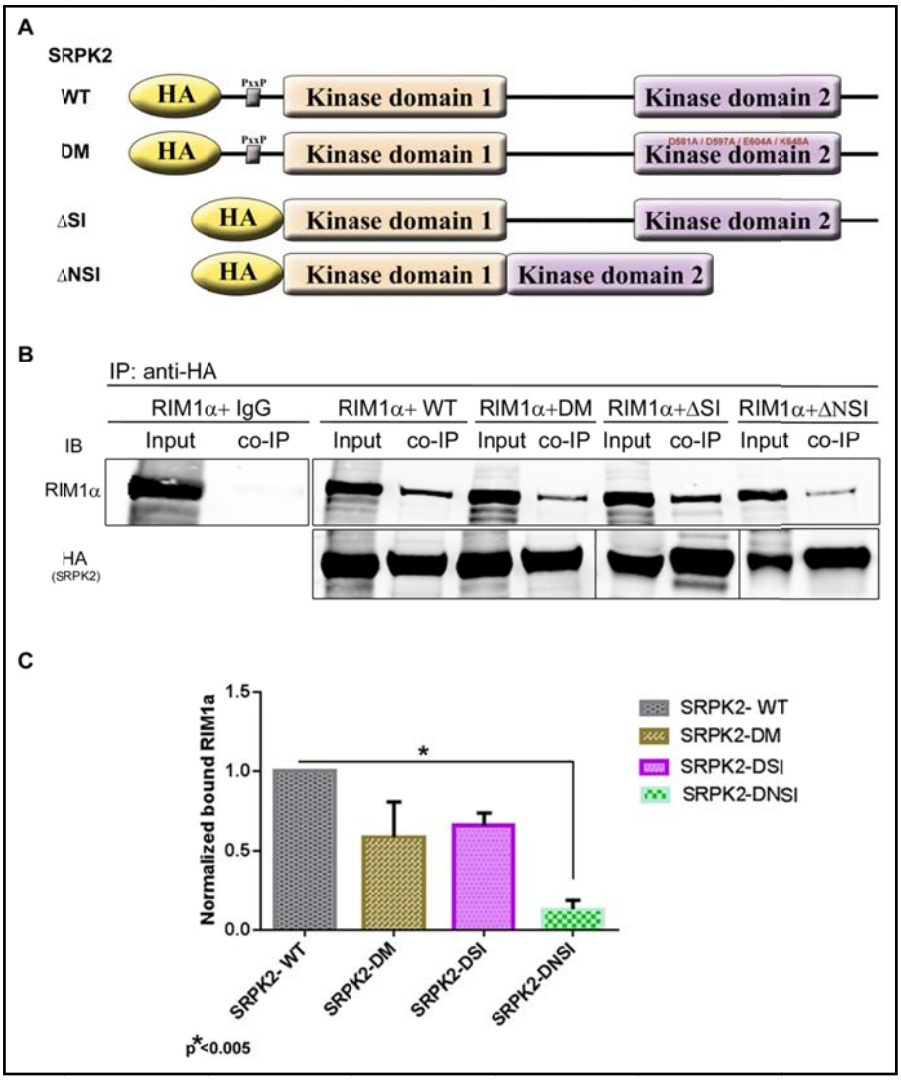

Figure 4.22:* The SRPK2 kinase domains mediate binding to RIM1α.** ***(A) Schematic representation of the WT and mutated proteins used in the binding assay. SRPK2-DM contains four point mutations in the docking groove (depicted in red); SRPK2-ΔSI lacks the N-terminal region, while in SRPK2-ΔNSI the entire non-kinase core regions are deleted. ***(B)*** HEK293T cells were transfected with above shown constructs and co-IP was performed with HA magnetic beads (N=4). After the incubation the beads were washed and boiled in SDS-Laemmlli buffer followed by SDS-PAGE and immunoblotting using anti-HA and anti-RIM1/2 antibodies. ***(C)*** Quantification of the binding affinity between overexpressed RIM1α, wild type SRPK2 and different mutants. The levels of RIM1α input and co-IPs were normalized to the level of HA-tagged SRPK2. Next, the input lane of each binding reaction was used to normalize the level of the corresponding co-IP. The final results were compared to SRPK2-WT. Error bars show SEM. Statistic was performed in PrismGraph using nonparametric ANOVA followed by Dunn's multiple comparisons test (N=4). N, number of independent experiments; IB, immunoblotting; IP, immunoprecipitations.

4.1.3.2.3 The effect of SRPIN340 inhibitor on the SRPK2 co-localization with endogenous RIM1α

Since the biochemistry data suggests a potential interaction between the SRPK2 kinase and the presynaptic protein RIM1α, co-localization of these proteins was further investigated in rat primary neuronal culture.

Additionally, to understand the effect of SRPK2 kinase activity on RIM1α, a selective inhibitor for serine-arginine protein kinases was studied in primary neuronal cells. SRPIN 340[6] is a specific inhibitor for SRPK1, shown not to inhibit other classes of Serine-Arginine-Rich Protein Kinases (SRPKs) (KARAKAMA et al., 2010). 10μM inhibitor was applied to primary cell culture at DIV12-14 for duration of 16h, followed by fixation and labelling against the endogenous SRPK2 and RIM1α proteins. Co-localization was measured using the Pearson's coefficient (JACOp plug-in, part of ImageJ program).

Analysis revealed that in comparison to the DMSO negative control, a slight increase in SRPK2 co-localisation with RIM1α (*Fig. 4.23; Fig. 4.24 p=0.0286*) was observed after treatment with SRPIN340. However, since the number of independent experiments is limited to N=2, further repetitions will be required to confirm these results.

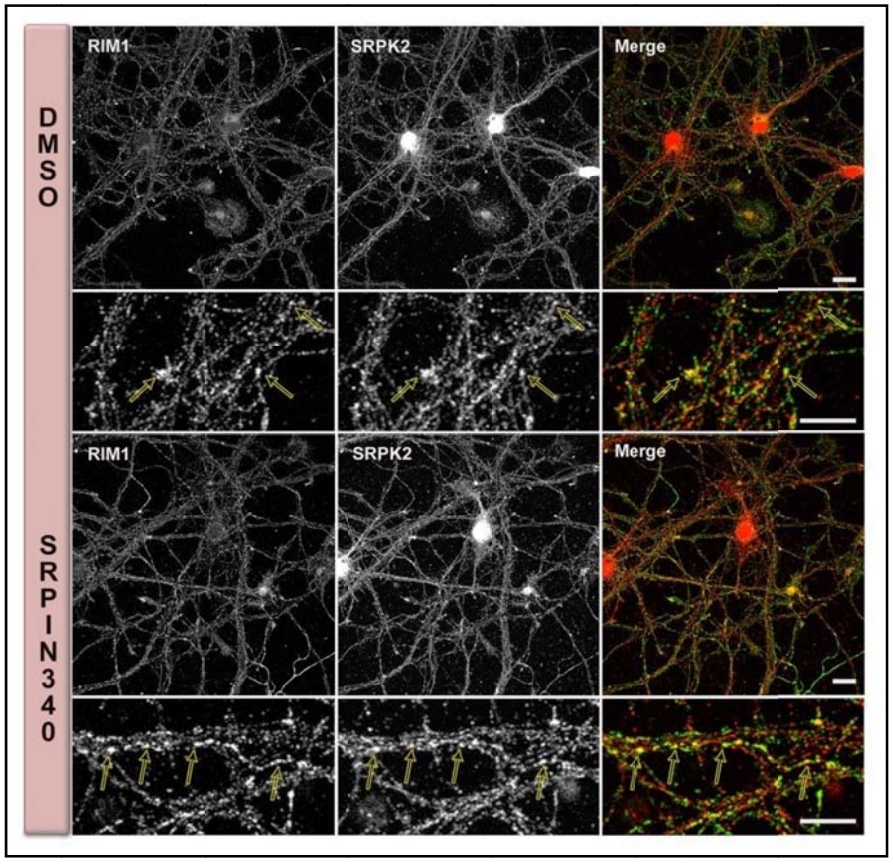

Figure 4.23: **The effect of SRPK inhibitor on RIM1α-SRPK2 co-localization.** DIV12-14 rat cortical neurons were incubated with 10μM SRPK inhibitor (SRPIN340, Axon Medchem) for 16h., followed by fixation in paraformaldehyde and staining for the endogenous SRPK2 (Bioss) and RIM1 (BD Bioscience). Negative control (*upper panel*) is represented by cells treated with the equivalent amount of DMSO. Images were acquired using a laser-scanning confocal microscope (Nikon A1/Ti). Yellow arrows indicate the co-localization between the SRPK2 kinase and the presynaptic protein RIM1. Scale bar: 20μm (overwiev); 10μm (insets).

[6] **SRPK1**: IC_{50} = 0.14 μM (mouse); **SRPK1**: K_i= 0.89 μM; **SRPK2**: IC_{50} = 1.8 μM (mouse) (source: Santa Cruz; Axon Medchem)

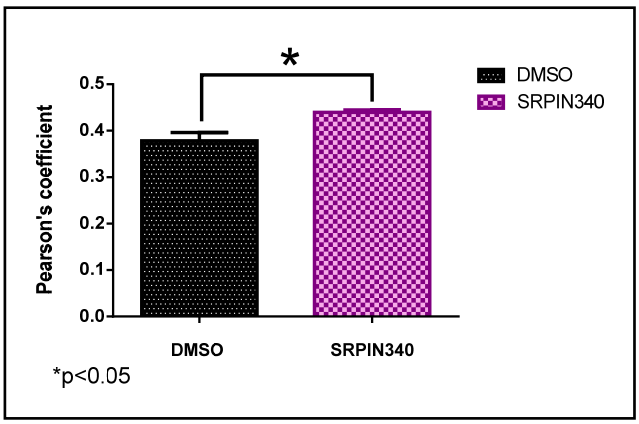

Figure 4.24: **SRPIN340 treatment induces a slight increase in co-localization of endogenous SRPK2 and RIM1/2 in primary cortical neurons.** At DIV14 rat cortical neurons were incubated with 10µM SRPK2 inhibitor (SRPIN340, Axon Medchem) for 16h, followed by fixation in paraformaldehyde and staining for the endogenous SRPK2 (Santa Cruz, 23) and RIM1/2. Co-localization was calculated using the Pearson's coefficient, part of the JACOp plug-in (ImageJ). Statistical analysis was performed in GraphPad Prism 6 using Man-Whitney test (two-tailed) (N=2). N, number of independent experiments.

4.1.3.3 Vesicle-associated membrane protein (VAMP) associated-protein A/B (VAPA/VAPB)

The first report on VAPA dates back to 1995 when, by using yeast two hybrid system, VAP-33 was identified in *Aplysia californica* to bind synaptobrevin-2/VAMP-2 and to play a role in synaptic transmission (SKEHEL et al., 1995). Several years later the mammalian homologs VAPA, VAPB and VAPC were characterized and their role in vesicle fusion and trafficking was suggested (WEIR et al., 1998; NISHIMURA et al., 1999). In accordance with the function of the *Aplysia californica* VAP-33, the *D.melanogaster* homologue DVAP-33 was reported to control synaptic bouton formation at the NMJ (PENNETTA et al., 2002) and to traffic proteins to axonal processes (YANG et al., 2012). VAPB protein was identified to contribute to normal dendrite morphology by taking part in ER-to-Golgi transport (KUIJPERS et al., 2013). A mutation in VAPB (P56S) was described to be the cause of a motor neuron disease (amyotrophic lateral sclerosis type 8-ALS8) (NISHIMURA et al., 2004). The role of VAP protein family in maintaining the AZ architecture has not been fully elucidated.

4.1.3.3.1 VAPA/VAPB binds RIM1α

The MS data revealed the VAPA protein as another possible candidate to bind the C2-domains of RIM1α (*Table 4.7*). The VAPA protein was identified, with a similar sequence coverage and number of unique peptides, in all three experimental conditions using crude synaptosomes. Analysis of the protein complexes co-immunoprecipitated with overexpressed RIM1α C2A-C2B domains in primary cortical neurons identified the VAPA protein with an even higher score (636, 10) and percentage of sequence coverage (40%).

Table 4.7: **Identification of VAPA as a novel RIM1α binding protein by MS.** Mascot scores are listed in correlation to various experimental conditions. Five independent experiments were performed.

Accession Number (UniProtKB)	*Gene name*	*Score*	*Sequence coverage*	*Unique peptides*	*Type of experiments*	*Description*
Q9WV55	VAPA-MOUSE	636,10	41,37	9	Co-IP – rat cortical neurons	**Vesicle-associated membrane protein-associated protein A**
		119,63	12,05	2	Control	
		127,37	12,05	2		
		47,79	13,25	2	Staurosporine	
		53,88	12,05	2		
		105,10	17,67	3		
		36,84	12,05	2	phosSTOP	
		31,27	12,05	2		

The VAP protein family includes besides VAPA (vap33) also VAPB/C protein. Although VAPB was not identified in the MS screen for novel RIM1α interaction partners, its interaction with RIM1α was examined, due to its high sequence homology with VAPA.

Next, *in vitro* binding assays were employed to investigate whether endogenous VAPA or VAPB/C could bind RIM1α. GST-pull down experiments were performed with GST-fusion proteins (GST-RIM1α C2A, GST-RIM1α C2B) and VAPA and VAPB proteins overexpressed in HEK293T cells. Immunoblotting revealed that VAP proteins bound strongly only the C2A-domain of RIM1α. These results were further validated by GST-pull downs using either whole mouse brain or primary rat cortical neurons (*Fig. 4.25B*).

Additionally, to identify which part of VAPA was mediating this interaction, different domains were separated and cloned into vectors containing the GST sequence. These newly generated GST- fusion proteins were incubated for several hours with HEK293T lysates containing overexpressed full-length RIM1α or FLAG- tagged C2A-C2B domains. Binding assays showed that only the major sperm protein domain associated with RIM1α, as well as with the C2-domains (*Fig. 4.25C*).

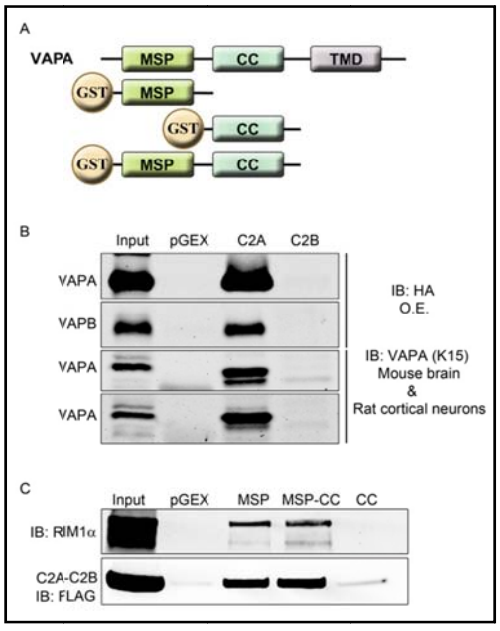

Figure 4.25: **Both VAPA and VAPB bind the C2A-domain of RIM1α.** ***(A)*** Schematic representation of full-length VAPA and the individual domains fused to GST. ***(B)*** Immunoblotting of the GST-pull downs showing the RIM1α C2A-domain to associate with VAPA from mouse brain (N=3), rat cortical neurons (N=1), HEK293T lysates (N=8) and VAPB (N=2). Detection of the endogenous or overexpresed VAPA was performed with an anti-VAPA antibody (K15, Santa Cruz). ***(C)*** The major sperm protein domain of VAPA binds both full-length as well as the truncated form of RIM1α (n=4). N, number of independent experiments; IB, immunoblotting.

4.1.3.3.2 Kinase inhibition strengthens the VAPA-RIM1α interaction

In our mass-spectrometry analysis, an increase in VAPA was detected when kinase activity was blocked. After the MS scores of controls were deduced from staurosporine and phosSTOP scores (treatment vs. control), the obtained values were plotted relative to control. An increase in detected VAPA protein was observed when kinase activity was inhibited compared to phosphatase inhibition (*Fig. 4.26A*).

To test whether the same treatment applied to crude synaptosomes had an effect on the binding affinity, GST-pull down experiments were performed in the presence of staurosporine or phosSTOP inhibitors. To this end, GST-fusion proteins (GST-RIM1α C2A and GST-RIM1α C2B) were incubated with crude synaptosomes or lysed primary rat cortical neurons pre-treated with 1µM staurosporine (30min) or 1x phosSTOP (1h), followed by immunoblotting and detection of VAPA protein. The binding reaction contained as well the same amount of staurosporine or phosSTOP inhibitors.

Compared to the phosSTOP and control conditions, an increase in binding affinity was observed in samples pre-treated with the kinase inhibitor (*Fig. 4.26B*).

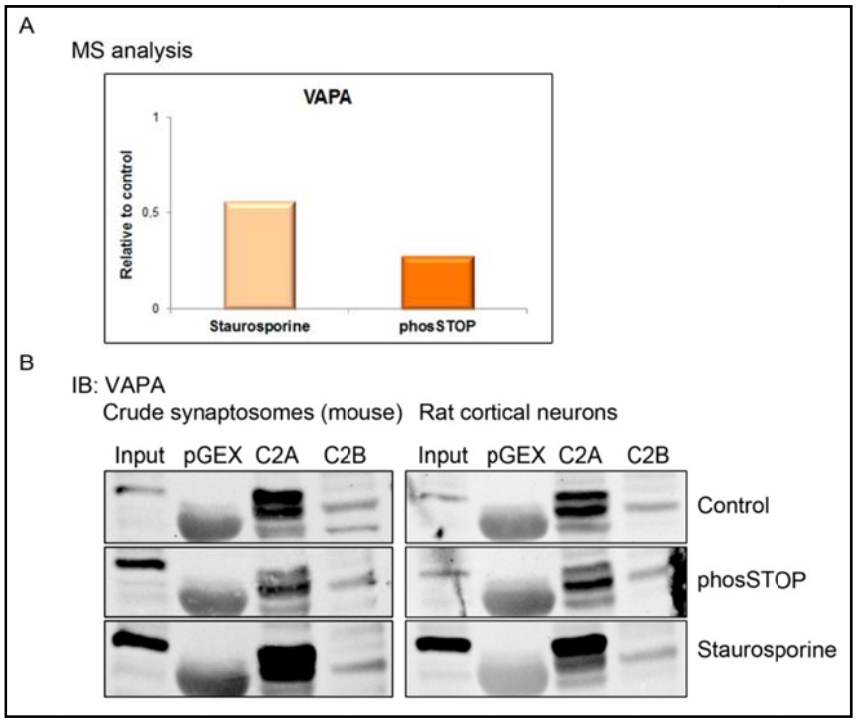

Figure 4.26: **Staurosporine treatment enhanced VAPA-RIM1α binding.** ***(A)*** VAPA was detected with higher scores in the MS, after kinase inhibition by stauroporine application. The data represents the mean of four independent experiments, and is plotted relative to control (N=4). ***(B)*** GST-RIM1α C2A and GST-RIM1α C2B were incubated with lysed crude synaptosomes (mouse brain) or with lysed primary rat cortical neurons for 2h/4°C, followed by SDS-PAGE and immunoblotting (N=4). In parallel samples were treated with staurosporine (1µM) or phosSTOP (1x) before and during the binding assays. Staurosporine treatment enhanced the association between the RIM1α C2A-domain and the endogenous VAPA compared to control or phosSTOP conditions. N, number of repetitions; IB, immunoblotting.

4.1.3.3.3 The T812/814A point mutations in the RIM1α C2A-domain impair binding to VAPA

Because the binding assays clearly indicated a direct binding between the RIM1α C2A-domain and VAP proteins, several RIM1α C2A mutants were tested in GST-pull downs. A previous report described a point mutation in the RIM1α C2A-domain (R844H) to be responsible for the autosomal dominant cone-rode dystrophy in humans (JOHNSON et al., 2003). Moreover, using bioinformatical tools, several amino acid residues were identified as potential targets for kinases. Two amino acids, predicted to be phosphorylated by protein kinase A, were mutated and tested in the binding assay.

GST-pull down experiments were performed with lysed rat primary cortical neurons, lysed crude synaptosomes or mouse whole brain. In all three cases, the T812/814A point mutations in the RIM1α C2A-domain impaired the binding to VAPA protein (*Fig. 4.27B*), while the R844H mutation did not have any influence on the binding affinity.

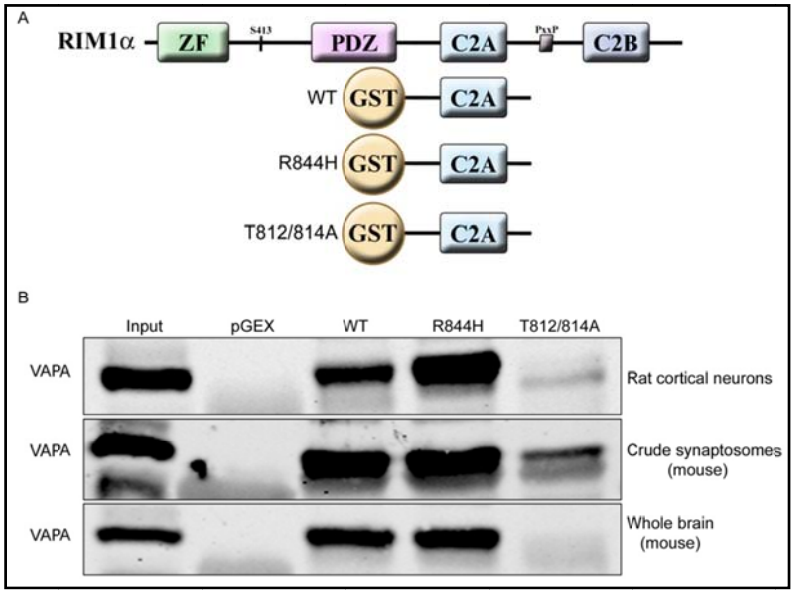

Figure 4.27: **Point mutations in the RIM1α C2A-domain impair VAPA binding.** ***(A)*** Representation of the full-length untagged RIM1α, the WT-C2A and the mutant C2A-domains (*R884H* and *T812/814A*) used in the GST-pull down assays. ***(B)*** The T812/814A mutations in the RIM1α C2A-domain, affecting the recognition motif for PKA, impaired binding to the endogenous VAPA (N=3). N, number of independent experiments.

4.1.3.3.4 VAP proteins bind RIM1α in co-IP assays

GST-pull down results were further confirmed by co-IP experiments. HEK293T cells overexpressing HA-tagged VAPA or VAPB and full-length RIM1α or FLAG-tagged RIM1α C2A-C2B, were subjected to co-immunoprecipitations using either HA- or FLAG-magnetic beads.

Full-length untagged RIM1α was precipitated by both VAPA and VAPB. The binding was also validated when only the truncated form, RIM1α C2A-C2B was used (*Fig. 4.28B and C*).

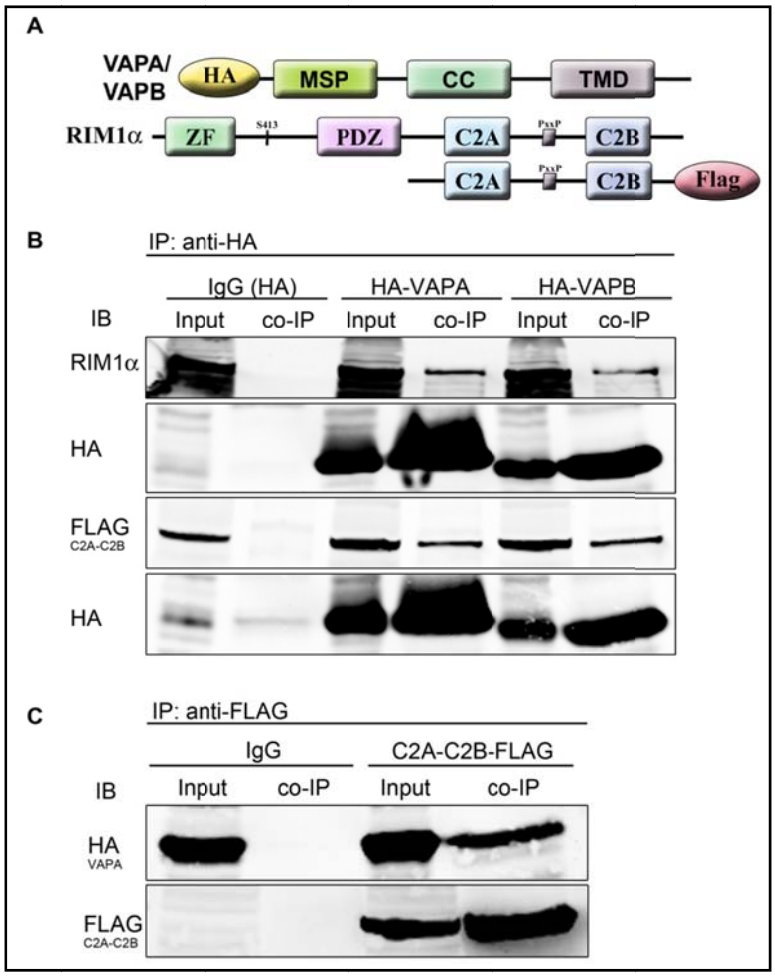

Figure 4.28: **Both VAPA and VAPB bind RIM1α.** ***(A)*** Schematic representation of the HA-tagged full-length VAPA and the untagged RIM1α. ***(B)*** Extracts of HEK293T cells transiently transfected with RIM1α (or RIM1α C2A-C2B-FLAG) and either HA-VAPA or HA-VAPB were subjected to co-IP with anti-HA magnetic beads. Co-IP reactions were incubated for 2h/4°C with HA-magnetic beads. Subsequently, beads were washed and boiled in SDS-Laemmlli buffer followed by SDS-PAGE. Input and precipitates were analyzed by immunoblot (IB) using RIM1α and FLAG antibodies (N=2-5). ***(C)*** A fusion protein consisting of only the C2-domains of RIM1α bound also full-length VAPA (N=3). N, number of independent experiments; IB, immunoblotting; IP, immunoprecipitations.

4.1.3.3.5 Co-localisation of VAP proteins with endogenous RIM1/2 in neuronal cell culture

Because the biochemistry data suggested, so far, the possibility of binding between RIM1α and VAP proteins, co-localization studies in primary cell culture were performed.

To study the co-localization of VAPA or VAPB/C with RIM1α, rat primary cortical neurons were transfected with full-length HA-tagged constructs, followed two weeks later by fixation and staining against endogenous RIM1α and the HA-tag. Both overexpressed VAPA and VAPB showed co-localization with endogenous RIM1/2 (*Fig. 4.29, upper panel; Fig. 4.30, upper panel*). Because protein overexpression might lead to aggregation and mislocalization, staining of the endogenous VAPA and VAPB/C was performed. Therefore, at DIV14, neurons were fixed, stained, and imaged for native VAPA and VAPB. The level of the protein was high in the soma and very weak in neurites. Nevertheless, some degree of co-localization was observed between RIM1/2 and VAPA or VAPB (*Fig. 4.29, lower panel; Fig. 4.30, lower panel*). A low degree of co-localization was also observed between the VAP proteins and the presynaptic marker, Bassoon (*Fig. 4.31*).

The co-localization between VAP proteins and different presynaptic proteins was calculated using the Pearson's coefficient, using the JACOp plug-in, integrated in the ImageJ software. The degree of co-localization between VAP proteins and the presynaptic protein Bassoon or RIM1/2 was similar (*Fig. 4.32*).

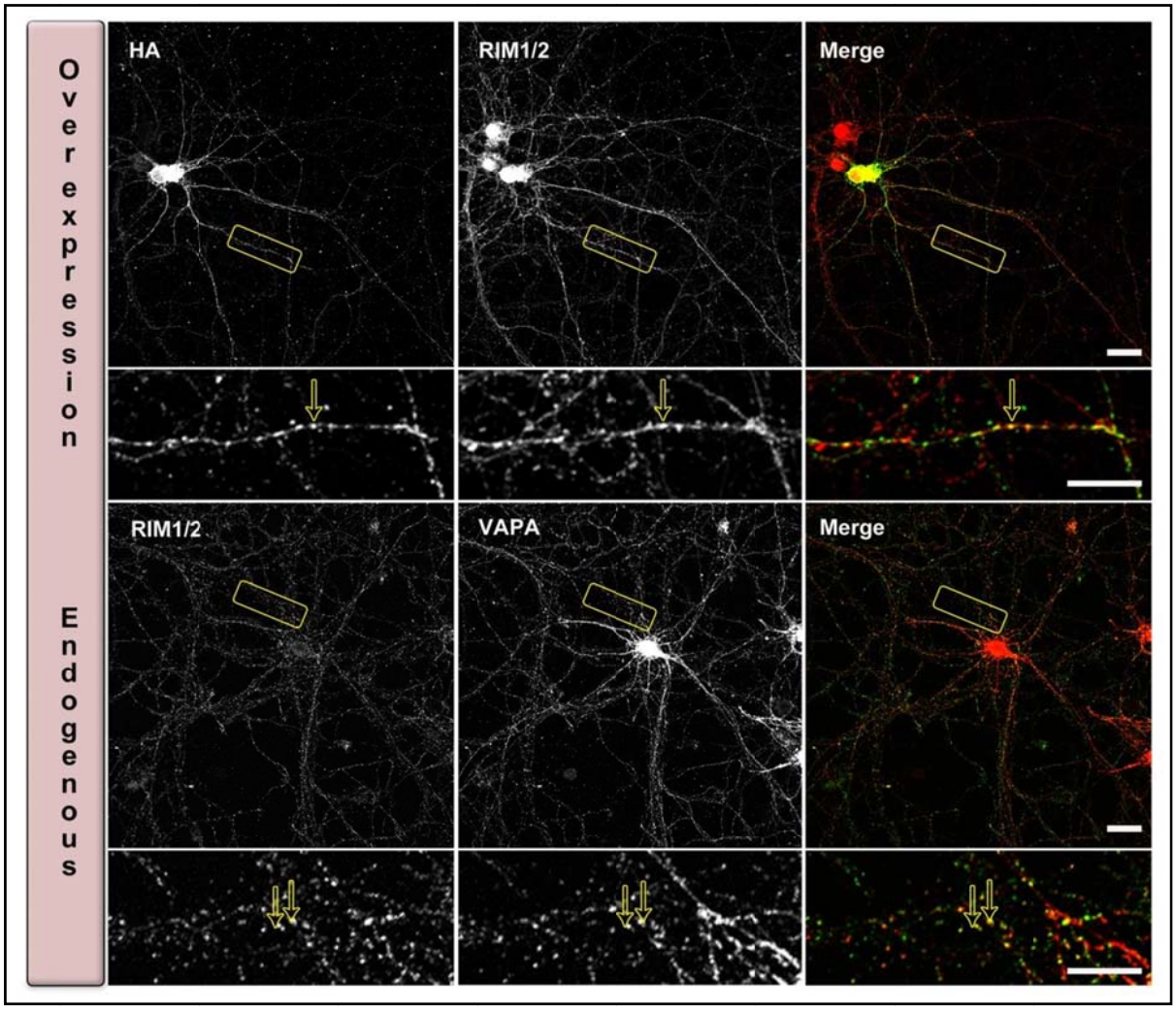

Figure 4.29: **Immunofluorescence labeling reveals a partial co-localisation of RIM1α with VAPA at synapses.** ***(Upper panel)*** At DIV3 primary rat cortical neurons were transfected with HA-tagged VAPA. Two weeks post-transfection neurons were fixed and stained against the HA-tag (HA.11 Clone 16B12, Covance) and endogenous RIM1/2 (Frank Schmitz). ***(Lower panel)*** DIV14 rat cortical neurons were fixed and stained for endogenous VAPA (H-40, Santa Cruz), and RIM1/2 (BD Bioscience). Images were acquired using a laser-scanning confocal microscope (Nikon A1/Ti). Yellow arrows indicate co-localization between these two proteins: RIM1α and VAPA. Scale bar: 20µm (overview); 10µm (insets).

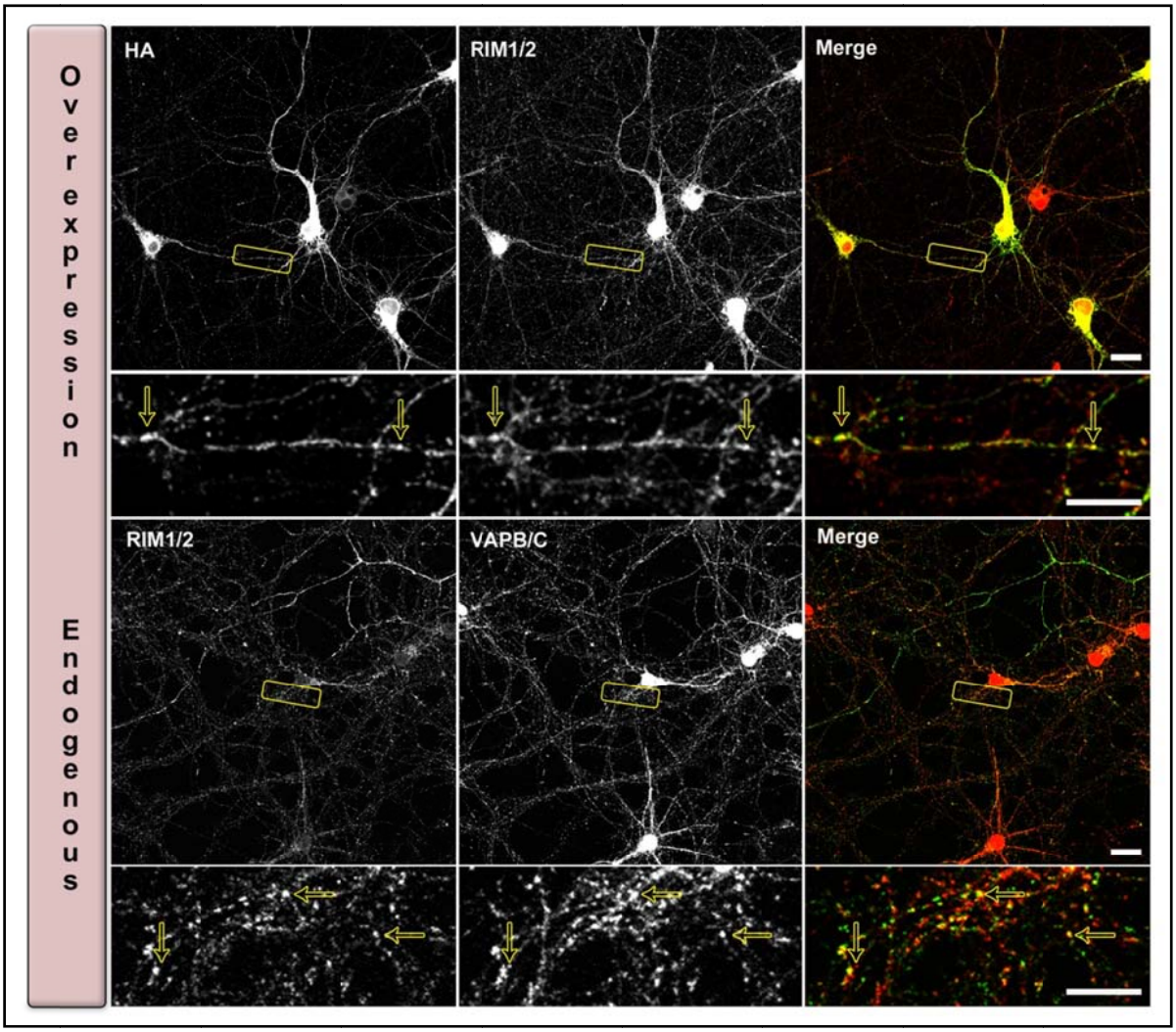

Figure 4.30: **Partial co-localisation of RIM1α with VAPB at synapses.** ***(Upper panel)*** At DIV3 primary rat cortical neurons were transfected with HA-tagged VAPB. Two weeks post-transfection neurons were fixed and stained against HA-tag (HA.11 Clone 16B12, Covance) and endogenous RIM1/2 (Frank Schmitz). ***(Lower panel)*** DIV14 rat cortical neurons were fixed and stained for endogenous VAPB (H-40, Santa Cruz), and RIM1/2 (BD Bioscience). Images were acquired using a laser-scanning confocal microscope (Nikon A1/Ti). Yellow arrows indicate co-localization between RIM1α and VAPB. Scale bar: 20µm (overview); 10µm (insets).

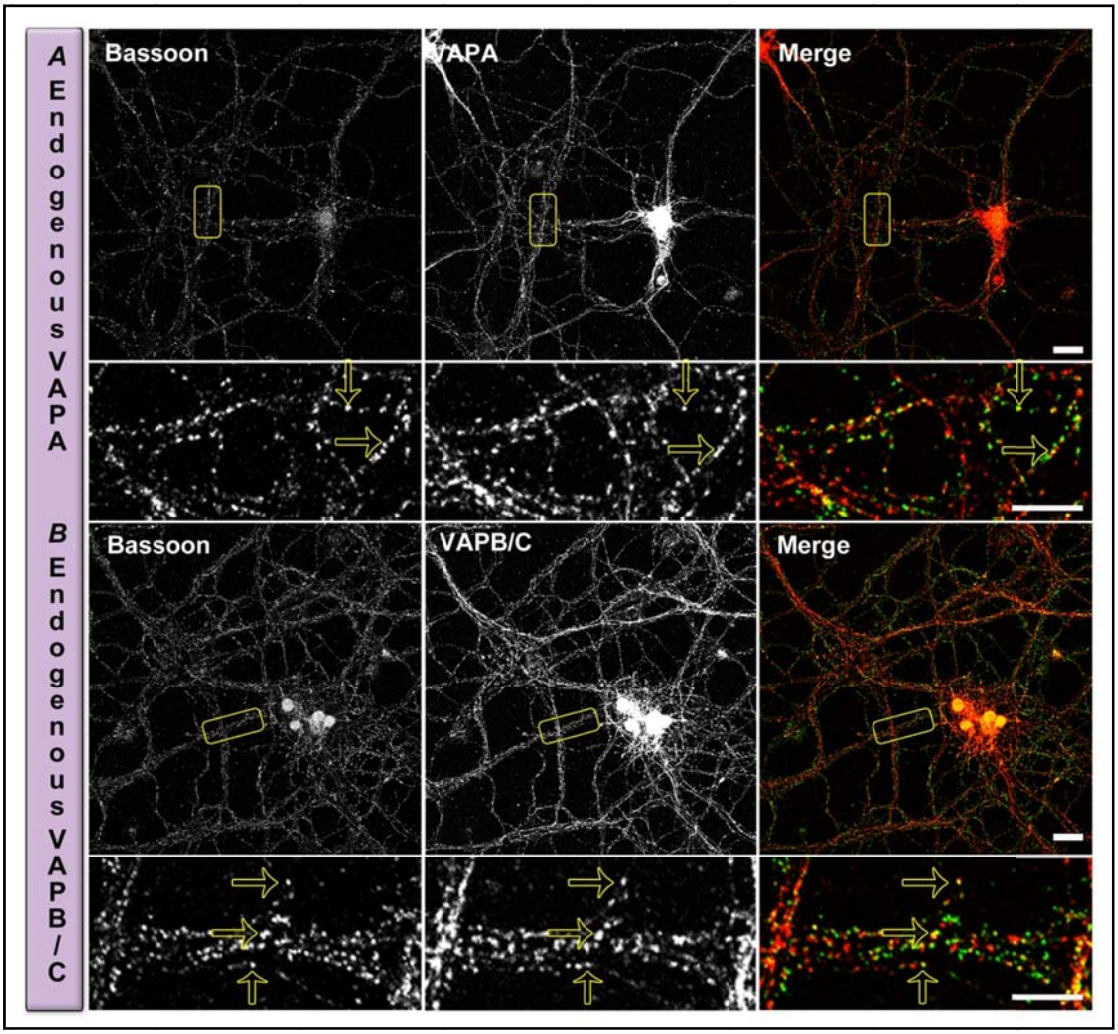

Figure 4.31: **Immunofluorescence labeling of VAPA, VAPB/C and Bassoon at synapses.** At DIV14 rat cortical neurons were fixed and stained for endogenous VAPA ***(A)*** (H-40, Santa Cruz), VAPB ***(B)*** (H-40, Santa Cruz), and the active zone protein Bassoon (Covance). The yellow arrows mark boutons positive for both endogenous proteins. Images were acquired using a laser-scanning confocal microscope (Nikon A1/Ti). Scale bar: 20µm (overview); 10µm (insets).

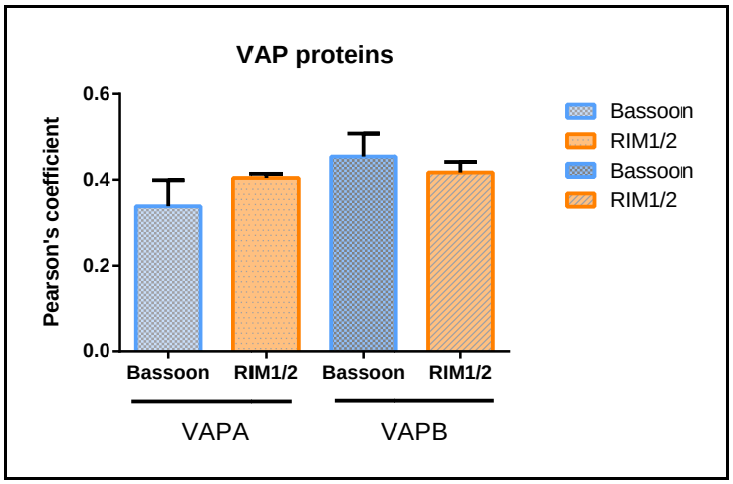

Figure 4.32: **Quantification of the co-localization of VAP proteins with different presynaptic markers.** Rat primary cortical neurons were stained against the endogenous proteins: VAPA, VAPB, Bassoon and RIM1/2. Pearson's coefficient was used for correlation analysis (JACOp plug-in, ImageJ). No significant differences were observed between different VAP proteins and RIM1/2 or Bassoon.

4.1.3.4 Copine VI

Highly expressed in the olfactory bulb and in the hippocampus Copine VI, known also as Copine N, is a calcium binding protein, whose gene expression level is up-regulated by kainate stimulation and LTP (NAKAYAMA et al., 1998, 1999). During embryonic development (E16.5), the mRNA and the protein expression is up-regulated in the axonal projections of the mitral cells in the olfactory bulb (YAMATANI et al., 2010). At the present, the function of Copine VI in the presynaptic terminal has not yet been fully investigated.

4.1.3.4.1 Copine VI binds RIM1α

A less studied protein, Copine VI, was detected in MS to associate with RIM1α (*Table 4.8*). Copine VI was identified with high scores both in co-IP experiments, using overexpressed RIM1α C2A-C2B domains in rat cortical neurons, as well as in crude synaptosomes. The level of detected Copine VI by MS was similar between different pharmacological treatments.

Table 4.8: **Copine VI.** Mascot scores are listed in correlation to the various experimental conditions. Five independent experiments were performed.

Accession Number (UniProtKB)	*Gene name*	*Score*	*Sequence coverage*	*Unique peptides*	*Type of experiments*	*Description*
Q9Z140	CPNE6-MOUSE	682,45	26,39	11	Neurons	Copine-6
		747,06	33,93	15	Control	
		139,28	6,82	2		
		306,17	9,16	5		
		574	19,39	9	Staurosporine	
		191,33	6,82	2		
		226,42	9,16	5		
		423,02	16,34	8	phosSTOP	
		397,20	12,21	4		
		89,75	3,59	2		
		121,64	9,34	5		

To investigate the direct binding between RIM1α and Copine VI, different binding assays were employed. GST-pull down assays with different GST-fusion proteins (RIM1α C2A or RIM1α C2B) and HA-tagged full-length Copine VI overexpressed in HEK293T cells, revealed a strong interaction between the calcium sensor and the C2B-domain of RIM1α (*Fig. 4.33B*). RIM1α C2A-domain did not bind the Copine VI.

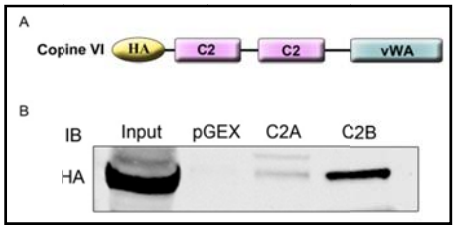

Figure 4.33: **Copine VI binds the C2B-domain of RIM1α.** ***(A)*** Schematic representation of full-length Copine VI, with the two C2-domains (C2A and C2B) in the N-terminal region, and von Willebrand factor type A-domain in the C-terminal region. ***(B)*** GST-pull down assay revealed that Copine VI has a stronger affinity for the C2B-domain of RIM1α (N=3). N, number of independent experiments; IB, immunoblotting.

4.1.3.4.2 The Copine VI-RIM1α interaction is calcium dependent

Given that previous studies have shown copines to be calcium-binding proteins (NAKAYAMA et al., 1998, 1999), the requirement of calcium in this binding was assessed. Thus, co-immunoprecipitations were carried out in the absence or presence of the calcium chelating agent, EGTA.

In the presence of EGTA the binding between RIM1α and Copine VI was strongly impaired (*Fig.4.34B*). The addition of calcium did not have any effect on the binding affinity compared to untreated control. The truncated form of RIM1α (C2A-C2B) also showed affinity for the HA-tagged Copine VI (*Fig. 4.34C*).

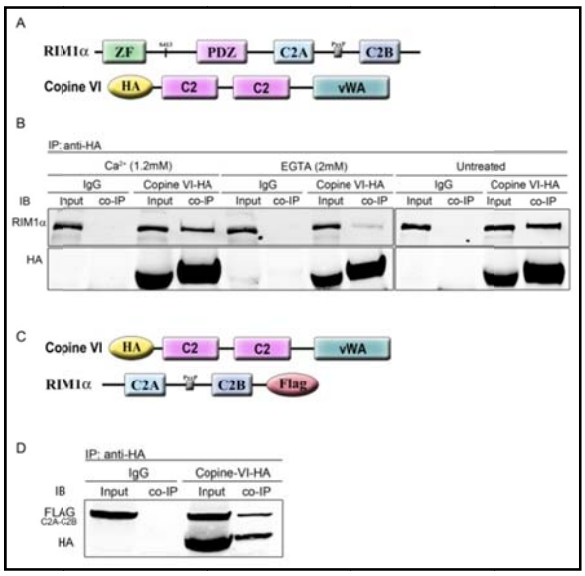

Figure 4.34:* Copine VI-RIM1α binding is calcium dependent.** ***(A/C) Schematic representation of the HA-tagged full-length Copine VI and the RIM1α. ***(B)*** Overexpressed proteins were subject to co-IPs using HA-magnetic beads in the presence of either calcium (1.2mM) or EGTA (2mM). EGTA weakened the interaction between Copine VI and RIM1α (N=4). ***(D)*** FLAG-tagged RIM1α C2A-C2B binds Copine VI (N=3). N, number of independent experiments; IB, immunoblotting; IP, immunoprecipitations.

4.1.3.4.3 Copine VI and RIM1/2 co-localized at a subset of synapses

Because of the direct binding between RIM1α and the calcium sensor, Copine VI, the co-localization of these two proteins was studied in primary rat cortical neurons. Primary cultures were fixed at DIV14 and the endogenous RIM1/2 and Copine VI proteins were labelled (*Fig. 4.35*).

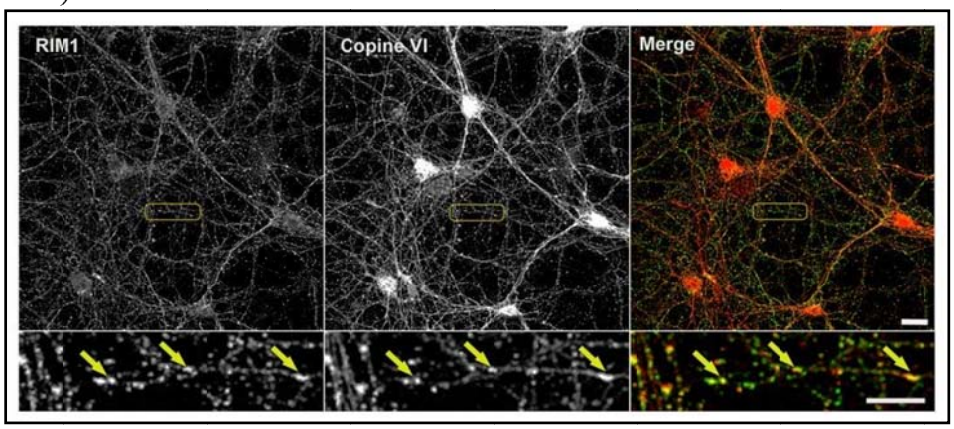

***Figure 4.35:* Immunofluorescence labelling of RIM1/2 and Copine VI at synapses.** At DIV14 rat cortical neurons were fixed and stained for endogenous proteins: RIM1 (BD Bioscience) and Copine VI (Ege Kavalali). The yellow arrows mark the positive boutons for both proteins. Images were acquired using a laser-scanning confocal microscope (Nikon A1/Ti). Scale bar: 20µm (overview); 10µm (insets).

4.2 SV2A

SV2A is a transmembrane synaptic vesicle protein with a suggested role in priming (CUSTER et al., 2006), in regulating the calcium level at the active zone (JANZ et al., 1999), and in controlling the amount and the co-trafficking of synaptotagmin1 in neurons (CHANG and SÜDHOF, 2009; YAO et al., 2010). However, up to date its precise mode of action has not been unequivocally determined. This might have been in part hampered by the fact that, except for synaptotagmin1, only few binding partners for SV2A have been identified (SCHIVELL et al., 1996). Therefore, one major goal of this thesis is to purify SV2A under native conditions by applying tandem affinity purification and to identify the potential novel binding partners by mass spectrometry.

4.2.1 Generation and characterisation of the TAP-tagged SV2A constructs

To purify SV2A under native conditions from mouse brain or neuronal cells using affinity chromatography techniques, the overexpression constructs had to be first designed and tested for proper expression and cellular localization.

Full-length SV2A from mouse was cloned with a short tandem affinity purification (TAP) tag, composed of one FLAG- and two Strep-sequences, both in N- as well as in C-terminal position. Furthermore, SV2A was fused in the C-terminal position also to GFP (*Fig.4.36A*). Rat cortical neurons were transfected with the newly generated plasmids or transduced with crude viral particles (rAAV serotype 1/2), expressing the above mentioned fusion proteins, at DIV2-5 (day in vitro). Two weeks later neurons were fixed and analysed by immunofluorescence using antibodies against SV2A, FLAG and the presynaptic marker Synapsin1/2. The TAP and GFP-tagged SV2A showed a punctate synaptic distribution along the axons and a co-localisation with the synapsin1/2 marker (*Fig.4.37A; B*). The expression of the tagged SV2A was confirmed by immunoprecipitation using FLAG-magnetic beads followed by immunoblotting against SV2A and the FLAG-tag. The resulting bands showed the expected molecular weight around 100-130kDa (*Fig.4.36B*). The IP using an anti-GFP antibody coupled to agarose beads did not give positive bands in the immunoblotting.

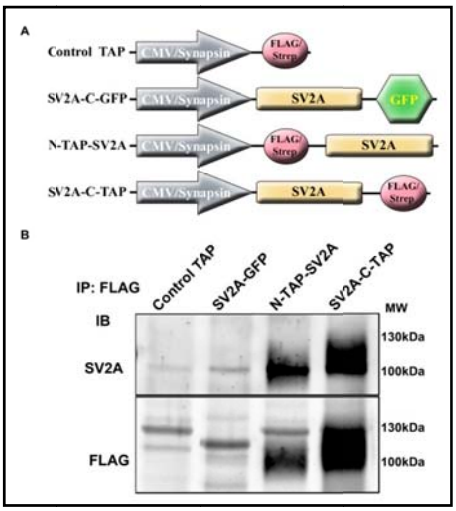

Figure 4.36: **Testing for SV2A overexpression in primary cultured neurons.** ***(A)*** Schematic representation of SV2A constructs. ***(B)*** Overexpression of SV2A-GFP, SV2A-N-TAP, SV2A-C-TAP in neuronal cell culture. Cell lysates were analysed by WB with antibodies against SV2A and FLAG.

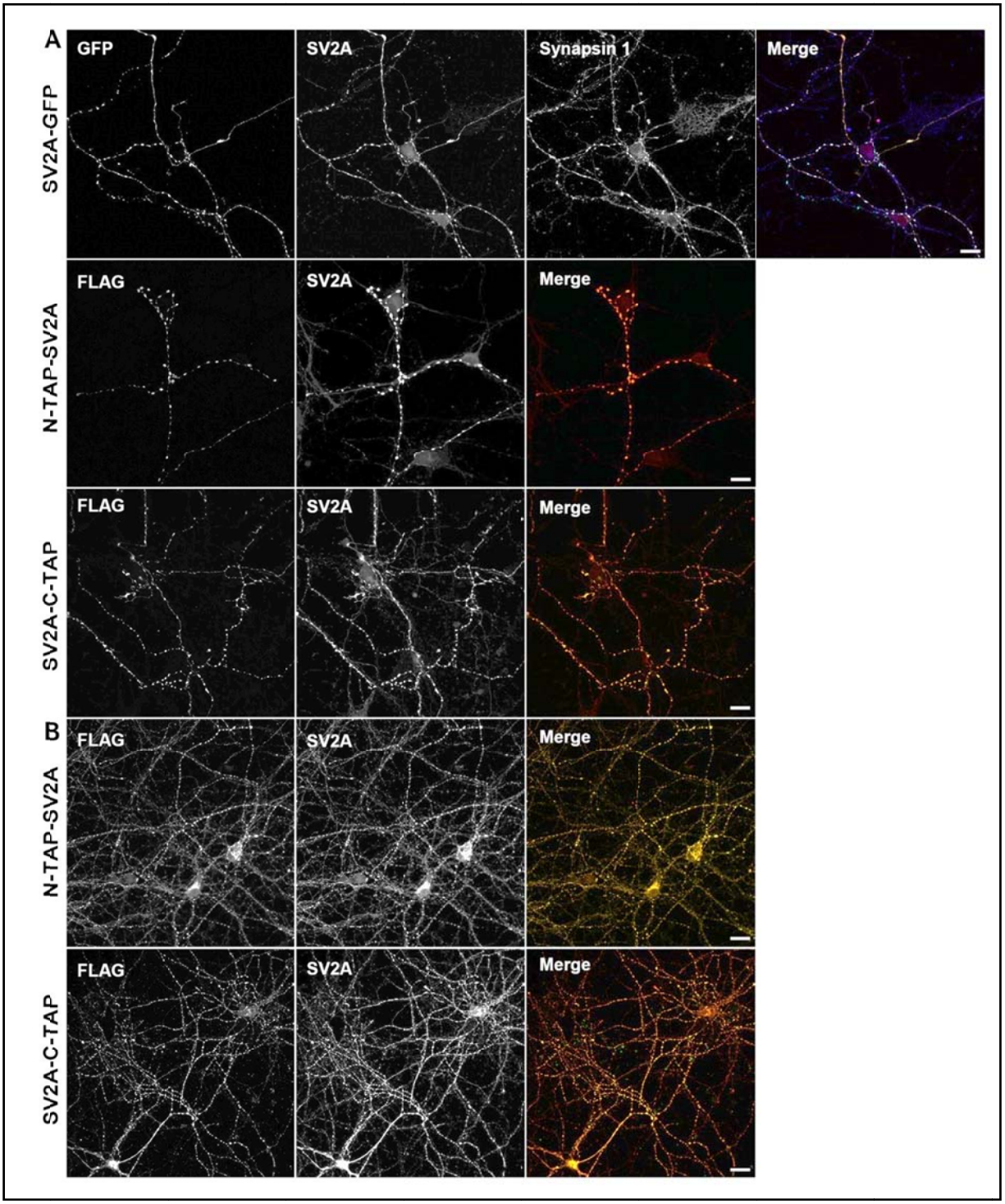

Figure 4.37: **Analysis of SV2A overexpression in cultured primary neurons.** ***(A)*** Rat cortical neurons were transfected at DIV4 with SV2A-GFP, SV2A-N- and -C-TAP, and analysed by immunofluorescence with antibodies against SV2A and FLAG. ***(B)*** At DIV2-3 rat cortical neurons were infected with rAAV serotype 1/2 expressing N- and C-TAP-tagged SV2A. Pictures were acquired using a laser-scanning confocal microscope (Nikon A1/Ti). Scale bar: 20µm.

4.2.2 Optimization of SV2A protein purification from primary rat cortical neurons

To test and optimze the affinity purification of SV2A, primary rat cortical neurons were transduced with viral particles (rAAV serotype 1/2) expressing SV2A with the TAP-tag either in the N- or C-terminal position. Two weeks after the transduction the cells were harvested, lysed in cold ice lysis buffer containing 3.9mM DDM (n-Dodecyl-ß-maltoside) and subjected to either a one- or two-step purification procedure.

4.2.2.1 One-step purification yields good recovery of TAP-tagged SV2A

Strep purification was based on the ability of the Strep-tactin matrices (streptavidin) to bind with high selectively to the strep sequence of the TAP-tag, allowing the purification of SV2A in one single step and in a column modus. To determine the purification efficiency, a small aliquot was kept after each purification step for further analysis by WB. The Strep purification alone showed a good recovery of the recombinant protein, since little material was lost during the procedure and the entire material was recovered after the 3rd and 4th elution steps. The disadvantage of this procedure was the limited binding capacity of the columns (50 to 100nmol/ml recombinant proteins), which were therefore unable to capture the entire applied tagged-SV2A protein. The bands present in the flow fraction and the first two washing steps may indicate that the column was over-saturated with the fusion protein (*Fig.4.38B*).

The capacity of the monoclonal M2-FLAG antibodies, covalently attached to the agarose beads, to recognise the octapeptide (DVKDDDDK) present in the TAP-tag allowed for the protein purification using the FLAG-tag (Batch modus). As in the case of the Strep purification, the column binding capacity was the limiting factor in capturing the whole amount of recombinant protein. However, the elution step performed with competitive FLAG peptides showed a sufficiently high recovery of the targeted protein (*Fig.4.38C*).

Since the purpose of these procedures was to purify proteins maintaining their native configuration, it was mandatory to control for SV2A structural integrity. For this purpose Synaptotagmin1 (Syt1) was chosen because it is one of the proteins known to bind to SV2A (SCHIVELL et al., 1996; PYLE et al., 2000). The immunoblotting experiments showed that a significant amount of Synaptotagmin1 was co-eluted in the Strep purification and to a lesser degree in the FLAG purification procedure, indicating that the recovered SV2A protein retained to a certain degree its native structure (*Fig.4.38*).

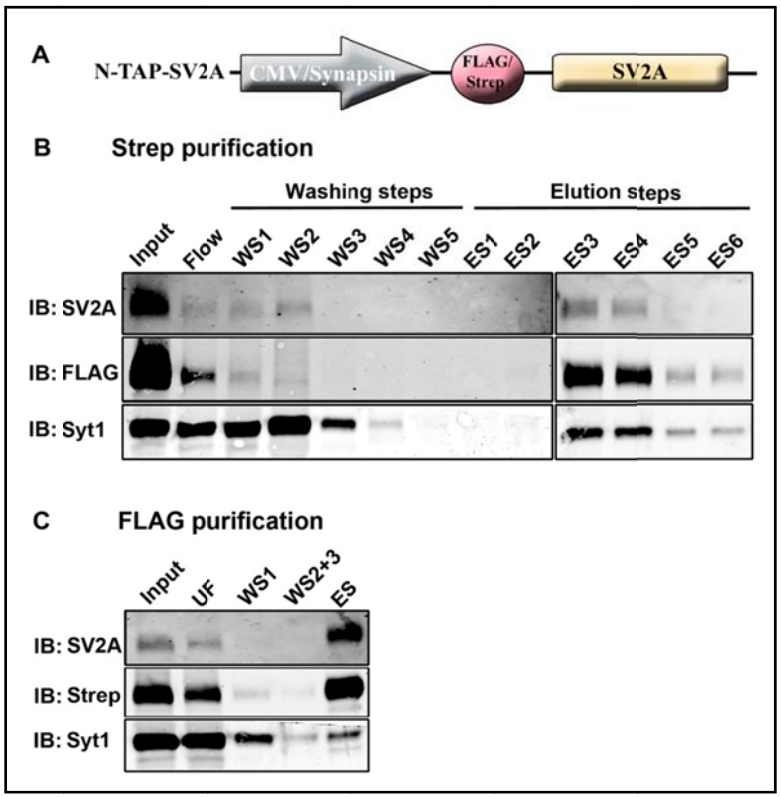

Figure 4.38: **Comparative analysis between FLAG- and Strep-one-step purification from rat primary neurons.** ***(A)*** Schematic representation of the N-TAP-SV2A. ***(B)*** Column purification using Strep-tactin matrix. ***(C)*** Batch purification using anti-FLAG M2 agarose beads. The efficiency of both single step purifications was verified by analysing each acquired fraction by WB. Purified SV2A maintains its ability to bind Synaptotagmin1 (Syt1), indicating structural integrity. WS, washing step; ES, elution step; UF, unbound fraction.

4.2.2.2 Two-step purification of fusion proteins leads to a decrease in elusion efficiency

In order to purify SV2A under native conditions retaining its binding partners and to minimize the large amounts of contaminants, two approaches were compared: a) the strep-tag followed by the FLAG-tag purification and b) the FLAG-tag followed by the strep-tag purification.

In *the first approach (strep-tag column purification followed by FLAG-tag batch purification)* most of the recombinant protein bound to the matrix was recovered in the elution steps, even though some material seemed to remain on the streptavidin matrix. All six collected fractions were than pooled and subjected to the FLAG purification procedure (anti FLAG M2 affinity gel). The recovery rate after the elution with FLAG peptides was rather poor. There were no detectable bands in the unbound fraction, pointing to an insignificant loss of recombinant protein during the incubation. This suggests that the total protein either remained bound to the beads or was rapidly degraded (*Fig.4.39B*).

The second approach started with the FLAG purification followed by a strep purification, which has proven to have a better efficiency. The amount of SV2A protein recovered from the M2 affinity gel was sufficiently high and no detectable material loss was noticed after the subsequent steps of strep purification. As a result, a higher yield of the protein of interest was achieved in the end (*Fig.4.39C*). The structural integrity of SV2A was estimated by its capacity to bind synaptotagmin1 (determined by WB). Since not the whole

amount of recombinant SV2A seemed to be recovered from the matrix, it was necessary to increase the number of elution steps from 6 to 8. This resulted in an increase in the final volume of eluate and a reduction in the protein concentration (*Fig.4.39B*). To circumvent this problem Amicon Ultra centrifugal filters were used to concentrate the samples.

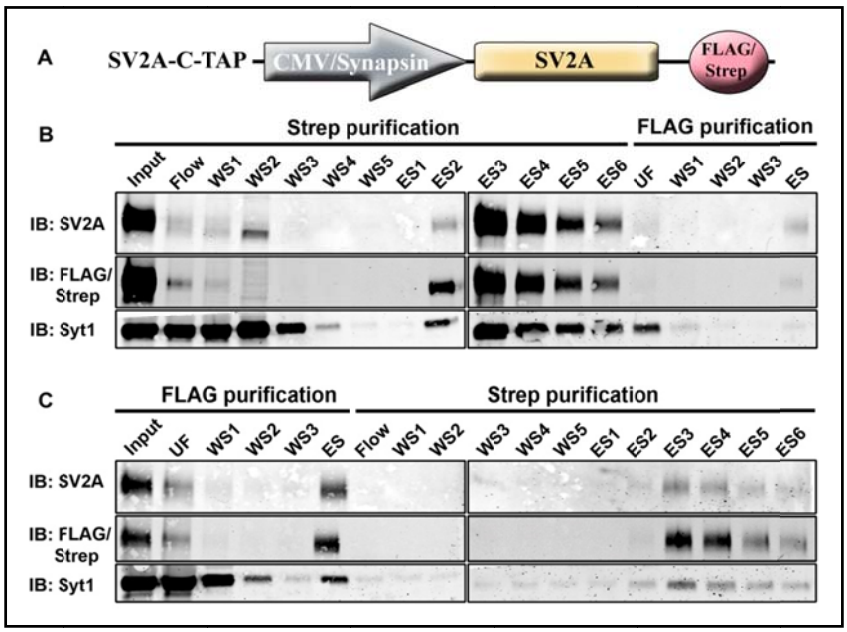

Figure 4.39: **Analysis of the efficiency of a two-step purification procedure for overexpressed SV2A-C-TAP.** ***(A)*** Schematic representation of the SV2A-C-TAP. ***(B)*** Strep purification followed by FLAG purification. After the binding of the Strep-fusion proteins and the washing steps, 6 elution steps were performed in the presence of 2.5mM desthiobiotin. All fractions were collected and mixed for 1h with anti-FLAG M2 agarose beads (FLAG purification). The proteins were eluted from the beads with 200µg/ml FLAG peptide. ***(C)*** FLAG purification followed by Strep purification. Protein complexes eluted from the FLAG beads (200µg/ml FLAG peptide) were added to the Strep column and the purification performed as described above. Purification did not alter SV2A's ability to bind Synaptotagmin1 (Syt1). WS, washing step; ES, elution step; UF, unbound fraction.

Following the strep/FLAG purification concentration of the protein solution using Amicon filters was also used to analyse the amount of protein lost during the entire tandem affinity purification. Washing fractions, flow fraction and the elution fraction were subjected to concentration. This approach resulted in a slight increase in the amount of eluted SV2A detected by WB. All other steps showed no detectable loss of SV2A during the entire tandem affinity purification procedure (*Fig.4.40C*).

Overall, in both approaches, a significant reduction in the protein recovery was observed after the elution steps compared to the initial input.

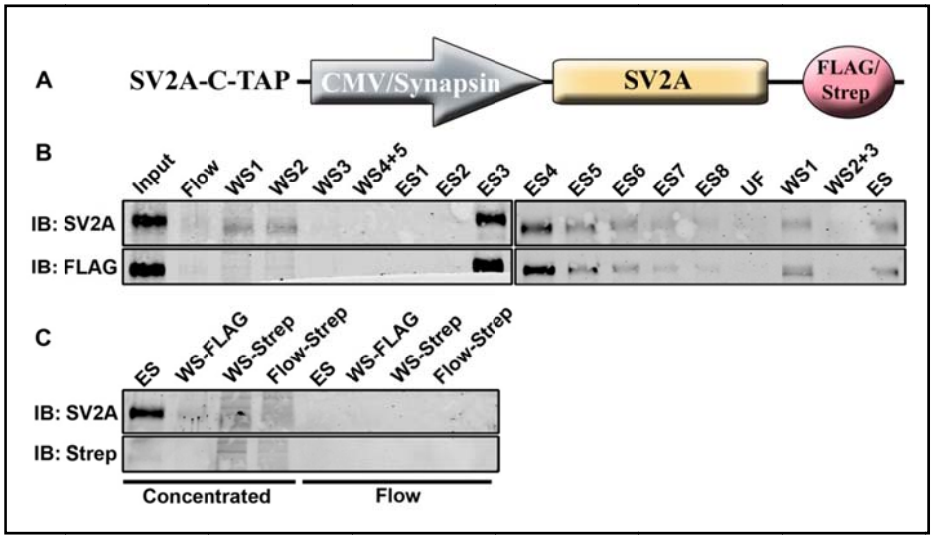

Figure 4.40: **Two-step purification of SV2A-C-TAP followed by concentration using Amicon Ultra Centrifugal filters.** ***(A)*** Schematic representation of the SV2A-C-TAP. ***(B)*** Strep purification followed by FLAG purification. After the binding and washing of the Strep fusion proteins, six elution steps were performed in the presence of 2.5mM desthiobiotin. All the fractions were pooled and mixed for 1h with anti-FLAG M2 agarose beads (FLAG purification), followed by elution with with 200µg/ml FLAG peptides. ***(C)*** Sample concentration with Amicon Ultra Centrifugal filters (3000 MWCO, Millipore). Similar fractions were pooled and concentrated by centrifugation at 14.000g for 30min. The concentrated protein solution and the flow through (the fraction, that has passed through the filter, < 3000 MWCO) were analysed by WB for the presence of SV2A. WS, washing step; ES, elution step; UF, unbound fraction; MWCO, molecular weight cut off.

4.2.3 SV2A overexpression and affinity purification from mouse brain

In order to scale up the amount of purified protein, a large amount of starting material would be required. As an alternative approach to overexpression in primary neuronal culture, purified viral particles (serotype 8; *Fig.4.41*) containing SV2A-N- and -C-TAP and the control N-TAP constructs were injected into ventricles of P0 mice (2µl/animal) once or 3 days (one injection/day) in a row. 2 to 5 weeks after the injection the mice were sacrificed, the brains extracted and prepared for affinity purification.

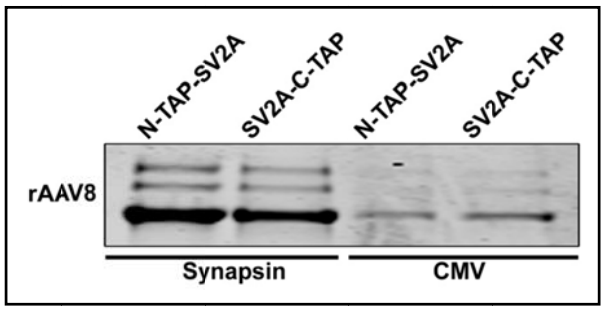

Figure 4.41: **Physical titer of purified rAAV viral particles serotype 8 visualized by Coomassie staining.** Virus purification using OptiPrep discontinuous gradient ultracentrifugation.

4.2.3.1 Analysis of mouse brain transduced with rAAV-SV2A-GFP indicates high levels of expression of recombinant protein

Viral particles expressing SV2A fused to GFP were used as positive control to check for the expression and the localisation of the protein. Two weeks following the injection animals were sacrificed, the brains homogenized in cold homogenisation buffer, and the recombinant protein purified by immunoprecipitation using anti-GFP antibodies coupled to magnetic beads. A strong signal was detected for overexpressed SV2A-GFP in the elution step (*Fig.4.42B*).

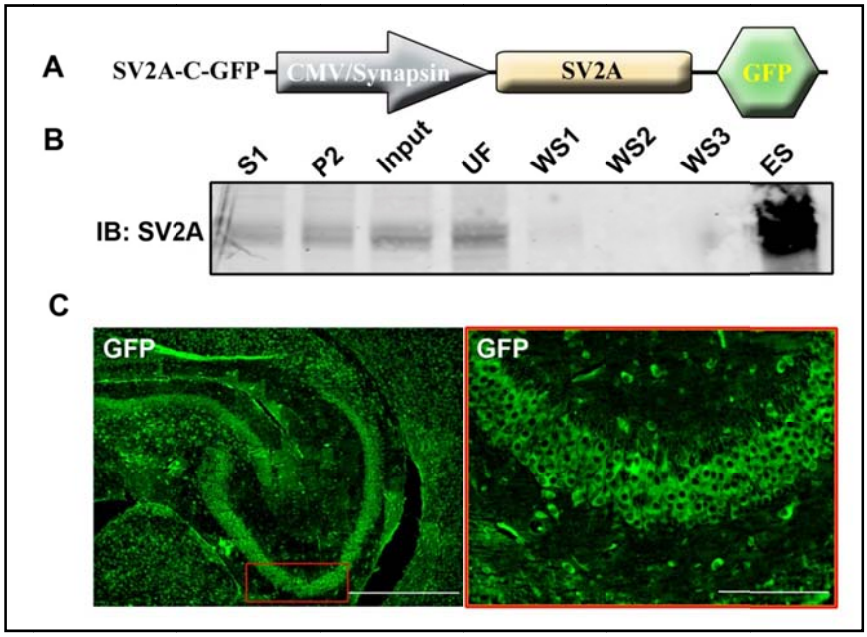

Figure 4.42: **Analysis of the overexpression of SV2A-GFP in Po mice.** ***(A)*** Schematic representation of SV2A-GFP. ***(B)*** Analysis of SV2A-GFP overexpresion in mouse brain (C57/BL6). P0 mice were injected into ventricles with 2µl of purified virus. Two weeks after injection crude synaptosomes were prepared and overexpressed SV2A was immunoprecipitated with anti-GFP antibodies (ab290) and detected by WB. ***(C)*** Immunohistochemistry of SV2A-GFP. Two weeks after injection brains were fixed in 4% paraformaldehyde and SV2A was detected by immunofluorescence with anti-GFP antibodies (ab290). S1, supernatant 1; P2, crude synaptosomes (pellet 2); WS, washing step; ES, elution step; UF, unbound fraction. Scale bar: 200µm (left picture); 100µm (right picture).

Furthermore, expression of SV2A-GFP was confirmed by immunohistochemistry on paraffin slides prepared from injected mice. A GFP signal could be detected almost everywhere in the brain, indicating a high overexpression of the fusion protein particularly in the soma of the cells (*Fig.4.42C*).

4.2.3.2 N- and C-tagged SV2A affinity purification from transduced mouse brain

4.2.3.2.1 Analysis of single-step purification method

The experiments with N- and C-TAP-tagged SV2A constructs were performed following the procedure as described for SV2A-GFP. Viral particles were injected into ventricles of P0 animals and two weeks later the brains were analysed for the overexpression of SV2A, both by immunohistochemistry as well as by tandem affinity purification and WB (*Fig.4.43 and 4.44*).

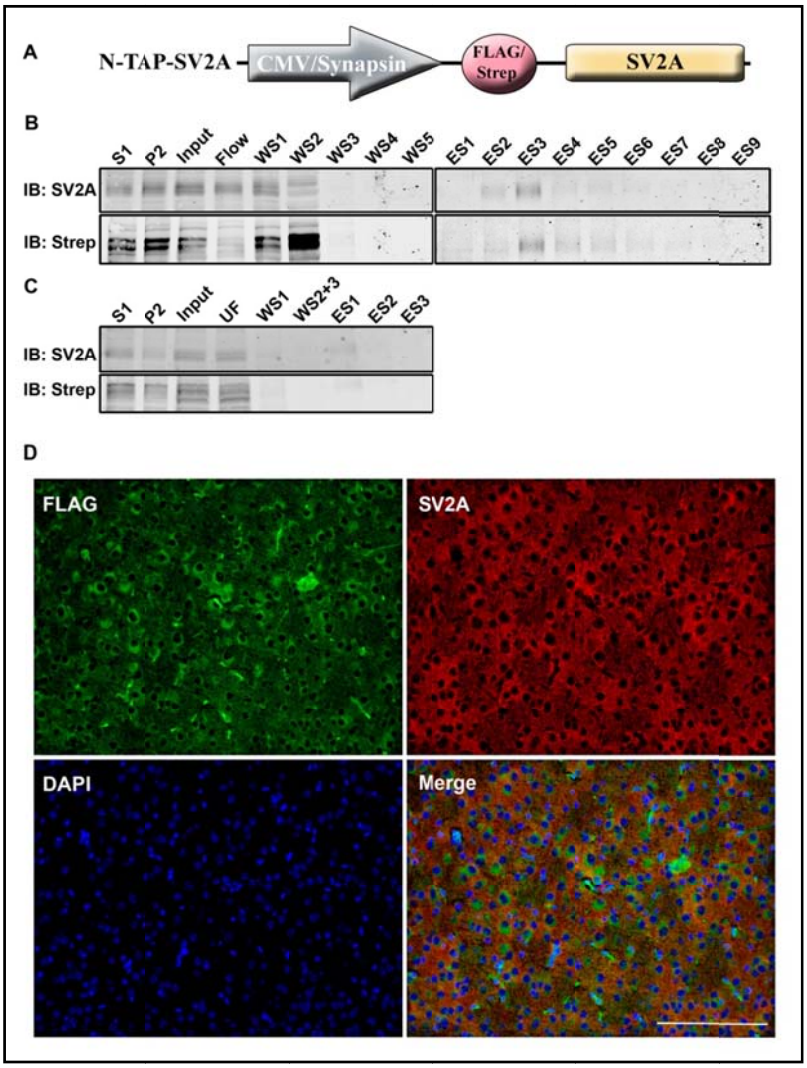

Figure 4.43: **Expression and purification of the N-TAP-SV2A from mouse brain.** ***(A)*** Schematic representation of the N-TAP-SV2A. ***(B)*** Strep purification of the N-TAP-SV2A. P0 mice were injected into ventricles with purified virus. Two weeks after injection crude synaptosomes were prepared and SV2A was purified using Strep columns. Each fraction was analysed for the presence of SV2A by WB. ***(C)*** FLAG purification of the N-TAP-SV2A. Crude synaptosomes were prepared and SV2A was purified using anti-FLAG M2 agarose beads. ***(D)*** Immunohistochemistry of N-TAP-SV2A. Two weeks after injection brains were fixed in 4% paraformaldehyde and SV2A was detected by labelling with FLAG (F1804, Sigma) and SV2A antibodies. S1, supernatant 1; P2, crude synaptosomes (pellet 2); WS, washing step; ES, elution step; UF, unbound fraction. Scale bar: 100µm.

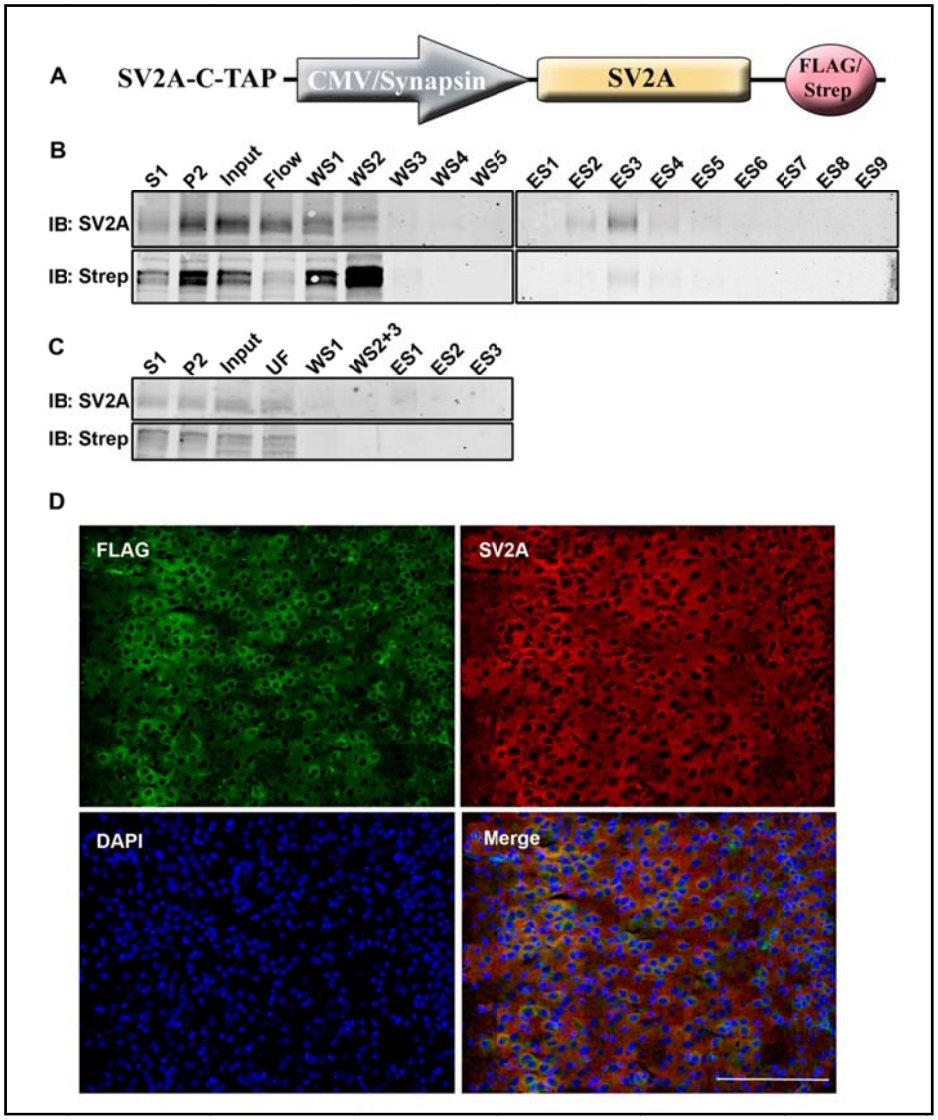

Figure 4.44: **Purification and analysis of SV2A-C-TAP.** ***(A)*** Schematic representation of SV2A-C-TAP. ***(B)*** Strep purification of the SV2A-C-TAP by. Two weeks after injection P0 mice were sacrificed and crude synaptosomes prepared. SV2A was purified using Strep columns. ***(C)*** FLAG purification of the SV2A-C-TAP. Crude synaptosomes were prepared and SV2A was purified and analysed by WB. ***(D)*** Immunohistochemistry of SV2A-C-TAP. Mice brains were fixed in 4% paraformaldehyde and SV2A detected by using FLAG (F1804, Sigma) and SV2A antibodies. S1, supernatant 1; P2, crude synaptosomes (pellet 2); WS, washing step; ES, elution step; UF, unbound fraction. Scale bar: 100µm.

From each injected brain, crude synaptosomes were prepared and lysed in the presence of the detergent DDM (3.9mM). Two different types of one-step purifications were performed: Strep and/or FLAG purification. The expression level of SV2A was low and furthermore, a large percentage of recombinant protein was lost in the first two washing steps of the Strep purification, while the remaining protein was poorly recovered in the elution step three (*Fig.4.43B and 4.44B*). The FLAG purification itself did not give satisfactory results, probably due to the low titre of the injected virus. Moreover, supplementary elution steps were performed in order to avoid SV2A remaining bound to the anti-FLAG M2 agarose

beads. Thus, the amount of peptide in the elution buffers was increased. However, the recombinant SV2A could not be detected in the elution fractions (*Fig.4.43C and 4.44C*).
In the immunohistochemistry experiments only a few cells showed a positive staining for FLAG and these cells were mostly located close to the initial site of injection. This suggested that the amount of expressed protein per brain was too low (*Fig.4.43D and 4.44D*). The purification efficiency for SV2A-C-TAP was similar to N-TAP-SV2A. Higher losses were detected in the Strep washing steps (WS1 and WS2). The protein yield after the second purification was low; pointing again to the fact that the titer of the virus is critical in order to obtain higher amounts of recombinant protein.

Purification of the TAP peptide alone showed that also the native SV2A displayed a slight affinity towards the matrices (*Fig.4.45*).

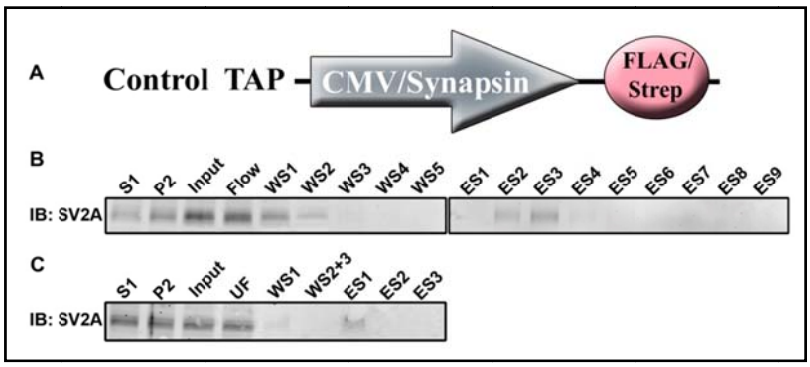

Figure 4.45: **Purification of the negative control, N-TAP from mouse brain.** ***(A)*** Schematic drawing of the negative control. ***(B)*** P0 mice were injected into ventricles with purified virus and two weeks later crude synaptosomes were prepared and Strep column purification was performed. ***(C)*** FLAG purification of the N-TAP negative control. Crude synaptosomes were prepared and N-TAP fragment was purified using anti-FLAG M2 agarose beads. Each fraction was analysed for the presence of SV2A by WB. S1, supernatant 1; P2, crude synaptosomes (pellet 2); WS, washing step; ES, elution step; UF, unbound fraction.

In order to increase the amount of recombinant protein expressed in the brain, the mice were injected 3 days in a row (2µl/mouse/day) with purified viral particles, overexpressing SV2A-N- and -C-TAP proteins. The protein expression was allowed to take place for 4 to 5 weeks. After the one-step Strep purification the amount of recombinant SV2A eluted from the matrix was strongly enriched and showed no obvious losses as was observed in the previous experiment (*Fig.4.46B*).

4.2.3.2.2 Two-step purification procedure

For Strep/FLAG tandem affinity purification two animals were sacrificed three weeks after the three consecutive injections. In this case, the elution fraction did not show any indication of SV2A protein enrichment, probably due to a low viral titer (*Fig.4.46C*). Still enough material was recovered to further proceed with the FLAG purification. Two different elution buffers were chosen in order to optimize the elution of the protein complexes containing SV2A from the FLAG beads. The classical elution protocol based on competition with FLAG

peptides yielded unsatisfactory results. All the recombinant SV2A still showed a high affinity for the antibodies coupled to the agarose matrix (*Fig.4.46D*).

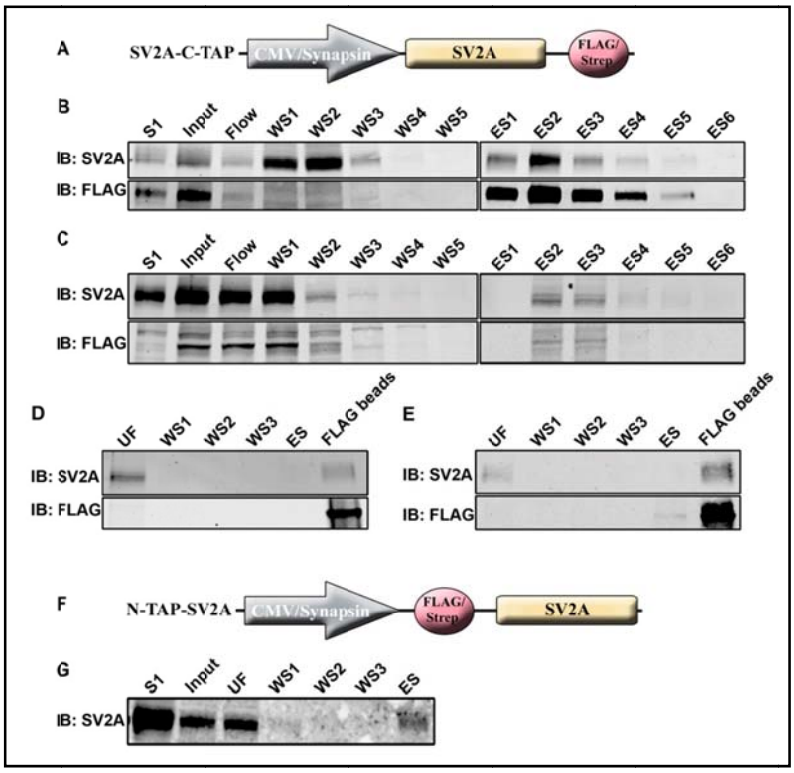

Figure 4.46:* Purification of SV2A-N- and -C-TAP from mouse brains injected with higher doses of purified viral particles.** ***(A)*/ *(F) Schematic representation of the constructs used in the purification. ***(B)*/ *(C)*** Analysis of SV2A-C-TAP after Strep purification. P0 mice were injected 3 days in a row with purified virus. 4-5 weeks after injection crude synaptosomes were prepared and SV2A was purified using Strep columns. Each fraction was analysed for the presence of SV2A by WB. Panel C represents the Strep purification step from the two-step purification. Collected elution fractions (panel C) were pooled and mixed with anti-FLAG M2 agarose beads and eluted with: ***(D)*** 200µg/ml FLAG peptide and ***(E)*** 1M Arg-HCl, pH 3.5. ***(G)*** Analysis of N-TAP-SV2A after FLAG purification using anti-FLAG M2 magnetic beads (Sigma). Elution was performed by boiling the magnetic beads in SDS-PAGE sample buffer. S1, supernatant 1; WS, washing step; ES, elution step; UF, unbound fraction.

An improved protocol for eluting membrane proteins from FLAG M2 antibodies using arginine-based buffers was described by Futatsumori-Sugai et al. (2009). Using the acidic arginine buffer brought a slight improvement in the elution efficiency of SV2A from the antibodies. Most of the protein remained bound to the agarose beads (*Fig.4.46E*). Since agarose supports may induce unspecific binding, magnetic beads coupled to FLAG antibodies were tested as well. The recovery of recombinant SV2A was improved when the magnetic beads were used instead of the agarose beads (*Fig.4.46G*).

4.2.4 Analysis of protein complexes co-immunprecipitated with overexpressed SV2A in primary neuronal cell culture

4.2.4.1 Enrichment of bound protein complexes to SV2A by using cross-linkers and primary neurons from hetero- and homozygous SV2A mice

To circumvent the problem of the low serotype 8 viral titer observed in animals, rat cortical neurons were transduced with crude rAAV viral particle serotype 1/2, TAP was performed, and proteins were resolved by SDS-PAGE, followed by staining with CCB (Coomassie

Colloidal blue). After tandem purification, fewer contaminants were detected in comparison to the one-step purification protocol (*Fig.4.47A and 4.49D*).

Since some of the interactions of SV2A may be transient or very week, only one step-purification procedure was applied, even though this resulted in an increase in the unspecific binding.

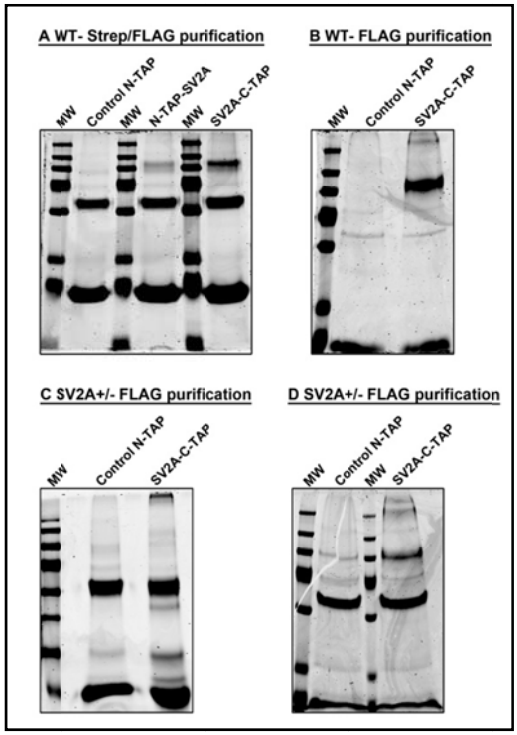

Figure 4.47: **Different purification protocols for SV2A from primary cultured neurons.** ***(A)*** Two-step purification of SV2A from wild type (WT) rat cortical neurons. ***(B)*** FLAG purification of SV2A from WT rat cortical neurons, fixed for 25-30min with 1% formaldehyde to cross-link proteins. ***(C)*** FLAG purification of SV2A from SV2A+/- (heterozygote) mice cortical neurons, fixed for 30 min with 25mM DSP cross-linker. ***(D)*** FLAG purification of SV2A from SV2A+/- (heterozygote) mice cortical neurons, fixed for 30-60min with the cross-linker DTBP (5mM).

As the number of SV2A molecules per vesicle is limited to a few copies and the amount of SV2A present might be critical for its function, (TAKAMORI et al., 2006) primary cultured neurons were prepared from heterozygous (SV2A +/-) and homozygous (SV2A-/-) embryos. Moreover, to stabilize the weak interaction that may occur, different cross-linkers were applied to fix the binding between amino groups of different proteins. Because formaldehyde had been previously described (VASILESCU et al., 2004; KLOCKENBUSCH and KAST, 2010) as a quick and fast method to cross-link proteins, different concentrations and time points were chosen (0.8% to 1% for 10 to 25min). None of the selected concentrations or time variations showed any significant difference in the pattern of bands observed compared to those obtained without cross-linkers (*Fig.4.47B*). Additional cross-linkers were tested: DSP and its water soluble analogue DTBP both in SV2A+/- (*Fig.4.47C and 4.47D*) as well as in SV2A -/- (*Fig.4.48*) neuronal cultures. These last two cross-linkers conferred a slight increase in the band patterns detected by CCB staining.

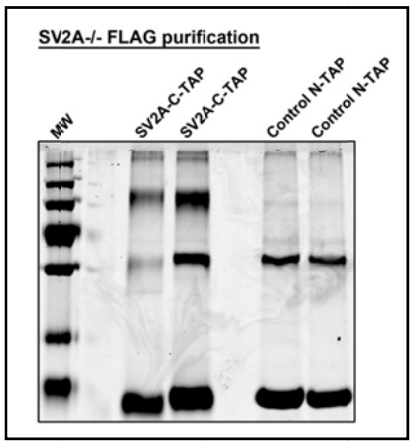

Figure 4.48: **Purification of TAP-tagged SV2A, overexpressed in knockout SV2A neuronal cell culture.** FLAG purification of SV2A from SV2A-/- (knock out) mouse cortical neurons, fixed for 60min with 5mM DTBP. The experiment was performed in duplicate.

4.2.4.2 Identification of novel potential binding partners for SV2A by mass-spectrometry

Primary rat cortical neurons were infected with viral particles expressing C-TAP-tagged SV2A. Following the affinity purifications (one-step and/or two-step affinity purification; no cross-linking) and visualization by Coomassie Colloidal Blue, several bands that were not present in the control lane were cut and analysed by MS (*Fig. 4.49*).

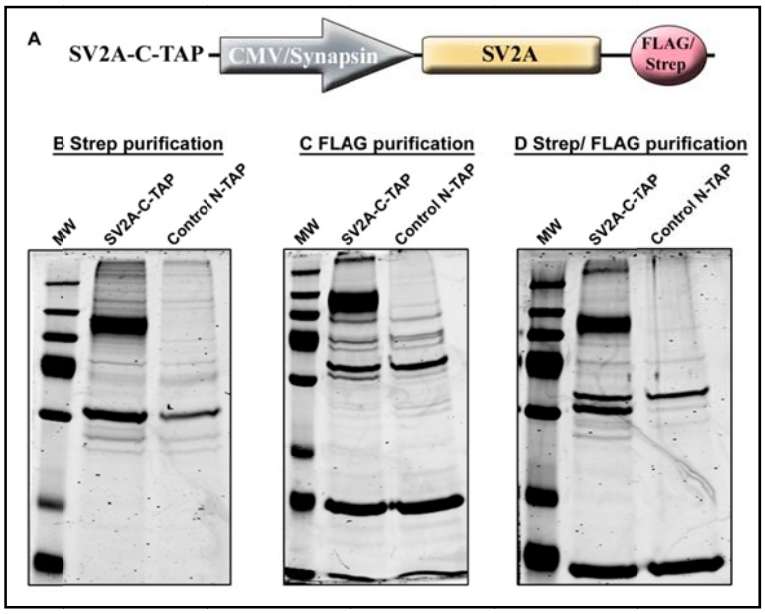

Figure 4.49: **Visualization by CCB staining of the protein complexes purified with SV2A.** Rat cortical neurons were infected with crude viral particles (rAAV, serotype 1/2) and SV2A was purified by: ***(B)*** One-step Strep purification, ***(C)*** one-step FLAG purification, ***(D)*** Strep/FLAG two-step purification.

In table 4.9, some of the newly identified potential binding partners for SV2A are summarized together with their functional roles. Three of these identified proteins (EH domain-containing protein 1, Rab3 and β-catenin) were further analysed in co-IP experiments, but a binding to SV2A could not be verified in biochemical assays.

Table 4.9: Potential novel SV2A binding proteins identified by affinity chromatography/MS.

Protein name	*Score*	*Role*
EH domain-containing protein 1	31	Modulates exocytosis
Protein lin-7 homolog C	37	Localizes synaptic vesicles at synapses
Rab3 GTPase-activating protein	31	Regulates exocytosis
Latrophilin-1	31	Receptor probably implicated in the regulation of exocytosis
Beta-catenin	80	
Ras GTPase-activating-like protein IQGAP1	23	Different signalling pathways
Rho GTPase-activating protein 44	37	
Rho guanine nucleotide exchange factor 33	24	
Ral GTPase-activating protein subunit alpha-1	30	
Ral GTPase-activating protein subunit alpha-2	30	
AP-1 complex	16	
Transcriptional activator protein Pur-beta	16	
Tubulin beta-2A chain	340	
Synaptophysin	77	Synaptic vesicle proteins
Synaptotagmin-1	35	
SV2A (Input)	*83*	

5. Discussion

Synaptic plasticity denotes the ability of neurons to respond to the ongoing network activity, by weakening or strengthening their activity. These adaptive changes can take place both at the pre- and postsynaptic terminals. Whereas the molecular mechanisms underlying postsynaptic plasticity have been studied in great detail, the cellular events mediating presynaptic plasticity are not as well understood. It has been hypothesized that presynaptic plasticity may involve the posttranslational modification of proteins. One of these modifications is the phosphorylation of proteins, which plays a role in the plasticity-induced remodelling of established AZs or in the assembly of novel active zones.

Two presynaptic proteins, the AZ protein RIM1α and the SV protein SV2A have been shown to be important in presynaptic plasticity, by modulating the function and properties of the presynaptic release machinery, e.g. SV priming. However, their precise mode of action is still unresolved. Thus, to gain a better understanding the following goals were pursued in this thesis:

(5.1) The effect of hyperphosphorylation on RIM1α at synapses.

(5.2) The identification of novel potential phospho-dependent binding partners for RIM1α.

(5.3) To gain insight into the enigmatic function of SV2A, we aimed to purify and analyse novel SV2A binding partners.

5.1 Hyperphosphorylation alters the distribution of the presynaptic protein RIM1α at synapses

Presynaptic plasticity involves the structural remodelling of the CAZ, which in turn engages dynamic changes in protein turnover and protein interactions. At the *D.melanogaster* NMJs an increase in the amount of the active zone protein Bruchpilot (Brp) and an enlargement of the presynaptic cytometrix structure was detected after the rapid induction of presynaptic strengthening. Moreover, the fast recruitment of Brp to the AZ led to an increase in the number of SVs and calcium channels at synapses (WEYHERSMÜLLER et al., 2011). The structural remodelling of the CAZ on a timescale of minutes was further supported by studies in hippocampal neurons using a fluorescently labelled Bassoon. The local redistribution of the AZ component led to rapid changes in the size of the AZ, which correlated with modifications in the RRP and the release probability (MATZ et al., 2010). Prolonged silencing of excitatory neurons caused a down-regulation of cellular expression levels of distinct presynaptic proteins, including RIM1α (LAZAREVIC et al., 2011). Interestingly, the decrease in the amount of RIM1α was not caused by UPS-dependent degradation but rather dependent on other

mechanisms, like the regulation of transcription and/or translation. Whereas the number of synapses labelled by RIM1α was decreased after silencing, the remaining positive puncta showed an increase in the level of RIM1α. This suggested a redistribution of RIM1α after prolonged activity deprivation (LAZAREVIC et al., 2011).

Even though the precise molecular mechanisms controlling synaptic adaptation are not well understood, protein phosphorylation has been postulated to contribute to the underlying synapse remodelling and plasticity. For example, ERK kinase, which can integrate a variety of signals, exerts many downstream effects, like, dendritic spine stabilization, modulation of ion channels or receptor insertion (review: SWEATT, 2004). Cdk5 was shown to be involved in LTP and LTD, acting as a homeostatic regulator of synaptic plasticity (review: SHAH and LAHIRI, 2014). One of the central enzymes actively involved in presynaptic plasticity is PKA, e.g. essential for mossy fiber (MF)-LTP (review: CASTILLO, 2012).

It has been shown that the presynaptic protein RIM1α acts as substrate for several kinases: PKA (LONART et al., 2003), ERK2 (SIMSEK-DURAN and LONART, 2008), CaMKII (SUN et al., 2003) and SAD-B (INOUE et al., 2006). Whereas the phosphorylation of the amino acid residue S^{413}in RIM1α by PKA was required for the induction of presynaptic LTP in cultured cerebellar granular and Purkinje cell neurons (LONART et al., 2003), studies in mice expressing mutations in this position were not able to confirm this (KAESER et al., 2008a; YANG and CALAKOS, 2010). Although RIM1α has been shown to be phosphorylated by a variety of kinases, the functional implications of phosphorylation/dephosphorylation of RIM proteins are not well understood. However, such posttranslational modifications regulated by synaptic activity, may directly impact RIM1α's properties, like its binding affinity to other proteins or its stability.

To test if the increased phosphorylation status of RIM1α affects its level or its association with the AZ, neuronal cell cultures were incubated with various phosphatase inhibitors. At different time intervals the neuronal cultures were fixed, endogenous RIM1/2 was labelled and the area of the bouton marked by RIM1α determined. Our results show, that by shifting the equilibrium to a hyperphosphorylated state, RIM1α distribution at synapses is altered. Application of phosSTOP led to a significant increase in the number of boutons with smaller RIM1α marked areas in comparison to control conditions. By blocking only the PP1 and PP2A phosphatases using either 10nM okadaic acid or 2nM Calyculin A, a non-significant increase in the number of RIM1/2 labelled boutons with smaller sizes compared to DMSO control conditions was detected.

High level of protein phosphorylation may affect RIM1α turn-over by either increasing or decreasing its stability. Computer-based simulations have described proteins to become more degradable if more sites are phosphorylated (multi-site phosphorylation). Such phosphorylation-dependent degradation processes are important for proteins involved in regulating the cell cycle (VAREDI et al., 2010). Because RIM1α is a protein with multiple phosphorylation sites, high kinase activity might trigger a degradation process. However, the total intensity of RIM1/2 labelling was not changed after phosSTOP treatment compared to the control condition. Therefore, these results do not suggest that a degradation mechanism might be induced by phosphorylation of RIM1α. On the other hand, phosphorylation may as well protect proteins from degradation, by blocking for example either the binding of E3 ubiquitin ligase to the substrate or by impairing its interaction with E2 ubiquitin-conjugation enzymes. It was hypothesised that RIM1α phosphorylation by PKA, may provide resistance to the degradation by the proteasome (CROWFORD and MENNERICK, 2012). However, to date there is no experimental evidence supporting this hypothesis.

In addition to protein stability, phosphorylation events may impact the association of RIM1α with the CAZ. It has been shown that certain phosphorylation events of CAZ components induce protein solubilisation by interfering with their intermolecular interactions. Binding of the 14-3-3 adapter protein to phosphorylated Bassoon (S^{2845}) decreased the attachment of Bassoon to the AZ (SCHRÖDER et al., 2013). Moreover, treatment of neuronal cultures with the phosphatase inhibitor okadaic acid inhibitor further induced solubilisation and diffusion of Bassoon, CAST and RIM proteins (SCHRÖDER et al., 2013). Accordingly, our experiments may indicate that hyperphosphorylated RIM1/2 protein becomes more soluble and diffuses away from the AZ and the bouton.

Prolonged exposure to okadaic acid has been shown to have cytotoxic effects on a variety of cells and to mediate neurodegenerative mechanisms by blocking PP2A phosphatase activity. The impairment of PP2A activity stimulates a large group of kinases, like ERK2, CaMKII, PKA (review: KAMAT et al., 2013). In our experiments, 1h stimulation did not induce neurotoxicity and moreover, the observed changes in the distribution of RIM1α may be a direct consequence of the interplay between multiple kinases that act at synapses.

However, in interpreting the functional relevance of our observation, it has to be considered that hyperphosphorylation of proteins induced by various pharmacological treatments is not physiological, but rather pushes the system to one side of the equilibrium. Secondly, our approach, immunocytochemistry, does not allow capturing the dynamic nature of phosphorylation events. In summary, our analysis revealed that the distribution of the

RIM1/2 protein is influenced by kinase activity and that hyperphosphorylation may affect the association of RIM1α with the CAZ.

5.2 Identification of novel phosphorylation-dependent RIM1α binding proteins

Over the years proteomics has emerged as an important tool to identify and characterize components of the pre- and postsynaptic terminals. Over 1000 proteins were identified in synaptosomes from whole mouse brain, representing the first inventory of the synaptic proteome (SCHRIMPF et al., 2005). Nevertheless the interactome of presynaptic proteins is not yet fully characterized, especially, when considering posttranslational modifications or transitory protein interactions.

To identify novel potential binding partners for the N- and C-terminal region of RIM1α we performed affinity purifications and mass spectrometry (MS). By using this approach more than 100 proteins were identified to associate with either the RIM1α ZF-PDZ or the RIM1α C2A-C2B domains. These proteins were classified in five categories: *signaling cascades/kinases* (SC), *synaptic vesicles* (SV), *plasma membrane/active zone* (AZ), *cytoskeleton* (C) and *others* (O). Of these, the proteins of the *signalling cascades/kinases* and *plasma membrane/active zone* group accounted for nearly half of the total identified proteins. Another large class was the *others* group, which included mitochondrial proteins or proteins whose localizations and functions were not well known.

In a recent study, the immunopurification and MS analysis of the presynaptic AZ resulted in the identification of 485 proteins, data that suggests the AZ to be enriched in proteins involved not only in neurotransmitter release but also in other cellular activities (WEINGARTEN et al., 2014). On the other hand, a comparison of the proteome of glutamatergic and GABA-ergic synapses showed no major differences between proteins involved in SV docking and release. Besides SV and AZ proteins, ion channels and transporters were also identified (BOYKEN et al., 2013). In accordance with Weingarten et al., we detected an overlap between our identified proteins and the purified AZ-proteins from their study. Similar proteins were presented in the *SV group* (vATPase subunit A, C1 and E1; synapsin-1, Rab-3A, phosphoglycerate kinase 1, peroxiredoxin-6, alpha-enolase, pyruvate kinase isozymes M1/M2, malate dehydrogenase, AP-2 subunit alpha-2, dynamin-1-like protein, clathrin light chain A and B); the *AZ group* (GLAST-1, synatxin-1B, EAAT2, SNAP-25, Thy-1, neuronal membrane glycoprotein M6-a, paralemmin-1, copine, thioredoxin-related transmembrane protein); the *SC group* (heat shock proteins, G proteins, 14-3-3 proteins, septin-5, calcineurin); the *C group* (tubulins, actin, septin-11, septin-6, cofilin-1, profilin-1).

In addition to these, the known binding partners of RIM1α were purified from mouse crude synaptosomes and rat primary cortical neurons: 14-3-3 proteins, ELKS2/CAST, RIM-BP, liprins. Other putative interacting proteins, like Munc13 or voltage-gated calcium channels, were not identified, probably due to a technical problem or due to the transitory nature of the interaction. The combination of buffer stringency and incubation time may be a limiting factor in analysing proteins that display transitory or weak interactions with RIM1α. Boyken et al. did also not identify Munc13 by MS, even though it was detected by WB in the same preparation (BOYKEN et al., 2013).

Whereas in the previous attempts at identifying novel RIM1α binding partners the posttranslational modifications were not taken into account, in this new experimental design we analysed the phosphorylation-dependent binding affinities between RIM1α and various proteins as well. Kinase and phosphatase blockade triggered changes in the phosphorylation status of RIM1α that were accountable for increasing or decreasing its binding affinity (*Table 5.1*). In this respect, RIM1α binding to certain proteins appeared to be phosphorylation dependent. This was, for example the case for SRPK2 (up-regulation with phosSTOP) and VAP proteins (up-regulation with staurosporine).

***Table 5.1*: The number of proteins binding the different regions of RIM1α under various pharmacological treatments.** The values represent the number of proteins binding RIM1α in only one condition. Four independent measurements were performed with the RIM1α C2A-C2B region, and two with the RIM1α ZF-PDZ region.

Region (RIM1α)	*Staurosporine treatment*	*phosSTOP treatment*
ZF-PDZ	18	3
C2A-C2B	29	25

Several proteins were chosen to be further investigated in biochemical assays, due to their direct involvement in AZ assembly. In this study we focused in particular, on four novel binding partners for RIM1α: two kinases (ULK and SRPK), trafficking proteins (VAPA, VAPB) and a calcium binding protein (copine VI).

5.2.1 Two novel potential kinases associate with RIM1α protein

The analysis of the protein complexes bound to the C2-domains of RIM1α identified two classes of kinases: serine/threonine kinases (ULK family) and serine/arginine kinases (SRPK family), which have been recently described as novel potential regulators of AZ assembly during synaptic plasticity and synaptogenesis (JOHNSON et al., 2009; NIERATSCHKER et al., 2009; WAIRKAR et al., 2009). To date nothing is known about the mammalian homologs with regard to

AZ function. Here, we report the direct binding between the presynaptic protein RIM1α and the members of the ULK and the SRPK family, respectively.

5.2.1.1 Unc-51-like kinase (ULK) binds the C2-domains of RIM1α

In our MS data, ULK2 was only identified with a low score. However, due to its suggested role in AZ assembly, the potential interaction with the presynaptic protein RIM1α was investigated. Using several independent biochemical approaches we found: (1) both ULK1 and ULK2 bind both C2-domains of RIM1α; (2) the interaction with RIM1α is mediated by their kinase domains; (3) inactivation of the catalytic activity of ULKs, by impairing the ATP binding site (K46R in ULK1, K39T in ULK2) (TOMODA et al., 1999; YAN et al., 1999), completely abolished its binding affinity for RIM1α. The presence of a lysine residue in the ATP pocket site ensures the autophosphorylation of the ULK1/2-spacer region that positively regulates kinase activity (TOMODA et al., 1999; YAN et al., 1999). It's believed that once autophosphorylation is impaired, the binding affinity of ULK1 and ULK2 for other substrates, like RIM1α protein, will decrease. Such is the case for fibroblast growth factor receptor substrate 2/3 that acts as substrate for WT-ULK1 and ULK2. In the presence of the kinase deficient form of ULK2 (K39T) the FRS2/3 is no longer bound and phosphorylated (AVERY et al., 2007).

Besides autophosphorylation, the activity of ULK1/2 is also under the control of other kinases. AMPK kinase for example, phosphorylates S^{555} of ULK1, thereby promoting the binding of ULK1 to 14-3-3 adapter proteins (BACH et al., 2011). 14-3-3 proteins are conserved regulatory molecules, able to bind a multitude of proteins, like S^{413} phosphorylated RIM1α (KAESER et al., 2008a) or S^{2845} phosphorylated Bassoon (SCHRÖDER et al., 2013). Thus, ULK kinases may act either directly, binding and phosphorylating RIM1α protein, or indirectly by modulating the function of other classes of proteins, such as adapter proteins.

ULK kinases have an unique phosphorylation recognition motif characterized by hydrophobic residues at multiple positions. According to peptide arrays the amino acids M, L and S are preferred in position -3; F, V, I and Y in positions +1 and +2; while L can be found at position +2 as well (PAPINSKI et al., 2014). Phosphorylation sites encompassing all these criteria were not found in RIM1α; however, this does not exclude phosphorylation at unconventional sites.

The positive interactions between ULKs and RIM1α were further supported by co-localization experiments in primary neuronal cultures. Both ULK kinases showed co-distribution with both the presynaptic proteins Bassoon and RIM1α, and the postsynaptic marker PSD-95. However, the degree of overlap with the presynaptic proteins was smaller

than with the postsynaptic marker. Studies in embryonic sensory neurons indicated that both ULK1 and ULK2 were present in axons and in growth cones, where punctuate structures were observed (ZHOU et al., 2007).

In all our biochemical studies RIM1α was able to bind both ULK1 and ULK2. This could be explained by the fact that both ULK1 and ULK2 have a high sequence homology (TOMODA et al., 1999). The mRNA expression profiles of ULK1 and ULK2 in adult mice indicate that the level of ULK1 in the cortex and hippocampus are much lower compared to ULK2 (Allen Brain Atlas[7]). Therefore, it remains to be elucidated if both isoforms or only one of them plays any significant role in the presynaptic compartment.

The ULK family, part of the serine/threonine kinase group, comprises five members, of which only two, ULK1 and ULK2, were shown to be expressed in brain (TOMODA et al., 1999). Whereas the role of ULK proteins in autophagy is documented (review: ALERS et al., 2012), their involvement in maintaining the CAZ is less well understood. ULK kinases have been linked to various processes from neurite outgrowth (TOMODA et al., 2004; ZHOU et al., 2007; OGURA et al., 2010) to the assembly of the AZ ultrastructure in *D.melanogaster* (WAIRKAR et al., 2009).

ULK kinase regulates axon formation in cerebellar neurons via the SynGAP-ULK-Syntenin-1 complex (TOMODA et al., 1999). Moreover, Syntenin-1 co-localizes within the presynaptic terminal with ELKS, contributing to the organization of the AZ (KO et al., 2006). ELKS, on the other hand, interacts with the PDZ-domain of RIM1α, possibly controlling either its distribution in cultured neurons (OHTSUKA et al., 2002; WANG et al., 2002) or inhibiting Ca^{2+}-channel binding to RIM1α and attenuating neurotransmitter release (KAESER et al., 2011). Via ELKS-Syntenin-1, ULK kinases might act on RIM1α and on other presynaptic proteins promoting changes in AZ architecture. Additionally, ULK may regulate the interaction between RIM1α-ELKS or RIM1α-Ca^{2+}-channels as well, which could have a direct impact on AZ ultrastructure or on the release machinery.

The postulated role of ULKs proteins in controlling AZ density and composition is based on studies in *D.melanogaster*, where ULKs regulate the localization of Bruchpilot (ELKS homolog) protein opposite to the glutamate receptors at synapses. The mechanism of action relies on the inactivation of ERK2 kinase by ULK, thereby promoting synapse development. Unc-51/ULK mutants displayed increased ERK2 kinase activity, while Bruchpilot was absent from many synapses (WAIRKAR et al., 2009). Since in mammalian cells RIM1α is a substrate for ERK2 kinase (SIMSEK-DURAN and LONART, 2008), it is tempting to speculate that ULK kinase may indirectly influence RIM1α phosphorylation level and in

[7] *http://mouse.brain-map.org*

consequence modulate its function by an unknown mechanism (*Fig. 5.1*). Further experimental data are needed to shed light on the potential function of ULK kinases in the presynaptic terminal and on the functional relevance of the binding between ULKs and RIM1α.

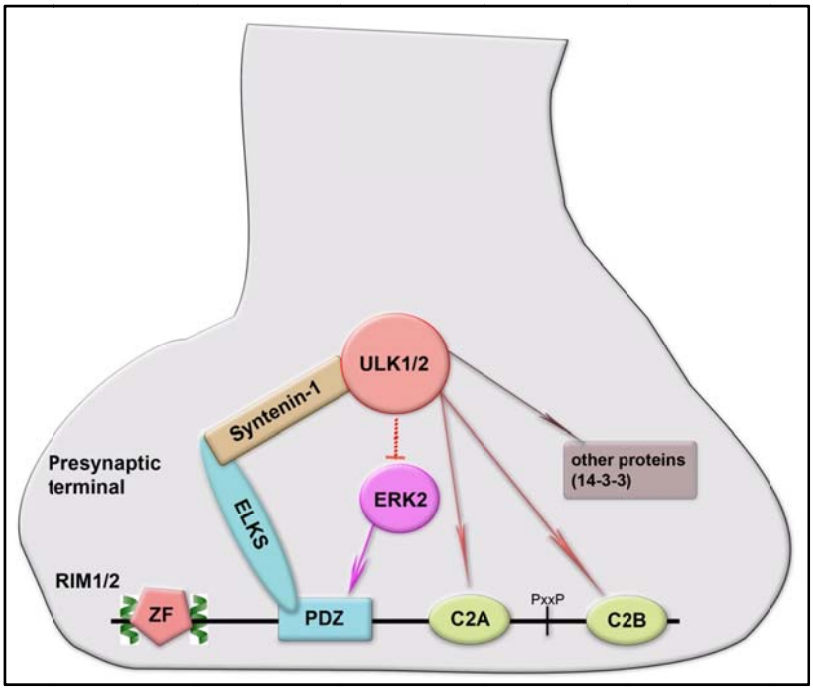

***Figure 5.1:* Hypothetical model for ULK kinase action in the presynaptic terminal.** ULK1/2, bound to Syntenin-1, blocks the activity of the ERK2 kinase. Simultaneously, RIM1α C2A-C2B domains might become the substrate for ULK1/2 kinase. In parallel ULK1/2 may also act on other active zone proteins (brown square).
ZF, zinc finger domain; PDZ, post synaptic density protein (PSD95), Drosophila disc large tumor suppressor (Dlg1), and zonula occludens-1 protein (zo-1); ULK, unc51-like kinase; ERK2, extracellular signal-regulated kinase 2.

5.2.1.2 Serine Arginine protein kinase 2 (SRPK2) targets specifically the C2A-domain of RIM1α

The second kinase identified with a high score by MS to associate with RIM1α, when using both crude synaptosomes and primary neuronal cultures, was SRPK2 (serine arginine protein kinase 2). By employing different *in vitro* binding assays, SRPK2 was detected to bind preferentially the C2A-domain of RIM1α.

The identification of SRPK2 to bind with high affinity RIM1α was unexpected, because this kinase has been mainly described to be involved in mRNA maturation by phosphorylating SR proteins, in chromatin reorganization and cell cycle progression (review: GIANNAKOUROS et al., 2011). Notably, two recent reports identified SRPK79D at *D.melanogaster*, as key protein in controlling the assembly of T-bars in neurons (JOHNSON et al., 2009; NIERATSCHKER et al., 2009). SRPK79D loss of function mutants displayed an accumulation of Bruchpilot (Brp) in the axons, while synapse morphology and synaptic transmission were unaffected. Given that both SRPK79D and Brp co-localized at the synapse, Brp might constitute a direct substrate for this kinase. However, the lack of a direct binding between these two proteins together with the absence of RS recognition sites in Brp (JOHNSON et al., 2009;

NIERATSCHKER et al., 2009) may indicate that other presynaptic proteins could act as mediators between SRPK79D and Brp.

One such protein could be RIM1α. The following data favours the idea that RIM1α could act as a possible substrate for SRPK2: (1) the high affinity of SRPK2 for the C2A-domain of RIM1α; (2) bioinformatical identification of RS dipeptides in the RIM1α sequence. Thus, SRPK2 could directly associate with RIM1α and phosphorylate it. Besides the RS dipeptides, SRPK2 may also phosphorylate unconventional sites in RIM1α, like the one previously described in Tau proteins-'PSLP' (HONG et al., 2012). Analysis of the RIM1α binding in the presence of a docking grove mutant (SRPK2-DM) revealed only a slight decrease in the RIM1α binding affinity compared to SRPK2-WT control. Moreover, deletion of both, the N-terminal region, important for the kinase activity, and the linker region, triggered as well a decrease in RIM1α binding affinity. Because in the presence of these truncated proteins, the binding to RIM1α was not completely abolished, the only regions from SRPK2 that could directly mediate these affinities are the catalytic domains. In consequence it remains to be elucidated, which kinase domain is directly involved in this interaction.

Up to date, only two proteins, SNAP25 and Syt1, were identified to bind the C2A-domain of RIM1α (COPPOLA et al., 2001). However, NMR studies were not able to confirm these findings (DAI et al., 2005). Identification of SRPK2 may represent the first specific binding partner for the RIM1α C2A-domain. The exact role of the C2A-domain in RIM proteins has not been fully elucidated. One point mutation in the C2A-domain of RIM1α (R844H) was linked to the autosomal dominant cone-rod dystrophy-CORD7, characterized by impaired vision due to the reduction in the cone and rod sensitivity (JOHNSON et al., 2003; MICHAELIDES et al., 2005). Individuals with such mutations display enhanced cognitive functions in at least the verbal and executive domains (SISODIYA et al., 2007).

IF studies support the co-localization of SRPK2 and RIM1α in the presynaptic compartment, despite the fact that the detected level of SRPK2 at synapses was significantly lower than at the soma. However, this is in agreement with the previous report of Nieratschker et al. (2009), where they could show that the expression level of SRPK79D was low and not well detected by the antisera raised against this protein. According to the Allen Brain Atlas, the mRNA expression level of SRPK2 in adult mouse brains seems to be low in the cortex compared to hippocampus. Because all our immunohistochemistry was performed with cortical neurons, a further investigation of the co-localization of SRPK2 and RIM1α in hippocampal neurons should be conducted as well.

Whereas studies in *D.melanogaster* suggested an important role for SRPK2 in preventing the ectopic formation of AZs within the axons (JOHNSON et al., 2009; NIERATSCHKER et al., 2009), the role of SRPKs in mammalian neurons, in particular in AZ formation, has not been fully addressed. The molecular mechanism by which SRPK79D prevents the unspecific accumulation of Brp at unconventional sites is not understood. However, it could be hypothesised that in mammalian cells SRPK2 might act in a similar way, regulating the assembly of AZ as well. Phosphorylation of RIM1α by SRPK2 may protect RIM1α against an unspecific accumulation/aggregation in different parts of the cell preventing in this way a premature assembly of the AZ. Once RIM1α reaches the correct destination (synaptic bouton), phosphatases could remove some of the phosphate groups promoting protein-protein interactions to occur. Additionally, certain functions of presynaptic proteins may be directly regulated by SRPK2 kinase activity. In this respect, the amount of SRPK2 present in the presynaptic terminal may be critical. Intriguingly, our IF data revealed that by blocking the activity of SRPK1 and SRPK2, a slight increase in the co-localization of SRPK2 with RIM1α was detected in the boutons. Because no sufficient data is available regarding the irreversibility of the inhibitor SRPIN340, we cannot conclude whether this presynaptic accumulation of SRPK2 represents active or inactive kinase.

Besides affecting the functions of presynaptic proteins, SRPK2 might promote changes in AZ architecture, by targeting the cytoskeleton as well. It has been reported that SRPK2 binds and phosphorylates Tau proteins (tau proteins stabilize the microtubules) impairing tau-dependent microtubule polymerization and neurite outgrowth (HONG et al., 2012). Hong et al. (2012) also showed that the knockdown of SRPK2 in the hippocampus of the Alzheimer's disease mouse model (APP/PS1) impact presynaptic functions. The amplitude of pair pulse facilitation (PPF), an indicator of presynaptic activity, was elevated in APP/PS1 mice, in which SRPK2 levels were decreased by injecting a lentivirus expressing a specific shRNA against this kinase (LV-shSRPK2), compared to WT. Unfortunately no electrophysiological data comparing the WT versus WT LV-shSRPK2 mice was presented. An increased in PPF was also measured in RIM1α KO mice, consistent with a reduced release probability (SCHOCH et al., 2002; PITSCH et al., 2012). Thus, it can be hypothesized that SRPK2 by phosphorylating various substrates may impact proper synaptic transmission. In *D.melanogaster* the deletion of SRPK79D does not induce any significant changes in the synaptic transmission at the NMJs (NIERATSCHKER et al., 2009). However, an overexpression of this kinase impaired synaptic transmission, probably by disrupting either the assembly of T-bars or the AZ organization (JOHNSON et al., 2009). Due to multiple effects this kinase might

have on various presynaptic proteins, further experimental data are necessary to explain whether SRPK2 acts as a negative regulator of AZ assembly, similar to *D.melanogaster*, or has a more subtle role in controlling diverse aspects in synaptic transmission.

5.2.2 VAPA/B proteins bind specifically the C2A-domain of RIM1α

The protein VAPA was identified with relative high scores in our MS analysis with both crude synaptosomes and neuronal cultures. In addition, the treatment of mouse crude synaptosomes with a kinase inhibitor (staurosporine) increased the level of VAPA detected by MS compared to the phosSTOP or control samples. These results corroborated with GST-pull down assays, in which kinase blockade increased not only the endogenous level of VAPA but also the binding affinity to the C2A-domain of RIM1α. Thus, a global kinase inhibition seems to favour the binding between RIM1α and VAPA.

The VAP protein family includes two highly homologous members: VAPA and VAPB/C (NISHIMURA et al., 1999). Both VAPA and VABP were identified to bind exclusively the C2A-domain of RIM1α in various biochemical assays, potencially due to their high degree of sequence homology. However, in our MS data we only detected VAPA, even though VAPB is expressed more abundantly in the brain (Allan Brain Atlas), indicating a preferential binding of VAPA to RIM1α.

Interestingly, the mutation of two threonine residues (T812/814A) in the RIM1α C2A-domain completely abolished the binding of RIM1α to VAPA. Bioinformatics predicts these threonines to be part of a PKA recognition motif. Either these threonine residues are necessary to mediate the direct binding of the RIM1α C2A-domain to VAPA or the phosphorylation status of these amino acid residues could impact the binding.

Taken together, this study shows that: **(1)** VAP proteins, and especially VAPA, bind specifically the RIM1α C2A-domain; **(2)** this association seems to be mediated by the threonine residues in the RIM1α C2A-domain.

Even though, Teuling et al. reported that VAPB did not co-distribute with presynaptic proteins, we observed that in rat cortical neurons these proteins were present in the same presynaptic compartment. The highest VAPA/B signal was detected, as previously published, in the soma, where the ER compartment is located (TEULING et al., 2007). However, IF analysis revealed that both VAP proteins showed a weak co-localization with endogenous RIM1α and Bassoon at the synapse. Because VAPs are actively involved in trafficking, their steady-state levels at synapses might be low.

Initially, VAP proteins were associated with plasma membrane fusion events in neuronal cells, via their interaction with Synaptobrevin/VAMP-2 protein (SKEHEL et al., 1995;

WEIR et al., 1998). However, later studies have shown that VAPA was not directly involved in SVs exocytosis but rather involved in regulating the organization of the ER (AMARILIO et al., 2005) and in ER-Golgi trafficking (KUIJPERS et al., 2013). Moreover, it was hypothesised that VAPA might play a role in trafficking or chaperoning vesicular components such as VAMP-2 through the ER to the presynaptic compartment (SKEHEL et al., 2000). The hypothesis of VAP proteins being actively involved in protein trafficking is supported by the fact that the *D.melanogaster* homolog, DVAP-33A was identified to selectively transport proteins to axonal processes (YANG et al., 2012). A reduction in the presynaptic DVAP-33A induced structural changes, like the disruption of synaptic microtubules and the accumulation of clusters of proteins and SVs along the axons (FORREST et al., 2013). In mouse cortical neurons VAPA is transported, through its interaction with protruding via KIF5, from the soma to neurites (MATSUZAKI et al., 2011). All these data could suggest a potential role of VAP proteins in assisting the selective transport of various axonal proteins, such as RIM1α, to either nascent or mature AZs. Therefore, we may speculate that besides VAMP-2, RIM1α could also be trafficked to the synaptic bouton via VAP proteins, a transport dependent on the phosphorylation status of both proteins. Future experiments will try to decipher the role of phosphorylation events in controlling the traffic of RIM1α.

Moreover, studies on DVAP-33A provide evidence of its importance in bouton formation by mediating the interaction between microtubules and presynaptic membranes (PENNETTA et al., 2002). DVAP-33 overexpression in presynaptic terminals induced an increase in the number of boutons that displayed a significantly reduced size and contained fewer vesicles (PENNETTA et al., 2002; CHAI et al., 2008). With respect to the total number of AZs Chai et al. (2008) did not observe any significant changes, while Ratnaparkhi et al. (2008) observed a decrease in the number of AZs. The study of Ratnaparkhi et al. suggests that VAP proteins might control the structural remodelling of AZs. However, up to date there not sufficient data connecting VAP proteins and AZ assembly in mammalian neurons.

Besides the suggested role in protein transport and bouton formation, VAP proteins could be actively involved in AZ protein sorting in ER-Golgi as well (*Fig. 5.2*). Active zone proteins are processed in the soma of neurons in different ways. While Piccolo, Bassoon and ELKS share a common Golgi-derived transport vesicle, Munc13 exits the soma on a distinct Golgi-derived vesicle. Surprisingly, RIM1α associates with transport vesicles in a post-Golgi compartment. However, to date the molecular mechanism governing this sorting is not well understood (MAAS et al., 2012). Thus, an intriguing question is the potential involvement of VAP proteins in sorting RIM1α in the ER-Golgi compartment. VAPA was shown to be involved

mainly in the ER-to-Golgi anterograde transport (PROSSER et al., 2008), while VAPB and its binding partner, YIF1A (Yip1-interacting factor homologue A) were reported to be necessary for the efficient transition of cargo proteins through the early secretory pathway (KUIJPERS et al., 2013). Since our binding assays showed a strong affinity between both VAP proteins and RIM1α, we can speculate that RIM1α might be assisted by both VAPA and VAPB in passing through ER-Golgi and exit the Golgi apparatus on a distinct transport vesicle.

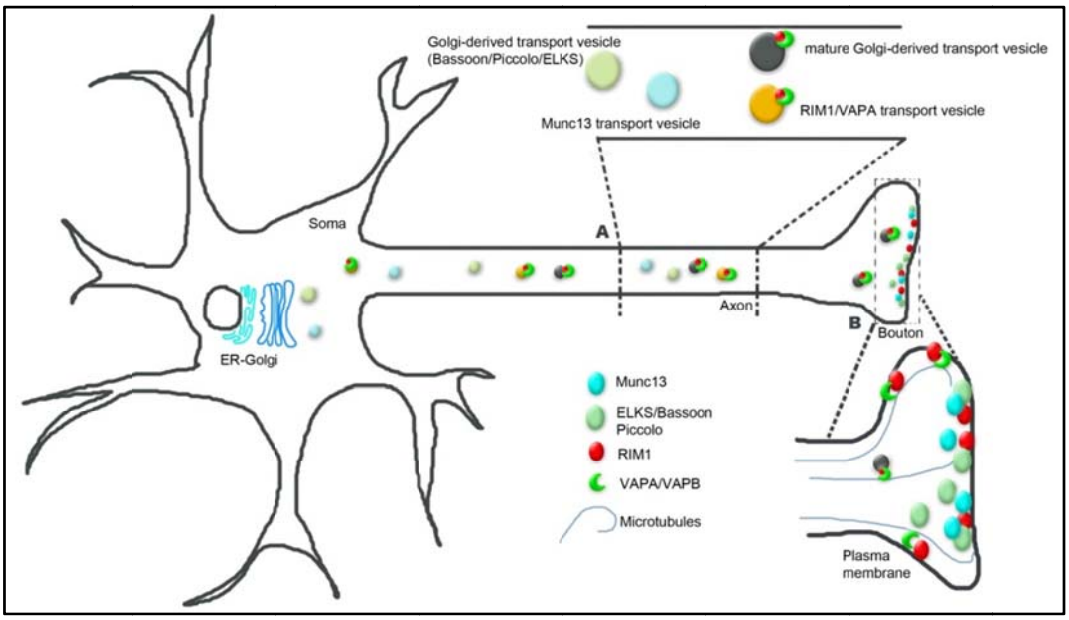

***Figure 5.2*: Hypothetical function of VAP proteins in sorting and transporting RIM1α to synapse (adapted after MAAS et al., 2012). (A)** Presynaptic proteins exit the Golgi apparatus via different vesicles. Bassoon, Piccolo and ELKS share a common Golgi-derived transport vesicle (**green**), whereas Munc13 (**blue**) and RIM1α (**red**) are trafficked independently. Model adapted after MAAS et al., 2012. Theoretically, the trafficking of RIM1α may be assisted by VAP proteins (**green**). During transport all these vesicles undergo maturation steps resulting in mature Golgi-derived transport vesicle (**grey**), which contain the entire set of AZ proteins. **(B)** According to Pennetta et al., DVAP may mediate the interaction between plasma membrane and microtubules. Hypothetically, VAPA/VAPB could facilitate the interaction between plasma membrane and various presynaptic proteins, like RIM1α. In this way VAP proteins could participate in targeting the AZ proteins to specific assembly sites.

5.2.3 Copine VI binds RIM1α in a calcium-dependent manner

Copine VI, a calcium binding protein highly enriched in the hippocampus (stratum radiatum in CA1 and CA3; inner molecular layer of dentate gyrus) and in the main olfactory bulb (NAKAYAMA et al., 1998; 1999), was identified with high scores in all approaches by MS. Up to date not much is known about the function of Copine VI at the synapse. Previous reports have shown that Copine VI, a C2-domain containing protein, associated with the plasma membrane and clathrin-coated membranes of internalized early endosomes in response to an increase in the intracellular calcium level in HEK293 cells. The C2-domains were necessary for the calcium-mediating membrane targeting, while the binding required the proximal region to the vWA-domain (PERESTENKO et al., 2010).

Our biochemistry data suggests a strong preference of Copine VI for the C2B-domain of RIM1α, while binding to full-length RIM1α is Ca^{2+}-dependent. Since RIM1α C2-domains lack the amino acids necessary to bind calcium ions (COPPOLA et al., 2001; GUAN et al., 2007), only the C2-domains of Copine VI are able to bind these divalent ions.

Because these C2-domains can form homo- or heterodimers, the MS data was analysed for increased occurrence of C2-domain containing proteins, such as Synaptotagmin1 or other copines. Such proteins, associating with the C-terminal part of RIM1α, were scarcely present in our MS data. Moreover, other copines were not detected in the MS. Together these observations support the specificity of the interaction.

Previous reports have suggested that Copine VI is enriched in the postsynaptic terminal (Alexander Kriz, 2010; *urn: urn:nbn:ch:bel-bau-diss89692*). However, our IF of endogenous Copine VI in primary cultured neurons also suggests a presynaptic localization, where it partially co-localizes with the presynaptic protein RIM1α. Therefore, Copine VI might be present on both pre- and postsynaptic terminals, mediating different cellular processes. Additionally, the study of Nakayama showed that Copine VI could be present in low amounts in some parts of axons as well (NAKAYAMA et al., 1999). Unpublished data of our collaborators attribute to Copine VI a presynaptic function as well, e.g. the regulation of SV fusion.

In summary, identification of Copine VI, as a potential binding partner for RIM1α, may point to a possible link between the function of RIM1α and the calcium-dependent events in the presynaptic terminal. Future experiments will be performed in order to examine the relevance of this interaction in the presynaptic terminal.

5.3 Identification of novel SV2A binding partners: new experimental approaches

Because of the still enigmatic function of the synaptic vesicle protein 2A (SV2A) in synaptic transmission and neuronal network plasticity, identification of novel potential binding partners for SV2A could provide insights into its role at synapses.

SV2A is 12-pass transmembrane protein with a high degree of posttranslational modifications that include a highly glycosylated intravesicular loop and a N-terminus containing at least ten phosphorylation sites (review: MENDOZA-TORREBLANCA et al., 2013). To date only a limited number of binding partners for SV2A have been identified, such as Synaptotagmin1 and clathrin adaptor proteins (review: MENDOZA-TORREBLANCA et al., 2013; YAO et al., 2010), whose functional relevance for the function of SV2A are still unclear.

Since the previous strategies to purify and identify novel SV2A binding partners were based mainly on GST pull-down or yeast two-hybrid assays using only parts of SV2A and did

not take into the account the posttranslational modifications (SCHIVELL et al., 1996; YAO et al., 2010), we attempted to analyse the binding partners of overexpressed SV2A using a tandem affinity purification method. By applying one- or two-step purifications we aimed at the identification of specific SV2A binding partners by maintaining at the same time the native SV2A protein conformation. Therefore, a FLAG/Strep sequence was tagged either in the N- or C-terminus of SV2A in order to detect any differences in SV2A binding affinities. Different approaches were tested in order to co-purify SV2A and its potential binding partners both from cortical neurons as well as from transduced mouse brain.

Purification of overexpressed SV2A from brain by employing the tandem-affinity methodology proved to be inconsistent between different trials. The major problems that we encountered were: **(1)** the expression level of the recombinant protein did not give a good yield after purification because either the viral titer was not high enough or the virus did not express high levels of protein; **(2)** the purification methodology used to co-purify the tagged-SV2A had an unsatisfactory efficiency. During different approaches of purification, in most of the cases, the recombinant protein was lost, especially when the Strep column was used, either because the column was not able to retain the applied material (technical problem) or the Strep sequence in the tag was masked by various protein contaminants. In the case of FLAG-beads, most of the captured SV2A could not be eluted from beads. In contrary to the poor yield of SV2A after purification from brain, sufficiently high amounts were obtained when mouse primary cultured neurons were used as starting material.

It has been demonstrated that the number of SV2A molecules per SV is critical for its function (TAKAMORI et al., 2006; NOWACK et al., 2011). Therefore, to avoid high levels of overexpressed SV2A in addition to the endogenous one, neuronal primary cultures were prepared from SV2A+/- or SV2A -/- mice. Moreover, to fix transient and/or weak interactions between SV2A and other proteins, a series of cross-linkers were used. However, neither the cross-linkers nor the primary cultures prepared from KO treatment produced a visible enrichment in the co-purified proteins. Because we could not see an improvement, wild-type neuronal cultures were further used for the final experiment. Compared to heterozygous or knock-out neurons, WT neurons allowed for a higher amount of starting material. Preparation of neuronal cultures from heterozygous or knock-out mice was limited to the number of embryos available at a certain time-point, since KO SV2A mice cannot be breed (CROWDER et al., 1999).

The analysis of protein complexes co-precipitated with SV2A by MS revealed several proteins previosly reported to associate with the N-terminal region of SV2A (YAO et al., 2010),

like: AP-1 complex, Transcriptional activator protein Pur-beta, Tubulin beta-2A chain, Syt1. Additionally, other proteins were identified by MS, e.g. Latrophilin, EHD1; however, none of these potential SV2A binding partners could be verified in binding assays.

Overall, the attempt to identify novel potential interacting partners for SV2A has been unsuccessful. This might be due to the fact that interactions require the native structure of the 12-transmembrane protein, a structure that in turn could have hampered the purifications of the SV2A proteome. Even though the detergent, used to solubilize SV2A under native conditions, was reported to maintain SV2A's binding properties to Syt1 and Keppra (anti-epileptic drug) (LAMBENG et al., 2006), it might not have preserved the native structure and therefore interactions might have been lost. According to various protein-protein databases[8], also for other multi-pass membrane proteins, e.g. synaptophysin or SCAMP, fewer binding partners are known.

Over the years different functions have been attributed to SV2A, like: neurotransmitter transport, gel matrix (the sugar moieties attached to the intravesicular loop may hold and release neurotransmitters) or modulator of exocytosis (review: MENDOZA-TORREBLANCA et al., 2013). Experimental data suggest that SV2A mediates SV fusion by regulating the action of Syt1. The N-terminal region of SV2A binds and keeps Syt1 inactive until the level of intracellular calcium rises. Once the calcium level is high the binding is disrupted and Syt1 interacts with the SNARE complex facilitating SV fusion. Additionally, during endocytosis SV2A binds Syt1 and prevents its diffusion. The recycling after SV fusion is mediated by clathrin adaptor proteins that bind both Syt1 and SV2A (review: MENDOZA-TORREBLANCA et al., 2013). The fact that these proteins, Syt1 and various adaptor proteins have been identified by our MS may suggest that SV2A, in order to fulfil its function, does not require a large number of interacting proteins.

Because our attempt to purify and resolve the SV2A proteome was not successful, other novel approaches are needed to be developed, e.g. generation of a knock-in mouse model expressing a tagged SV2A. Such a model would give the opportunity to study more closely not only the potential binding partners of SV2A but also the function of this protein.

[8] *http://www.uniprot.org/uniprot/P07825 (synaptophysin, R.norvegicus)*
http://www.uniprot.org/uniprot/P56603 (SCAMP, R.norvegicus)

6. Outlook

Taken together, the results of this thesis identified four novel RIM1α binding partners: two kinases, a calcium binding protein and proteins involved in trafficking and bouton formation. The next step will be to investigate the functional relevance of these new RIM1α binding proteins. Therefore, the following three major questions will need to be addressed in future experiments:

1. The role of SRPK2 and ULK1/2 in maintaining or/and controlling the AZ architecture and composition. In this regard, the role of these novel kinases in the presynaptic terminal should be investigated by using a specific SRPK2 inhibitor (SRPIN340) as well as shRNA-mediated knock-down in neuronal cultures. In addition, it will be necessary to examine the possible contribution of these kinases in controlling the release machinery, for example by measuring the SV exo- and endocytosis using the fluorescent FM-dyes. Moreover, electrophysiological recordings of neuronal cultures treated with either shRNA or SRPIN340 would be useful to reveal any changes that may occur during synaptic transmission when kinase function is blocked. Additionally, it will be necessary to examine whether RIM1α is a direct substrate of these kinases.

2. The role of VAP proteins in modulating the function or trafficking of RIM1α. It should be tested if VAP proteins play a role in trafficking presynaptic proteins to the boutons, in particular RIM1α. Analysing if the absence of VAPA and/or VAPB results in an impairment of RIM1α trafficking, could be tested by confocal live-imaging. Next, it should be examined the functional relevance of C2A-domain phosphorylation in respect to the function of VAPA. To evaluate whether VAP proteins may constitute a link between the core release machinery and RIM1α, electrophysiological recordings of neuronal cultures overexpressing WT or T812/814A RIM1α (point mutations in the C2A-domain that abolished the binding to VAPA) could be performed.

3. The role of the interaction between the calcium-binding protein, Copine VI and RIM1α in presynaptic plasticity. To address the function of Copine VI, shRNAs targeting specifically Copine VI will be used to investigate whether this protein has any major impact on the function of RIM1α and on synaptic transmission.

Because the amount of SV2A seems to be critical for its function, a knock-in mouse model could be generated by inserting a tag in SV2A locus. Expression of this new tagged protein could be analysed in the whole brain. Moreover, the tagged SV2A could be purified from either whole brain or specific brain area in order to identify novel interacting partners.

7. Summary

Synaptic plasticity encompasses various cellular mechanisms, which confer synapses the ability to react and adapt to ongoing changes in network activity. Some of the suggested mechanisms include remodelling and/or assembly of active zones (AZ), and modulation of neurotransmitter release. At the molecular level posttranslational modifications of proteins, e.g. phosphorylation, have been reported to be associated with these events. Two components of the release machinery, RIM1α and synaptic vesicle protein 2A (SV2A) were shown to be actively involved in presynaptic plasticity. However, the impact of posttranslational modifications, like phosphorylation, on the function of these proteins is not well understood. Therefore, the goals of this thesis were:

(1) To examine the impact of phosphorylation on the binding properties of RIM1α;

(2) To identify and analyse novel binding partners for SV2A.

We found that the distribution of RIM1α at synapses is altered after globally increasing the level of phosphorylation, while its total level remained unchanged, suggesting that the association of RIM1α with the CAZ is controlled by its phosphorylation status. Affinity purification and MS revealed that alterations in the phosphorylation status of RIM1α affected its affinity to specific binding partners. Out of the identified proteins, four candidates with a potential functional link were chosen to be further analysed in binding assays: two kinases (unc-51-like kinase 1/2, serine arginine protein kinase 2), one calcium-binding protein (Copine VI), and proteins involved in trafficking (vesicle-associated membrane protein (VAMP) associated-protein A/B). Interestingly, RIM1α may represent the first AZ substrate for ULKs and SRPK2, which in *D.melanogaster* have already been linked to the assembly of AZs. This may support the hypothesis that both ULKs and SRPK2 could be actively involved in controlling not only RIM1α's function but also its association with the CAZ. VAP proteins, by specifically binding the C2A-domain of RIM1α, may contribute to control the trafficking of RIM1α to the synapse. Copine VI may regulate the function of RIM1α in a calcium-dependent manner. Further analysis will reveal if these novel interactions may have any functional relevance for the function of RIM1α. In summary, we identified novel RIM1α binding partners, of which some interact with RIM1α in a phosphorylation-dependent manner. Further studies will have to examine if these are involved in mediating the association of RIM1α with the CAZ or its role in plasticity.

The last part of the study was dedicated to another presynaptic protein, SV2A. To date the role played by SV2A in SV priming is not fully elucidated. Therefore, to gain insight into the enigmatic function of SV2A identification of novel binding partners was pursued.

Different affinity purification strategies coupled to MS were performed in order to identify the SV2A proteome. However, none of these approaches resulted in the identification of novel interacting proteins, which could be further verified in biochemical assays.

Taken together, the findings of this thesis may form the basis for further functional studies in order to decipher the molecular mechanisms underlying the function of RIM1α and in consequence, the role of RIM1α in presynaptic plasticity.

8. Appendix

8.1 Plasmid Maps

8.1.1 pAAV-MCS

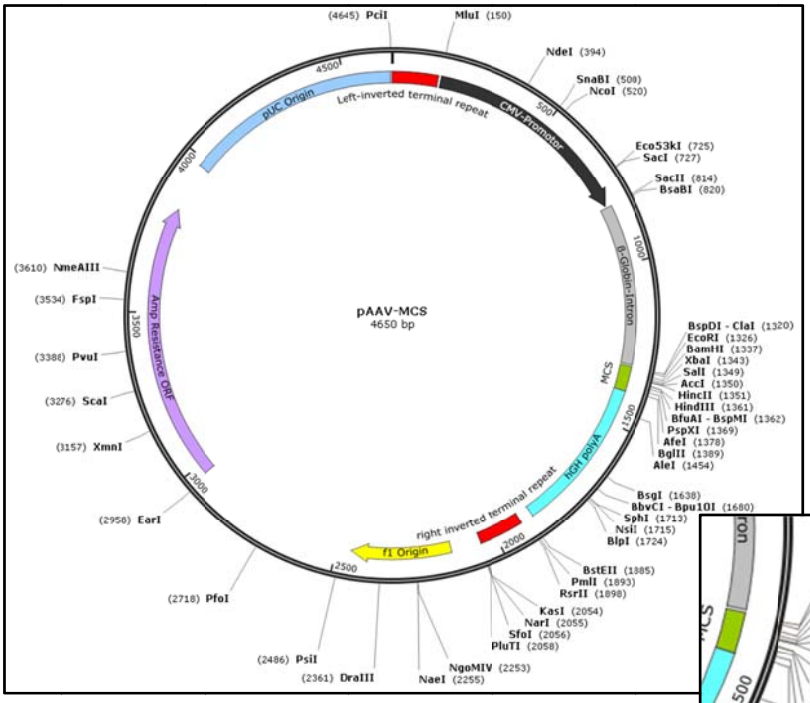

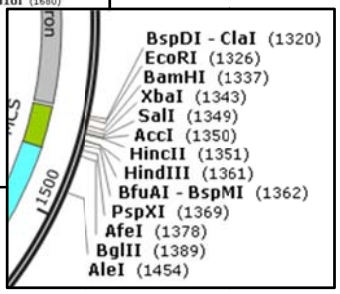

Figure 8.1: **Circular map of the pAAV-MCS plasmid** (adapted from Stratagene AAV Helper Free-system instruction manual). The plasmid contains a cytomegalovirus (CMV) promoter with a beta-globin intron, a MCS and a polyadenilation site. These elements are flancked by a left inverted terminal repeat (L-ITR) and a right inverted terminal repeat (R-ITR) neecessary for the synthesis of recombinant adeno-associated viruses (rAAV) genome. The order of the restriction enzymes in the MCS is depicted in the inset.

8.1.2 CMV-MCS

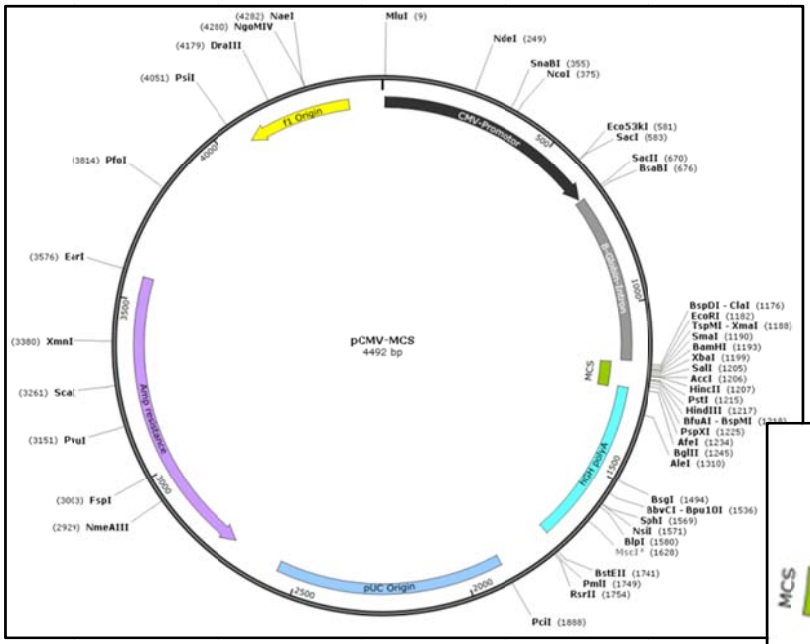

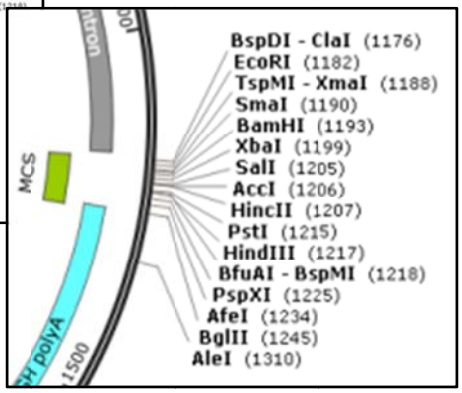

Figure 8.2: **Circular map of the pCMV-MCS plasmid** (adapted from Stratagene AAV Helper Free-system instruction manual). The plasmid contains a cytomegalovirus (CMV) promoter with a beta-globin intron, a MCS and a polyadenilation site (hGH pA). The enzyme restriction sites in the MCS are detailed in the inset.

8.2 cDNA and Protein sequences

8.2.1 RIM1α cDNA sequence (R.norvegicus)- NCBI Ref. seq: NM_052829.1

[atgtcctcggccgtggggccccgaggtcctcgcccacccacggtgcctccccctatgcaagaactgcccgacctgagccacctgaccgaggaggagaggaac
attatcatggcagtgatggaccggcagaaggaagaggaggaaaaagaagaggccatgctcaa]E1gtgtgttgtcagggacatggcgaagcctgctgcctgcaa
aacaccaagaaatgctgaaagccagccccatcaaccaccact]E2gaacattttcagatgtgtctgtgttcccagaaagccaagcagcgaagagggaggcccaga
aagagactg]E3gagattgcatcaacagtttgaaagctacaaggagcaagtgagaaaaatcggagaggaagcgaggcgttaccagggcgagcacaaggatgat
gccccgacgtgtggaatctgtcataagacaaagtttgctgatggatgtggccatctctgctcctattgtcgcaccaagttctgtgcacgctgcggaggccgtgtgtctc
tgcgatcgaacaatgaggacaaagtg]E4gttatgtgggtatgcaatttatgtcgaaagcaacaagaaatcttaacgaaatctggagcgtggttctttggaagtggccc
tcagcagcctagtcaagatgggactctgagtgacacggccacaggtgctggatctgaggtgccaagagaaaagaaagcaaggctccaagagcgatcaaggtctc
agacgcccttgagtacagcagctgtctcttcccaagacactgctacccccggtgcaccgttgcacaggaacaaaggggctgagccctcacagcaagccttgggtc
ctgaacagaagcaggcatcaagatcaagaagcgagccaccgagggaaag]E5gaagaaggctccagggctttcagagcagaatggcaagggaggccagaag
agcgagcgcaaacgtgtccccaagtctgtggtgcaacccggggaagggatcgcggatgagagggagaggaaagagaggcgggaaacccgcaggttggaga
aagggcgctcccaggactactcagaccggcctgagaaacgcgacaatggcagggtggcggaagaccagaagcagaggaaggaggaggagtaccagactag
gtaccgcagcgaccctaacctggctcgctacccggtgaaggcgccgccagaggagcagcagatgcgcatgcacgcccgggtgtcccgagcgaggcacgagc
ggcgccacagcgacgtggcgctcccgcacaccgaggcagctgccgccgcgccggctgaggccacggcgggcaagcgcgcgccggccaccgccagggtct
ctcccccggagtcccgcgcgcacgcgcggcggccgcccagcctcccaccgagcacgggccaccgccgccgcggccagccccgggtcccgcagagccac
ccgagccgcgcgtccccgagccgctccgtaagcagggccgcctggacccgggctcggccgtgcttctgcgcaaggccaagcgcgagaaggcggagagcatg
ctgcggaacgactcgctgagctccgatcagtccgagtccgtgcggccatcccgcccaagcctcaccggcccaagcggggaggcaagagacgtcagatgtcg
gtgagcagctcggaggaggagggcgtgtccacaccggagtacacgagctgcgaggacgtggagctggagagcgagagcgtgagcgagaaag]E6gtgactt
ggattactactggttggatcccgccacgtggcacagcagggaaacgtcgcctatcagttcg]E7catcctgtaacgtggcagccgtctaaagagggagatcgacta
atcggccgtgttattcttaacaaaagaacaaccatgcccaaagaatcaggtgcattattgggtctgaag]E8gtggttggaggaaaaatgacggacttagggcgcctt
ggtgctttcatcaccaaagtaaagaagggcagcctggcagacgtcgtcggacacctaagagcag]E9gggacgaagtcctagagtggaatggtaaacccctgcc
gggagcaacaaacgaagaagtttacaacattatcttagaatcaaaatcagaacctcaagttgagattattgtttcaaggcctattgg]E10tgacatccccaggatccct
gagagttcccatcctcccctggagtcca]E11gttcaagttcctttgaatctcagaaaatggaaaggccttctatttctgttatttctccaaccagccctggagctctgaaa
gatgccccacaagtcttaccagggcaactctca]E12gtgaagctatggtatgataaagtggggcaccagctgattgtaaatgttctacaagcaacagatctacccct
agagtagatggccgtcccaggaatccctatgtaaaaatgtattttcttccagatagaag]E13cgacaaaagtaaaaggagaaccaaaacagtaaagaaacttctaga
gccaaaatggaaccagacatttgtctactcacacgtacatcgtagagattttcgagagcgaatgttagagattaccgtgtgggaccagccgagagtacaggacgaa
gagagtgaatttcttggagag]E14atcctcatagagttggaaacagcgcttttagatgatgagccccattggtataaactccagacacatgacgaatcttcactacctct
gcctcagccatcaccgttcatgcccaggcggcatattcatggagagagctccagcaaaaagctacaaa]E15gatctcagcgaatcagtgatagtgacatctcagatt
atgaggttgatgatggtattggagtagtgcctccag]E16tgggttatagagctagtgctagagagagtaaagcaaccacgttaacagtgccagagcaacaaagaac
tacacatcaccgctcacgttccgtgtctcctcatcgcggcgatgatcagggaaggcctcgttcacgtttaccaaatgtgccattacagag]E17gagcttagatgaaatt
catccaacacgaaggtcacgttctccaacccgacaccatgatgcctcccgaagcccggccgatcacagatccagacatgtggaaagtcaatattcgtcagagcca
gacag]E18tgagcttctcatgctgcccagagcaaaacgaggacgaagtgcagaaagcctacacatgaccaga]E19gaccttgttaggtactctaacacattacca
cccaagatgcctttattacaaaacgactaccgttggagcagcagt]E20gaactgcagccctctcttgacagggctaggagtgctagtaccaactgcttgagaccaga
tactagtttgcattcaccagaacgagaaag]E21gggtagatggtccccctccctagataggaggcgacctgctagccccaggattcaaatccagcatgcatctccg
gagaatgacag]E22gcactccagaaagtctgaaagatgtagcatccaaaaacagtctaggaaaggcacagcctctgatgcagacag]E23ggttctcccaccatg
cctttctagaaggggatacgcaaccccaagagcaaccgatcaaccggtcgttaggggaaagcatcccactcgttcacggtcgagcgagcactctagtgtcagaac
cctgtgttctatgcaccaccttgcccccggagggtcggcgccaccttctccacttctgacaag]E24aacgcaccgacaaggaagcccaacccagtctcctccagca
gacacatccttcggcagtcgccgtggaagacagctcccacaggtgccagttcgaagcggcagtatagaacaag]E25caagcttagtagtggaggagcgaacga
gacagatgaaagtgaaagttcaccgatttaagcagacaacagggtctgggtctagtcaagaacttgaccacgagcaatactccaag]E26tacaacatacataaaga
tcagtacagaagctgtgataacgcgtctgccaagtcttcagatagtgatgtcagtgatgtgtccgccatttccagagccagcagtacctcacgcctcagcagcacaa
gctttatgtcagagcagtctgagcgcccccaggggtaggatcag]E27ttcatttacccccaaaatgcaaggcagacggatggggacttcaggaagagccatcatca
agagcaccagtgtaagtggagagatatatacactggaacgtaatgacggtagccagtcggacacggccgtaggtaccgtcggagccggtggaaagaaacgaag
atccagcctgagcgccaaagtggtagccattgtgtctcgaagaagcaggagcacgtcacagctcagccagacag]E28agtcgggccacaagaagttgaaaagc
accatccagaggagtacggaaacaggaatggcagctgaaatgcggaagatggtgagacagccgagccgggagtccacggatggcagcatcaacagttatagct
cggaaggaaa]E29cttgatatttcctggagttcgagtaggacccgacagtcagttcagtgatttccttgatgggttgggaccagcgcagctcgttggccgtcagacg
ctcgccacccccggccatgg]E30gcgatatccaaatcgggatggaggataagaagggtcagttggaggttgaggttatcagagcccggagccttacacaaaaacc
tggttccaaatctacacccg]E31ctccctatgtgaaagtatatcttttggaaaatggagcctgtattgccaaaaagaagacaagaattgcacggaaaactctcgatcctt
tgtatcagcagtccctggtttttgatgaaagtccacagggtaaagttcttcag]E32gtgattgtctggggtgactatggaagaatggaccacaaatgctttatgggtgtg
gctcaaatcttgttggaagaacttgatctatccagcatggtgattggatggtataaattgttccctccgtcctcactggtggatcccactctcgctccctgacccgccg
ggcttcccaatcatctctggaaagttcgtccgggcctccctgcatccggtcatag]E33

8.2.2 RIM1α protein sequence (R.norvegicus)

MSSAVGPRGPRPPTVPPPMQELPDLSHLTEEERNIIMAVMDRQKEEEEKEEAMLKCVVRDMAKPAACKTPRNAESQ
PHQPPLNIFRCVCVPRKPSSEEGGPERDWRLHQQFESYKEQVRKIGEEARRYQGEHKDDAPTCGICHKTKFADGCG
HLCSYCRTKFCARCGGRVSLRSNNEDKVVMWVCNLCRKQQEILTKSGAWFFGSGPQQPSQDGTLSDTATGAGSEV
PREKKARLQERSRSQTPLSTAAVSSQDTATPGAPLHRNKGAEPSQQALGPEQKQASRSRSEPPRERKKAPGLSEQNG
KGGQKSERKRVPKSVVQPGEGIADERERKERRETRRLEKGRSQDYSDRPEKRDNGRVAEDQKQRKEEEYQTRYRS
DPNLARYPVKAPPEEQQMRMHARVSRARHERRHSDVALPHTEAAAAAPAEATAGKRAPATARVSPPESPRARAAA

AQPPTEHGPPPPRPAPGPAEPPEPRVPEPLRKQGRLDPGSAVLLRKAKREKAESMLRNDSLSSDQSESVRPSPPKPHR
PKRGGKRRQMSVSSSEEEGVSTPEYTSCEDVELESESVSEKGDLDYYWLDPATWHSRETSPISSHPVTWQPSKEGDR
LIGRVILNKRTTMPKESGALLGLKVVGGKMTDLGRLGAFITKVKKGSLADVVGHLRAGDEVLEWNGKPLPGATNE
EVYNIILESKSEPQVEIIVSRPIGDIPRIPESSHPPLESSSSSFESQKMERPSISVISPTSPGALKDAPQVLPGQLSVKLWYD
KVGHQLIVNVLQATDLPPRVDGRPRNPYVKMYFLPDRSDKSKRRTKTVKKLLEPKWNQTFVYSHVHRRDFRERML
EITVWDQPRVQDEESEFLGEILIELETALLDDEPHWYKLQTHDESSLPLPQPSPFMPRRHIHGESSSKKLQRSQRISDS
DISDYEVDDGIGVVPPVGYRASARESKATTLTVPEQQRTTHHRSRSVSPHRGDDQGRPRSRLPNVPLQRSLDEIHPTR
RSRSPTRHHDASRSPADHRSRHVESQYSSEPDSELLMLPRAKRGRSAESLHMTRDLVRYSNTLPPKMPLLQNDYRW
SSSELQPSLDRARSASTNCLRPDTSLHSPERERGRWSPSLDRRRPASPRIQIQHASPENDRHSRKSERCSIQKQSRKGT
ASDADRVLPPCLSRRGYATPRATDQPVVRGKHPTRSRSSEHSSVRTLCSMHHLAPGGSAPPSPLLTRTHRQGSPTQS
PPADTSFGSRRGRQLPQVPVRSGSIEQASLVVEERTRQMKVKVHRFKQTTGSGSSQELDHEQYSKYNIHKDQYRSC
DNASAKSSDSDVSDVSAISRASSTSRLSSTSFMSEQSERPRGRISSFTPKMQGRRMGTSGRAIIKSTSVSGEIYTLERND
GSQSDTAVGTVGAGGKKRRSSLSAKVVAIVSRRSRSTSQLSQTESGHKKLKSTIQRSTETGMAAEMRKMVRQPSRE
STDGSINSYSSEGNLIFPGVRVGPDSQFSDFLDGLGPAQLVGRQTLATPAMGDIQIGMEDKKGQLEVEVIRARSLTQK
PGSKSTPAPYVKVYLLENGACIAKKKTRIARKTLDPLYQQSLVFDESPQGKVLQVIVWGDYGRMDHKCFMGVAQI
LLEELDLSSMVIGWYKLFPPSSLVDPTLAPLTRRASQSSLESSSGPPCIRS*

8.2.3 ULK1 cDNA and Protein sequence (M.musculus)- Clone ID:6406755/GenBank: BC059835

```
ATGGAGCCGGGCCGCGGCGGCGTCGAGACCGTGGGCAAGTTCGAGTTCTCTCGCAAGGACCTGATTGGACACGGCGCCTT
 M  E  P  G  R  G  G  V  E  T  V  G  K  F  E  F  S  R  K  D  L  I  G  H  G  A  F
CGCGGTGGTCTTCAAGGGTCGACACCGCGAGAAGCACGACCTGGAGGTGGCCGTCAAATGCATTAACAAGAAGAACCTTG
  A  V  V  F  K  G  R  H  R  E  K  H  D  L  E  V  A  V  K  C  I  N  K  K  N  L
CCAAGTCCCAAACACTGCTGGGAAAGGAAATCAAAATCCTGAAGGAACTAAAGCACGAAAACATCGTGGCGCTGTATGAC
A  K  S  Q  T  L  L  G  K  E  I  K  I  L  K  E  L  K  H  E  N  I  V  A  L  Y  D
TTCCAGGAAATGGCTAATTCTGTCTACCTGGTCATGGAGTATTGTAATGGTGGAGACCTGGCTGACTACCTGCACACTAT
 F  Q  E  M  A  N  S  V  Y  L  V  M  E  Y  C  N  G  G  D  L  A  D  Y  L  H  T  M
GCGCACACTGAGTGAAGACACTGTCAGGCTTTTCCTACAGCAGATCGCTGGCGCCATGCGGCTGCTGCACAGCAAGGGCA
  R  T  L  S  E  D  T  V  R  L  F  L  Q  Q  I  A  G  A  M  R  L  L  H  S  K  G
TCATCCACCGGGACCTGAAGCCCCAAAACATCCTGCTGTCCAACCCTGGGGGCCGCCGGGCCAACCCCAGCAACATCCGA
I  I  H  R  D  L  K  P  Q  N  I  L  L  S  N  P  G  G  R  R  A  N  P  S  N  I  R
GTCAAGATTGCTGACTTTGGATTCGCTCGGTACCTCCAGAGCAACATGATGGCGGCCACACTCTGTGGTTCTCCTATGTA
 V  K  I  A  D  F  G  F  A  R  Y  L  Q  S  N  M  M  A  A  T  L  C  G  S  P  M  Y
CATGGCTCCTGAGGTCATTATGTCCCAGCACTACGATGGAAAGGCTGACCTGTGGAGCATTGGCACCATTGTCTACCAGT
  M  A  P  E  V  I  M  S  Q  H  Y  D  G  K  A  D  L  W  S  I  G  T  I  V  Y  Q
GTCTGACAGGGAAGGCCCCTTTTCAGGCCAGCAGCCCTCAGGATTTGCGCCTGTTTTATGAGAAGAACAAGACACTAGTT
C  L  T  G  K  A  P  F  Q  A  S  S  P  Q  D  L  R  L  F  Y  E  K  N  K  T  L  V
CCTGCCATCCCCCGGGAGACATCAGCTCCCCTGCGGCAGCTGCTCCTGGCTCTGTTGCAGCGGAACCACAAGGACCGCAT
 P  A  I  P  R  E  T  S  A  P  L  R  Q  L  L  L  A  L  L  Q  R  N  H  K  D  R  M
GGACTTTGATGAATTTTTCCACCACCCTTTCTTGGATGCCAGCACCCCCATCAAGAAATCCCCACCTGTGCCTGTGCCCT
  D  F  D  E  F  F  H  H  P  F  L  D  A  S  T  P  I  K  K  S  P  P  V  P  V  P
CATATCCAAGCTCAGGGTCTGGCAGCAGCTCCAGCAGCAGCTCTGCCTCCCACCTGGCCTCTCCACCGTCCCTGGGGGAG
S  Y  P  S  S  G  S  G  S  S  S  S  S  S  S  A  S  H  L  A  S  P  P  S  L  G  E
ATGCCACAGCTACAGAAGACCCTTACCTCCCCAGCCGATGCTGCTGGCTTTCTTCAGGGCTCCCGGGACTCTGGTGGCAG
 M  P  Q  L  Q  K  T  L  T  S  P  A  D  A  A  G  F  L  Q  G  S  R  D  S  G  G  S
CAGCAAAGACTCCTGTGACACAGATGACTTTGTCATGGTCCCAGCCCAGTTTCCAGGTGATCTAGTTGCTGAGGCAGCCA
  S  K  D  S  C  D  T  D  D  F  V  M  V  P  A  Q  F  P  G  D  L  V  A  E  A  A
GTGCCAAGCCCCCACCTGATAGCCTGCTGTGTAGTGGGAGCTCATTGGTGGCCTCTGCTGGCCTAGAGAGCCACGGCCGT
S  A  K  P  P  P  D  S  L  L  C  S  G  S  S  L  V  A  S  A  G  L  E  S  H  G  R
ACCCCCTCTCCCTCTCCGACCTGCAGCAGCTCTCCCAGCCCCTCTGGCCGGCCTGGCCCCTTCTCCAGCAACAGGTACGG
 T  P  S  P  S  P  T  C  S  S  S  P  S  P  S  G  R  P  G  P  F  S  S  N  R  Y  G
TGCCTCGGTCCCCATTCCTGTCCCCACTCAGGTGCACAATTACCAGCGCATCGAGCAAAACCTGCAATCGCCCACTCAAC
  A  S  V  P  I  P  V  P  T  Q  V  H  N  Y  Q  R  I  E  Q  N  L  Q  S  P  T  Q
AGCAGACAGCCAGGTCCTCTGCCATCCGAAGGTCAGGGAGCACCAGCCCCCTGGGCTTTGGCCGGGCCAGCCCATCACCC
Q  Q  T  A  R  S  S  A  I  R  R  S  G  S  T  S  P  L  G  F  G  R  A  S  P  S  P
CCCTCCCACACCGATGGAGCCATGCTGGCCAGGAAGCTGTCACTTGGAGGTGGCCGTCCCTACACACCTTCTCCCCAAGT
 P  S  H  T  D  G  A  M  L  A  R  K  L  S  L  G  G  G  R  P  Y  T  P  S  P  Q  V
GGGAACCATCCCAGAGCGACCCAGCTGGAGCAGAGTGCCCTCCCCACAAGGAGCTGATGTGCGGGTTGGCAGGTCACCAC
  G  T  I  P  E  R  P  S  W  S  R  V  P  S  P  Q  G  A  D  V  R  V  G  R  S  P
GACCCGGTTCCTCTGTGCCTGAGCACTCTCCAAGAACCACTGGGCTGGGCTGCCGCCTGCACAGTGCCCCTAACCTGTCC
R  P  G  S  S  V  P  E  H  S  P  R  T  T  G  L  G  C  R  L  H  S  A  P  N  L  S
GACTTCCATGTTGTGCGTCCCAAGCTGCCTAAGCCCCCAACAGACCCACTGGGAGCCACCTTTAGCCCACCCCAGACCAG
 D  F  H  V  V  R  P  K  L  P  K  P  P  T  D  P  L  G  A  T  F  S  P  P  Q  T  S
CGCACCCCAGCCATGCCCAGGGCTACAGTCTTGCCGGCCACTGCGTGGCTCACCTAAGCTGCCTGACTTCCTACAGCGGA
  A  P  Q  P  C  P  G  L  Q  S  C  R  P  L  R  G  S  P  K  L  P  D  F  L  Q  R
GTCCCCTACCCCCCATCCTAGGCTCTCCTACCAAGGCCGGGCCCTCCTTTGACTTCCCCAAAACCCCCAGCTCTCAGAAT
S  P  L  P  P  I  L  G  S  P  T  K  A  G  P  S  F  D  F  P  K  T  P  S  S  Q  N
```

```
TTGCTGACCCTGTTGGCTAGGCAGGGGGTAGTAATGACACCACCTCGGAACCGTACACTGCCTGACCTCTCCGAGGCCAG
 L  L  T  L  L  A  R  Q  G  V  V  M  T  P  P  R  N  R  T  L  P  D  L  S  E  A  S
TCCTTTCCATGGCCAGCAGCTGGGCTCTGGCCTTCGGCCCGCTGAAGACACCCGGGGTCCCTTTGGACGGTCCTTCAGCA
   P  F  H  G  Q  Q  L  G  S  G  L  R  P  A  E  D  T  R  G  P  F  G  R  S  F  S
CCAGCCGCATTACGGACCTGCTGCTTAAGGCTGCATTTGGGACTCAGGCCTCTGACTCAGGCAGCACAGACAGCCTACAG
T  S  R  I  T  D  L  L  L  K  A  A  F  G  T  Q  A  S  D  S  G  S  T  D  S  L  Q
GAGAAACCTATGGAGATTGCTCCCTCTGCTGGCTTTGGAGGGACTCTGCATCCAGGAGCTCGTGGTGGAGGGGCCAGCAG
 E  K  P  M  E  I  A  P  S  A  G  F  G  G  T  L  H  P  G  A  R  G  G  G  A  S  S
CCCAGCACCTGTGGTATTTACTGTAGGCTCCCCACCCAGTGGTGCCACCCCACCCCAGAGTACCCGTACCAGAATGTTCT
   P  A  P  V  V  F  T  V  G  S  P  P  S  G  A  T  P  P  Q  S  T  R  T  R  M  F
CAGTGGGCTCTTCCAGCTCCCTGGGCTCTACTGGCTCCTCCTCTGCCCGCCACTTAGTGCCTGGGGCCTGTGGAGAGGCC
S  V  G  S  S  S  S  S  L  G  S  T  G  S  S  S  A  R  H  L  V  P  G  A  C  G  E  A
CCGGAGCTTTCTGCCCCAGGCCACTGCTGTAGCCTTGCTGACCCCCTTGCTGCCAACTTGGAGGGGGCTGTGACCTTCGA
 P  E  L  S  A  P  G  H  C  C  S  L  A  D  P  L  A  A  N  L  E  G  A  V  T  F  E
GGCTCCTGACCTCCCAGAGGAGACCCTCATGGAGCAAGAGCACACGGAAACCCTACACAGTCTGCGCTTCACACTAGCGT
   A  P  D  L  P  E  E  T  L  M  E  Q  E  H  T  E  T  L  H  S  L  R  F  T  L  A
TTGCACAGCAAGTTCTGGAGATTGCAGCCCTGAAGGGAAGTGCCAGTGAGGCCGCCGGTGGCCCTGAGTACCAGCTCCAG
F  A  Q  Q  V  L  E  I  A  A  L  K  G  S  A  S  E  A  A  G  G  P  E  Y  Q  L  Q
GAAAGTGTGGTGGCTGACCAGATCAGTCAGTTGAGCCGAGAGTGGGGCTTTGCAGAGCAACTGGTTCTGTACTTGAAGGT
 E  S  V  V  A  D  Q  I  S  Q  L  S  R  E  W  G  F  A  E  Q  L  V  L  Y  L  K  V
GGCTGAGCTGCTGTCCTCAGGCCTACAGACTGCCATTGACCAGATTCGAGCTGGCAAACTCTGCCTTTCATCTACTGTGA
   A  E  L  L  S  S  G  L  Q  T  A  I  D  Q  I  R  A  G  K  L  C  L  S  S  T  V
AGCAGGTGGTACGCAGACTAAATGAGCTGTACAAGGCCAGCGTGGTATCCTGCCAGGGCCTCAGCTTGCGACTTCAGCGC
K  Q  V  V  R  R  L  N  E  L  Y  K  A  S  V  V  S  C  Q  G  L  S  L  R  L  Q  R
TTCTTTCTGGACAAACAACGGCTGCTGGACGGGATCCATGGTGTCACTGCAGAGCGGCTCATCCTCAGCCATGCTGTGCA
 F  F  L  D  K  Q  R  L  L  D  G  I  H  G  V  T  A  E  R  L  I  L  S  H  A  V  Q
AATGGTACAATCAGCTGCCCTTGATGAGATGTTCCAGCACCGAGAGGGCTGTGTACCGAGATATCACAAAGCCCTGCTAT
   M  V  Q  S  A  A  L  D  E  M  F  Q  H  R  E  G  C  V  P  R  Y  H  K  A  L  L
TGCTGGAGGGGTTGCAGCACACTCTCACGGACCAGGCAGACATTGAGAACATTGCCAAATGCAAGCTGTGCATTGAGAGG
L  L  E  G  L  Q  H  T  L  T  D  Q  A  D  I  E  N  I  A  K  C  K  L  C  I  E  R
AGACTCTCGGCCCTGCTGAGTGGTGTCTATGCCTGA
 R  L  S  A  L  L  S  G  V  Y  A  *
```

8.2.4 ULK2 cDNA and Protein sequence (M.musculus)- Clone ID:5709559/GenBank: BC046778

```
ATGGAGGTGGTGGGCGACTTCGAGTACTGCAAGCGGGACCTCGTGGGACACGGGGCCTTCGCTGTGGTCTTCCGGGGGCG
 M  E  V  V  G  D  F  E  Y  C  K  R  D  L  V  G  H  G  A  F  A  V  V  F  R  G  R
GCACCGCCAGAAAACTGATTGGGAGGTGGCTATTAAAAGTATTAATAAAAAGAACTTGTCAAAATCACAAATTCTGCTTG
   H  R  Q  K  T  D  W  E  V  A  I  K  S  I  N  K  K  N  L  S  K  S  Q  I  L  L
GAAAGGAAATAAAAATCTTAAAGGAGCTTCAGCATGAAAACATCGTAGCGCTCTATGATGTTCAGGAATTGCCCAACTCT
G  K  E  I  K  I  L  K  E  L  Q  H  E  N  I  V  A  L  Y  D  V  Q  E  L  P  N  S
GTCTTTCTGGTGATGGAGTATTGCAATGGTGGAGACCTGGCAGATTATTTGCAAGCTAAAGGAACTCTGAGTGAAGATAC
 V  F  L  V  M  E  Y  C  N  G  G  D  L  A  D  Y  L  Q  A  K  G  T  L  S  E  D  T
TATCAGAGTGTTTCTCCATCAGATTGCGGCAGCCATGCGAATCCTGCACAGCAAAGGGATAATCCACAGGGATCTCAAAC
   I  R  V  F  L  H  Q  I  A  A  A  M  R  I  L  H  S  K  G  I  I  H  R  D  L  K
CACAGAATATCCTGTTGTCTTATGCCAATCGAAGGAAGTCGAATGTCAGTGGTATTCGTATTAAAATAGCTGATTTTGGT
P  Q  N  I  L  L  S  Y  A  N  R  R  K  S  N  V  S  G  I  R  I  K  I  A  D  F  G
TTCGCACGGTACCTACATAGTAACACAATGGCAGCGACACTGTGTGGATCCCCAATGTACATGGCTCCCGAGGTTATTAT
 F  A  R  Y  L  H  S  N  T  M  A  A  T  L  C  G  S  P  M  Y  M  A  P  E  V  I  M
GTCTCAACATTATGATGCTAAGGCAGATTTATGGAGCATAGGAACAGTGATCTATCAATGCCTAGTTGGAAAACCACCTT
   S  Q  H  Y  D  A  K  A  D  L  W  S  I  G  T  V  I  Y  Q  C  L  V  G  K  P  P
TTCAGGCTAATAGTCCTCAGGACCTAAGGATGTTTTATGAAAAAAACAGGAGCTTAATGCCTAGTATTCCCAGAGAAACA
F  Q  A  N  S  P  Q  D  L  R  M  F  Y  E  K  N  R  S  L  M  P  S  I  P  R  E  T
TCACCTTACTTGGCTAATCTCCTTTTGGGTTTGCTTCAGAGAAATCAAAAGGATAGAATGGACTTTGAAGCATTTTTCAG
 S  P  Y  L  A  N  L  L  L  G  L  L  Q  R  N  Q  K  D  R  M  D  F  E  A  F  F  S
CCATCCTTTCCTTGAGCAAGTTCCAGTTAAAAAATCTTGCCCAGTCCCAGTGCCTGTGTATTCTGGCCCTGTCCCTGGAA
   H  P  F  L  E  Q  V  P  V  K  K  S  C  P  V  P  V  P  V  Y  S  G  P  V  P  G
GCTCCTGCAGCAGCTCACCATCTTGTCGCTTTGCTTCTCCACCATCCCTTCCAGATATGCAGCATATTCAGGAAGAAAAC
S  S  C  S  S  S  P  S  C  R  F  A  S  P  P  S  L  P  D  M  Q  H  I  Q  E  E  N
TTATCCTCCCCACCGTTGGGTCCTCCCAACTATCTACAGGTGTCCAAAGACTCTGCGAGTAATAGTAGCAAGAACTCTTC
 L  S  S  P  P  L  G  P  P  N  Y  L  Q  V  S  K  D  S  A  S  N  S  S  K  N  S  S
TTGTGACACGGATGACTTTGTTTTGGTTCCACACAACATCTCGTCAGACCACTCATATGACATGCCAATGGGGACTACGG
   C  D  T  D  D  F  V  L  V  P  H  N  I  S  S  D  H  S  Y  D  M  P  M  G  T  T
CCAGACGTGCTTCAAATGAATTCTTTATGTGTGGAGGGCAGTGTCAACCTACTGTGTCACCTCACAGCGAAACAGCCCCA
A  R  R  A  S  N  E  F  F  M  C  G  G  Q  C  Q  P  T  V  S  P  H  S  E  T  A  P
ATTCCAGTTCCTACTCAAGTAAGGAATTATCAGCGCATAGAACAGAATCTTATATCCACTGCCAGCTCTGGCACAAACCC
 I  P  V  P  T  Q  V  R  N  Y  Q  R  I  E  Q  N  L  I  S  T  A  S  S  G  T  N  P
```

```
ACATGGTTCTCCAAGATCTGCAGTAGTACGAAGGTCTAATACCAGCCCCATGGGCTTCCTCCGGGTTGGGTCCTGCTCCC
  H  G  S  P  R  S  A  V  V  R  R  S  N  T  S  P  M  G  F  L  R  V  G  S  C  S
CTGTACCAGGAGACACAGTGCAGACAGGAGGACGAAGACTCTCTACTGGCTCTTCCAGGCCTTACTCACCATCCCCTTTG
P  V  P  G  D  T  V  Q  T  G  G  R  R  L  S  T  G  S  S  R  P  Y  S  P  S  P  L
GTTGGTACCATTCCTGAACAGTTTAGTCAGTGCTGCTGTGGACATCCTCAGGGCCATGAAGCCAGGAGTAGGCACTCCTC
 V  G  T  I  P  E  Q  F  S  Q  C  C  C  G  H  P  Q  G  H  E  A  R  S  R  H  S  S
AGGTTCTCCAGTGCCACAGACCCAGGCACCACAGTCACTCTTACTGGGTGCTAGACTGCAGAGTGCACCCACCCTCACCG
  G  S  P  V  P  Q  T  Q  A  P  Q  S  L  L  L  G  A  R  L  Q  S  A  P  T  L  T
ATATCTATCAGAACAAGCAGAAGCTCAGAAAGCAGCACTCTGACCCTGTGTGTCCGTCCCATGCTGGAGCTGGGTATAGT
D  I  Y  Q  N  K  Q  K  L  R  K  Q  H  S  D  P  V  C  P  S  H  A  G  A  G  Y  S
TACTCACCTCAGCCTAGTCGGCCTGGCAGCCTTGGGACCTCTCCCACCAAGCACACGGGGTCCTCTCCACGGAATTCTGA
 Y  S  P  Q  P  S  R  P  G  S  L  G  T  S  P  T  K  H  T  G  S  S  P  R  N  S  D
CTGGTTCTTTAAAACTCCTTTACCAACAATCATTGGCTCTCCTACTAAGACTACAGCTCCTTTCAAAATCCCTAAAACAC
  W  F  F  K  T  P  L  P  T  I  I  G  S  P  T  K  T  T  A  P  F  K  I  P  K  T
AAGCATCTTCTAACCTGTTAGCCTTGGTTACTCGTCATGGGCCTGCTGAAAGCCAGTCCAAAGATGGGAATGACCCTCGT
Q  A  S  S  N  L  L  A  L  V  T  R  H  G  P  A  E  S  Q  S  K  D  G  N  D  P  R
GAGTGTTCCCACTGCCTCTCAGTACAAGGAAGCGAGAGGCATCGATCTGAGCAGCAGCAGAGCAAGGCAGTGTTTGGCAG
 E  C  S  H  C  L  S  V  Q  G  S  E  R  H  R  S  E  Q  Q  Q  S  K  A  V  F  G  R
ATCTGTCAGTACTGGGAAGTTATCAGAACAACAAGTAAAGGCACCTTTAGGTGGACACCAGGGCAGCACGGATAGTTTAA
  S  V  S  T  G  K  L  S  E  Q  Q  V  K  A  P  L  G  G  H  Q  G  S  T  D  S  L
ACACAGAACGACCAATGGATGTAGCTCCTGCAGGAGCCTGTGGTGTTATGCTGGCATTGCCAGCAGGAACAGCAGCAAGC
N  T  E  R  P  M  D  V  A  P  A  G  A  C  G  V  M  L  A  L  P  A  G  T  A  A  S
GCCAGAGCTGTCCTCTTCACCGTGGGGTCTCCTCCACACAGTGCCACAGCCCCCACTTGTACTCATATGGTCCTTCGAAC
 A  R  A  V  L  F  T  V  G  S  P  P  H  S  A  T  A  P  T  C  T  H  M  V  L  R  T
AAGAACCACCTCAGTGGGGTCCAGCAGCTCAGGAGGTTCCTTGTGTTCTGCAAGTGGCCGAGTATGTGTGGGCTCCCCTC
  R  T  T  S  V  G  S  S  S  S  G  G  S  L  C  S  A  S  G  R  V  C  V  G  S  P
CTGGACCAGGGTTGGGCTCTTCCCCACCAGGAGCAGAGGGAGCTCCCAGCCTAAGATACGTGCCTTATGGTGCTTCACCA
P  G  P  G  L  G  S  S  P  P  G  A  E  G  A  P  S  L  R  Y  V  P  Y  G  A  S  P
CCCAGCCTAGAGGGTCTCATCACCTTTGAAGCCCCTGAACTACCAGAGGAGACACTGATGGAGCGAGAGCACACAGACAC
 P  S  L  E  G  L  I  T  F  E  A  P  E  L  P  E  E  T  L  M  E  R  E  H  T  D  T
CTTACGCCATCTGAACATGATGTTAATGTTTACTGAGTGTGTGCTGGACCTGACGGCAGTGAGGGGTGGGAACCCTGAGC
  L  R  H  L  N  M  M  L  M  F  T  E  C  V  L  D  L  T  A  V  R  G  G  N  P  E
TGTGCACATCTGCTGTGTCCTTGTACCAGATTCAGGAGAGTGTAGTTGTGGACCAGATCAGCCAGCTAAGCAAAGATTGG
L  C  T  S  A  V  S  L  Y  Q  I  Q  E  S  V  V  V  D  Q  I  S  Q  L  S  K  D  W
GGGCGGGTGGAGCAGCTGGTGTTGTACATGAAGGCAGCACAGCTGCTGGCGGCTTCCCTGCATCTCGCCAAAGCTCAGGT
 G  R  V  E  Q  L  V  L  Y  M  K  A  A  Q  L  L  A  A  S  L  H  L  A  K  A  Q  V
CAAGTCTGGGAAGCTGAGCCCATCCATGGCTGTGAAACAAGTTGTTAAAAATCTGAATGAAAGATACAAATTCTGCATCA
  K  S  G  K  L  S  P  S  M  A  V  K  Q  V  V  K  N  L  N  E  R  Y  K  F  C  I
CCATGTGCAAGAAACTTACAGAAAAGCTGAATCGCTTCTTCTCCGATAAACAGAGATTTATTGATGAAATCAACAGTGTG
T  M  C  K  K  L  T  E  K  L  N  R  F  F  S  D  K  Q  R  F  I  D  E  I  N  S  V
ACTGCAGAGAAACTCATCTATAATTGTGCTGTGGAAATGGTTCAATCTGCAGCCCTGGATGAGATGTTTCAGCAGACTGA
 T  A  E  K  L  I  Y  N  C  A  V  E  M  V  Q  S  A  A  L  D  E  M  F  Q  Q  T  E
AGACATCGTTTATCGCTACCACAAGGCAGCCCTTCTTTTGGAAGGCTTAAGTAAGATCCTGCAGGACCCTACAGATGTTG
  D  I  V  Y  R  Y  H  K  A  A  L  L  L  E  G  L  S  K  I  L  Q  D  P  T  D  V
AAAATGTGCATAAGTATAAATGTAGTATTGAAAGAAGATTGTCAGCACTCTGCTGTAGCACTGCAACTGTGTGA
E  N  V  H  K  Y  K  C  S  I  E  R  R  L  S  A  L  C  C  S  T  A  T  V  *
```

Kinase domain of ULK1/2 is depicted in **blue**, *serine proline rich domain* in **black** and *C-terminal domain* in **orange**.

8.2.5 VAPA cDNA sequence (M.musculus)- Clone ID:3490082/GenBank:BC003866

ATGGCGTCCGCCTCCGGGGCCATGGCGAAGCACGAGCAGATCCTGgTCCTCGACCCTCCTTCAGACCTCAAATT
CAAAGGCCCCTTCACAGATGTAGTCACTACAAATCTTAAATTGCAAAATCCATCGGATAGAAAAGTGTGTTTC
AAAGTGAAGACTACAGCACCTCGCCGGTACTGTGTGCGGCCCAACAGTGGGATTATTGACCCGGGGTCAATTG
TGACTGTTTCAGTAATGCTGCAACCCTTTGATTATGATCCGAATGAAAAGAGTAAACATAAGTTCATGGTACAG
ACAATTTTTGCTCCACCAAACATTTCAGATATGGAAGCTGTGTGGAAAGAAGCAAAACCTGATGAATTAATGG
ATTCTAAATTGAGATGTGTGTTTGAAATGCCGAATGAAAATGATAAGCTGAATGATATGGAACCTAGCAAAGC
TGTTCCACTGAATGCATCCAAACAAGACGGACCCCTGCCAAAACCAcACAGTGTTTCACTCaATGATACGGAAA
CAAGGAAACTGATGGAAGAGTGCAAGCGACTCCAGGGAGAAATGATGAAGCTCTCAGAAGAAAACCGACACC
TGAGAGATGAAGGCCTAAGGCTCAGAAAGGTAGCACATTCGGATAAACCTGGATCCACCTCAGCCGTGTCCTT
CAGAGATAATGTCACCAGTCCTCTTCCTTCTCTTCTGGTTGTAATTGCAGCCATTTTCATTGGATTCTTTCTAGG
GAAATTCATCTTG

8.2.6 VAPA Protein sequence (M.musculus)

MASASGAMAKHEQILVLDPPSDLKFKGPFTDVVTTNLKLQNPSDRKVCFKVKTTAPRRYCVRPNSGIIDPGSIVTVS
VMLQPFDYDPNEKSKHKFMVQTIFAPPNISDMEAVWKEAKPDELMDSKLRCVFEMPNENDKLNDMEPSKAVPLNA
SKQDGPLPKPHSVSLNDTETRKLMEECKRLQGEMMKLSEENRHLRDEGLRLRKVAHSDKPGSTSAVSFRDNVTSPL
PSLLVVIAAIFIGFFLGKFIL

8.2.7 VAPB cDNA sequence (M.musculus)- NCBI Ref. seq: NM_019806.5

ATGGCGAAGGTGGAACAGGTCCTGAGCCTCGAGCCACAACACGAGCTCAAGTTCCGAGGTCCCTTCACTGATG
TTGTCACCACCAACCTAAAGCTTGGCAACCCAACAGACCGAAATGTGTGTTTTAAAGTGAAGACCACAGCACC
TCGCAGGTACTGCGTGCGGCCCAACAGTGGGGTCATTGATGCCGGGGCCTCTCTCAATGTGTCTGTGATGTTAC
AGCCTTTCGATTATGATCCCAATGAGAAAAGTAAACACAAGTTTATGGTTCAGTCTATGTTTGCTCCGCCTGAC
ACTTCTGATATGGAGGCAGTATGGAAGGAGGCAAAACCGGAAGACCTTATGGATTCAAAACTTAGATGTGTGT
TTGAATTGCCAGCAGAAAATGCTAAACCACATGATGTAGAAATAAATAAAATCATACCTACGAGTGCATCCAA
GACAGAAGCACCGGCAGCCGCAAAGTCCCTGACATCGCCCCTCGATGACACAGAAGTAAAGAAGGTGATGGA
AGAGTGCAGGCGGCTGCAGGGGGAGGTGCAGAGGCTTCGGGAGGAGAGCAGGCAGCTCAAGGAAGAAGACG
GACTTCGGGTGAGGAAGGCGATGCCGAGCAACAGCCCCGTGGCGGCTCTGGCGGCCACTGGGAAGGAGGAGG
GCCTGAGCGCCCGGCTGCTGGCCCTGGTGGTTCTGTTCTTTATCGTTGGTGTCATTATAGGGAAGATTGCCTTG

8.2.8 VAPB Protein sequence (M.musculus)

MAKVEQVLSLEPQHELKFRGPFTDVVTTNLKLGNPTDRNVCFKVKTTAPRRYCVRPNSGVIDAGASLNVSVMLQPF
DYDPNEKSKHKFMVQSMFAPPDTSDMEAVWKEAKPEDLMDSKLRCVFELPAENAKPHDVEINKIIPTSASKTEAPA
AAKSLTSPLDDTEVKKVMEECRRLQGEVQRLREESRQLKEEDGLRVRKAMPSNSPVAALAATGKEEGLSARLLAL
VVLFFIVGVIIGKIAL

8.2.9 Copine VI cDNA sequence (M.musculus)- Clone ID:6591063/GenBank:BC050766

atgtcggacccagagatgggatgggtgcctgagcccccggccatgaccctgggagcctctcgagtggagctgcgggtgtcctgccatggcctgctggaccgag
acacgctcacaaagccgcatccatgtgtgctgctcaaactctactcggatgagcagtgggtggaggtggaacgcacggaggtgcttcgctcctgttcaagcccagt
cttctcccgggtgctggccattgaatacttttttgaagagaagcagcctttgcagttccacgtgttcgatgccgaggatggagccaccagccccagcagcgacacctt
cctcgggtctacggagtgcaccttgggccagattgtgtcacaaaccaaggtcactaagccattactgctgaagaatgggaagacggcgggcaagtctactatcacg
attgtggctgaggaggtatcaggtaccaacgactatgtgcaacttaccttcagagcccacaagctggataacaaggatctgttcagcaagtctgacccccttcatggag
atttataagaccaatggagaccagagtgaccaactggtctggaggactgaggtggtgaaaaacaacctgaaccccagctgggagccattccgcctgtccttgcatt
ctttgtgcagctgtgacatccacaggccgctcaagttcctggtatatgactatgactccagtggaaagcacgacttcatcggcgagttcaccagcacattccaggaaa
tgcaagaggggaccgcaaaccctgggcaggagatgcagtgggactgtatcaaccccaagtaccgagacaagaagaagaattacaagagctcagggacagtcgt
gctggcccagtgcaccgtggaaaaagtccacaccttcctggattatatcatgggtggctgccagatcagcttcacggtggctatcgacttcactgcctccaatgggg
acccaaggagcagccagtctctgcactgcctcagcccccgacagcccaaccactacctgcaggccttgcgcacagtgggcggtatctgccaggactatgacagt
gataagcggttcccagcttttggcttcggagctcgaatccccccaaactttgaggtctcccatgactttgctatcaactttgacccagaaaatcctgaatgtgaagagat
ctcaggggtcatagcctcctaccgccgctgcttgcctcagatccagctctatggtcctaccaacgtggcccctatcatcaaccgtgtggctgaaccagcccagcgag
agcagagcaccggccaagccacgaagtattcagtactgctggtgctcactgacggtgtggtgagtgatatggcagagacccgaacagccattgtgcgagcctccc
gcctgcccatgtcaatcatcatcgtgggtgtgggcaacgctgacttctctgacatgaggctactggacggagatgatggtcccctgcgttgcccaaaggggtacct
gcagcccgtgacattgtccagtttgtgcccttcagggacttcaaggacgctgccccctctgcactagctaagtgtgtcctggcagaggtgccacggcaggtggtag
agtactatgccagccaaggtatcagtcccggggctcccaggccctccacgccagctatgactcccagccctagccca

---

8.2.10 Copine VI Protein sequence (M.musculus)

MSDPEMGWVPEPPAMTLGASRVELRVSCHGLLDRDTLTKPHPCVLLKLYSDEQWVEVERTEVLRSCSSPVFSRVLA
IEYFFEEKQPLQFHVFDAEDGATSPSSDTFLGSTECTLGQIVSQTKVTKPLLLKNGKTAGKSTITIVAEEVSGTNDYVQ
LTFRAHKLDNKDLFSKSDPFMEIYKTNGDQSDQLVWRTEVVKNNLNPSWEPFRLSLHSLCSCDIHRPLKFLVYDYD
SSGKHDFIGEFTSTFQEMQEGTANPGQEMQWDCINPKYRDKKKNYKSSGTVVLAQCTVEKVHTFLDYIMGGCQISF
TVAIDFTASNGDPRSSQSLHCLSPRQPNHYLQALRTVGGICQDYDSDKRFPAFGFGARIPPNFEVSHDFAINFDPENPE
CEEISGVIASYRRCLPQIQLYGPTNVAPIINRVAEPAQREQSTGQATKYSVLLVLTDGVVSDMAETRTAIVRASRLPM
SIIIVGVGNADFSDMRLLDGDDGPLRCPKGVPAARDIVQFVPFRDFKDAAPSALAKCVLAEVPRQVVEYYASQGISP
GAPRPSTPAMTPSPSP

8.2.11 SRPK2 cDNA sequence (M.musculus)-Clone ID: 4507346/GenBank:BC020178

ATGTCAGTTAACTCTGAGAAGTCGTCCTCTTCAGAAAGGCCGGAGCCTCAACAGAAAGCTCCTTTAGTTCCTCC
TCCTCCACCACCACCACCGCCACCACCACTGCCAGACCCCGCACCCCCAGAGCCAGAGGAGGAGATTCTGGGG
TCAGATGATGAGGAGCAGGAGGACCCCGCAGATTACTGCAAAGGTGGCTATCATCCAGTGAAAATTGGAGATC
TCTTCAATGGTCGATATCATGTCATTAGAAAGCTAGGATGGGGGCACTTTTCTACTGTATGGCTGTGCTGGGAT
ATGCAAGGGAAAAGATTTGTTGCAATGAAAGTTGTAAAAAGTGCCCAGCATTATACAGAGACAGCCTTGGATG
AAATTAAACTACTCAAATGCGTTCGAGAAAGTGACCCCAGTGACCCAAACAAAGACATGGTAGTTCAGCTAAT
TGATGACTTCAAGATCTCAGGCATGAATGGGATACATGTCTGCATGGTCTTTGAAGTACTTGGTCACCATCTCC
TCAAATGGATCATCAAATCCAACTATCAAGGCCTCCCAGTACGTTGTGTGAAGAGTATCATTCGACAGGTCCTT
CAAGGGTTAGATTATCTACACAGTAAGTGCAAGATAATTCACACCGACATAAAGCCGGAAAACATCTTGATGT
GTGTGGATGACGCTTACGTGAGAAGAATGGCAGCCGAAGCCACGGAGTGGCAGAAAGCAGGTGCTCCTCCTCC
CTCTGGGTCTGCAGTGAGTACGGCTCCACAGCAAAAACCTATAGGAAAAATATCTAAAAACAAAAAGAAAAA
GCTGAAAAAGAAACAGAAGAGACAGGCTGAGTTGCTGGAGAAACGCCTACAGGAGATTGAGGAATTGGAGCG
AGAAGCCGAAAGGAAAATCCTAGAGGAGAACATCACCTCTGCAGAAGCTTCCGGGGAGCAGCAGGATGGAGA
GTACCAGCCGGAGGTGACACTGAAAGCAGCCGACTTAGAGGACACAACTGAGGAAGAGACAGCAAAGGATAA
TGGTGAAGTTGAAGACCAGGAAGAGAAAGAAGATGCAGAGAAGGAGAACGCGGAGAAGGATGAAGATGATG
TTGAACAGGAACTTGCAAACTTAGACCCTACCTGGGTGGAGTCCCCGAAAGCCAATGGCCATATTGAAAATGG
CCCGTTCTCACTGGAGCAGCAGCTGGAGGATGAAGAGGACGATGAAGATGACTGTGCAAATCCCGAGGAGTA
TAACCTCGATGAGCCAAATGCAGAGAGTGATTACACGTATAGCAGCTCCTATGAACAATTCAATGGTGAATTG
CCAAATGGACAACATAAGACTTCAGAGTTTCCCACACCGTTGTTTTCTGGGCCCTTAGAACCTGTGGCCTGTGG
CTCTGTGATTTCAGAGGGATCGCCACTTACCGAGCAGGAGGAAAGCAGTCCCTCCCATGACAGAAGCAGGACA
GTTTCAGCCTCTAGTACTGGAGATTTGCCAAAAACAAAAACCCGGGCGGCTGACCTGTTGGTGAACCCTCTGG
ATCCACGGAATGCAGATAAAATTAGAGTAAAAATTGCTGACCTGGGAAATGCTTGTTGGGTGCATAAACATTT
CACAGAGGATATCCAGACACGTCAGTATAGGTCCATAGAGGTTTTAATAGGAGCAGGCTACAGCACACCTGCA
GACATTTGGAGTACAGCTTGCATGGCATTTGAGCTCGCCACAGGAGACTATTTGTTCGAACCGCATTCTGGGGA
AGACTATTCCAGAGATGAAGACCACATAGCCCACATCATAGAGCTGCTAGGCAGTATCCCAAGGCACTTTGCT
CTGTCTGGAAAATATTCTCGGGAATTCTTCAATCGCAGAGGAGAACTGCGGCACATCACCAAGCTGAAGCCCT
GGAGCCTCTTTGATGTACTTGTGGAAAAGTATGGCTGGCCCCATGAAGATGCTGCACAATTTACAGATTTCCTG
ATCCCAATGTTAGAGATGGTTCCAGAAAAACGAGCCTCAGCTGGCGAATGCCTTCGACATCCTTGGTTGAATTC
T

8.2.12 SRPK2 Protein sequence (M.musculus)

MSVNSEKSSSSERPEPQQKAPLVPPPPPPPPPPLPDPAPPEPEEEILGSDDEEQEDPADYCKGGYHPVKIGDLFNGRY
HVIRKLGWGHFSTVWLCWDMQGKRFVAMKVVKSAQHYTETALDEIKLLKCVRESDPSDPNKDMVVQLIDDFKIS
GMNGIHVCMVFEVLGHHLLKWIIKSNYQGLPVRCVKSIIRQVLQGLDYLHSKCKIIHTDIKPENILMCVDDAYVRRM
AAEATEWQKAGAPPPSGSAVSTAPQQKPIGKISKNKKKKLKKKQKRQAELLEKRLQEIEELEREAERKILEENITSAE
ASGEQQDGEYQPEVTLKAADLEDTTEEETAKDNGEVEDQEEKEDAEKENAEKDEDDVEQELANLDPTWVESPKA
NGHIENGPFSLEQQLEDEEDDEDDCANPEEYNLDEPNAESDYTYSSSSYEQFNGELPNGQHKTSEFPTPLFSGPLEPVA
CGSVISEGSPLTEQEESSPSHDRSRTVSASSTGDLPKTKTRAADLLVNPLDPRNADKIRVKIADLGNACWVHKHFTE
DIQTRQYRSIEVLIGAGYSTPADIWSTACMAFELATGDYLFEPHSGEDYSRDEDHIAHIIELLGSIPRHFALSGKYSREF
FNRRGELRHITKLKPWSLFDVLVEKYGWPHEDAAQFTDFLIPMLEMVPEKRASAGECLRHPWLNS

8.2.13 SV2A (R.norvegicus)-NCBI Ref. seq: NM_057210.2

atggaagaaggctttcgagaccgagcagcgttcatccgtggggccaaagacattgccaaggaagttaagaagcacgcggccaagaaggtggtgaagggtctcg
acagagtccaggatgaatattcccgaaggtcctactcccgctttgaggaggaggaggatgatgatgacttccctgcccctgctgacggctattaccgcggagaagg
ggcccaggatgaggaggaaggtggcgcttccagtgatgccactgagggccacgatgaggatgatgagatctacgagggagaatatcagggcatccccgggc
agagtctgggggcaaaggcgaacggatggcagatggggcacccctggctggagtgagaggggcttaagtgatggggagggtcccctgggggtcgcgggg
aggcgcagcggcgtaaagatcgggaagaattggctcagcagtatgagaccatcctccgggagtgcggccatggtcgcttccagtggacactctacttcgtgctgg
gtctggcgctgatggccgatggtgtagaggtctttgtggtgggctttgtgctgcccagtgctgagaaagatatgtgcctgtcggactccaacaaaggcatgctaggc
ctcattgtgtacctgggcatgatggtgggggccttcctctggggaggcctggctgatcggctgggtcggagacagtgtctgctcatctcgctctcagtcaacagcgt
cttcgctttcttctcatccttcgtccagggttatggcaccttccttttctgccgcctcctttctgggattgggattggtggttccatccccattgtcttctcctatttttcggagtt
tctggcccaggagaaacgtggggagcatttgagctggctctgtatgttctggatgattggtggcgtgtatgcagctgcaatggcctgggccatcatccccactatgg
gtggagtttccagatgggctctgcttaccagttccacagctggagggtctttgtcctcgtctgtgcctttccctctgtgtttgccatcggggctctgactacgcagccgg
agagtccccgcttcttcttagagaatgggaagcacgatgaggcctggatggtgctgaagcaggttcatgacaccaacatgcgagccaagggccatcctgagcgag
tcttctcagtaacccacattaaaacgattcatcaggaggatgaattgattgagatccagtcagacacaggaacctggtaccagcgctggggagtgcgggctttgagc
ctgggggtcaggtttgggggaacttcctctcctgcttcagtccagagtaccggcgcatcactctgatgatgatggggtatggttcaccatgtccttcagctactacg
gtttgactgtctggtttcccgacatgatccgccatctccaggctgtggactatgcagcccgaaccaaagtgttcccaggggagcgcgtggagcacgtgacatttaact
tcacactggagaatcagatccaccgaggggacagtacttcaatgacaagttcatcgggctgcgtctgaagtcagtgtcctttgaggattccctgtttgaggaatgtta
ctttgaagatgtcacatccagcaacacattcttccgcaactgcacattcatcaacaccgtgttctacaacacggacctgtttgagtacaagttcgtgaacagccgcctg
gtgaacagcacattcctgcacaataaggaaggttgcccactagatgtgacagggacgggcgaaggtgcctacatggtgtactttgtcagcttcttggggacactgg

ctgtgctccctggaaatattgtgtctgctctgctcatggacaagattggcaggctcagaatgcttgctggttccagtgtgttgtcctgtgtttcctgcttcttcctgtctttg
ggaacagtgagtcagccatgatcgctctgctctgccttttgggggagtcagtattgcatcctggaacgcgctggacgtgctgactgttgaactctacccttccgacaa
gaggacgacggccttcggcttcctgaatgccctgtgtaagctggcagctgtactgggcatcagcatcttcacgtcctttgtgggaatcaccaaggccgctcccatcct
cttcgcctcagctgcgcttgcccttggtagctctctggctctgaagctgcctgagacccggggacaggtgctgcag

8.2.14 SV2A Protein sequence (R. norvegicus)

MEEGFRDRAAFIRGAKDIAKEVKKHAAKKVVKGLDRVQDEYSRRSYSRFEEEEDDDDFPAPADGYYRGEGAQDEE
EGGASSDATEGHDEDDEIYEGEYQGIPRAESGGKGERMADGAPLAGVRGGLSDGEGPPGGRGEAQRRKDREELAQ
QYETILRECGHGRFQWTLYFVLGLALMADGVEVFVVGFVLPSAEKDMCLSDSNKGMLGLIVYLGMMVGAFLWGG
LADRLGRRQCLLISLSVNSVFAFFSSFVQGYGTFLFCRLLSGVGIGGSIPIVFSYFSEFLAQEKRGEHLSWLCMFWMIG
GVYAAAMAWAIIPHYGWSFQMGSAYQFHSWRVFVLVCAFPSVFAIGALTTQPESPRFFLENGKHDEAWMVLKQV
HDTNMRAKGHPERVFSVTHIKTIHQEDELIEIQSDTGTWYQRWGVRALSLGGQVWGNFLSCFSPEYRRITLMMMG
VWFTMSFSYYGLTVWFPDMIRHLQAVDYAARTKVFPGERVEHVTFNFTLENQIHRGGQYFNDKFIGLRLKSVSFED
SLFEECYFEDVTSSNTFFRNCTFINTVFYNTDLFEYKFVNSRLVNSTFLHNKEGCPLDVTGTGEGAYMVYFVSFLGTL
AVLPGNIVSALLMDKIGRLRMLAGSSVLSCVSCFFLSFGNSESAMIALLCLFGGVSIASWNALDVLTVELYPSDKRTT
AFGFLNALCKLAAVLGISIFTSFVGITKAAPILFASAALALGSSLALKLPETRGQVLQ

9. Abbreviations

A	
AAV	Adeno associated virus
AC	Adenylyl cyclase
ADBE	Activity-dependent bulk endocytosis
APS	Ammonium peroxodisulphate
ATP	Adenosine tri-phosphate
AZ	Active Zone
B	
BDNF	Brain-derived neurotrophic factor
BES	N,N, Bis-(2-hydroxyethyl)-2-amino-ethansulfonic acid
BME	Basal Medium Eagle
Brp	Bruchpilot
BSA	Bovine serum albumin
β-ME	Beta mercaptoethanol
C	
Ca^{2+}	Calcium ions
$CaCl_2$	Calcium chloride
CaMKII	Ca2+/calmodulin-dependent protein kinase II
cAMP	Cyclic adenosine-3,5-monophosphate
CASK	Calcium/calmodulin-dependent serine protein kinase
CAZ	Cytomatrix at the active zone
CC	Coiled-coil domain
CCB	Coomassie Colloidal Blue
cDNA	Complementary DNA
Cdk5	Cyclin-dependent kinase 5
CMV	Cytomegalovirus
CNS	Central nervous system
CO_2	Carbon dioxide
Co-IP	Co-immunoprecipitation
CTD	C-terminal domain
C-terminus	Carboxyl terminus
D	
DAPI	4',6-diamidin-2-phenylindol
DDM	n-dodecyl-β-maltoside
dH_2O	Distillate water
DIV	Day *in vitro*
DMEM	Dulbecco's Modified Eagle's Medium
DMSO	Dimethyl sulfoxide
DNA	Deoxyribonucleic acid
dNTP	Deoxyribonucleotide triphosphate
DSP	Dithiobis (succinimidylpropionate)
DTBP	Dimethyl 3,3'-dithiobispropionimidate-2HCl
DTT	Ditiothreitol
E	
E18,5	Embryo at day 18.5 after fertilization
EDTA	Ethylenediaminetetraacetic acid
ELKS	Name stems from the proteins high content in glutamate (E), leucine (L), lysine (K), and serine (S)
EM	Electron microscopy
ER	Endoplasmic reticulum
ERK2	Extracellular signal-regulated kinase2
ES	Elution steps
F	
FCS	Fetal calf serum
FM	Name after Fei Mao, who synthetized for the first time these dyes
Fw	Forward
G	
G	Gravitational
GFP	Green fluorescent protein
GPCR	G-protein coupled receptor
GSH	Glutathione
GST	Glutathione S-transferase
GTP	Guanosintriphosphate
H	
h	Hour
HA	Human influenza hemaglutinin
HBS	HEPES buffered saline
HBSS	Hanks buffered salt solution
HEK 293T	Human embryonic kidney cell line 293T
HEPES	2-[4-(2-hydroxyethyl)piperazin-1-yl]ethanesulfonic acid
I	
IAA	Iodamidacetate
IB	Immunoblotting
IC50	Half inhibitory concentration
IF	Immunofluorescence
IgG	Immunoglobulin G
IHC	Immunohistochemistry
IMDM	Iscove's Modified Dulbecco's Medium
IP	Immunoprecipitation
IPTG	Isopropyl-β-D-thiogalactoside
IRDye	InfraRed Dye
K	
kb	Kilo base
KCl	Potassium chloride
KD	Kinase domain
kDa	Kilo Dalton
KH_2PO_4	Potasium dihydrogenphosphate
KO	Knock-out
L	
LAR	Leukocyte common antigen related
LB-medium	Luria broth medium
LC-MS	Liquid chromatography- mass spectrometry
LTD	Long-term depression
LTP	Long-term potentiation

M	
M	Molar
MCS	Multiple cloning site
MEM	Minimal essential medium
MF	Mossy fibres
mg	Miligram
$MgCl_2$	Magnesium chloride
$MgSO_4$	Magnesium sulphate
min	Minute
ml	Millilitre
mM	Milimolar
mRNA	Messenger RNA
MS	Mass spectrometry
MSP	Major sperm protein domain
MW	Molecular weight
MWCO	Molecular weight cut off
Mg	Microgram
µl	Microliter
µm	Micromolar
N	
NaCl	Sodium chloride
NAD	Nicotinamide adenine dinucleotide
$NaHCO_3$	Sodium carbonate
Na_2HPO_4	Disodiumhydrogenphosphat
NaOH	Sodium hydroxide
NCBI	National Center for Biotechnology Information
ng	Nanogram
NGS	Normal goat serum
nm	Nanometer
nM	Nanomolar
NMJ	Neuromuscular junction
N-terminus	Amino-terminus
O	
OD	Optical density
OE	Over expression
ON	Over night
P	
P2	Pellet 2- crude synaptosomes
PAGE	Polyacrylamide gel electrophoresis
PBS	Phosphate buffered saline
PCR	Polymerase chain reaction
PDZ	**P**ost synaptic density; Drosophila **d**isc large tumour suppressor; **z**onula occludens-1 protein
Pen/Strep	Penicillin/Streptomycin
PFA	Paraformaldehyde
PKA	Protein kinase A
PKC	Protein kinase C
PP1	Protein phosphatase 1
PP2A	Protein phosphatase 2A
R	
Rev	Reverse
RIM	Rab3 interacting molecule
RIM-BPs	RIM-binding proteins
RNA	Ribonucleic acid
rpm	Rotation per minute
RRP	Readily releasable pool
RS	Arginine/serine dipeptides
RT	Room temperature
RT-PCR	Reverse transcription PCR
S	
S1	Supernatant 1
sec	Seconds
SEM	Standard error of the mean
shRNA	Short hairpin RNA
SDS	Sodium dodecyl sulfate
SNAP25	Synaptosomal-associated protein 25
SNARE	Soluble N-ethylmaleimide-sensitive factor (NSF) attachment protein receptors
SPRD	Serine proline rich domain
SRPK	Serine arginine protein kinase
SS	Splice site
SV	Synaptic vesicle
SV2A	Synaptic vesicle protein 2 A
Syt1	Synaptotagmin1
T	
TAP	Tandem affinity purification
TBS	Tris buffered saline
TEMED	N,N,N',N'-Tetramethylethylendiamin
Tm	Melting temperature
TMD	Transmembrane domain
TMR	Transmembrane region
U	
U	Units
ULK	Unc51-like kinase
UF	Unbound fraction
UNC	Uncoordinated
UPS	Ubiquitin-proteasome system
V	
VAPA/VAP B	Vesicle-associated membrane protein (VAMP) associated protein A/B
VAMP-2	Vesicle associated membrane protein 2
VGCG	Voltage gated calcium channels
vWA	Von Willebrand factor type A
W	
WB	Western blot
WS	Washing steps
WT	Wild-type
Z	
ZF	Zinc finger domain

10. References

Alers, S., Löffler, A. S., Wesselborg, S., and Stork, B. (2012). The incredible ULKs. *Cell Communication and Signaling : CCS*, *10*(1), 7.

Amarilio, R., Ramachandran, S., Sabanay, H., and Lev, S. (2005). Differential regulation of endoplasmic reticulum structure through VAP-Nir protein interaction. *The Journal of Biological Chemistry*, *280*(7), 5934–44.

Andrews-Zwilling, Y. S., Kawabe, H., Reim, K., Varoqueaux, F., and Brose, N. (2006). Binding to Rab3A-interacting molecule RIM regulates the presynaptic recruitment of Munc13-1 and ubMunc13-2. *The Journal of biological chemistry*, *281*(28), 19720–19731.

Avery, A. W., Figueroa, C., and Vojtek, A. B. (2007). UNC-51-like kinase regulation of fibroblast growth factor receptor substrate 2/3. *Cellular Signalling*, *19*(1), 177–84.

Bach, M., Larance, M., James, D. E., and Ramm, G. (2011). The serine/threonine kinase ULK1 is a target of multiple phosphorylation events. *The Biochemical Journal*, *440*(2), 283–291.

Bajjalieh, S. M., Peterson, K., Shinghal, R., and Scheller, R. H. (1992). Synaptic Vesicle Protein Homologous. *Science*, *257*(8), 1271–1273.

Bajjalieh, S. M., Peterson, K., Linial, M., and Scheller, R. H. (1993). Brain contains two forms of synaptic vesicle protein 2. *PNAS*, *90*(6), 2150–2154.

Bajjalieh, S. M., Frantz, G. D., Weimann, J. M., McConnell, S. K., and Scheller, R. H. (1994). Differential expression of synaptic vesicle protein 2 (SV2) isoforms. *The Journal of neuroscience, 14*(9), 5223–5235.

Barria, A., Derkach, V., Soderling, T.R., and (2001). Protein Phosphorylation and Long-term Synaptic Plasticity. *Encyclopedia of Life Sciences*, 1–7.

Betz, A., Okamoto, M., Benseler, F., Brose, N., (1997). Direct Interaction of the Rat unc-13 Homologue Munc13-1 with the N Terminus of Syntaxin. *Journal of Biological Chemistry, 272*(4), 2520–2526.

Betz, A., Thakur, P., Junge, H. J., Ashery, U., Rhee, J. S., Scheuss, V., Rosenmund, C., Rettig, J., and Brose, N. (2001). Functional interaction of the active zone proteins Munc13-1 and RIM1 in synaptic vesicle priming. *Neuron*, *30*(1), 183–196.

Bolte, S., and Cordeliers, F.P. (2006). A guided tour into subcellular colocalization analysis in light microscopy. *J Microsc., 224,* 213–232.

Blundell, J., Kaeser, P. S., Südhof, T. C., and Powell, C. M. (2010). RIM1alpha and interacting proteins involved in presynaptic plasticity mediate prepulse inhibition and additional behaviors linked to schizophrenia. *The Journal of neuroscience, 30*(15), 5326–5333.

Boyken, J., Grønborg, M., Riedel, D., Urlaub, H., Jahn, R., and Chua, J. J. E. (2013). Molecular profiling of synaptic vesicle docking sites reveals novel proteins but few differences between glutamatergic and GABAergic synapses. *Neuron*, *78*(2), 285–297.

Calakos, N., Schoch, S., Südhof, T. C., and Malenka, R. C. (2004). Multiple roles for the active zone protein RIM1alpha in late stages of neurotransmitter release. *Neuron*, *42*(6), 889–896.

Castillo,P. E., Schoch, S., Schmitz, F., Südhof, T. C., and Malenka, R. C. (2002). RIM1α is required for presynaptic long-term potentiation. *Nature*, *415*(6869), 327–330.

Castillo, P. E. (2012). Presynaptic LTP and LTD of excitatory and inhibitory synapses. *Cold Spring Harbor Perspectives in Biology*, *4*(2).

Chai, A., Withers, J., Koh, Y. H., Parry, K., Bao, H., Zhang, B., Budnik, V., and Pennetta, G. (2008). hVAPB, the causative gene of a heterogeneous group of motor neuron diseases in humans, is functionally interchangeable with its Drosophila homologue DVAP-33A at the neuromuscular junction. *Human Molecular Genetics*, *17*(2), 266–280.

Chang, W.-P., and Südhof, T. C. (2009). SV2 renders primed synaptic vesicles competent for Ca2+ -induced exocytosis. *The Journal of neuroscience, 29*(4), 883–897.

Cheung, G., and Cousin, M. a. (2013). Synaptic vesicle generation from activity-dependent bulk endosomes requires calcium and calcineurin. *The Journal of Neuroscience*, *33*(8), 3370–3379.

Choi, U. B., Strop, P., Vrljic, M., Chu, S., Brunger, A. T., and Weninger, K. R. (2010). Single-molecule FRET-derived model of the synaptotagmin 1-SNARE fusion complex. *Nature structural & molecular biology*, *17*(3), 318–324.

Coppola, T., Magnin-Luthi, S., Perret-Menoud, V., Gattesco, S., Schiavo, G., and Regazzi, R. (2001). Direct interaction of the Rab3 effector RIM with Ca2+ channels, SNAP-25, and synaptotagmin. *The Journal of Biological Chemistry*, *276*(35), 32756–32762.

Crawford, D. C., and Mennerick, S. (2012). Presynaptically silent synapses: dormancy and awakening of presynaptic vesicle release. *The Neuroscientist : a review journal bringing neurobiology, neurology and psychiatry*, *18*(3), 216–223.

Crowder, K. M., Gunther, J. M., Jones, T. a, Hale, B. D., Zhang, H. Z., Peterson, M. R., Scheller, R. H., Chavkin, C., and Bajjalieh, S. M. (1999). Abnormal neurotransmission in mice lacking synaptic vesicle protein 2A (SV2A). *PNAS*, *96*(26), 15268–15273.

Custer, K. L., Austin, N. S., Sullivan, J. M., and Bajjalieh, S. M. (2006). Synaptic vesicle protein 2 enhances release probability at quiescent synapses. *The Journal of neuroscience, 26*(4), 1303–1313.

Dai, H., Tomchick, D. R., García, J., Südhof, T. C., Machius, M., and Rizo, J. (2005). Crystal structure of the RIM2 C2A-domain at 1.4 A resolution. *Biochemistry*, *44*(41), 13533–13542.

Dai, H., Shen, N., Araç, D., and Rizo, J. (2008). A Quaternary SNARE-Synaptotagmin-Ca2+ -Phospholipid Complex in Neurotransmitter Release. *J Mol Bio,367*(3), 848–863.

Deng, L., Kaeser, P. S., Xu, W., and Südhof, T. C. (2011). RIM proteins activate vesicle priming by reversing autoinhibitory homodimerization of Munc13. *Neuron*, *69*(2), 317–331.

Dulubova, I., Sugita, S., Hill, S., Hosaka, M., Fernandez, I., and Südhof, T. C. (1999). A conformational switch in syntaxin during exocytosis : role of munc18. *The EMBO Journal*, *18*(16), 4372–4382.

Dulubova, I., Lou, X., Lu, J., Huryeva, I., Alam, A., Schneggenburger, R., Südhof, T. C., and Rizo, J. (2005). A Munc13/RIM/Rab3 tripartite complex: from priming to plasticity? *The EMBO journal*, *24*(16), 2839–2850.

el-Husseini, A. el-D., and Bredt, D. S. (2002). Protein palmitoylation: a regulator of neuronal development and function. *Nature Reviews. Neuroscience*, *3*(10), 791–802.

Fernández-Busnadiego, R., Zuber, B., Maurer, U. E., Cyrklaff, M., Baumeister, W., and Lucic, V. (2010). Quantitative analysis of the native presynaptic cytomatrix by cryoelectron tomography. *The Journal of cell biology*, *188*(1), 145–156.

Fernández-Busnadiego, R., Asano, S., Oprisoreanu, A.-M., Sakata, E., Doengi, M., Kochovski, Z., Zürner, M., Stein, V., Schoch, S., Baumeister, W., and Lucic, V. (2013). Cryo-electron tomography reveals a critical role of RIM1α in synaptic vesicle tethering. *The Journal of cell biology*, *201*(5), 725–740.

Forrest, S., Chai, A., Sanhueza, M., Marescotti, M., Parry, K., Georgiev, A., Sahota, V., Mendez- Castro, R., and Pennetta, G. (2013). Increased levels of phosphoinositides cause neurodegeneration in a Drosophila model of amyotrophic lateral sclerosis. *Human Molecular Genetics*, *22*(13), 2689–704.

Fukuda, M. (2003). Distinct Rab binding specificity of Rim1, Rim2, rabphilin, and Noc2. Identification of a critical determinant of Rab3A/Rab27A recognition by Rim2. *The Journal of biological chemistry*, *278*(17), 15373–15380.

Futatsumori-Sugai, M., Abe, R., Watanabe, M., Kudou, M., Yamamoto, T., Ejima, D., Arakawa, T., and Tsumoto, K. (2009). Utilization of Arg-elution method for FLAG-tag based chromatography. *Protein expression and purification*, *67*(2), 148–155.

Giannakouros, T., Nikolakaki, E., Mylonis, I., and Georgatsou, E. (2011). Serine-arginine protein kinases: a small protein kinase family with a large cellular presence. *The FEBS journal*, *278*(4), 570–586.

Girach, F., Craig, T. J., Rocca, D. L., and Henley, J. M. (2013). RIM1α SUMOylation Is Required for Fast Synaptic Vesicle Exocytosis. *Cell Reports*, 1–8.

Glockner, C.J., Boldt, K., and Ueffing, M. (2009). UNIT 19.20 Strep/FLAG Tandem Affinity Purification (SF-TAP) to Sudy Protein Interactions. *Current Protocols in Protein Science.*

Graf, E. R., Valakh, V., Wright, C. M., Wu, C., Liu, Z., Zhang, Y. Q., and DiAntonio, A. (2012). RIM promotes calcium channel accumulation at active zones of the Drosophila neuromuscular junction. *The Journal of Neuroscience, 32*(47), 16586–16596.

Guan, R., Dai, H., Tomchick, D. R., Dulubova, I., Machius, M., Südhof, T. C. and Rizo, J. (2007). Crystal Structure of the RIM1α C2B Domain at 1.7 Å Resolution. *Biochemistry*, (46), 8988–8998.

Han, Y., Kaeser, P. S., Südhof, T. C., and Schneggenburger, R. (2011). RIM determines Ca^2+ channel density and vesicle docking at the presynaptic active zone. *Neuron*, *69*(2), 304–316.

Harlow, M. L., Ress, D., Stoschek, a, Marshall, R. M., and McMahan, U. J. (2001). The architecture of active zone material at the frog's neuromuscular junction. *Nature*, *409*(6819), 479–484.

Harlow, M. L., Szule, J. a, Xu, J., Jung, J. H., Marshall, R. M., and McMahan, U. J. (2013). Alignment of synaptic vesicle macromolecules with the macromolecules in active zone material that direct vesicle docking. *PloS One*, *8*(7), e69410.

Hebb D. O (1949) The Organization of Behavior, New York : Wiley , Introduction and Chapter 4, "The first stage of perception : growth of the assembly," pp. xi - xix , 60–78.

Hibino, H., Pironkova, R., Onwumere, O., Vologodskaia, M., Hudspeth, A. J., and Lesage, F. (2002). RIM - binding proteins (RBPs) couple Rab3 - interacting molecules (RIMs) to voltage - gated Ca 2 + channels. Neuron, *34*(3), 411–423.

Hong, Y., Chan, C. B., Kwon, I.-S., Li, X., Song, M., Lee, H.-P., Liu, X., Sompol, P., Jin, P., Lee, H-gon., Yu, S. P., and Ye, K. (2012). SRPK2 phosphorylates tau and mediates the cognitive defects in Alzheimer's disease. *The Journal of neuroscience*, *32*(48), 17262–17272.

Horridge, B. G. A., and Mackay, B. (1962). Naked axons and symmetrical synapses in coelenterates. *Quarterly Journal of Microscopical Science*, *103*, 531–41.

Inoue, E., Mochida, S., Takagi, H., Higa, S., Deguchi-Tawarada, M., Takao-Rikitsu, E., Inoue, M., Yao, I., Takeuchi, K., Kitajima, I., Setou, M., Ohtsuka, T., and Takai, I. (2006). SAD: a presynaptic kinase associated with synaptic vesicles and the active zone cytomatrix that regulates neurotransmitter release. *Neuron*, *50*(2), 261–275.

Janz, R., Goda, Y., Geppert, M., Missler, M., and Südhof, T. C. (1999). SV2A and SV2B Function as Redundant Ca 2+ Regulators in Neurotransmitter Release. *Neuron 24*, 1003–1016.

Jiang, X., Litkowski, P. E., Taylor, A. a, Lin, Y., Snider, B. J., and Moulder, K. L. (2010). A role for the ubiquitin-proteasome system in activity-dependent presynaptic silencing. *The Journal of neuroscience*, *30*(5), 1798–1809.

Johnson, E. L., Fetter, R. D., and Davis, G. W. (2009). Negative regulation of active zone assembly by a newly identified SR protein kinase. *PLoS biology*, *7*(9), e1000193.

Johnson, S., Halford, S., Morris, A. G., Patel, R. J., Wilkie, S. E., Hardcastle, A. J., Moore, A. T., Zhang, K., and Hunt, D. M. (2003). Genomic organisation and alternative splicing of human RIM1, a gene implicated in autosomal dominant cone-rod dystrophy (CORD7)☆. *Genomics*, *81*(3), 304–314.

Kaeser, P. S., Kwon, H.-B., Blundell, J., Chevaleyre, V., Morishita, W., Malenka, R. C., Powell, C. M., Castillo, P. E., and Südhof, T. C. (2008a). RIM1alpha phosphorylation at serine-413 by protein kinase A is not required for presynaptic long-term plasticity or learning. *PNAS*, *105*(38), 14680–14685.

Kaeser, P. S., Kwon, H.-B., Chiu, C. Q., Deng, L., Castillo, P. E., and Südhof, T. C. (2008b). RIM1alpha and RIM1beta are synthesized from distinct promoters of the RIM1 gene to mediate differential but overlapping synaptic functions. *The Journal of neuroscience, 28*(50), 13435–13447.

Kaeser, P. S., Deng, L., Wang, Y., Dulubova, I., Liu, X., Rizo, J., and Südhof, T. C. (2011). RIM Proteins Tether Ca 2 + Channels to Presynaptic Active Zones via a Direct PDZ-Domain Interaction. *Cell, 144*, 282-295.

Kaeser, P. S., Deng, L., Fan, M., and Südhof, T. C. (2012). RIM genes differentially contribute to organizing presynaptic release sites. *PNAS*, *109*(29), 11830–11835.

Kamat, P. K., Rai, S., and Nath, C. (2013). Okadaic acid induced neurotoxicity: an emerging tool to study Alzheimer's disease pathology. *Neurotoxicology*, *37*, 163–172.

Karakama, Y., Sakamoto, N., Itsui, Y., Nakagawa, M., Tasaka-Fujita, M., Nishimura-Sakurai, Y., Kakinuma, S., Oooka, M., Azuma, S., Tsuchiya, K., Onogi, H., Hagiwara, M., and Watanabe, M. (2010). Inhibition of hepatitis C virus replication by a specific inhibitor of serine-arginine-rich protein kinase. *Antimicrobial Agents and Chemotherapy*, *54*(8), 3179–3186.

Kiyonaka, S., Wakamori, M., Miki, T., Uriu, Y., Nonaka, M., Bito, H., Beedle, A. M., Mori, E., Hara, Y., Waard, D. M., Kanagawa, M., Itakura, M., Takahashi, M., Campbell, P. K., and Mori, Y. (2007). RIM1 confers sustained activity and neurotransmitter vesicle anchoring to presynaptic Ca2+ channels. *Nature neuroscience*, *10*(6), 691–701.

Klockenbusch, C., and Kast, J. (2010). Optimization of formaldehyde cross-linking for protein interaction analysis of non-tagged integrin beta1. *Journal of Biomedicine and Biotechnology*, *2010*, 927585.

Ko, J., Yoon, C., Piccoli, G., Chung, H. S., Kim, K., Lee, J.-R., Lee, H. W., Kim, H., Sala, C., and Kim, E. (2006). Organization of the presynaptic active zone by ERC2/CAST1-dependent clustering of the tandem PDZ protein syntenin-1. *The Journal of neuroscience*, *26*(3), 963–970.

Köhrmann, M., Haubensak, W., Hemraj, I., Kaether, C., Leßmann, V. J., and Kiebler, M. A. (1999). Rapid Communication Fast, Convenient , and Effective Method to Transiently Transfect Primary Hippocampal Neurons. *Journal of neuroscience research, 58,* 831–835.

Koushika, S. P., Richmond, J. E., Hadwiger, G., Weimer, R. M., Jorgensen, E. M., and Nonet, M. L. (2001). A post-docking role for active zone protein Rim. *Nature neuroscience*, *4*(10), 997–1005.

Kriz, A. (2010). Copine 6, a novel calcium sensor translating synaptic activity into spine plasticity. PhD Thesis, University of Basel, Faculty of Science. *http://edoc.unibas.ch/diss/DissB_8969*; *urn: urn:nbn:ch:bel-bau-diss89692*.

Kuijpers, M., Yu, K. Lou, Teuling, E., Akhmanova, A., Jaarsma, D., and Hoogenraad, C. C. (2013). The ALS8 protein VAPB interacts with the ER-Golgi recycling protein YIF1A and regulates membrane delivery into dendrites. *The EMBO journal*, *32*(14), 2056–2072.

Kutzleb, C., Sanders, G., Yamamoto, R., Wang, X., Lichte, B., Petrasch-Parwez, E., and Kilimann, M. W. (1998). Paralemmin, a prenyl-palmitoyl-anchored phosphoprotein abundant in neurons and implicated in plasma membrane dynamics and cell process formation. *The Journal of cell biology*, *143*(3), 795–813.

Lambeng, N., Grossmann, M., Chatelain, P., and Fuks, B. (2006). Solubilization and immunopurification of rat brain synaptic vesicle protein 2A with maintained binding properties. *Neuroscience letters*, *398*(1-2), 107–112.

Lazarevic, V., Schöne, C., Heine, M., Gundelfinger, E. D., and Fejtova, A. (2011). Extensive remodeling of the presynaptic cytomatrix upon homeostatic adaptation to network activity silencing. *The Journal of Neuroscience*, *31*(28), 10189–10200.

Liang, N., Zeng, C., Tao, K. P., Sou, W. H., Hsia, H. P., Qu, D., Lau, S. N., and Ngo, K. (2014). Primary structural features of SR-like protein acinusS govern the phosphorylation mechanism by SRPK2. *Biochemical Journal, 459*(1), 181–191.

Llinás, R. R. (2003). The contribution of Santiago Ramón y Cajal to functional neuroscience. *Nature Reviews. Neuroscience*, *4*(1), 77–80.

Lonart, G., Schoch, S., Kaeser, P. S., Larkin, C. J., Südhof, T. C., and Linden, D. J. (2003). Phosphorylation of RIM1alpha by PKA triggers presynaptic long-term potentiation at cerebellar parallel fiber synapses. *Cell*, *115*(1), 49–60.

Maas, C., Torres, V. I., Altrock, W. D., Leal-Ortiz, S., Wagh, D., Terry-Lorenzo, R. T., Fejtova, A., Gundelfinger, E. D., Noam, E. Z., and Garner, C. C. (2012). Formation of Golgi-Derived Active Zone Precursor Vesicles. *Journal of Neuroscience*, *32*(32), 11095–11108.

Matz, J., Gilyan, A., Kolar, A., Mccarvill, T., and Krueger, S. R. (2010). Rapid structural alterations of the active zone lead to sustained changes in neurotransmitter release. *PNAS, 107*(19), 8836–8841.

Matsuzaki, F., Shirane, M., Matsumoto, M., and Nakayama, K. I. (2011). Protrudin serves as an adaptor molecule that connects KIF5 and its cargoes in vesicular transport during process formation. *Molecular Biology of the Cell*, *22*(23), 4602–4620.

Mendoza-Torreblanca, J. G., Vanoye-Carlo, A., Phillips-Farfán, B. V., Carmona-Aparicio, L., and Gómez-Lira, G. (2013). Synaptic vesicle protein 2A: basic facts and role in synaptic function. *The European Journal of Neuroscience*, *38*(11), 3529–3539.

Mercer, A.J., and Thoreson, W. B. (2011). The dynamic architecture of photoreceptor ribbon synapses: Cytoskeletal, extracellular matrix, and intramembrane proteins. *Vis Neuroscience*, 28 (6), 453–471.

Michaelides, M., Holder, G. E., Hunt, D. M., Fitzke, F. W., Bird, a C., and Moore, a T. (2005). A detailed study of the phenotype of an autosomal dominant cone-rod dystrophy (CORD7) associated with mutation in the gene for RIM1. *The British journal of ophthalmology*, *89*(2), 198–206.

Mittelstaedt, T., Alvaréz-Baron, E., and Schoch, S. (2010). RIM proteins and their role in synapse function. *Biological Chemistry*, *391*(6), 599–606.

Müller, M., Liu, K. S. Y., Sigrist, S. J., and Davis, G. W. (2012). RIM Controls Homeostatic Plasticity through Modulation of the Readily-Releasable Vesicle Pool. *Journal of Neuroscience*, *32*(47), 16574–16585.

Nakayama, T., Yaoi, T., and Kuwajima, G. (1999). Localization and subcellular distribution of N-copine in mouse brain. *Journal of neurochemistry*, *72*(1), 373–379.

Nakayama, T., Yaoi, T., Yasui, M., and Kuwajima, G. (1998). N-copine: a novel two C2-domain-containing protein with neuronal activity-regulated expression. *FEBS letters*, *428*(1-2), 80–84.

Nieratschker, V., Schubert, A., Jauch, M., Bock, N., Bucher, D., Dippacher, S., Krohne, G., Asan, E., Buchner, S., and Buchner, E. (2009). Bruchpilot in ribbon-like axonal agglomerates, behavioral defects, and early death in SRPK79D kinase mutants of Drosophila. *PLoS genetics*, *5*(10), e1000700.

Nishimura, A. L., Mitne-Neto, M., Silva, H. C. a, Richieri-Costa, A., Middleton, S., Cascio, D., Kok, F., Oliveira, J. R. M., Gilingwater, T., Webb, J., Skehel, P., and Zatz, M. (2004). A mutation in the vesicle-trafficking protein VAPB causes late-onset spinal muscular atrophy and amyotrophic lateral sclerosis. *American journal of human genetics*, *75*(5), 822–831.

Nishimura, Y., Hayashi, M., Inada, H., and Tanaka, T. (1999). Molecular cloning and characterization of mammalian homologues of vesicle-associated membrane protein-associated (VAMP-associated) proteins. *Biochemical and biophysical research communications*, *254*(1), 21–26.

Nowack, A., Yao, J., Custer, K. L., and Bajjalieh, S. M. (2010). SV2 regulates neurotransmitter release via multiple mechanisms. *American journal of physiology. Cell physiology*, *299*(5), C960–967.

Nowack, A., Malarkey, E. B., Yao, J., Bleckert, A., Hill, J., and Bajjalieh, S. M. (2011). Levetiracetam reverses synaptic deficits produced by overexpression of SV2A. *PloS One*,*6*(12),e29560.

O'Callaghan, D. W., Hasdemir, B., Leighton, M., and Burgoyne, R. D. (2003). Residues within the myristoylation motif determine intracellular targeting of the neuronal Ca2+ sensor protein KChIP1 to post-ER transport vesicles and traffic of Kv4 K+ channels. *Journal of Cell Science*, *116*(23), 4833–4845.

Ogura, K., Okada, T., Mitani, S., Gengyo-Ando, K., Baillie, D. L., Kohara, Y., and Goshima, Y. (2010). Protein phosphatase 2A cooperates with the autophagy-related kinase UNC-51 to regulate axon guidance in Caenorhabditis elegans. *Development (Cambridge, England)*, *137*(10), 1657–1667.

Ohtsuka, T., Takao-Rikitsu, E., Inoue, E., Inoue, M., Takeuchi, M., Matsubara, K., Deguchi-Tawarada, M., Satoh, K., Morimoto, K., Nakanishi, H., and Takai, Y. (2002). Cast: a novel protein of the cytomatrix at the active zone of synapses that forms a ternary complex with RIM1 and munc13-1. *The Journal of cell biology*, *158*(3), 577–590.

Palade, G. E. and Palay, S. L. (1954). Electron microscope observations of interneuronal and neuromuscular synapses. *Anatomical Record* 118, 335–336.

Papinski, D., Schuschnig, M., Reiter, W., Wilhelm, L., Barnes, C. a, Maiolica, A., Hansmann, I., Pfaffenwimmer, T., Kijanska, M., Stoffel, I., Lee, S. S., Brezovich, A., Lou, J. H., Turk, B. E., Aebersold, R., Ammerer, G., Peter, M., and Kraft, C. (2014). Early steps in autophagy depend on direct phosphorylation of Atg9 by the Atg1 kinase. *Molecular Cell*, *53*(3), 471–483.

Pennetta, G., Hiesinger, P. R., Fabian-Fine, R., Meinertzhagen, I. a, and Bellen, H. J. (2002). Drosophila VAP-33A directs bouton formation at neuromuscular junctions in a dosage-dependent manner. *Neuron*, *35*(2), 291–306.

Perestenko, P. V, Pooler, A. M., Noorbakhshnia, M., Gray, A., Bauccio, C., and Jeffrey McIlhinney, R. A. (2010). Copines-1, -2, -3, -6 and -7 show different calcium-dependent intracellular membrane translocation and targeting. *The FEBS Journal*, *277*(24), 5174–89.

Pitsch, J., Opitz, T., Borm, V., Woitecki, A., Staniek, M., Beck, H., Becker, A. J., and Schoch, S. (2012). The presynaptic active zone protein RIM1α controls epileptogenesis following status epilepticus. *The Journal of neuroscience, 32*(36), 12384–12395.

Powell, C. M., Schoch, S., Monteggia, L., Barrot, M., Matos, M. F., Feldmann, N., Südhof, T. C., and Nestler, E. J. (2004). The presynaptic active zone protein RIM1alpha is critical for normal learning and memory. *Neuron*, *42*(1), 143–153.

Pozo, K., and Goda, Y. (2010). Unraveling mechanisms of homeostatic synaptic plasticity. *Neuron*, *66*(3), 337–351.

Prokop, A., and Meinertzhagen, I. a. (2006). Development and structure of synaptic contacts in Drosophila. *Seminars in cell and developmental biology*, *17*(1), 20–30.

Prosser, D. C., Tran, D., Gougeon, P.-Y., Verly, C., and Ngsee, J. K. (2008). FFAT rescues VAPA-mediated inhibition of ER-to-Golgi transport and VAPB-mediated ER aggregation. *Journal of Cell Science*, *121*(Pt 18), 3052–3061.

Pyle, R. a, Schivell, a E., Hidaka, H., and Bajjalieh, S. M. (2000). Phosphorylation of synaptic vesicle protein 2 modulates binding to synaptotagmin. *The Journal of biological chemistry*, *275*(22), 17195–17200.

Ratnaparkhi, A., Lawless, G. M., Schweizer, F. E., Golshani, P., and Jackson, G. R. (2008). A Drosophila model of ALS: human ALS-associated mutation in VAP33A suggests a dominant negative mechanism. *PloS One*, *3*(6), e2334.

Rizo, J., and Südhof, T. C. (2002). Snares and Munc18 in synaptic vesicle fusion. *Nature reviews. Neuroscience*, *3*(8), 641–653.

Schivell, a E., Batchelor, R. H., and Bajjalieh, S. M. (1996). Isoform-specific, calcium-regulated interaction of the synaptic vesicle proteins SV2 and synaptotagmin. *The Journal of biological chemistry*, *271*(44), 27770–27775.

Sambrook, J. and Russell, D. W. (2001). Molecular Cloning. A Laboratory Manual. 3rd Edition. *Cold Sprin Harbour Laboratory press*.

Schoch, S., Castillo, P. E., Jo, T., Mukherjee, K., Geppert, M., Wang, Y., Schmitz, F., Malenka, R. C., and Südhof, T. C. (2002). RIM1alpha forms a protein scaffold for regulating neurotransmitter release at the active zone. *Nature*, *415*(6869), 321–326.

Schoch, S., and Gundelfinger, E. D. (2006). Molecular organization of the presynaptic active zone. *Cell Tissue Research*, 326 (2), 379–391.

Schoch, S., Mittelstaedt, T., Kaeser, P. S., Padgett, D., Feldmann, N., Chevaleyre, V., Castillo, P. E., Hammer, R. E., Han, W., Schmitz, F., Lin, W., and Südhof, T. C. (2006). Redundant functions of RIM1alpha and RIM2alpha in Ca (2+)-triggered neurotransmitter release. *The EMBO journal*, *25*(24), 5852–5863.

Schoch, S., Müller, A. J., and Oprisoreanu A. M., (2014). Liprins, ELKS, and RIM-BP Proteins. (In press). Reference Module in Biomedical Sciences. Elsevier

Schrimpf, S. P., Meskenaite, V., Brunner, E., Rutishauser, D., Walther, P., Eng, J., Aebersold, R., and Sonderegger, P. (2005). Proteomic analysis of synaptosomes using isotope-coded affinity tags and mass spectrometry. *Proteomics*, *5*(10), 2531–2541.

Schröder, M. S., Stellmacher, A., Romorini, S., Marini, C., Montenegro-Venegas, C., Altrock, W. D., Gundelfinger, E. D., and Fejtova, A. (2013). Regulation of presynaptic anchoring of the scaffold protein bassoon by phosphorylation-dependent interaction with 14-3-3 adaptor proteins. *PloS One*, *8*(3), e58814.

Shah, K., and Lahiri, D. K. (2014). Cdk5 activity in the brain - multiple paths of regulation. *Journal of Cell Science*, *127*(Pt 11), 2391–400.

Siksou, L., Triller, A., and Marty, S. (2011). Ultrastructural organization of presynaptic terminals. *Current Opinion in Neurobiology*, *21*(2), 261–268.

Simsek-Duran, F. and Lonart, G. (2008). The role of RIM1alpha in BDNF-enhanced glutamate release. *Neuropharmacology*, *55*(1), 27–34.

Sisodiya, S. M., Thompson, P. J., Need, A., Harris, S. E., Weale, M. E., Wilkie, S. E., Michaelides, M., Free, S. L., Walley, N., Gumbs, C., Gerrelli, D., Ruddle, P., Whalley, L. J., Starr, J. M., Hunt, D. M., Goldstein, D. B., Deary, I. J., and Moore, A. T. (2007). Genetic enhancement of cognition in a kindred with cone-rod dystrophy due to RIMS1 mutation. *Journal of Medical Genetics*, *44*(6), 373–380.

Skehel, P. a, Armitage, B. a, Bartsch, D., Hu, Y., Kaang, B. K., Siegelbaum, S. a, Kandel, E. R. and Martin, K. C. (1995). Proteins functioning in synaptic transmission at the sensory to motor synapse of Aplysia. *Neuropharmacology*, *34*(11), 1379–1385.

Skehel, P. a, Fabian-Fine, R., and Kandel, E. R. (2000). Mouse VAP33 is associated with the endoplasmic reticulum and microtubules. *PNAS*, *97*(3), 1101–1106.

Stevens, D. R., Wu, Z., Matti, U., Junge, H. J., Schirra, C., Becherer, U., Wojcik, S. M., Brose, N., and Rettig, J. (2005). Report Identification of the Minimal Protein Domain Required for Priming Activity of Munc13-1, *15*, 2243–2248.

Stigloher, C., Zhan, H., Zhen, M., Richmond, J., and Bessereau, J.-L. (2011). The presynaptic dense projection of the Caenorhabditis elegans cholinergic neuromuscular junction localizes synaptic vesicles at the active zone through SYD-2/liprin and UNC-10/RIM-dependent interactions. *The Journal of neuroscience, 31*(12), 4388–4396.

Su, S. C., Seo, J., Pan, J. Q., Samuels, B. A., Rudenko, A., Ericsson, M., Neve, R. L., Yue, D. T., and Tsai, L.-H. (2012). Regulation of N-type voltage-gated calcium channels and presynaptic function by cyclin-dependent kinase 5. *Neuron*, *75*(4), 675–687.

Südhof, T. C. (2004). The synaptic vesicle cycle. *Annual Review of Neuroscience*, *27*, 509–47.

Südhof, T. C. (2012). The presynaptic active zone. *Neuron*, *75*(1), 11–25.

Südhof, T. C. (2013). Neurotransmitter release: the last millisecond in the life of a synaptic vesicle. *Neuron*, *80*(3), 675–690.

Sun, L., Bittner, M. a, and Holz, R. W. (2001). Rab3a binding and secretion-enhancing domains in Rim1 are separate and unique. Studies in adrenal chromaffin cells. *The Journal of biological chemistry*, *276*(16), 12911–12917.

Sun, L., Bittner, M. a, and Holz, R. W. (2003). Rim, a component of the presynaptic active zone and modulator of exocytosis, binds 14-3-3 through its N terminus. *The Journal of biological chemistry*, *278*(40), 38301–38309.

Sweatt, J. D. (2004). Mitogen-activated protein kinases in synaptic plasticity and memory. *Current Opinion in Neurobiology*, *14*(3), 311–317.

Szule, J. a, Harlow, M. L., Jung, J. H., De-Miguel, F. F., Marshall, R. M., and McMahan, U. J. (2012). Regulation of synaptic vesicle docking by different classes of macromolecules in active zone material. *PloS One*, *7*(3), e33333.

Takamori, S., Holt, M., Stenius, K., Lemke, E. a, Grønborg, M., Riedel, D., Urlaub, H., Schenck, S., Brügger, B., Ringler, P., Müller, S.A. Rammner, B., Gräter, F., Hub, J.S., De

Groot, B. L., Mieskes, G., Moriyama, Y., Klingauf, J., Grubmüller, H., Heuser, J., Wieland, F., and Jahn, R. (2006). Molecular anatomy of a trafficking organelle. *Cell*, *127*(4),831–846.

Takao-Rikitsu, E., Mochida, S., Inoue, E., Deguchi-Tawarada, M., Inoue, M., Ohtsuka, T., and Takai, Y. (2004). Physical and functional interaction of the active zone proteins, CAST, RIM1, and Bassoon, in neurotransmitter release. *The Journal of cell biology*, *164*(2), 301–311.

Teuling, E., Ahmed, S., Haasdijk, E., Demmers, J., Steinmetz, M. O., Akhmanova, A., Jaarsma, D., and Hoogenraad, C. C. (2007). Motor neuron disease-associated mutant vesicle-associated membrane protein-associated protein (VAP) B recruits wild-type VAPs into endoplasmic reticulum-derived tubular aggregates. *The Journal of Neuroscience, 27*(36), 9801–15.

Tomoda, T., Bhatt, R. S., Kuroyanagi, H., Shirasawa, T., and Hatten, M. E. (1999). A mouse serine/threonine kinase homologous to C. elegans UNC51 functions in parallel fiber formation of cerebellar granule neurons. *Neuron*, *24*(4), 833–846.

Tomoda, T., Kim, J. H., Zhan, C., and Hatten, M. E. (2004). Role of Unc51.1 and its binding partners in CNS axon outgrowth. *Genes Dev, 18*, 541–558.

Varedi K, S. M., Ventura, A. C., Merajver, S. D., and Lin, X. N. (2010). Multisite Phosphorylation Provides an Effective and Flexible Mechanism for Switch-Like Protein Degradation. *PloS One, 5*(12), e14029.

Vasilescu, J., Guo, X., and Kast, J. (2004). Identificationof protein-protein interactions using in vivo cross-linking and massspectrometry. *Proteomics*, *4*(12), 3845–3854.

Vrljic, M., Strop, P., Ernst, J. a, Sutton, R. B., Chu, S., and Brunger, A. T. (2010). Molecular mechanism of the synaptotagmin-SNARE interaction in Ca2+-triggered vesicle fusion. *Nature structural and molecular biology*, *17*(3), 325–331.

Wairkar, Y. P., Toda, H., Mochizuki, H., Furukubo-Tokunaga, K., Tomoda, T., and Diantonio, A. (2009). Unc-51 controls active zone density and protein composition by downregulating ERK signaling. *The Journal of Neuroscience, 29*(2), 517–528.

Waites, C. L., Leal-Ortiz, S. a, Okerlund, N., Dalke, H., Fejtova, A., Altrock, W. D., Gundelfinger, E.D., and Garner, C. C. (2013). Bassoon and Piccolo maintain synapse integrity by regulating protein ubiquitination and degradation. *The EMBO journal*, *32*(7), 954–969.

Wang, Y., Okamoto, M., Schmitz, F., Hofmann, K., and Südhof, T. C. (1997). Rim is a putative Rab3 effector in regulating synaptic-vesicle fusion. *Nature*, *388*(6642), 593–598.

Wang, H. Y., Lin, W., Dyck, J. a, Yeakley, J. M., Songyang, Z., Cantley, L. C., and Fu, X. D. (1998). SRPK2: a differentially expressed SR protein-specific kinase involved in mediating the interaction and localization of pre-mRNA splicing factors in mammalian cells. *The Journal of cell biology*, *140*(4), 737–750.

Wang, Y., Sugita, S., and Südhof, T. C. (2000). The RIM/NIM family of neuronal C2 domain proteins. Interactions with Rab3 and a new class of Src homology 3 domain proteins. *The Journal of biological chemistry*, *275*(26), 20033–20044.

Wang, X., Hu, B., Zimmermann, B., and Kilimann, M. W. (2001). Rim1 and rabphilin-3 bind Rab3-GTP by composite determinants partially related through N-terminal alpha -helix motifs. *The Journal of biological chemistry*, *276*(35), 32480–32488.

Wang, Y., Liu, X., Biederer, T., and Südhof, T. C. (2002). A family of RIM-binding proteins regulated by alternative splicing: Implications for the genesis of synaptic active zones. *PNAS*, *99*(22), 14464–14469.

Wang, Y., and Südhof, T. C. (2003). Genomic definition of RIM proteins: evolutionary amplification of a family of synaptic regulatory proteins. *Genomics*, *81*(2), 126–137.

Weimer, R. M., Gracheva, E. O., Meyrignac, O., Miller, K. G., Richmond, J. E., and Bessereau, J.-L. (2006). UNC-13 and UNC-10/rim localize synaptic vesicles to specific membrane domains. *The Journal of neuroscience, 26*(31), 8040–8047.

Weingarten, J., Laßek, M., Mueller, B. F., Rohmer, M., Lunger, I., Baeumlisberger, D., Dudek, S., Gogesch, P., Karas, M., and Volknandt, W. (2014). The proteome of the presynaptic active zone from mouse brain. *Molecular and Cellular Neurosciences*, *59*, 106–118.

Weir, M. L., Klip, A., and Trimble, W. S. (1998). Identification of a human homologue of the vesicle-associated membrane protein (VAMP)-associated protein of 33 kDa (VAP-33): a broadly expressed protein that binds to VAMP. *Biochem. J., 333*, 247–251.

Westfall, I. a. (1996). Ultrastructure of synapses in the first-evolved nervous systems. *Journal of neurocytology*, *25*(12), 735–746.

Weyhersmüller, A., Hallermann, S., Wagner, N., and Eilers, J. (2011). Rapid active zone remodeling during synaptic plasticity. *The Journal of Neuroscience*, *31*(16), 6041–52.

Xu, T., and Bajjalieh, S. M. (2001). SV2 modulates the size of the readily releasable pool of secretory vesicles. *Nature cell biology*, *3*(8), 691–698.

Yamatani, H., Kawasaki, T., Mita, S., Inagaki, N., and Hirata, T. (2010). Proteomics analysis of the temporal changes in axonal proteins during maturation. *Developmental Neurobiology*, *70*(7), 523–537.

Yan, J., Kuroyanagi, H., Kuroiwa, a, Matsuda, Y., Tokumitsu, H., Tomoda, T., Shirasawa, T., and Muramatsu, M. (1998). Identification of mouse ULK1, a novel protein kinase structurally related to C. elegans UNC-51. *Biochemical and biophysical research communications*, *246*(1), 222–227.

Yan, J., Kuroyanagi, H., Tomemori, T., Okazaki, N., Asato, K., Matsuda, Y., Suzuki, Y., Ohshima, Y., Mitani, S., Masuho, Y., Shirasawa, T., and Muramatsu, M. (1999). Mouse ULK2, a novel member of the UNC-51-like protein kinases: unique features of functional domains. *Oncogene*, *18*(43), 5850–5859.

Yang, Y., and Calakos, N. (2010). Acute in vivo genetic rescue demonstrates that phosphorylation of RIM1alpha serine 413 is not required for mossy fiber long-term potentiation. *The Journal of Neuroscience*, *30*(7), 2542–2546.

Yang, Z., Huh, S. U., Drennan, J. M., Kathuria, H., Martinez, J. S., Tsuda, H., Hall, M. C., and Clemens, J. C. (2012). Drosophila Vap-33 Is Required for Axonal Localization of Dscam Isoforms. *Journal of Neuroscience*, *32*(48), 17241–17250.

Yao, I., Takagi, H., Ageta, H., Kahyo, T., Sato, S., Hatanaka, K., Fukuda, Y., Chiba, T., Morone, N., Yuasa, S., Inokuchi, K., Ohtsuka, T., MacGregor, G. R., Tanaka, K., and Setou, M. (2007). SCRAPPER-dependent ubiquitination of active zone protein RIM1 regulates synaptic vesicle release. *Cell*, *130*(5), 943–957.

Yao, J., and Bajjalieh, S. M. (2008). Synaptic vesicle protein 2 binds adenine nucleotides. *The Journal of biological chemistry*, *283*(30), 20628–20634.

Yao, J., Nowack, A., Kensel-Hammes, P., Gardner, R. G., and Bajjalieh, S. M. (2010). Cotrafficking of SV2 and synaptotagmin at the synapse. *The Journal of neuroscience, 30*(16), 5569–5578.

Zhai, R. G., and Bellen, H. J. (2004). The architecture of the active zone in the presynaptic nerve terminal. *Physiology*, *19*, 262–270.

Zhou, X., Babu, J. R., Silva, S., Shu, Q., Graef, I. A., Oliver, T., Tomoda, T., Tani, T., Wooten, M. W., and Wang, F. (2007). Processes regulate filopodia extension and branching of sensory axons. *PNAS, 104*(14), 5842–5847.

Zolotukhin, S., Potter, M., Zolotukhin, I., Sakai, Y., Loiler, S., Fraites, T. J., Chiodo, V. a, Phillipsberg, T., Muzyczka, N., Hauswirth, W. W., Flotte, T. R., Byrne, B. J., and Snyder, R. O. (2002). Production and purification of serotype 1, 2, and 5 recombinant adeno-associated viral vectors. *Methods*, *28*(2), 158–167.

11. Acknowledgments

Today, finding myself at the end of my PhD studies and looking back, I cannot stop thinking that this work would not have been possible without a lot of goodwill and support from many other persons, on whom I could rely on for advice and assistance.

To my PhD supervisor and my boss, Prof. Dr. Susanne Schoch, I would like to convey my deepest gratitude for believing in me, and giving me the chance to complete my studies in her lab. The intellectual and professional support, as well as the freedom I was granted in performing the experimental part, since I was often given the opportunity to rethink some of the experiments in my own way, helped me to unfold myself into the more confident person I am today. In times of distress and crisis of faith, when nothing seemed to fall into place, she always found the time to encourage me and give me new directions to follow. The huge optimism she is gifted with is something I could always link to and for me at least, she is the best of the mentors.

Deep gratitude goes to Prof. Dr. Albert Haas for taking the necessary time to read and supervise my PhD thesis.

To Prof. Dr. Walter Witke, who kindly accepted to be part of my thesis committee I would like to extend my sincere thanks and appreciation.

Prof. Alf Lamprecht I would like to thank for his willingness to be part of my thesis committee.

I am awfully thankful to Sabine Opitz for the huge work she has done and the patience she had to prepare hundreds of plates of neuronal cultures, especially from SV2A KO mice. Many thanks go to, Vanessa Schmitt, Lioba Dammer and Daniela Frangenberg, who performed exceptionally in their duties making the life in the lab very pleasant, as well as to the former Master students Sarah Lenz, Katharina Schulenburg, Alexander Müller and Andrea Franz for their help within these projects.

The entire collective Schoch/Becker I would like to thank also for their help and constructive discussions over the past years, for they showed me what teamwork really means.